A NUMERICAL AND EXPERIMENTAL INVESTIGATION OF RADAR COUPLING AND PROPAGATION THROUGH CONCRETE

BY

IVO JOSE PADARATZ

BSc MSc Eng.

THESIS SUBMITTED TO THE UNIVERSITY OF EDINBURGH
FOR THE DEGREE OF DOCTOR OF PHILOSOPHY
NOVEMBER 1996

UNIVERSITY OF EDINBURGH
DEPARTMENT OF CIVIL AND ENVIRONMENTAL ENGINEERING
1996

DECLARATION

I HEREBY DECLARE THAT THIS THESIS WAS COMPOSED BY MYSELF, AND THE ORIGINAL WORKS AND RESULTS REPORTED WERE OBTAINED SOLELY BY MYSELF, UNLESS OTHERWISE STATED.

EDINBURGH, NOVEMBER 1996

I. J. PADARATZ

TO MY PARENTS †

ACKNOWLEDGEMENTS

The author wishes to thank Prof. M.C.Forde, head of the Department of Civil and Environmental Engineering, for providing all the necessary facilities during the whole research.

The author is grateful to Prof. M. C. Forde and to Dr. M. S. A. Hardy for their supervision. Their suggestions, criticism and constructive comments decisively contributed for the exit of this work.

The author is particularly grateful to Mr. K. Broughton, technician of the NDT Laboratory of this Department, for his friendship and high technical support.

The author wishes to thank Mrs. G. Temple, Mr. J. Hutchenson and remaining staff for providing the general secretarial and technical assistance during this work.

The author also wishes to thank the fellows of the NDT Research Group for their friendship and general assistance.

The author wishes to express his special gratitude to his wife Sonia and daughters Pricilla, Rejane and Aline. Their help, patience and encouragement at all times, were decisive to make this work a reality.

NOTATION

A_1 , A_2	amplitude
a	unit vector
B	magnetic flux density
c	velocity of wave propagation in free space
D	electric displacement, depth
DFT	discrete Fourier transform
DS	degree of saturation
d	distance, path length, depth, thickness
d'	characteristic dimension of heterogeneity
E	electric field intensity, dynamic modulus of elasticity
e	emissivity
FFT	Fast Fourier Transform
f	frequency, centre frequency
f_d [n]	discrete time function representing a sampled waveform
f_o	centre frequency of the antenna in air
f(t)	time domain function
H	magnetic field intensity
J	current density
j	$=\sqrt{-1}$
k, k_c	wavenumber, a coefficient
k_o	wavenumber in free space
MC	moisture content
N	number of samples
P_i	initial weight
P_{od}	weight after oven dried
P_{sat}	saturated weight
R	receiver, acoustic reflection coefficient, rate of energy radiation
r	radius of the first Fresnel zone

S	saturation
S_f	sampling rate or sampling interval
T	transmitter, acoustic transmission coefficient, period, absolute temperature
T_w	time window size
t	time, travel time
$\tan \delta$	loss tangent, dissipation factor
V, V_L, V_p	longitudinal ultrasonic wave velocity
v	velocity of wave propagation, phase velocity
$X(\omega)$	coefficients of the Fourier integral
X_d [k]	Fourier coefficients of a discrete time function
x	antennas' position
Z	intrinsic impedance, acoustic impedance
α	attenuation constant
β	phase-shift constant
Δ_t	time delay
Δ_f	frequency interval (or frequency resolution)
δ	skin depth
ε	dielectric permittivity
ε_a	relative permittivity of air
ε_c	complex permittivity
ε_{cr}	relative complex permittivity
ε_m	relative permittivity of concrete solids (real part)
ε_o	dielectric permittivity of free space
ε_r	dielectric constant
ε_{sw}	relative complex permittivity of water
ε'	real part of the complex permittivity
ε_e'	effective value of ε'
ε''	imaginary part of the complex permittivity
ε_e''	effective value of ε''
ε'_r	real part of the relative complex permittivity

ε''_r	imaginary part of the relative complex permittivity
ϕ	porosity
γ	propagation constant
η_i	refractive index
λ	wavelength
μ	magnetic permeability
μ_o	magnetic permeability of free space
μ_r	relative magnetic permeability
ν	Poisson's ratio
θ_i	angle of the incident wave
θ_r	angle of the reflected wave
θ_t	angle of refraction of the transmitted wave
ρ	charge density, reflection coefficient, density
σ	conductivity, Stefan-Boltzmann constant
σ_c	complex conductivity
σ'	real part of the complex conductivity
σ''	imaginary part of the complex conductivity
τ	transmission coefficient
ω	angular frequency
ω_0	fundamental frequency

LIST OF TABLES

LIST OF PLATES

LIST OF FIGURES

LIST OF CONTENTS

ABSTRACT

The main purpose of this research was to obtain numerical and experimental information that may support Radar survey design. The reference material is usually concrete, but the results can be extended to other materials.

Other techniques currently being employed either on concrete or masonry are also critically described. Justification for this research into Radar is clearly identified.

A numerical study was carried out giving emphasis to Radar resolution (horizontal and vertical) and clutter (signal scattered from material heterogeneity). Assumptions are made for the centre frequency of transmitted pulses, and the results are compared to experiments.

The experimental work focuses on signal distortion due to antenna coupling and wave attenuation during propagation in lossy media. The centre frequency of the recorded signals is used as a reference for comparisons.

Digital signal processing techniques are used to analyse the experimental data, in both time domain and frequency domain.

Other important aspects that could influence the accuracy of travel time measurements are also discussed, such as the antenna size for short ranges and the change in pulse shape.

Radar confirms its potential as a non-destructive technique, however users have to be aware of its limitations. Experiments suggest that manufactures of Radar need to improve their systems, particularly for their portability and antenna efficiency.

CHAPTER 1

INTRODUCTION

CHAPTER 1

1. INTRODUCTION

Over the past decades a growing number of concrete structures world-wide have presented signs of deterioration earlier than initially expected. This has been associated with the changes in cement manufacture, increased use of cement replacements and admixtures, and a decline in standards of workmanship and construction supervision [1]. Political disputes which accelerate the process of new construction combined with limited economic resources have also been blamed, mainly in developing countries.

The problems mentioned above have led to a dramatic increase in the amount of research into techniques that could be used to quickly assess concrete properties of existing structures, in particular the in-place strength of concrete for safety. However, more recently the growing interest in the rehabilitation of existing constructions has required improvements in methods for condition assessment. These methods might provide information regarding structural performance of the concrete, such as: member thickness, location of cracking and delamination, degree of concrete consolidation, presence of voids and honeycombing, location of reinforcement and corrosion activity. Planned restoration can extend the lifetime of an existing structure, and testing of concrete structures, to verify their existing conditions, can provide the basis for an economically and viable rehabilitation. In all this context a set of techniques and methods generally denominated as non-destructive tests (NDT) play a very important rule.

In most cases, inspections have been a visual appraisal of the external envelope of a structure and little use has been made of the modern non-destructive techniques. It is thought that little information is available to suggest that they can

be used cost effectively [2]. The main factors that contributed to the increase in the application of NDT methods include:

- the ability to perform rapid surveys of existing construction;

- the possibility of assessing large volumes of concrete with economic advantages when compared to core extraction, and giving a clearer and more statistically representative picture of the integrity of the structure;

- the technological developments in hardware and software allowing more efficient data collection and analysis.

Research in the field of non-destructive testing has advanced in recent years due to the demand of a better understanding of the mechanism and extent of deterioration in structures before starting any repair and/or rehabilitation work [3]. Traditionally concrete strength tests have been the main type of in-situ measurement. Even though quantitative testing is usually preferred in practice, a major repair, rehabilitation or strengthening work requires a prior determination of the structural integrity. There is therefore an increasing demand for methods that are able to scan large portions of a structure, in order to extrapolate the test results from single point techniques over a whole structure.

Non-destructive testing is a well accepted practice in the inspection of metal-based materials. Radiographic and ultrasonic techniques are routinely used to detect anomalies in steel frameworks of buildings and bridges [4,5]. However concrete is an inhomogeneous composite material, where NDT methods are still subject to limitations. The variability of results can be very high, and expertise as well as experience in data interpretation are required in many cases. This is caused by the fact that most concrete is ready-mixed away from the site before placing, consolidation and curing in the field. Lack of control over material handling and treatment in the field leads to a variable final product.

One of the most effective non-destructive tests is visual inspection, and normally represents one of the first steps in any evaluation of concrete structures [6]. It requires broad knowledge in structural engineering, concrete materials, and construction methods. Its evaluation is basically confined to the surface of a structure, even though nowadays the use of optical tools (fiberscopes and borescopes) can help in the inspection of some regions not accessible to the naked eye. Visual inspection usually takes part of the planning stage of a test programme and should allow an experienced professional to indicate the relevant further tests to be carried out in any given situation [7].

The principal tests that may be applied for assessing concrete in structures are listed in Table 1.1 [1]. It classifies the tests according to the property under investigation:

- corrosion of embedded steel;
- concrete quality, durability and deterioration;
- concrete strength;
- integrity and performance.

In terms of non-destructive testing of concrete, the tests listed in Table 1.1 may also be re-grouped into two major groups: those used to estimate in-place mechanical properties and those that are used to locate embedments or hidden anomalies.

In the first group some are truly non-destructive, such as rebound hammer and ultrasonic pulse velocity. Others normally produce some surface damage such as pullout, torque or break-off tests.

Property under investigation	Test	Equipment type
Corrosion of embedded steel	Half-cell potential	Electrochemical
	Resistivity	Electrical
	Linear polarization resistance	Electrochemical
	A.C. Impedance	Electrochemical
	Cover depth	Electromagnetic
	Carbonation depth	Chemical/microscopic
	Chloride concentration	Chemical/electrical
Concrete quality, durability and deterioration	Surface hardness	Mechanical
	Ultrasonic pulse velocity	Electromechanical
	Radiography	Radioactive
	Radiometry	Radioactive
	Neutron absorption	Radioactive
	Relative humidity	Chemical/electronic
	Permeability	Hydraulic
	Absorption	Hydraulic
	Petrographic	Microscopic
	Sulphate content	Chemical
	Expansion	Mechanical
	Air content	Microscopic
	Cement type and content	Chemical/microscopic
	Abrasion resistance	Mechanical
Concrete strength	Cores	Mechanical
	Pull-out	Mechanical
	Pull-off	Mechanical
	Break-off	Mechanical
	Internal fracture	Mechanical
	Penetration resistance	Mechanical
	Maturity	Chemical/electrical
	Temperature-matched curing	Electrical/electronic
Integrity and performance	Tapping	Mechanical
	Pulse-echo	Mechanical/electronic
	Dynamic response	Mechanical/electronic
	Acoustic emission	Electronic
	Thermoluminescence	Chemical
	Thermography	Infra-red
	Radar	Electromagnetic
	Reinforcement location	Electromagnetic
	Strain or crack measurement	Optical/mechanical/electrical
	Load test	Mechanical/electronic/ electrical

Table 1.1 Principal test methods, after Bungey [1]

The second group of NDT methods comprises those applied for condition assessment of existing structures. They are based on the propagation of either electromagnetic or stress waves, and have been applied to measure physical properties other than the strength of concrete in structures, as well as to detect flaws or discontinuities, and to provide data for condition assessment. Infrared thermography, ground penetrating radar and impact-echo are a few of these methods.

The main methods that have been employed for condition assessment will be described in chapter 2. Radar is the non-destructive testing method used during the work which forms the subject of this thesis, and will be described in more detail in chapter 3.

The aim of this research is to investigate numerically and experimentally the propagation of electromagnetic waves through concrete using the radar technique, giving emphasis to the effects of antenna coupling and wave distortion. Chapter 5 covers the numerical analysis, including the behaviour of signal attenuation and velocity of wave propagation. It also presents recommendations for a preliminary choice of suitable antenna for survey design purposes. Aspects such as vertical and horizontal target resolution, energy scattering from material heterogeneity (clutter) and depth of penetration are discussed.

Experimental work was carried out to obtain quantitative information regarding antenna coupling and wave distortion for 900 MHz antennas, and is covered in chapters 6 and 7. The findings give support to the numerical analysis mentioned before, where these problems were considered only using an empirical approach. Extensive signal processing was applied to the experimental data, and the respective techniques and specific considerations are described in chapter 4.

Chapters 8 and 9 present the overall discussion of the findings and recommendations for future research.

CHAPTER 2

NON-DESTRUCTIVE TESTING OF CONCRETE IN STRUCTURES

CHAPTER 2

2. NON-DESTRUCTIVE TESTING OF CONCRETE IN STRUCTURES

2.1 INTRODUCTION

As mentioned in the previous chapter, the main technique employed during the experiments of the present research is ground penetrating radar (GPR), and will be covered in detail in chapter 3. This chapter will briefly introduce the radar technique, and cover the methods that are complementary to it. What these techniques have in common is the potential of detecting features not visible at the surface. Their basic principles will be described, and their main applications, advantages and disadvantages highlighted. This will be followed by a discussion in order to justify the relevance of choosing radar for the numerical and experimental work.

The complementary NDT methods used in the investigation of reinforcement corrosion, concrete strength and properties such as surface hardness, sulphate content and abrasion, are deemed to be outside the scope of this thesis.

2.2 NDT METHODS FOR CONDITION ASSESSMENT OF CONCRETE IN STRUCTURES

2.2.1 Stress waves methods

The relevant stress wave methods that will be covered in this section are ultrasonic pulse velocity (UPV), pulse-echo and impact echo methods. All methods

are based on the propagation of stress waves in the ultrasonic range, which is above the audible limit, usually assumed as about 20 kHz.

Stress waves are generated when the surface of a solid material is suddenly submitted to pressure or deformation, such as by impact or electro-mechanical transducers. They can be of three types: longitudinal or compressional waves (P-waves), transverse or shear waves (S-waves) and surface waves (R-waves). These waves are schematically represented in Figure 2.1. Longitudinal waves are the fastest and can provide useful information on the interior of a concrete body. The particle displacement is in the direction of wave propagation.

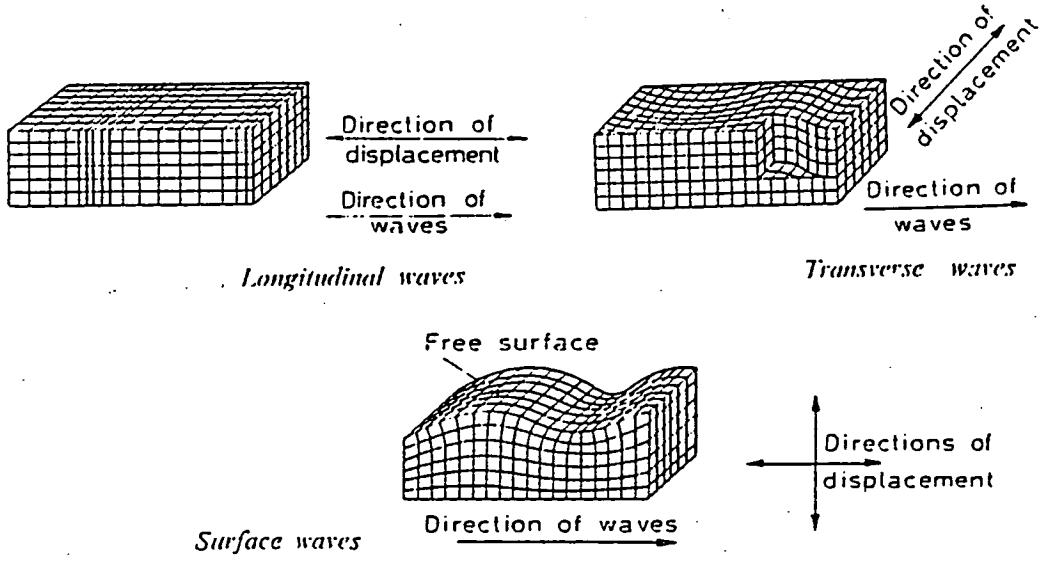

Figure 2.1 Types of stress waves, after Filipczynski *et al.* [8]

The velocity of the longitudinal waves is given by the equation 2.1, valid for an infinite, homogeneous, isotropic and elastic solid [9]. Concrete may not satisfy all these conditions, and therefore this equation should be used as reference only.

$$V_L = \sqrt{\frac{E(1-\nu)}{\rho(1+\nu)(1-2\nu)}} \qquad (2.1)$$

Where,

V_L = longitudinal wave velocity

E = dynamic modulus of elasticity

ρ = density

ν = Poisson's ratio

When stress waves reach an interface between two media with significant contrast in their densities and elastic properties, reflection and transmission will occur. The reflection coefficient for normal incidence waves (angle of incidence 90°) can be obtained by [9],

$$R = \frac{Z_2 - Z_1}{Z_2 + Z_1} \qquad (2.2)$$

Z_1, Z_2 = acoustic impedance of material 1 and 2 respectively.

The corresponding transmission coefficient is given by

$$T = \frac{2Z_1}{Z_2 + Z_1} \qquad (2.3)$$

The acoustic impedance Z of a material is given by $Z = \rho V_L$. Table 2.1 contains the acoustic impedance for some materials of interest, extracted from the references [10,11]. Applying the values for a concrete/air interface, equation (2.2) computes a value that approximates to unity, which means nearly total reflection. This information becomes very useful when using ultrasonic techniques for the detection of internal defects in concrete.

Table 2.1 Characteristic acoustic impedance of some materials, based on references [10,11]

Material	Characteristic acoustic impedance (kg $m^{-2}s^{-1}$)
Air	0.420×10^3
Water	1480×10^3
Soils	$280 - 4300 \times 10^3$
Concrete	$7200 - 10800 \times 10^3$ (*)
Steel	46600×10^3

(*): Assuming a density of 2400 kg/m^3

a) Ultrasonic pulse velocity (UPV)

Also known as "ultrasonic through transmission", the ultrasonic pulse velocity is one of the oldest methods that has been used for concrete. The field instruments for measuring pulse velocity appeared almost at the same time in Canada and England in the late 1940s [12]. Figure 2.2 shows a schematic representation of the ultrasonic test instrument. The portability of the commercial units is one of their main advantages, allowing easy handling in field works: examples are the V-Meter [13] manufactured in the USA, and the PUNDIT [14] in England-UK.

Discs of piezo-electric materials form the basis of most transducers used in the present technique. When an alternating voltage is applied across the thickness of a piezo-electric material, it contracts and expands generating a compression wave normal to the disc [9]. This transducer vibration is then transferred to the surrounding medium as a mechanical energy, and the process will be most efficient if the transducer crystal vibrates at its natural frequency.

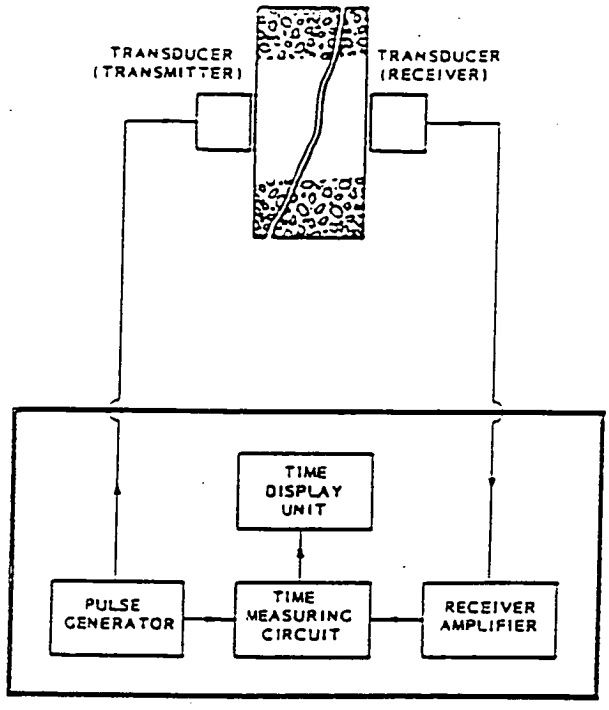

Figure 2.2 Typical diagram of UPV testing equipment, after Naik [15]

As seen at the beginning of this section, the presence of air gaps in the ultrasonic travel paths obstructs the waves' propagation. This can also happen between the transducers and material surface, requiring the use of couplants such as petroleum jelly, liquid soap and grease, to ensure that the transducer vibration is transferred to the medium under investigation. For very rough surfaces, special probes called exponential receivers with a tip diameter of only 6 mm may be employed, or the surface has to be smoothed using for example plaster of Paris [12,15].

The waves generated for the non-destructive testing inspection of concrete in structures are usually within the range of 20 to 200 kHz. This is much less than the range used for metallic materials, where the frequency varies from 0.5 to 20 MHz [9]. Special probes such as electromagnetic acoustic transducers are employed, which have the advantage over piezo-electric transducers of being totally non-contact

devices [16]. Higher frequency waves provide better resolution, but will attenuate more rapidly when propagating through heterogeneous materials such as concrete. This drastically limits the operational frequencies for applications on concrete structures.

The measurements with the ultrasonic pulse velocity method can be made with three possible transducer arrangements, as shown in Figure 2.3: direct transmission, semi-direct transmission and indirect transmission. The first one normally presents the most reliable results, because maximum energy is directed to and picked-up at the receiver. The semi-directed transmission may be convenient if high concentration of reinforcement is present [15]. The indirect arrangement provides only information from a layer near to the surface.

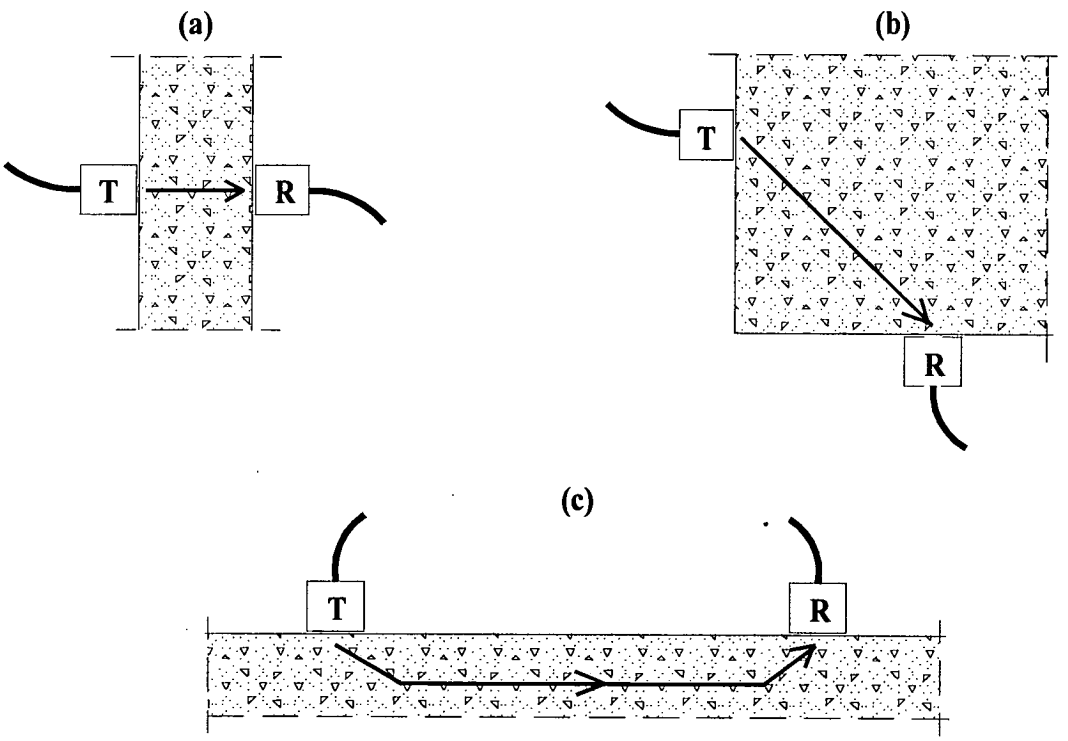

Figure 2.3 Transducer arrangements for UPV testing, based on reference [14]: (a) direct, (b) semi-direct, and (c) indirect transmission

The ultrasonic equipment provides the time of arrival of the first compression wave. If the wave travel path length is known, then the velocity can be determined by,

$$v = \frac{d}{t} \qquad (2.4)$$

d = direct path length

t = travel time of the first arrival, given by the equipment.

The direct and semi-direct transmissions have for long been be used to provide data for detecting features in the interior of concrete such as cracks, voids and other imperfections [10]. However this technique only measures the transmission time between the source and detector. For condition assessment of concrete and other materials, such as masonry, it is possible to improve the approach by employing the acoustic tomography, that can also include the detection of embedments [17,18]. It is similar to that used in medical applications of X-ray tomography. The main difference is that X-rays travel in a straight line whilst acoustic waves can refract and reflect at interfaces between materials with different elastic properties. Since the presence of air voids, contrasts in material density and reinforcements can affect the travel times, acoustic tomography may be able to produce an image showing the existence and location of these features.

The use of tomography will be effective if a large amount of data is available. Therefore the collection of data is primarily important, and using the normal point-by-point UPV test method becomes a very slow process, making the tomographic analysis impractical. Recently, improvements have been made by developing an UPV scanning method that allows much more rapid data acquisition [19]. Basically, the method uses a fixed receiver and moving source as shown in Figure 2.4. The scanner source is made up of a piezo-electric transducer in a cylindrical

configuration, which allows it to roll while generating vibrations into the object under test.

Whatever the mode of data acquisition, the data is later fed into tomographic processing software to produce a 2-dimensional slice image. Recent software developments have been made for analysis considering curved wave paths for three-dimensional reconstruction [20].

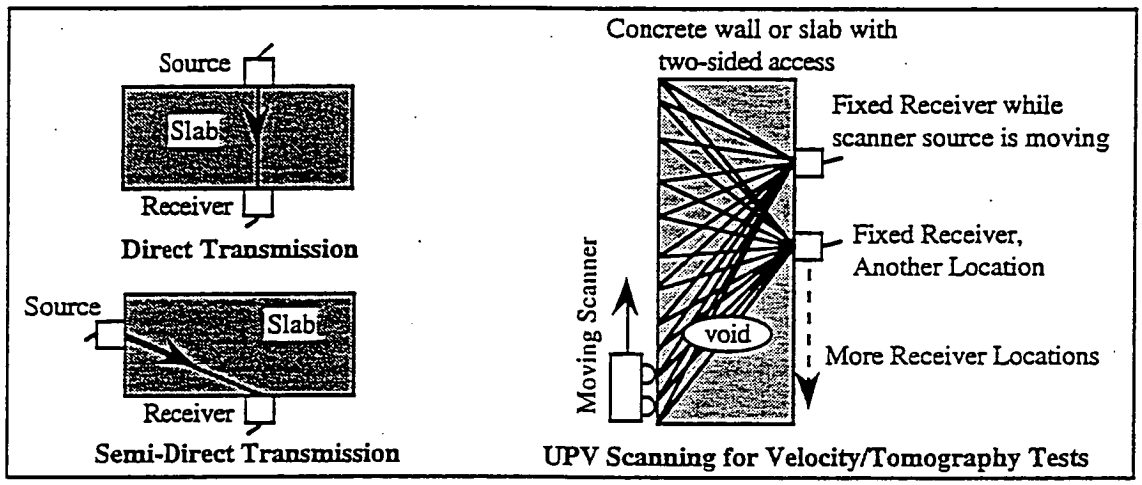

Figure 2.4 UPV scanning for tomography, from reference [21]

Although tomography has shown its capabilities in detecting internal defects and embedments in concrete, the accuracy of their size and precise location can be affected by factors such as extreme operating temperatures, concrete stress, path length, microcracks, and moisture [1,22]. Regarding the path length, BS 1881: Part 203 [23] recommends a minimum path length of 100 mm and 150 mm for concrete with maximum aggregate size of 20 mm and 40 mm respectively. In addition, the separation of significant anomalies from false artifacts may be difficult when interpreting tomographic velocity reconstructions. It is assumed that defects with dimensions less than 10 % of the smallest specimen dimension are considered non-

recognizable, and are filtered out [24]. This can eliminate spurious anomalies from the data, but also represents a limitation of the technique in terms of resolution.

The main applications regarding condition assessment, advantages and limitations of ultrasonic pulse velocity method are summarised below [15,25].

Applications

- Verification of concrete relative quality and uniformity.
- Detection of internal discontinuities such as cracks, voids and honeycombing.
- Assessment of concrete deterioration resulting from fire, mechanical, frost or chemical attack.
- Detection of embedments using acoustic tomography.

Advantages

- The test is well established and has been standardised by several organisations world-wide, including ASTM (American Standards) and BSI (British Standards).
- The equipment is portable and relatively inexpensive.
- The test procedure is simple, allowing easy use at both in the laboratory and in the field.

Limitations and disadvantages

- Requires access to two sides of test element.
- Results are affected by several factors such as amount and size of aggregates, moisture variations, material density, wave path length, and presence of reinforcement.
- If using tomographic velocity reconstructions, the resolution is limited to 10 % of the specimen minimum dimension.
- The presence of aggregates, with size larger than the component wavelengths, produce high signal attenuation that reduces the accuracy of the readings.
- The use of couplants such as oil and grease leave undesirable marks on the concrete surface.

- The UPV method is a vibration technique and therefore any other sources of vibration should be eliminated during the tests.

b) Pulse-echo method

This method involves introducing a stress wave at one accessible side of the structure by means of a transducer that works as transmitter and as receiver, or by using a pair of transducers (one transmitter and one receiver) closely spaced. In the first case a true pulse-echo is obtained, whilst the second one is known as "pitch-catch" mode [11]. Figure 2.5 depicts the two techniques illustrating the detection of a flaw in concrete, and Figure 2.6 shows an application of a true pulse-echo system on a concrete slab with an artificial defect. If the wave velocity in the material is known, the measured travel time of the echo can be used to work out the depth of the reflector as follows,

$$D = \frac{V\Delta t}{2} \qquad (2.5)$$

Δt = time delay between the start of the transmitted pulse and the arrival of the echo.

The capability of detecting the defects depends primarily on the wave frequency. The higher the frequency (or shorter the wavelength) the better is the resolution, but as a consequence the pulse attenuation increases rapidly due to the scattering effect at the interfaces between the mortar matrix and the aggregates. This will limit the penetration of the pulses and the surveys will be confined to small depths. To increase the penetration in concrete lower frequency transducers have to be employed. However it will often result in larger transducers, making the use of the pulse-echo technique difficult in practice [11].

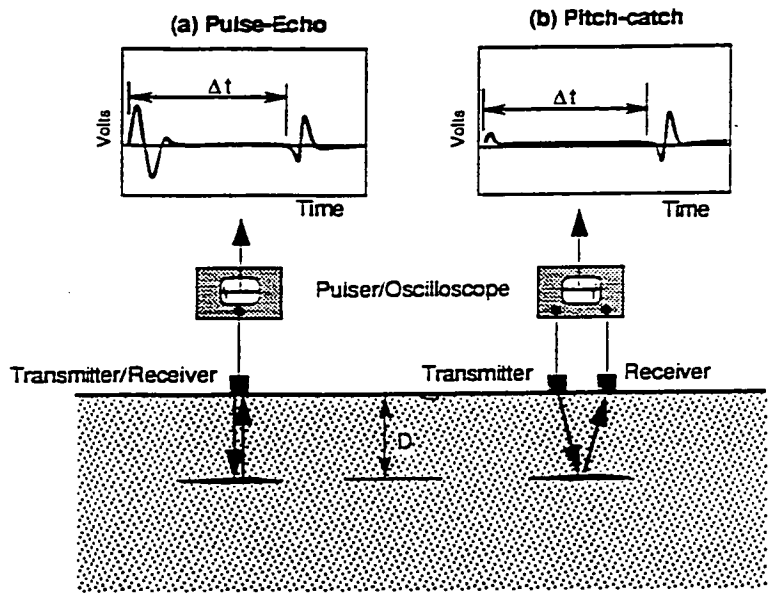

Figure 2.5 Pulse-echo and pitch-catch techniques, after reference [11]

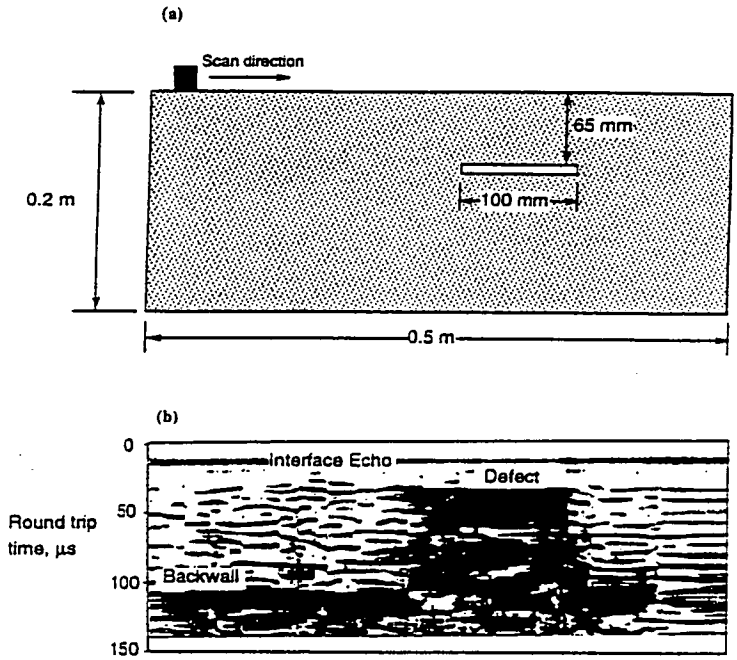

Figure 2.6 Imaging of defects in concrete by ultrasonic pulse-echo technique, based on reference [26]

Krause *et al.* carried out an extensive laboratory work testing different set-ups of ultrasonic pulse-echo methods, and comparative partial results can be found in the reference [27]. The experiments determine the state of the art of concrete testing in Germany using these and other NDT methods.

New developments are under way attempting to replace the traditional ultrasonic piezo-electric transducers by totally non-contact devices. In this direction laser systems have been tested in the laboratory to generate ultrasonic waves in concrete and to detect their reflections [28]. It has been shown that lasers can provide the basis of a non-contacting system for inspecting metals with ultrasound [29]. A source of laser pulses is extremely efficient at generating waves that propagate along the surface of the medium under testing, but also generates bulk waves that radiate away from the surface into the medium, as shown in Figure 2.7 [30]. Limited success has been achieved so far when using laser on concrete. To produce detectable reflections, sufficient acoustic energy has to be generated in the material, which is still a difficulty associated with this technique [28].

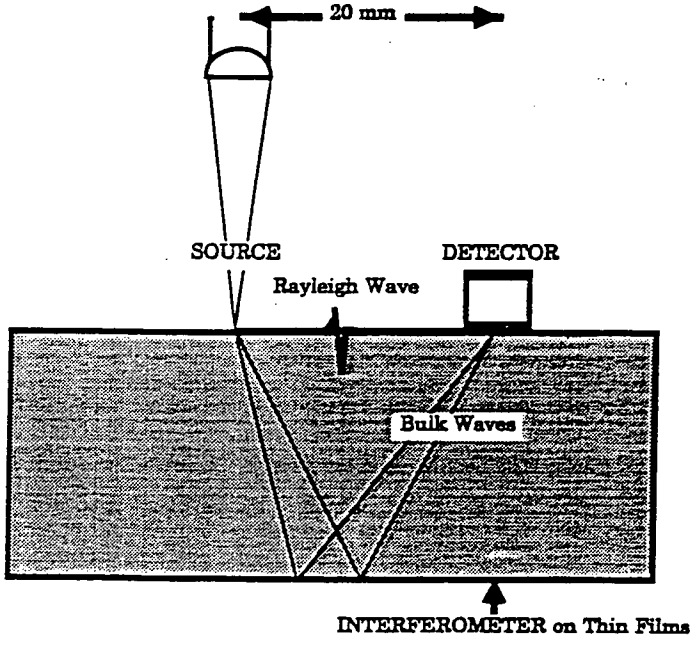

Figure 2.7 Schematic representation of ultrasonic waves generated by a laser system, from reference [30]

The main applications and limitations of the pulse-echo technique are listed below [25,31].

Applications

- Can determine thickness of concrete elements.
- Can locate reinforcement, defects, voids and delaminations.
- Estimates uniformity and relative quality of concrete.

Limitations

- Limited depth of penetration.
- Requires experienced operator.
- Expertise is necessary for interpretation of results.
- Multiple scattering at aggregates can difficult the identification of the echoes produced by a defect.

c) Impact-echo method

To overcome the necessity of large transducers for generating ultrasonic pulses, mentioned in the previous technique, a mechanical impact method has been proposed called *impact-echo* [32]. It is used to produce short duration pulses which travel through the test object. Three types of wave (longitudinal, transverse and surface waves) are generated. The basic principle is illustrated in Figure 2.8.

The impact-echo method is a point source generator, and therefore will present less directionality than can be achieved with transducers in the pulse-echo method. Large transducers can produce a more focused beam of pulses, and thus fewer reflections of the surrounding medium will occur. This allows easier interpretation of the results [33]. Therefore the quality of the results of the present method will depend of the way the impact is applied. The longer the impact duration

the lower the frequency components of the waves, though longer amplitudes will be achieved. Conversely, a shorter contact time produces a broader range of frequencies, but the amplitudes will decrease [34].

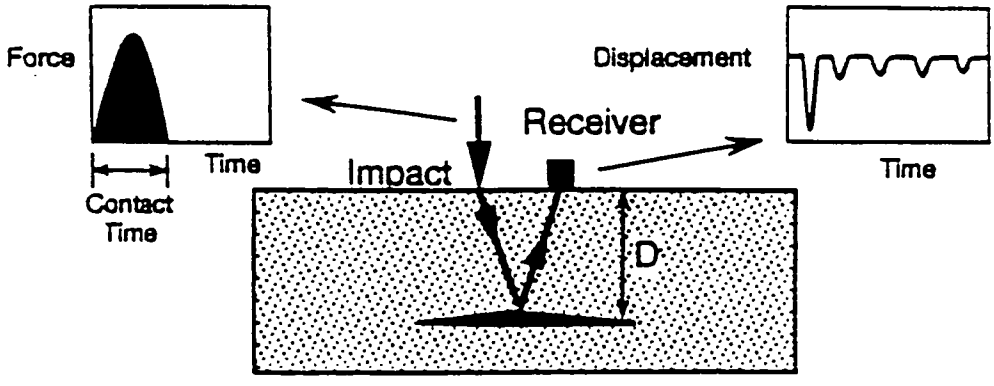

Figure 2.8 Basic principle of impact-echo method, after Carino and Sansalone [33]

Impact method has traditionally been used for evaluation of concrete piles [35]. A single blow is applied by hammer to the top and the reflections detected by an accelerometer. It is better known as sonic-echo or seismic-echo method. The data are displayed on an oscilloscope and can be analysed in the time domain, as there is enough time delay between the transmitted signal and reflections from the pile. The length of piles and existing defects across them can be determined [36]. Clear peaks in the time domain are normally present, because the interface between the piles and surrounding soils works as a wave guide giving better directionality to the impact waves [11].

If the structure under investigation is plate-like, such as slabs and pavements, shorter duration impacts are needed as they will contain higher frequency components. Due to the broader beam and shorter travel paths, the response may become too complex to be analysed in the time domain. Thus the main feature of the "new" impact-echo method, is the analysis in the frequency domain [37]. The analysis in the frequency domain is not a new approach, as it was already employed in transient dynamic response pile testing [38]. It is a vibration method developed by the Centre Expérimental de Recherches et d'Études du Bâtiment et des Travaux Publics (CEBTP) of France, which involves the use of an electro-dynamic shaker at the pile head. It was shown to be a useful tool for identifying faults in concrete piles. Similar results are obtained with the transient shock method, where the excitation of the pile is achieved by impact with an instrumented hammer [35]. The impact-echo method was developed in the U.S.A. for testing features on concrete highway pavements under the SHRP program [39].

From Figure 2.8, one may observe that the travel time of the multiple reflections of the initial pulse will repeat many times. This indicates that the waveform undergoes a periodic behaviour, and the period will be given by [40]

$$T = \frac{2D}{V_p} \qquad (2.6)$$

$2D$ = travel path

V_p = longitudinal wave speed

The frequency is the inverse of the period, and therefore it follows that

$$f = \frac{1}{T} = \frac{V_p}{2D} \qquad (2.7)$$

The wave speed can be calculated using the test on a structural element with known thickness. The frequency in equation (2.7) can be determined from the frequency

domain amplitude spectrum, which is obtained applying the Fourier transform (see chapter 4) on the recorded signals. A typical example of the frequency domain results is shown in Figure 2.9 [33]. The simulated defect produces a much higher frequency response (smaller period), because it is located at half a way of the slab thickness.

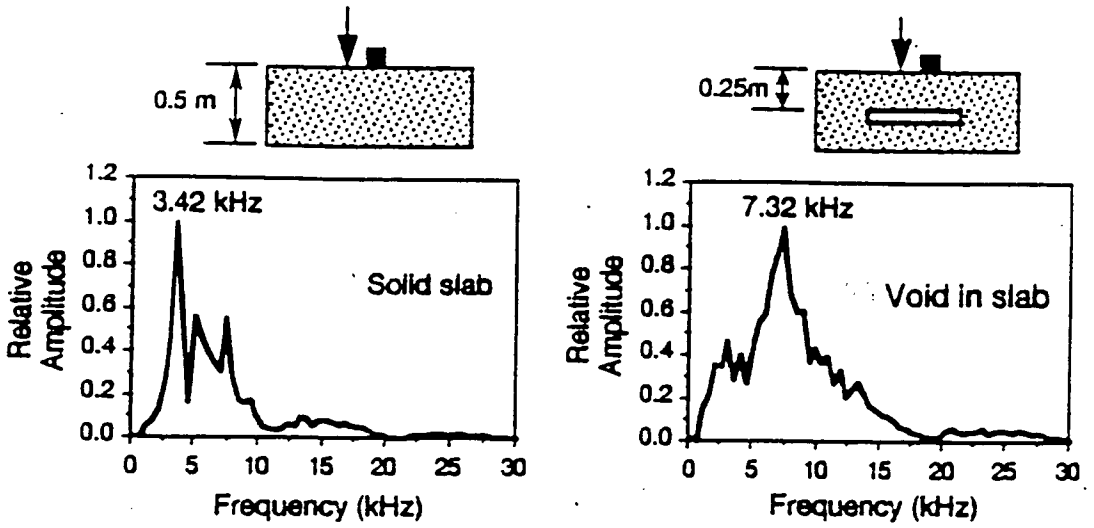

Figure 2.9 Example of frequency domain analysis of impact-echo method, based on reference [33]

The transducer used as the receiver has been a conical-tipped piezoelectric one. The advantage is that this kind of transducer does not require liquid or viscous couplants, only a thin lead strip is used to provide the necessary coupling [11].

Currently, typical applications of the impact-echo method include the location and extent of cracks, delaminations, honeycombing, and lack of bond between reinforcement and concrete. The detection of voids in post-tensioned ducts and unbonded area between two concretes has also been reported [41].

Commercial equipment is already available, but an experienced operator is required and is limited to testing members less than 2 metres thick. Another limitation is the impulse frequency. If the concrete surface crumbles upon impact then a larger contact time occurs, resulting in a lower frequency of input signal [42]. This can obscure target reflections initially expected. Therefore one can mistakenly make the hypothesis "if no defect is identified, then no defect exists", on the false premise that the intended input frequency has been achieved [39]. The wave velocity determined with this technique has been reported to be about 10 % less than that achieved by UPV test [34,43]. Experiments carried out by Martin and Forde [42] have shown however that the results are nearly the same. This suggests that more experimental data is necessary to explain this divergence, in order to better identify the factors involved and their influence on the velocity values.

The main advantage of this technique (as in all pulse-echo methods) is that access to only one side of the structure is required to carry out the tests. The best results have been for plate-like structures, such as slabs and pavements. More complex shape targets will produce divergent beam reflections, making the interpretation of data difficult.

2.2.2 Infrared thermography

Infrared thermography or infrared scanning is a measure of the surface radiation related to temperature and emissivity of materials [44]. It is based on the principle that the presence of an anomaly having a lower thermal conductivity than the surrounding material (e.g. cracks and delaminations) will affect the flow of heat and consequently change the distribution of the surface temperature. The heating source present during the measurements and the thermal conductivity contrast of materials must be great enough to permit the development of temperature anomalies.

The source of heat can be created artificially by using heating lamps or it can occur naturally [45]. In the latter case it can be by solar heating (heat flow into structure) and night-time cooling (heat flow out of structure).

The principle of infrared thermography is illustrated in Figure 2.10 [45]. It considers the simple case of a discontinuity in a concrete slab, which produces a localised insulation effect. The presence of the discontinuity interferes in the heat flow within the slab and affects the surface distribution of temperature. The differences in the surface temperature are then detected by an imaging infrared scanner (similar to a video camera). It measures the amount of the emitted radiation by means of special sensors and displays a television image of the temperature distribution of the scanned surface. The radiation is in the infrared region of the electromagnetic energy spectrum, not visible by the naked eye. A conventional video camera provides a visual record of the same surface. All the information is initially recorded in analog video images, and after converted into digital data for storage, signal processing and interpretation.

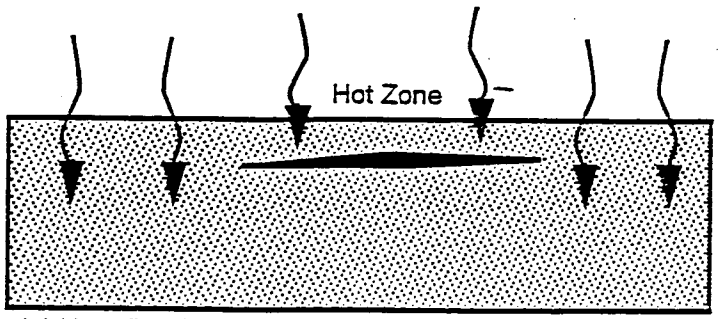

(a) Heat flow inward results in hot zone above flaw

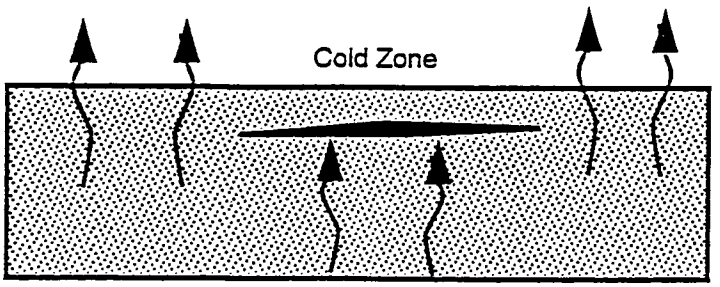

(b) Heat flow outward results in cold zone above flaw

Figure 2.10 Basic principle of the infrared thermography method, after Weil [45]

The background theory that gives support to the infrared thermography technique is based on the rate of electromagnetic energy emitted by a surface, given by the Stefan-Boltzmann law [46], as follows,

$$R = e\sigma T^4 \qquad (2.8)$$

where,

R = rate of energy radiation per unit area of surface (W/m^2)

e = emissivity of the surface

σ = the Stefan-Boltzmann constant = 5.67×10^{-8} $W/m^2 \cdot K^4$

T = absolute temperature of the surface (K)

The emissivity is defined as the ability of a material to radiate energy compared to a perfect black body radiator. Its value ranges from 0 to 1. The higher the roughness of a surface the higher the emissivity.

The main applications of infrared thermography has been in the detection of delaminations in concrete bridge decks due to reinforcement corrosion [47], defects associated with the waterproof membrane in bridge decks [48,49],and deterioration in and below highway, airport and parking pavements [50]. Weil [51] has also reported the detection of pipelines, Ward [52] has studied the insulation properties of buildings, and Titman [53] reported the use of thermography for detecting leaking in a central heating system.

The technique is quite well established for the investigation of delaminations in bridge decks with and without asphalt concrete overlays and has been standardised. Procedures for using thermography in this case are given in the American Standard ASTM D 4788 [54].

Advantages and limitations

Infrared thermography may become a cost effective non-destructive technique because it can quickly and efficiently evaluate greater areas than other methods. Its results can provide a good indication of the location and horizontal size of delaminated areas and other concrete defects. The technique requires however special skills and equipment. Its main limitations are [25,55]:

- requires training to make sure that useful data are collected and high level of expertise to correctly interpret the results;

- environmental conditions, such as air temperature, wind speed, shaded or direct light and presence of surface moisture, may affect the results;

- due to a smaller gradient of temperature, the detection of deeper defects may be more difficult;

- the depth or thickness of a subsurface anomaly cannot be determined.

2.2.3 Nuclear methods

Nuclear methods, also known as radioactive methods, employ high-energy electromagnetic radiation. The results are produced by the interaction between this energy and the material under investigation. These methods can be broadly classified into two groups [56]: radiometric methods and radiological methods.

The radiometric methods involve the use of a concentrated radiation source (radiometric isotope) in one side of the concrete element to be tested, and a detector at the opposite side to pick up and measure the received emissions [1]. It is analogous

to the ultrasonic through transmission technique, and is mainly used for measuring the in-place concrete density, both in fresh and hardened condition. The Figure 2.11 depicts the direct radiometric method, but it can also be used as a backscatter method where it requires only access to one side. In the latter case source and detector are placed on the same side and the measurements are confined in the surface zone of the concrete element.

In the present case however, the radiographic methods are more relevant as they can be employed for the detection of voids, delaminations and embedments [25], like other techniques for condition assessment. They can be of two types: X-ray radiography and γ-ray radiography.

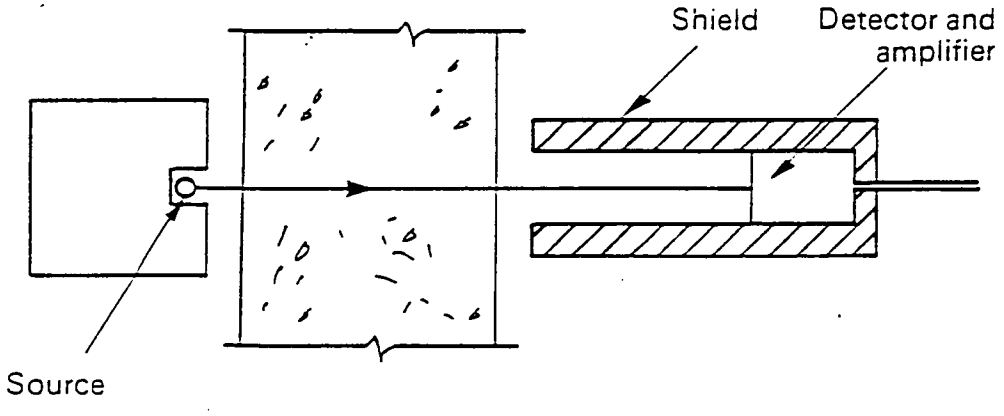

Figure 2.11 Direct transmission radiometry with source and detector external to test object, after Bungey [1]

The γ-ray radiography has gained more acceptance due to its portability and low cost for field applications, if compared to the X-ray type. The latter has however the advantage that the equipment can be turned off after using it, while in the γ-ray

radiography the rays are emitted continuously from a radioactive source and heavy shielding is required for personnel protection [57].

Radiography involves the use of radiation passing through the object under investigation to produce an image ("photograph") of the interior of the concrete. Basically, it consists in placing a radioactive source on one side of the concrete element while a standard X-ray film is held against the opposite side, as shown in Figure 2.12. The graphic picture reveals the position and condition of reinforcement, air voids in the concrete or grouting of post-tensioned construction, segregation and variable consolidation [56]. High density material, such as reinforcement, appears as a light area in the developed film, whilst a region of low density is shown as dark areas. The concrete element thickness is limited up to 500 mm, after that the radiation exposure times are considered unacceptable in practice.

Radiography is applicable to a variety of materials and the results are permanently recorded on film. The information can be further used for recording, evaluation and for keeping archives of the results. However, radiographic films have the disadvantage that after their exposure, it is necessary to develop them in a dark room not always available at the field site. In addition, they may become time consuming and expensive when used for a systematic inspection. To overcome these problems, digital radioscope using X-rays detectors coupled to an image acquisition and processing system (instead of films) is being developed [58]. This technique permits real-time inspection.

The radiographic equipment is in general quite expensive and the operators must be licensed. Another limitation is that radiography requires access to both sides of a concrete element.

The main concern in the use of any nuclear method is safety. The radiation sources are a health and safety hazard. The British standard BS 1881: Part 205 (Recommendations for radiography of concrete) provides guidance on radiography

work, including suitable sources of radiation, safety precautions and testing procedures [59].

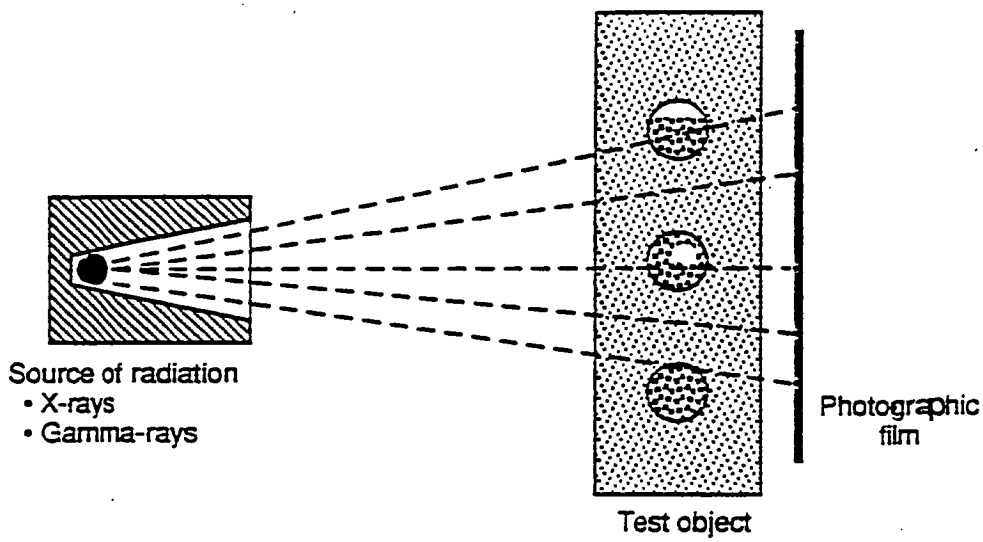

Figure 2.12 Schematic representation of the radiographic method, after Mitchell [57]

2.2.4 Ground penetrating radar (GPR)

This technique is similar to the seismic reflection technique, sonar surveying , and sonic or ultrasonic pulse-echo methods [60,61], differing only by the kind of energy used. The basic radar system and its principles are depicted in Figure 2.13.

In simple terms, short electromagnetic energy pulses of high nominal centre frequency (50 - 2500 MHz) are sent into the ground (pulse systems) by the antenna.

Here the term ground assumes a quite broad meaning and may represent any different medium to air, depending on the application: natural ground, concrete structures, masonry structures, pavements, bridge decks, etc. Besides, every "ground" may contain more than two layers with distinct electrical properties. The antenna represents a transition device, or transducer, between a guided wave and a free-space (or ground) wave. The guiding device or transmission line transports electromagnetic energy to or from the antenna [62,63]. In the first case it works as "transmitter", and in the second as "receiver".

When the dielectric properties of two consecutive layers produce enough contrast, the transmitted energy will be partially reflected back as it strikes the layers' boundary or targets. The remainder of the energy is transmitted and refracted at the same interface and continues propagating through the next layer until it finds a new interface, and then the process repeats.

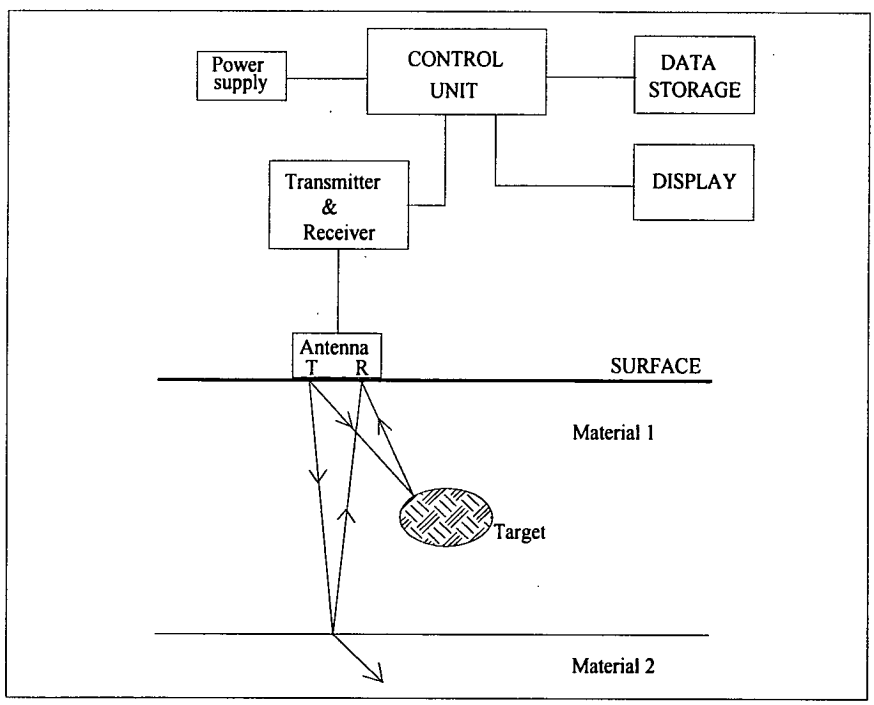

Figure 2.13 Basic principles and components of a radar system with a monostatic antenna

The velocity of the waves, their attenuation during propagation and the amount of energy scattered back are mainly governed by the materials electrical properties.

Since the energy radiated by the antenna is a divergent beam, reflections from targets may be recorded even if they are not at the same vertical position. Typical signatures will be displayed according to the targets' shape when the antenna is scanned across the surface. For instance, if a localised object, like the target shown in Figure 2.13, has a circular section, a parabolic signature will be recorded. This is the case of buried tanks or pipes, reinforcement bars, some voids, etc. (See Figure 3.4). These signatures may differ as the shapes vary, and become even more complex when closer targets reflections are recorded.

Radar has proved to be a powerful tool in the investigation of a quite wide range of applications. Particularly as an NDT technique, using high resolution antennas (> 500 MHz), radar has succeeded with more or less reliability in:

a) detecting and locating reinforcing bars, metallic and plastic ducts;
b) identifying moisture and voids (air or water filled);
c) monitoring pavement deterioration (delaminations and asphalt separation);
d) locating the presence of chlorides;
e) identifying construction details;
f) estimating the thickness of pavements and structure elements;
g) detecting variations in material density, provided that there is sufficient contrast in the electrical properties.

2.2.5 Advantages and limitations of Radar

The main advantages of Radar compared to other techniques, described in the previous sections, are:

- rapid tool to inspect large areas, without much disruption of local activities;
- it is truly non destructive;
- does not depend upon special weather conditions;
- low power requirements;
- can be used either in transmission mode with a pair of transducers where two sides are accessible, or in reflection mode using a transducer with in-built transmitter and receiver at only one side of the test object;
- is not obtrusive, and the radiated electromagnetic energy is normally low, not requiring special protection to operators;
- does not require special couplants, and transducers do not even need to be in contact with the ground;
- radar waves propagate through air.

On the other hand, there are still several disadvantages to be considered, which probably explains why radar has not succeeded in many applications. The main disadvantages usually referred to are described below:
- requires considerable personnel expertise to operate the equipment;

- interpretation of data is still in many cases comparative in nature, often necessitating visual inspection and drilling, coring or excavation;

- frequently requires sophisticated signal processing when the data presents high noise level or complex signatures. Yet signal processing does not always improve the results significantly, and thus is not always economically justifiable;

- the commercial systems available are still quite expensive, restricting their availability as an NDT technique for most of potential users in civil engineering field;

- the radiated energy is not like a laser beam, it diverges with angles depending on the electrical properties of the medium;

- radar waves do not propagate through metallic materials, impeding for example the internal investigation of metal post-tensioned cable ducts or behind heavy reinforcements.

2.3 CONCLUSIONS

The aim of this chapter was to give a brief description of the main non-destructive testing methods that may be employed for condition assessment of concrete in structures.

The common point considered here to select the NDT techniques was the capability "to see" the interior of concrete, in order to detect and locate defects and embedments, as well as to measure the thickness of structural elements.

Basically two kinds of energy were involved, acoustic and electromagnetic. In the former mostly high frequency waves in the ultrasonic range only were considered, because resolution was the key factor.

As seen, all techniques have proven to be valuable for condition assessment, but each one has advantages and disadvantages. None of them provides all answers in a particular test. Usually in practice the best results are achieved when a combination of techniques is employed. For example, infrared thermography can rapidly survey large areas and locate hidden anomalies if enough temperature gradient is produced. However it cannot determine depths, where other techniques such as impact-echo or radar may provide this information. Ultrasonic pulse velocity only provides the transmission velocity values, and can produce an internal picture of concrete if data are processed with the tomographic technique. Impact-echo works very well for plate-like structures, but may fail in the case of more complex target shapes, and the input frequency may change if the surface concrete crushes due to the impact. Radiography requires licensed operators and is subjected to severe

regulation. Radar does not propagate through metallic materials, and may produce complex signatures which frequently requires sophisticated signal processing.

From the above, one may conclude that any one method does not totally replace the others. Research and development are necessary for all techniques, and in this direction several groups are being set up world-wide in universities and research centres. The techniques employed by each research group depend to some extent on the kind of problems being demanded by the local construction industry.

In the present work, several reasons have led to the decision to choose ground penetrating radar (GPR) as the non-destructive test method for the numerical and experimental investigation, including:

- the growing interest by the construction industry in acquiring alternative NDT methods for condition assessment;

- the successful applications in the field shown by many case histories already reported, proving that radar can become a very useful NDT tool;

- on the other hand, considering the many cases where radar has failed in producing good results, there is a need of more understanding of its functionality to inform users of its limitations;

- the provision of quantitative information that may help non radar experts to decide whether the technique is applicable in a particular field work, and if so the appropriate antenna to be used.

- the availability of a complete radar system in the NDT laboratory at the University of Edinburgh without restrictions of time and operational cost.

CHAPTER 3

GROUND PENETRATING RADAR (GPR)

CHAPTER 3

3. GROUND PENETRATING RADAR (GPR)

3.1 INTRODUCTION

3.1.1 History

Radar is an innovative inspection technique for non-destructive evaluation, that has been used on concrete and masonry structures and highway pavements. More traditionally this kind of electromagnetic sounding technique has been largely employed in the remote sensing of buried objects, encased in concrete or other material, or hidden behind walls or other structures [64]. Radar, which denotes "Radio detection and ranging", has its background based on applications of electromagnetic signals at the beginning of this century.

Detection of buried objects was first reported in Germany in 1910 and 1926 [65]. Afterwards this technology received increasing interest mainly during the Second World War and later in the 1960's during the Vietnam War, due to its importance for military purposes. During this period the technology available allowed the development of equipment that could accurately detect any airborne object that reflected electromagnetic waves, such as planes, ships, and land forms. This was possible because distinct objects present their own scattering characteristics and reflection properties, and the electromagnetic waves propagate through air at the constant speed of light [61].

In the early 1950's, the same technology was employed experimentally as a ground probing tool. Since electromagnetic waves can also propagate through most

solids and liquids, it was not difficult to recognise the ability of this technique being used also in profiling subsurface geological features. This relied on the fact that electrical properties are distinctive for each material, producing variations in the waves' speed and their amplitude, and reflections and refractions will occur at the interfaces of different materials. As result, several radar systems were developed under the name of "ground penetrating (or probing) radars" (GPR).

Presently the main manufacturers of commercial radar systems that allow data acquisition with non-contacting high resolution antennas (horn antennas) are Pulse Radar (Houston, Texas, USA), Penetradar (Buffalo, New York, USA) and GSSI (North Salem, New Hampshire, USA). Systems that use ground coupled antennas, which operate in a wider range of nominal centre frequencies (80 - 1000 MHz), are Geophysical Survey Systems, Inc. - GSSI (USA), Sensor and Software Inc. (Canada), ERA Technology (UK), MALA (Sweden) and OYO (Japan) [65,66].

The Radar system developed by GSSI has become the most widely used for structural inspections, mainly in the frequency range of 500 MHz to 1 GHz.

3.1.2 Ground penetrating radar applications

The applications of GPR received great attention in the early 1970's, covering the determination of thickness and structures of glaciers, locating ice in permafrost [67], location of sewer lines and buried cables [68], measurement of the thickness of sea ice [69], profiling the bottom of rivers and lakes [70], investigation of lunar sub-surface [71,72], and detection of corpses [73]. This was followed by the detection of buried containers with hazardous waste [74,75], investigation of scour around bridge foundations [76-79], location of buried pipes [80,81], detection of hidden objects in walls [82], and detection of concealed objects behind the linings of tunnel walls [83].

Regarding engineering applications, the first works reported were related to the inspection of airfields for voids underneath non-concrete pavements [84], and location of voiding underneath concrete sidewalks [85], and underneath concrete pavements [66,86-88]. Radar evaluation of bridge decks were first reported in the United States in the early 1980's by Clemena [89-91], and more recently by Maser [92], Saarenketo [93] and Chung [94], looking for materials deterioration and delaminations of concrete pavements caused by reinforcing steel corrosion.

The use of Radar has also been employed for detecting changes in subgrade moisture content, and sinkholes under a pavement [66]. Increased chloride content has been seen in GPR data as strong signal attenuation in concrete bridge decks [95], as well as in site investigation of salt water saturated sand [96].

The measurement of pavement thickness is important in many aspects of engineering and management. Radar data has been shown to be quite accurate for evaluating pavement thickness, as well as identifying changes in pavement section, using antennas of very high resolution [92,97,98].

Another successful application has been in the field of archaeology. In this case radar has been shown to be useful in mapping buried structures, in locating buried artefacts and in identifying target zones, all valuable information that will be available before any excavation. The size of the targets and their approximate depth can be estimated, making the excavation more cost effective [99,100,129].

The use of radar for structural applications as a non-destructive inspection technique, has received major interest only over the past few years [101]. Fenning [102] reported the investigation of voids below reservoir floor slabs, constructional details and assessment of reinforcement provision. Bailey [103] employed radar for the investigation of structural faults, location of leakage zones on concrete bridge decks and below swimming pools. Attempts were made to verify the effectiveness of

radar in assessing the integrity of in-situ joints in precast concrete structures [104]. Location of tendons in post-tensioning and prestressed concrete structures have been carried out with relative success [105-108].

Masonry structures have also been object of investigation with radar for identifying materials' thickness, voids and condition of mortar fills in historic buildings [109], for detecting moisture movement in masonry walls [110], and for identifying hidden geometry and characteristics of the soil fillings in arch bridges [111].

3.1.3 Advantages and limitations of radar

The advantages and limitations of radar were already covered in chapter 2, section 2.2.5. The interpretation of radar data has been one of the most difficult tasks of this technique. Considering that impulse radar has grown rapidly as an NDT method within the construction industry, and given the increasing financial support, systematic research work has been started by universities and government organisations. Laboratory approaches have been set up using simpler models to obtain a better understanding of more complex structural features [112], and to investigate the response of concrete under electromagnetic waves using special high resolution antennas [113].

Presently computer modelling is also used to aid in the interpretation of radar data. Models are mathematical descriptions of NDT techniques expressed as algebraic equations or computer programs that can predict inspection performance. In several models this means predicting the waveforms which could result from simulated subsurface targets [114].

Archaeological sites [115,116], masonry structures geometry [117], subsurface objects within concrete [118,119], delaminations in concrete bridge decks

[120], and bridge scour [78] are examples where computer simulation has been tested.

Tomographic techniques have also been proposed to construct images of the interior of concrete using the recorded Radar data [121,122]. These techniques require multiple measurements and extensive computational time processing.

3.2 RADAR SYSTEM

The basic principles of ground penetrating radar were described in detail in chapter 2. The main components of a traditional radar system consist of a control unit, display unit, tape recorder, power supply and antennas. In modern equipment data may also be stored digitally on hard discs and later can be transferred directly to a computer. Antennas are called monostatic when the same antenna works as transmitter and receiver, or bistatic with separate transmitter and receiver.

A radar system for non-destructive evaluation should present among others the following features [123]:

(a) ability to transmit signals with sufficient power to reach the targets and return to the surface;

(b) enough receiver sensitivity for signal detection;

(c) ability to resolve two consecutive targets in the direction of the signal (vertical resolution);

(d) ability to resolve targets in the lateral direction (spatial or horizontal resolution);

(e) reduced clutter noise (multiple reflections within the radar system and signal scattering from material heterogeneity);

(f) easy handling (portability).

Factors (c), (d) and (e) are described and discussed in numerical terms in chapter 5, for commercial antennas applied on concrete.

It is known that higher frequency components attenuate quite rapidly during the wave propagation. However since the transmitted pulses carry energy over a broad frequency spectrum, most commercial systems are designed to be sensitive enough to record data even when returned from very lossy media.

To get the most of a radar survey, one has to decide what is most relevant: resolution or more penetration. Unfortunately both represent opposite extreme conditions, and always a compromise must be achieved. For non-destructive evaluation usually high resolution is desired and therefore high frequency antennas should be employed. Conversely, penetration will be deeper when using lower frequencies.

3.3 ELECTROMAGNETIC BACKGROUND THEORY

All the equations which govern the propagation of electromagnetic waves are derived from the well known Maxwell's equations, the latter summarised below

$$\nabla \times \mathbf{E} = -\frac{\partial \mathbf{B}}{\partial t} \tag{3.1}$$

$$\nabla \times \mathbf{H} = \mathbf{J} + \frac{\partial \mathbf{D}}{\partial t} \tag{3.2}$$

$$\nabla \cdot \mathbf{D} = \rho \tag{3.3}$$

$$\nabla \cdot \mathbf{B} = 0 \tag{3.4}$$

where: $\mathbf{B}$ = magnetic flux density

$\mathbf{E}$ = electric field intensity

$\mathbf{J}$ = current density

$\mathbf{H}$ = magnetic field intensity

$\mathbf{D}$ = electric displacement

ρ = charge density

In ground penetrating radar practice we are often more concerned in how an electromagnetic wave propagates rather how it is generated. This implies the assumption in the region ρ zero and that any currents are conduction currents ($\mathbf{J} = \sigma \mathbf{E}$). These considerations are quite general ones and include practical cases of free space ($\sigma = 0$) as well as most conductors and dielectric materials [124].

Maxwell's equations may be rewritten as follows, for a wave in a linear isotropic and homogenous medium characterized by ε (dielectric permittivity), μ (magnetic permeability) and σ (conductivity):

$$\nabla \times \mathbf{E} = -\mu \frac{\partial \mathbf{H}}{\partial t} \tag{3.5}$$

$$\nabla \times \mathbf{H} = \sigma \mathbf{E} + \varepsilon \frac{\partial \mathbf{E}}{\partial t} \tag{3.6}$$

$$\nabla \cdot \mathbf{E} = 0 \tag{3.7}$$

$$\nabla \cdot \mathbf{H} = 0 \tag{3.8}$$

The equations above may also be represented by vector field phasors that depend on space coordinates but not on time [125], called time-harmonic Maxwell's equations:

$$\nabla \times \mathbf{E} = -j\omega\mu\mathbf{H} \tag{3.9}$$

$$\nabla \times \mathbf{H} = \sigma\mathbf{E} + j\omega\varepsilon\mathbf{E} \tag{3.10}$$

$$\nabla \cdot \mathbf{E} = 0 \tag{3.11}$$

$$\nabla \cdot \mathbf{H} = 0 \tag{3.12}$$

ω = angular frequency

μ = magnetic permeability

ε = dielectric permittivity

σ = conductivity

The equations (3.9, 3.10, 3.11 and 3.12) can be combined to produce the so called homogenous vector Helmholzt's equations:

$$\nabla^2 \mathbf{E} + k^2 \mathbf{E} = 0 \tag{3.13}$$

$$\nabla^2 \mathbf{H} + k^2 \mathbf{H} = 0 \tag{3.14}$$

Where: k = wavenumber

$$k = \omega \sqrt{\mu \varepsilon} \tag{3.15}$$

In free space: $k = k_0 = \omega \sqrt{\mu_0 \varepsilon_0} = \dfrac{\omega}{c}$

and $$c = \frac{1}{\sqrt{\mu_0 \varepsilon_0}} \cong 3 \times 10^8 \quad \text{(m/s)},$$

is the velocity of wave propagation in free space, with

$\varepsilon_0 = 8.854 \times 10^{-12}\ Farad / meter$ = dielectric permittivity of free space

$\mu_0 = 4\pi \times 10^{-7}\ Henry / meter$ = magnetic permeability of free space

In a lossy medium the wavenumber k is a complex number:

$$k_c = \omega \sqrt{\mu \varepsilon_c} \tag{3.16}$$

$$\varepsilon_c = \varepsilon' - j\varepsilon'' \quad \text{(Complex permittivity)} \tag{3.17}$$

Conventionally, it is customary to define a propagation constant γ, such that:

$$\gamma = j k_c = j\omega \sqrt{\mu \varepsilon_c} \tag{3.18}$$

Or, since γ is also complex:

$$\gamma = \alpha + j\beta = j\omega\sqrt{\mu(\varepsilon' - j\varepsilon'')} = j\omega\sqrt{\mu\varepsilon'}\left(\sqrt{1 - j\frac{\varepsilon''}{\varepsilon'}}\right) \tag{3.19}$$

with,

ε' = real part of the complex permittivity

ε'' = imaginary part of the complex permittivity, commonly referred to as loss factor

$j = \sqrt{-1}$

If the medium has a certain amount of free charge carriers, dielectric losses occur as a result of conduction currents. In this case an equivalent conductivity may be defined, which relates to the imaginary part of the complex permittivity in Eq. (3.19) as

$$\sigma = \omega\varepsilon'' \tag{3.20}$$

Expressions for α and β can then be derived from equation (3.19) [126], as follows:

$$\alpha = \omega\left[\frac{\mu\varepsilon'}{2}\left(\sqrt{1 + \frac{\sigma^2}{\omega^2\varepsilon'^2}} - 1\right)\right]^{1/2} \tag{3.21}$$

$$\beta = \omega\left[\frac{\mu\varepsilon'}{2}\left(\sqrt{1 + \frac{\sigma^2}{\omega^2\varepsilon'^2}} + 1\right)\right]^{1/2} \tag{3.22}$$

The physical meaning of α and β is very important and may be explained using the equation (3.13). Considering a lossless medium, where $\sigma = 0$ ($\varepsilon''=0$, $\varepsilon=\varepsilon'$), $\alpha = 0$, and $\beta = k = \omega\sqrt{\mu\varepsilon}$, equation (3.13) becomes

$$\nabla^2 \mathbf{E} - \gamma^2 \mathbf{E} = 0 \tag{3.23}$$

The solution of equation (3.23), representing a uniform plane wave propagating in the +z-direction and polarized in the x-direction is

$$\mathbf{E} = \mathbf{a}_x E_x = \mathbf{a}_x E_0 e^{-\gamma z} \tag{3.24}$$

$\mathbf{a}_x$: unit vector at x-direction

Using equation (3.24) the propagation factor $e^{-\gamma z}$ can be written as

$$E_x = E_0 e^{-\alpha z} e^{-j\beta z} \tag{3.25}$$

As $e^{-\alpha z}$ decreases with z it represents an attenuation factor, and so α is called an *attenuation constant*. The second factor, $e^{-j\beta z}$, is a phase factor and β is called a *phase-shift constant.*

The velocity of wave propagation (*phase velocity*) will be given by (3.26):

$$v = \frac{\omega}{\beta} \tag{3.26}$$

3.3.1 Conductors and dielectrics

Materials are classified according to their electrical properties into three types: *conductors*, which have high electrical conductivity; *insulators*, which are characterised for having low conductivity, and *semiconductors*. Most metals belong to the first group, while most geological and building materials are classified as insulators (or dielectrics).

When an electric field is applied to a material, a movement of electric charges (electric current) will occur. Two types of current may exist, depending on the nature of the material: *conduction current* and *displacement current*. The first type is dominant in metals, because they present free electrons that will flow through the metallic matrix whilst the material is submitted to an electric field. Energy is dissipated in the form of heat and definitely transferred to the medium, representing an energy loss mechanism [124].

Displacement currents are associated with bound charges, typical of insulators. In this case the charges are constrained from free movement. When an external electric field is applied to an insulator the electric charges simply move to a new stable configuration causing charges of opposite polarity to separate and remain so. This charge separation produces an electric field that opposes the external one, creating a balance called polarization. Energy from the applied electric field is also transferred to the material, but in this case characterizing an energy storage mechanism. Once the electric field is removed, the charges move back to the original configuration, and the energy stored during the process is released [124].

Natural materials, when submitted to an electric field, will present in general the two kinds of current described above. This is because they are classified as dielectric, and will respond as an insulator or conductor depending on their constitutive parameters σ (conductivity) and ε (dielectric permittivity), described in section 3.3.5, and the rate of change of the electric field.

Concrete, in particular, may behave either as an insulator or conductor of electromagnetic waves. In the equation (3.6), the first term on the right represents conduction current density and the second one displacement current density [126]. Lets we consider the ratio between these terms, $\sigma/\omega\varepsilon$, which simply represents the ratio of conduction current density to displacement current density. The value $\sigma/\omega\varepsilon$=1 can be considered a frontier between conductors and dielectrics, despite knowing that in reality the transition from a conductor to an insulator is a gradual one without any clear cut-off point. Good conductors will present values much greater than unity, and conversely dielectrics will present values much less. In summary:

if $\frac{\sigma}{\omega\varepsilon} >> 1$, the material is classified as a good conductor and means that a significant amount of the energy input to a medium will be dissipated;

if $\frac{\sigma}{\omega\varepsilon} << 1$, the material is classified as a good dielectric (or lowloss material).

3.3.2 Electromagnetic wave attenuation

From the theory presented in the previous section, it can be shown that for conductive dielectric materials Eq. 3.21 may be rewritten as [127]:

$$\alpha = \omega\left[\frac{\mu\varepsilon'}{2}\left(\sqrt{1+tan^2\delta}-1\right)\right]^{1/2} \tag{3.27}$$

where: α = attenuation constant

$\omega = 2\pi f$ - angular frequency

μ = magnetic permeability

ε' = real part of the complex permittivity

$$\tan\delta = \frac{\varepsilon''}{\varepsilon'} \cong \frac{\sigma}{\omega\varepsilon'} \quad \text{- loss tangent (or dissipation factor)} \tag{3.28}$$

At radar frequencies, ε' (real part of 3.17) can be assumed approximately constant and independent of frequency [128]. This hypothesis was considered for the numerical analysis described later in chapter 5. The conductivity depends on the water content of the material and the frequency used for measuring it. A more accurate determination over the frequency range 10 MHz to 10 GHz should consider the frequency dependence of the material's electrical properties, where the loss tangent would be given by [129]

$$tan\delta = \frac{\varepsilon_e''}{\varepsilon_e'} \tag{3.28a}$$

Where: $\varepsilon_e' = \varepsilon' - \frac{\sigma''}{\omega}$ and $\varepsilon_e'' = \varepsilon'' + \frac{\sigma'}{\omega}$

σ',σ": real and imaginary parts of the complex conductivity (Eq. 3.49)

Thus, equation (3.28a) would result in

$$tan\delta = \frac{\sigma' + \omega\varepsilon''}{\omega\varepsilon' - \sigma''} \tag{3.28b}$$

However experimental values for the electrical properties have been reported only for frequencies up to 100 MHz (See section 3.3.6).

Dividing Eq. 3.17 by ε_0 (permittivity of free space), the complex permittivity becomes dimensionless

$$\varepsilon_{c_r} = \varepsilon_r' - j\varepsilon_r'' \tag{3.29}$$

where: $\varepsilon_{c_r} = \frac{\varepsilon_c}{\varepsilon_0}$ = relative complex permittivity

$\varepsilon_r' = \frac{\varepsilon'}{\varepsilon_0}$ = real part of the relative complex permittivity

$\varepsilon_r'' = \frac{\varepsilon''}{\varepsilon_0}$ = imaginary part of the relative complex permittivity

Knowing that $\varepsilon_0 = 8.854 \times 10^{-12}$ F/m, $\mu_0 = 4\pi \times 10^{-7}$ H/m and $\mu_r \cong 1$ for non-magnetic materials, equation (3.30) can be derived from equation (3.27)

$$\alpha = 1.482 \times 10^{-8} f \sqrt{\varepsilon_r}\left[\sqrt{1 + tan^2\delta} - 1\right]^{1/2} \tag{3.30}$$

where α = attenuation constant in nepers/m

f = centre frequency of the transmitted signal (in Hz)

$\varepsilon_r = \varepsilon_r'$ = dielectric constant (see section 3.3.5)

or in decibels/m:

$$8.686\ \alpha = 12.9 \times 10^{-8} f \sqrt{\varepsilon_r} \left[\sqrt{1+tan^2\,\delta} - 1\right]^{1/2} \tag{3.31}$$

It can also be demonstrated that

$$tan\,\delta = \frac{\varepsilon''}{\varepsilon'} = 1.8 \times 10^{10}\ \frac{\sigma}{f\varepsilon_r} \tag{3.32}$$

σ: in Sm^{-1}

According to section 3.3.1, for slightly conducting materials tanδ << 1, typical of concrete with low to medium salt and moisture content, the attenuation might be calculated in a simplified form as follows:

$$\sqrt{1+tan^2\,\delta} = \sqrt{1+\frac{\sigma^2}{\omega^2\varepsilon'^2}} \cong 1 + \frac{\sigma^2}{2\omega^2\varepsilon'^2} \tag{3.33}$$

$$\text{Thus, } \alpha = \frac{\sigma}{2}\sqrt{\frac{\mu}{\varepsilon'}} = \frac{\sigma}{2}\sqrt{\frac{\mu_r\mu_o}{\varepsilon_r\varepsilon_o}} \tag{3.34}$$

With $\mu_r \cong 1.0$, equation (3.34) becomes

$$\alpha = 1.64 \times 10^3 \frac{\sigma}{\sqrt{\varepsilon_r}}\ ^{(*)} \qquad \text{(In dB/m)} \tag{3.35}$$

*Some authors [130,131] have reported this equation with the numerical coefficient 1.69, which is incorrect. However this error is small (<4%).

3.3.3 Electromagnetic wave velocity

In most practical applications, geological and building materials are classified as low loss materials (tanδ << 1) at radar frequencies and therefore the general equation for wave velocity (3.37) is often simplified to [130]:

$$v = \frac{c}{\sqrt{\varepsilon_r}} \tag{3.36}$$

which is independent of frequency and conductivity.

However all materials except ferromagnetics do absorb, in different levels, some amount of electromagnetic energy. In doing so they change the electromagnetic wave velocity.

Since radar gives the travel time of the wave between transmitter and target and back to the receiver, it is very important to know the velocity when the aim is to estimate the depth of the target. Estimating the velocity depends on prior knowledge of the relative permittivity, which in turn is very dependent on water content.

In a general form the velocity can be calculated by equation (3.37), derived from the equations (3.22) and (3.26), valid for conductive dielectric materials [65]:

$$v = \frac{1}{\left[\frac{\mu\varepsilon'}{2}\left(\sqrt{1+tan^2\,\delta}+1\right)\right]^{1/2}} \tag{3.37}$$

Using the definitions given in section 3.3.2, the following equation can be derived:

$$v = \frac{c}{\left[\frac{\varepsilon_r}{2}\left(\sqrt{1+tan^2\,\delta}+1\right)\right]^{1/2}} \tag{3.38}$$

3.3.4 Electromagnetic pulse wavelength

The wavelength is the distance between corresponding adjacent peaks on the wave, (or the period in space of a travelling wave), and can be calculated by equation (3.39):

$$\lambda = \frac{v}{f} \tag{3.39}$$

where v = wave propagation velocity

f = frequency

Equation (3.39) is valid for single frequencies. In a survey design (described in chapter 5), when using ground penetrating radar (GPR), as an estimate one can use the simplified equation for the velocity (3.36) (lowloss materials) and the centre frequency of the transmitted signal. Therefore taking (3.36) and (3.39) we obtain

$$\lambda = \frac{c}{f\sqrt{\varepsilon_r}} \qquad \text{c = 0.30 m/ns (light speed)} \tag{3.40}$$

$$\text{Thus,} \quad \lambda = \frac{300}{f\sqrt{\varepsilon_r}} \tag{3.41}$$

where: f = centre frequency in MHz

λ = wavelength in metres (see Figure 3.1)

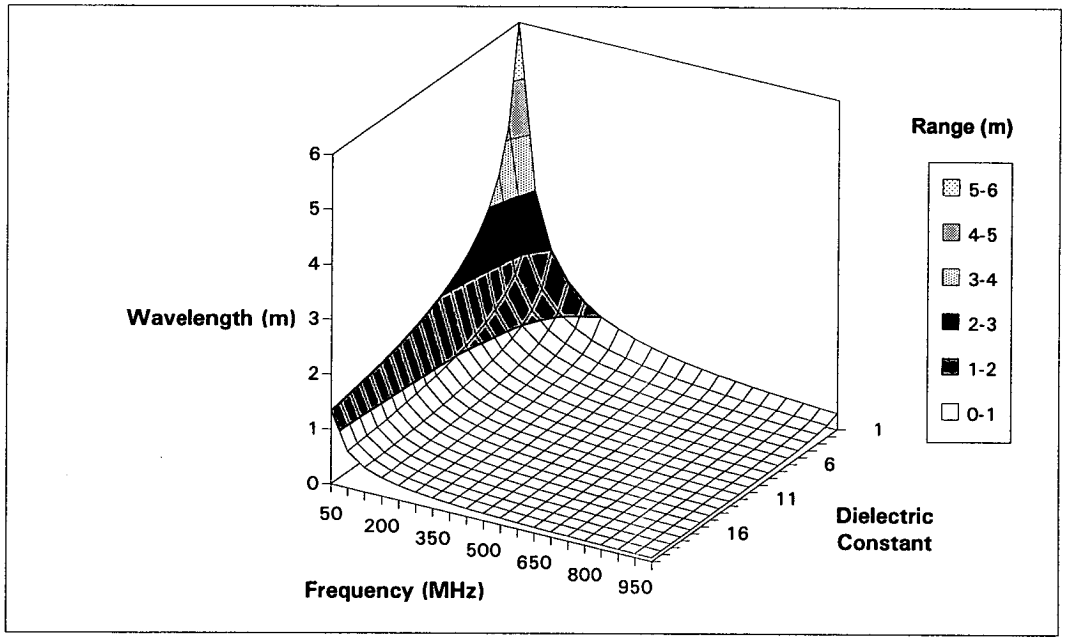

Figure 3.1 Electromagnetic wavelength for lowloss materials

3.3.5 Reflection, transmission and refraction of electromagnetic waves

As described in section 2.2.4, electromagnetic energy transmitted into the ground will be partially reflected back from interfaces of different dielectrics. The amount of the reflected energy is dictated by the reflection coefficient given by the classical Fresnel equations [125].

Based on Figure (3.2), the reflection coefficient for an incident plane wave polarized with its electric field vector normal to the plane of incidence, is

$$\rho = \frac{Z_2 \cos\theta_i - Z_1 \cos\theta_t}{Z_2 \cos\theta_i + Z_1 \cos\theta_t} \tag{3.42}$$

where : ρ = reflection coefficient

Z_1 , Z_2 = intrinsic impedance of materials 1 and 2

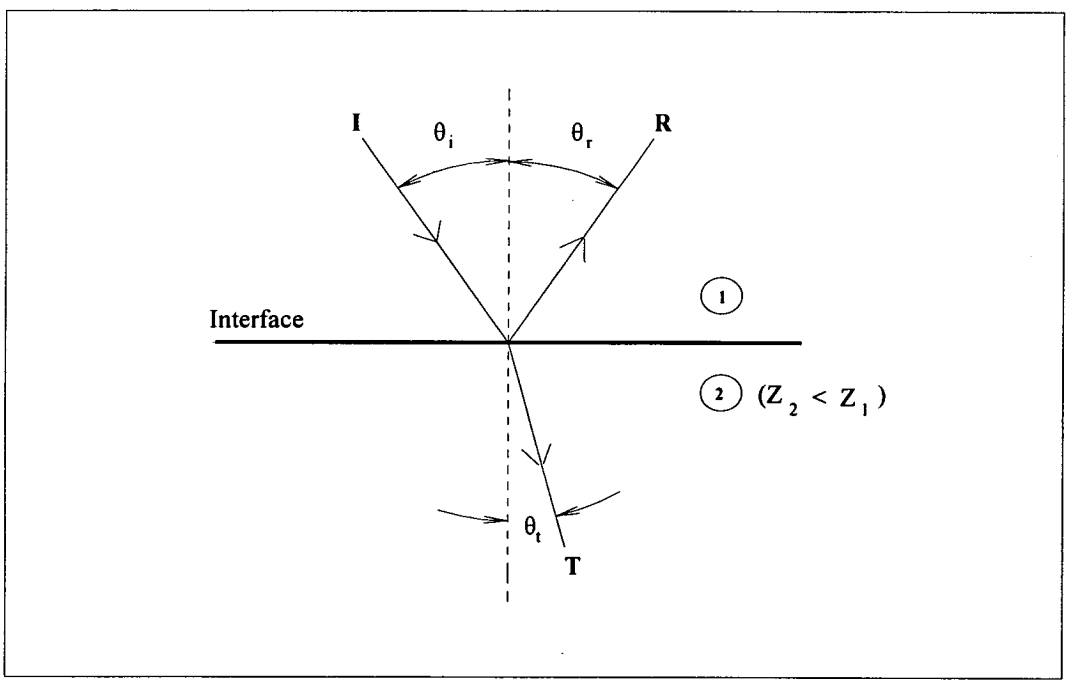

Figure 3.2 Reflection and refraction of a ray obliquely incident on an interface of electromagnetic impedance contrast

The intrinsic impedance for a conductive medium is given by

$$Z = \sqrt{\frac{j\omega\mu}{\sigma + j\omega\varepsilon}} = \sqrt{\frac{j2\pi f\mu_r\mu_0}{\sigma + j2\pi f\varepsilon_r\varepsilon_0}} \tag{3.43}$$

where :

f = frequency

μ_r = relative magnetic permeability of material

μ_0 = magnetic permeability of free space

σ = conductivity

ε_r = relative permittivity of material (real part)

ε_0 = permittivity of free space

The intensity of the transmitted wave at the same interface is given by the transmission coefficient

$$\tau = \frac{2Z_2\cos\theta_i}{Z_2\cos\theta_i + Z_1\cos\theta_t} \tag{3.44}$$

For a normal incidence plane wave $\theta_i = 0$ and $\theta_t = 0$.

Most geological and building materials may be classified as lowloss materials (low conductivity) and non-magnetics with $\mu_r = 1$. For these materials equation (3.43) may be reduced to

$$Z = \sqrt{\frac{\mu_0}{\varepsilon_r\varepsilon_0}} \tag{3.45}$$

Thus for normal incidence, equations (3.42) and (3.44) may be rewritten only as functions of the respective real parts of the relative complex permittivity as follows

$$\rho = \frac{\sqrt{\varepsilon_{r1}} - \sqrt{\varepsilon_{r2}}}{\sqrt{\varepsilon_{r1}} + \sqrt{\varepsilon_{r2}}} \tag{3.46}$$

and $$\tau = \frac{2\sqrt{\varepsilon_{r1}}}{\sqrt{\varepsilon_{r1}} + \sqrt{\varepsilon_{r2}}} \tag{3.47}$$

In reality the interface between two different materials is not perfect, since some roughness is always present. This means that equations (3.46) and (3.47) will give approximated maximum results [132].

The absolute value of equations (3.42) and (3.46) gives the relative strength of the reflected wave. A negative number will indicate a change in its polarity. For metals, which are considered in practice as perfect conductors, the reflection coefficient will result $\cong$ -1, and virtually no penetration occurs.

The angle of refraction of the transmitted wave can be derived from Snell's law of refraction [133],

$$\theta_t = \sin^{-1}\left(\sin\theta_i \frac{Z_2}{Z_1}\right) \tag{3.48}$$

3.3.6 Electrical properties of materials

According to section 3.3.1, to characterise a dielectric material such as concrete, the constitutive parameters σ (conductivity) and ε (permittivity), as well as the electromagnetic wave frequency, must be considered. This is particularly important when using Radar or microwave techniques on concrete structures to allow realistic interpretation of the achieved data.

The conductivity σ is a measure of the response of free charges to an imposed electric field [134]. The permittivity ε is a measure of the response of bound charges to an electric field, or " a measure of the extent to which the electric charge distribution in the material can be distorted or polarized by the application of an

electric field" [135]. Both may be frequency dependent, and at very high frequencies may present an out-of-phase component. Therefore, they will be represented by complex quantities:

$$\varepsilon_{c_r} = \varepsilon_r' - j\varepsilon_r'' \qquad \text{(Eq. 3.29)}$$

$$\sigma_c = \sigma' - j\sigma'' \qquad (3.49)$$

In both equations, the first and second terms represent the in-phase and out-of-phase components, respectively. At most radar frequencies, σ'' is normally small.

The real part of equation (3.29) ε_r' is commonly called the "dielectric constant". Actually for most porous materials (like concrete), this property may vary with frequency as well as other parameters including porosity, water content (or saturation), air content, temperature and salinity [136]. Therefore it is in fact not "constant". However, the name dielectric constant is largely used in practice as well as in the literature and should not produce a misleading interpretation, keeping in mind its possible variability. The name "dielectric constant" will be from now on kept throughout this thesis, unless stated otherwise.

Reporting back again to equation (3.29), we can see that its real part is associated with the wave velocity (v), and the imaginary part (normally called loss factor) relates to the conductivity or attenuation (α) of electromagnetic waves. These parameters are of the most interest in ground penetrating radar applications and were already described in sections 3.3.2 and 3.3.3, respectively.

There are basically three ways to obtain values for the electrical properties of materials: on site measurements (e.g. using Radar and resistivity methods); in the laboratory with special experimental apparatus, and empirically by numerical modelling.

On site measurements

With on site measurements the dielectric constant is normally obtained. There are basically two techniques to achieve it: reflection or transmission.

The reflection technique has largely been used in highway pavements and asphalt covered bridge decks evaluation [64,92]. Here the dielectric constant of asphalt for instance can be determined by measuring the reflection coefficient at the air-asphalt interface, positioning the antennas far from the surface (approx. 0.30 m). This reflection coefficient will be the ratio between the amplitude of the signal representing the surface asphalt reflection (A_2) and a reference signal obtained at the same distance but with the antenna directed to a metal plate (A_1). Thus,

$$\rho = -\frac{A_2}{A_1} \tag{3.50}$$

The dielectric constant (or relative permittivity) is calculated by the following equation

$$\varepsilon_r = \left(\frac{1+\rho}{1-\rho}\right)^2 \tag{3.51}$$

The same approach may be employed in concrete structures [137], however the results will only reflect the characteristics of the concrete zone near to the surface.

More accurate results will be achieved if cores are drilled at the same locations where the time measurements are taken. However they will not necessarily be representative of the rest of the structure mainly when large areas are to be surveyed.

It is well known that concrete is not a homogenous material, and moreover, normally contains a moisture gradient. Therefore the transmission method will normally give more representative values of the bulk of the concrete. Even so it will be an average value of the whole concrete at the path of propagation. It is essentially based on the determination of travel times of electromagnetic waves, either reflected from buried targets (using the radar technique in reflection mode), or transmitted between two points. In both modes the simplified equation (3.36) of velocity is usually employed, which is non-frequency dependent. This equation can be rewritten as

$$\varepsilon_r = \left(\frac{c}{v}\right)^2 \tag{3.52}$$

$$v = \frac{d}{t} \tag{3.53}$$

where: d = path length

t = travel time

Thus $$\varepsilon_r = \left(\frac{ct}{d}\right)^2 \tag{3.54}$$

When only one side of a concrete structure is accessible and two antennas are available (one as transmitter and one as receiver), the depth to a reflector may be obtained taking multiple reflections from the same reference point called Common Depth Point (CDP) [138].This is made by moving the antennas apart at equal distances relative to an initial centre point (Figure 3.3). This process is quite familiar in reflection seismics.

The depth "d" can be determined by

$$d = \sqrt{\frac{t_2^{\,2}x_1^{\,2} - t_1^{\,2}x_2^{\,2}}{4\left(t_1^{\,2} - t_2^{\,2}\right)}} \tag{3.55}$$

Knowing the depth and using the time delay for the antennas as separation zero (point x_0 in Figure 3.3), the average velocity can be calculated by equation (3.53), and the dielectric constant may be estimated by either equation (3.52) or (3.54).

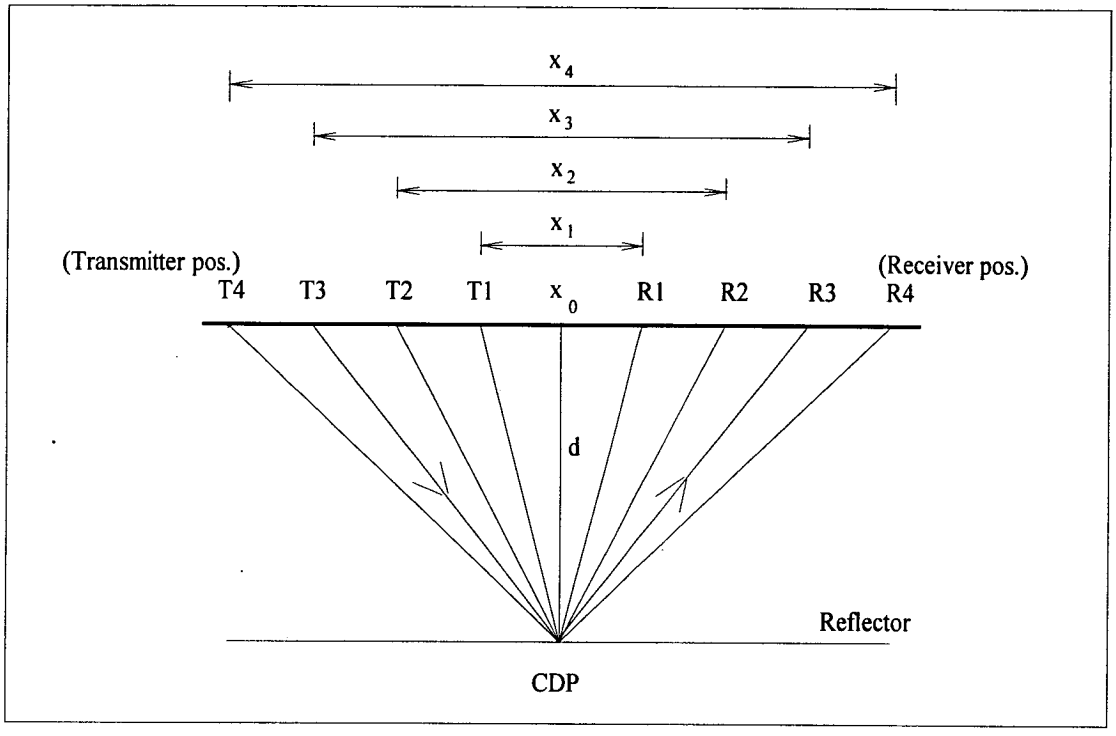

Figure 3.3 The common depth point method, after Ulriksen [138]

In a similar situation but with only one monostatic antenna at hand (with in-built transmitter and receiver), after recording the two-way transit time a core should be drilled at the same point for depth calibration.

Another alternative is suggested by GSSI and described by Ulriksen [138], as depicted in Figure 3.4. Here a point target in the profiling plane is required. When the antenna moves over the buried target, the distance values to the target "s" will follow a hyperbolic variation in function of "x" and "d" according to

$$s = \sqrt{x^2 + d^2} \tag{3.56}$$

The distances "d" and "s" are proportional to the delay times "t_0" and "t", respectively. Thus, the depth to point target will be given by

$$d = \frac{|x|}{\sqrt{\left(\frac{t}{t_0}\right)^2 - 1}} \tag{3.57}$$

Therefore the average velocity and estimated dielectric constant can be calculated with equations (3.53) and (3.52) respectively.

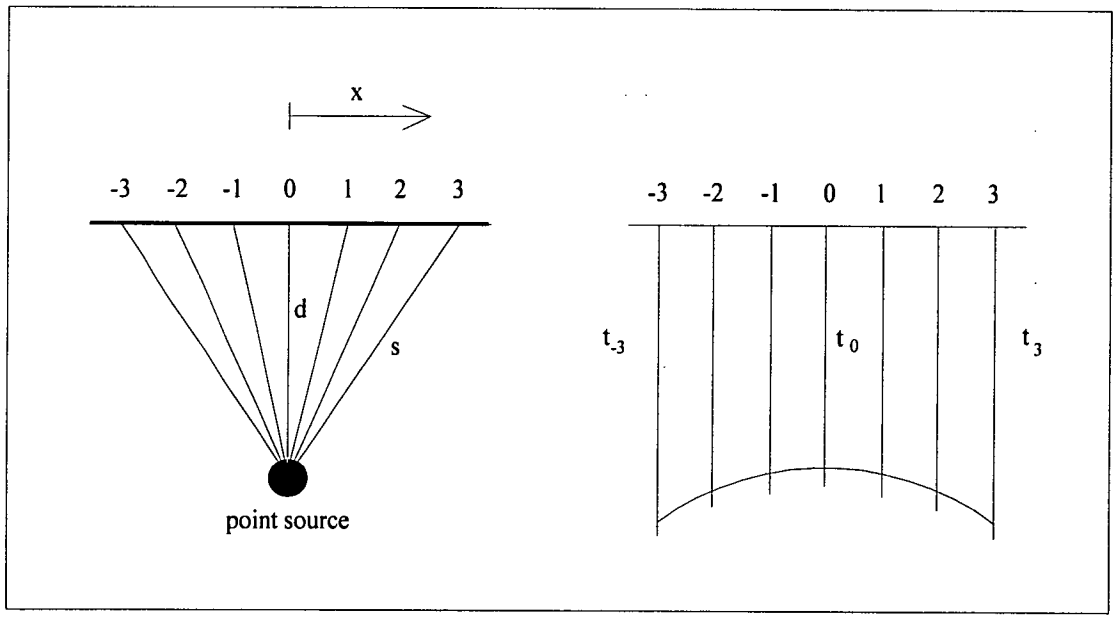

Figure 3.4 Velocity analysis from a point target, with monostatic antenna

Wherever the structure is accessible on opposite faces, the transmission technique should be employed. In this case two antennas are necessary and are

conveniently positioned at opposite sides, according to Figure 3.5 . This technique has proved to be more accurate [139].

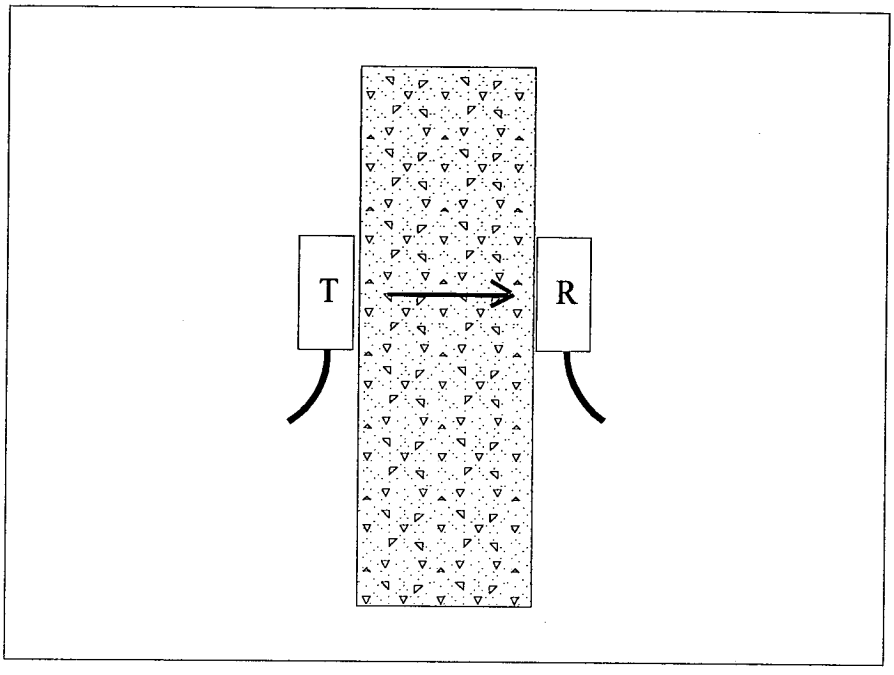

Figure 3.5 Transmission technique

So far only the determination of the dielectric constant has been briefly described, which is related to the propagation velocity. However, the conductivity will be of paramount importance if one wants to estimate either the attenuation of the signals or the depth of penetration. On-site measurements have been done only at low frequencies, up to 100 MHz, using for example conductivity meters [140,141] and resistivity methods. The latter, giving values at DC levels with frequencies < 1 kHz, associated with the corrosion of embedded reinforcing steel [142]. In both cases the results will underestimate the actual values of the conductivity, as it is expected to increase at higher frequencies. It is also well known that both dielectric constant and conductivity increase with water content. The presence of salts in the pore water will increase the conductivity further, without affecting significantly the dielectric constant [112,143].

Laboratory measurements

Laboratory setups may include the use of a parallel plate capacitor, a transmission line, a waveguide, a resonator and others. The type of material and the frequency range of interest will indicate the appropriate technique to be used [144]. For the particular case of concrete, which presents two different physical phases depending on its age, the first two approaches have traditionally been used.

Wilson [145] used a parallel plate capacitor to measure electrical properties of fresh concrete at very early ages , during the first 24 hours. Al-Qadi [144] has used the same technique to monitor the variation of the permittivity in concrete for ages up to 28 days, for frequencies up to 40 MHz. In both cases low radio frequencies are used. For hardened concrete, more important in non-destructive evaluation of existing structures using high resolution antennas, the transmission line technique has proved to be more suitable.

A transmission line consists of a pair of conductors which transports electromagnetic waves. The propagation velocity of the waves varies with the electrical properties of the material between the conductors. For every different filling material the electrical response of the transmission line changes, from which the electrical properties of the material can be inferred.

Recently three different research groups have started work using the same technique on concrete, differing basically in the size of the equipment. Shaw *et al.* [146] designed a transmission line which accommodates concrete with aggregate size up to 10 mm (Figure 3.6). Values for the dielectric constant were measured for frequencies ranging from 1 MHz to 1.5 GHz, which covers the usual range of commercial broad bandwidth antennas. However frequency limitations arose during the testing when concretes with higher moisture content were used. The dielectric constant was calculated based on the time delay between the reflections at the ends of

the filling material and using the simplified equation for wave velocity (Eq. 3.34). When the frequency applied was too high, the far end reflection resulted very much attenuated, yelding difficulty in the accurate determination of time propagation. In this case the reflection technique was employed, where only the first reflection at the interface air/material was considered.

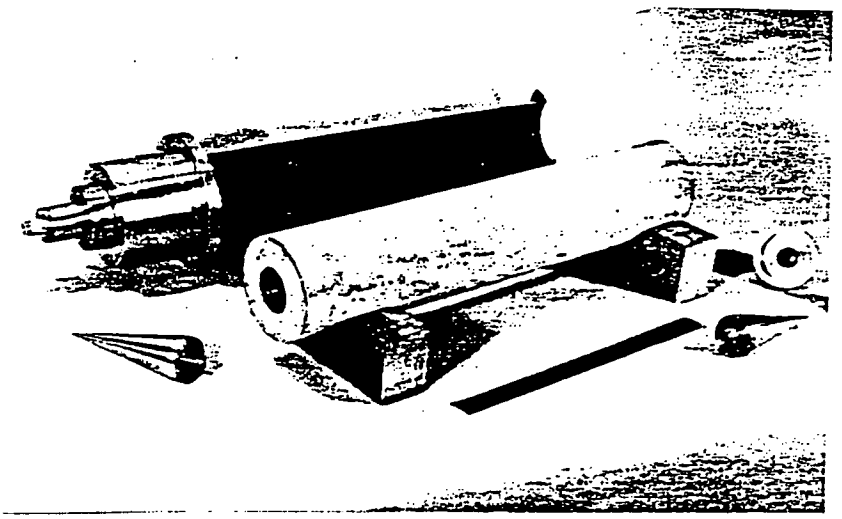

Figure 3.6 Large diameter transmission line, after Shaw *et al.* [146]

Al-Qadi *et al.* [144] have reported the measurements of electrical properties of Portland cement concrete in a quite wide range of frequencies (0.1 MHz - 10 GHz), using three different set-ups: parallel plate capacitor (0.1 MHz-40 MHz), coaxial transmission line (100 MHz - 1GHz) and a TEM Horn antenna (0.5 GHz - 10 GHz). The first set-up was already mentioned above. Experimental results were also reported for the second one, obtained from both time and frequency domain measurements. Different curing times were considered.

Baillon *et al.* [147] developed a large transmission line of a coaxial wave guide type. The main difference compared to the previous one is that it supports

samples with larger aggregate sizes, up to 30 mm. Therefore the scattering effect due to size of aggregates could also be analysed. They used concrete samples with ages varying from 1 day to 24 days. The measurements were taken with frequencies ranging from 50 MHz to 1 GHz.

All results have shown variation of the electrical properties with applied frequency and age and composition of concrete. The researches are still in their early stage and no definitive accurate results are yet available for practical applications at radar frequencies. More research is necessary in the future to get more detailed information concerning the influence of moisture content, salinity of pore water, porosity and aggregate size.

Numerical modelling

Numerical modelling is another way which may be used to estimate electrical properties of concrete or other heterogeneous materials. Based on models set up for partially saturated rocks [148], similar models were developed for concrete. Concrete is a mixture of solid particles, air, water and salt, and may be classified as an artificial rock. Two kinds of problem may be considered: knowing the characteristics and volumetric proportion of the constituents to work out properties of the composite material, or conversely to predict the composition based on field measurements. The second case is quite important in non-destructive evaluation.

Three methods have been studied in depth for concrete [149]: *Complex refractive index method (CRIM)*, *Continuous grain size distribution model(CGSDM)* and *Discrete grain size distribution model(DGSDM)*. The first one is a volumetric model where only the volume fraction of the constituents is considered. The last two are geometrical models where beyond the volumetric fraction they also consider the spatial distribution (continuous or discrete) and shapes of the constituents. These models assume that the solid grain and air voids in concrete are spherical. Halabe *et*

al. [149] claim that results given by the DGSDM model are better than CRIM and the continuous model. Endres and Knight [150] proposed models for partially saturated rocks suggesting that the shape of the inclusions also affects the dielectric constant of a mixture. In this direction Tsui and Matthews [151] have studied these inclusion models for mature concrete considering the geometrical variation of the pore shape. Results were compared to CRIM and CGDSM models. The five models showed significant differences in predicting the values of dielectric constants. They also concluded that it is necessary for further mathematical development of the models in order to match experimental data more closely.

The theory behind all models and their validity when applied to concrete is presented in more detail in the references quoted above.

The CRIM method is the one which has been widely used in soils, rocks and concrete due to its simplicity. This method lacks a theoretical basis [149]. However it gives a sensible estimation of the electrical properties at higher radio frequencies and materials with low conductivity ($\frac{\sigma}{\omega \varepsilon'}$ <1). This represents the normal case when using radar on concrete in existing structures.

The refractive index for a medium is defined as

$$\eta = c\sqrt{\mu\ \varepsilon_0 \varepsilon_{cr}} \tag{3.58}$$

where: c = velocity of electromagnetic waves in free space

μ = permeability of medium

ε_0 = dielectric permittivity of free space

ε_{cr} = relative complex permittivity of medium

The CRIM method states that the effective complex-refractive index for the mixture is given by the volume average of the complex refractive indices of the constituents [148], as follows:

$$\sqrt{\varepsilon_{cr}} = (1-\phi)\sqrt{\varepsilon_m} + (1-S)\phi\sqrt{\varepsilon_a} + \phi S\sqrt{\varepsilon_{sw}} \tag{3.59}$$

where: ϕ = porosity of concrete

S = degree of saturation

ε_m = relative permittivity of concrete solids (real)

ε_a = relative permittivity of air (real)

ε_{sw} = relative complex permittivity of water

ε_{cr} = relative complex permittivity of concrete mixture

Figure (3.7) gives an indication of the variation of relative permittivity of concrete with porosity and saturation, assuming ε_m = 5.0, ε_a = 1.0 and ε_{sw} = 80 (ignoring the imaginary part). The results will represent only the real part of concrete relative permittivity or the dielectric constant, valid for lowloss conditions.

The CRIM method can also predict the conductivity when the imaginary part of the complex permittivity of water is included, taking into account the salinity. However the results may not be realistic in the case of very high salinity and lower frequencies [149]. There are well defined equations to work out the complex permittivity of saline water [152,153].

As described in this section, research is ongoing to improve published data for electrical properties of concrete. However, while new accurate data are not yet available, one may use values for ε_r and σ which have been published in the literature. Table 3.1 shows a list of typical values for most common building and geological materials. These values are based on experimental measurements at frequencies up to 100 MHz. A more comprehensive list of values for the dielectric

constant published in the literature can be found in Petroy's paper presented at the conference SAGEEP '94 [154].

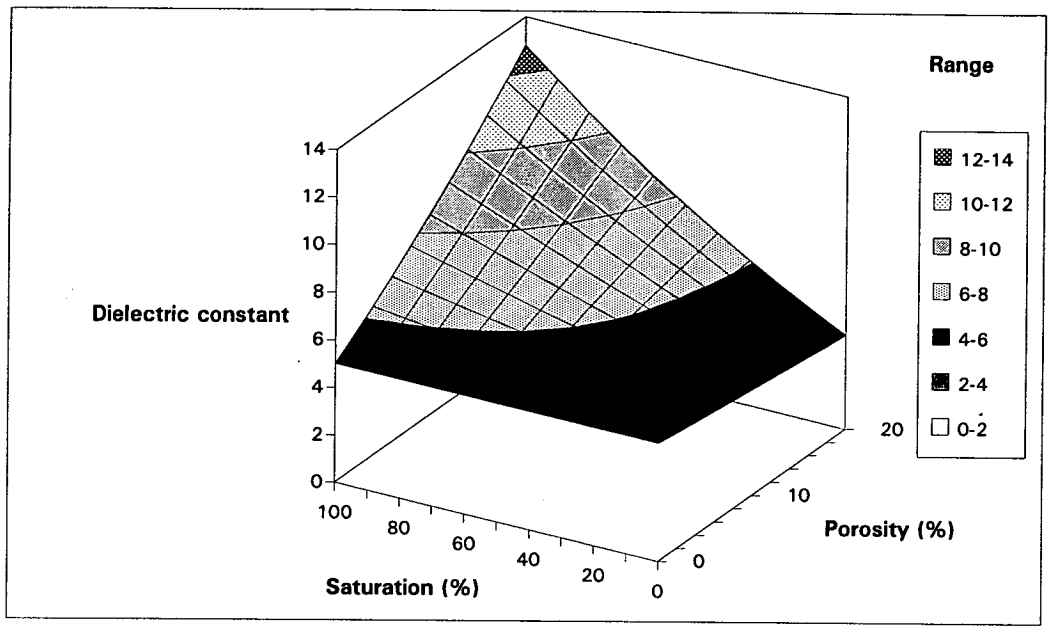

Figure 3.7 Dielectric constant of concrete using CRIM method

The values given in Table 3.1 should be used as guidance only, as properties of natural materials may vary substantially.

3.4 DISCUSSION

Throughout this chapter a basic overview of the radar technique was given comprising its background theory, main applications, the available commercial systems, its limitations and capabilities. Also the methods of measuring or estimating the electrical properties of materials were briefly described: measurements on-site, in the laboratory and employing numerical models. Further information will be presented in following chapters related to the subjects that are being covered.

Table 3.1 Approximate electrical properties of typical building and geological materials [78,131,140,155]

Material	Dielectric constant (ε_r)	Conductivity mS/m
Air	1	0
Metal (Iron)	1	10^8
Fresh water	81	1
Sea water	81	$4x10^3$
Dry sand	3	10^{-4} - 1
Saturated sand (*)	25	10^{-1} - 10
Dry clay	3	1 - 10
Saturated clay (*)	15	10^2 - 10^3
Dry granite	5	10^{-5}
Wet granite	7	1
Dry concrete	6	1
Saturated concrete	12	10^2

(*) Fresh water

Numerical modelling is essentially based on the volume fraction, spatial distribution, shape and electrical properties of material constituents. Therefore estimation of the mixture properties can be made without complete information regarding pulse propagation (e.g. travel times). On the other hand on site and laboratory measurements essentially rely on the knowledge of distance and travel times.

When employing special apparatus like transmission lines, the results in the time domain may be affected by signal distortion due to attenuation. The pulses of the near and far reflections do not necessarily keep the same length, and therefore

travel times may be overestimated. Moreover when using a radar equipment with contact antennas another aspect that cannot be ignored is the antenna coupling effect. Both antenna coupling and wave propagation in lossy media may produce distortion that broadens the signal and can introduce errors in time measurements. As a result, dielectric constant values may lack accuracy. Conversely if the electrical properties are known, estimation of depths may present variations.

In other situations the resolution or the capability of detecting targets in recorded data might be the main factor. Here the signal distortion may also cause problems. With the increase in pulse length, lower frequency components will predominate. Hence the resolution will be limited and potential targets may not be distinguishable. Here the analysis in the frequency domain is required.

3.5 CONCLUSIONS

The main remark that can be made at this stage is that there is a necessity of more knowledge about the behaviour of electromagnetic waves propagating through concrete. The determination of the electrical properties (experimentally or numerically) is fundamental and has been recently addressed by several researchers. However the performance of the Radar equipment itself is also important, not only in the field where many case histories have been successfully reported, but also and principally in laboratory conditions. Here, employing more simple models its capabilities and limitations might be easier identified.

Little laboratory work has been done on a systematic basis using the Radar equipment, perhaps because only a few universities or research centres own a system or have it available for long periods of time. In most cases Radar equipment is used in research in the field and by private companies for professional purposes. The University of Edinburgh owns a complete Radar system with additional signal

processing package and laboratory support. Therefore a decision was taken to develop basic numerical and experimental research using concrete as the reference material.

Chapter 5 covers a numerical analysis of electromagnetic waves through concrete, taking already into account the possible change in pulse frequency contents. The aim is to obtain elements that could feed a Radar survey design.

Chapters 6 and 7 present the results of the experimental work carried out in laboratory condition, giving emphasis on signal distortion. The idea is to see how antenna coupling and wave attenuation during propagation might affect the recorded data. In this case extensive signal processing in frequency domain was necessary, and the results could be compared to the assumptions made for the numerical study described in chapter 5.

CHAPTER 4

DIGITAL SIGNAL PROCESSING

CHAPTER 4

4. DIGITAL SIGNAL PROCESSING

4.1 INTRODUCTION

A signal that varies continuously in time and amplitude is called an *analog signal*. Conversely, if it assumes discrete values it represents a *digital signal* (Figure 4.1). Signals normally contain information. However, often signals do not produce information directly because disturbances (noise) may be present. It is in this context that signal processing represents the means for enhancing, extracting, storing and transmitting useful information.

Digital signal processing (DSP) techniques have been traditionally quite familiar in the fields of electrical and electronic engineering, mechanical engineering and geophysics. However the development of digital systems that deal with data acquisition has grown in other branches of engineering and science, including civil engineering. Therefore professionals involved with data analysis and interpretation from other backgrounds have to become familiar with the DSP techniques.

Due to advances in electronics and computing it has become attractive in recent years to collect data in a digital format on a computer. This gives flexibility in the analysis of the data and the formats available for presentation.

Nowadays many techniques for digital signal processing are available. Their employment in practice relies fundamentally on user experience and skills, since he has to know what kind of information is being addressed. Too much processing or the use of inadequate techniques can also deteriorate the original data.

(a)

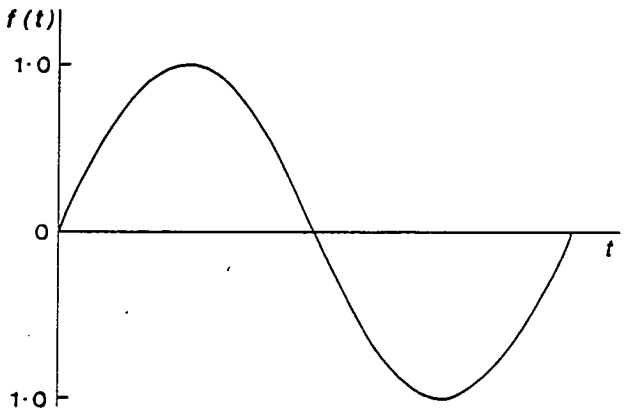

(b)

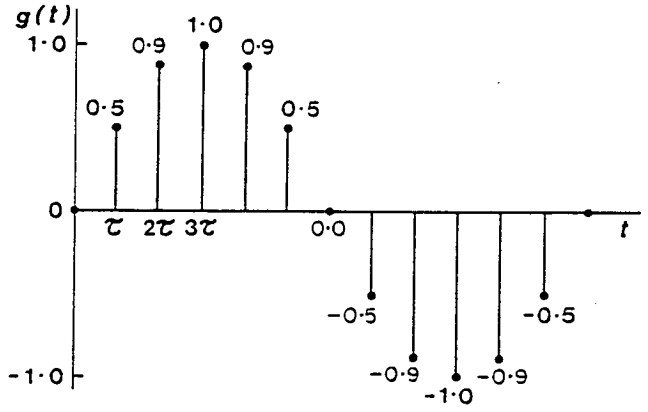

Figure 4.1 Types of signals, after Kearey [60]: a) analog, and b) digital

Radar is the non-destructive technique employed during the present research. In radar the signals are always superimposed on unwanted noise. In favourable circumstances the signal-to-noise ratio is high, so that the signal is readily identified and extracted for subsequent analysis. In this context, "signal processing" allows the extraction of information collected by a radar system. It can for instance make weaker signals detectable, enhance specific components of the data, or produce quantitative information such as wave velocity and amplitude attenuation with depth.

The final presentation of the information should make its interpretation by a user easier.

Despite having most of the DSP techniques available for the present research, the idea was to keep signal processing to a minimum. It has mainly focused on frequency spectrum analysis of data regarding the radar antenna coupling and wave distortion during propagation. Filtering was applied only where it was necessary to make visible targets that has been obscured by the transmitted signal and to remove noise of very high frequency.

DSP techniques are well established and many standard books have been published covering this subject. A few are mentioned in the reference list in chapter 10 [156-160]. This chapter will therefore describe, without much mathematical manipulation, only the basics of the theory and related topics that were mostly applied on the experimental data: frequency domain analysis, signal windowing and data filtering.

4.2 ANALYSIS IN THE FREQUENCY DOMAIN

As mentioned before, most of the data analysis in this research (described in chapters 6 and 7) is concentrated on the frequency spectrum of the recorded experimental data. Fourier decomposition is used to obtain information in the frequency domain. In the case of radar, the data are sampled and recorded as digitised waveforms. Therefore the Discrete Fourier Transform (DFT) is used to produce the frequency contents of waveforms of interest.

The Fourier analysis can be made using either Fourier series or Fourier integral (transform). The first one is used for periodic waveforms, which are characterised by repeating themselves during all time ($-\infty$ to $+\infty$). A periodic waveform can be composed as a sum of sine and cosine waves, and each one will be

represented by a single frequency in the frequency spectrum. Thus, the Fourier series provides a link between the time and frequency representation of periodic signals. The Fourier transform extends this link to transient signals, and the frequencies of the component sine and cosine waves are represented by a continuous function, the spectrum in the frequency domain.

As radar signals are transient the Fourier integral must be used in this analysis. The Fourier integral can be derived considering a periodic waveform whose period is allowed to approach infinity [158,161]. A transient signal can be considered as the integral of component harmonics,

$$f(t) = \frac{1}{2\pi} \int_{-\infty}^{\infty} X(\omega) e^{j\omega t} d\omega \qquad (4.1)$$

where,

$j = \sqrt{-1}$

$X(\omega)$ = the Fourier transform of $f(t)$

$$X(\omega) = \int_{-\infty}^{\infty} f(t) e^{-j\omega t} dt \qquad (4.2)$$

The two integrals (4.1) and (4.2) are known as the Fourier Transform pair. The second one transforms a non-periodic continuous waveform from a function of time to a function of frequency, and is called the Fourier Transform. The first integral, transforms the frequency-domain function back to the time-domain function and is called the Inverse Fourier Transform.

In the modern ground penetrating radar (GPR) systems, the data are recorded in digital form. This means that the signals in the time domain are not continuous but sampled (see section 4.3.1). Furthermore the period of the waves is no longer infinite. A consequence is that the resolution (Δf) of the frequency spectra will be defined by the time window size T_w :

$$\Delta f = \frac{1}{T_w} \tag{4.3}$$

The Fourier Transform pair still applies in such cases, however expressions (4.1) and (4.2) have to be adjusted, as follows,

$$f_d[n] = \frac{1}{N}\sum_{k=0}^{N-1} X_d[k] e^{j2\pi kn/N} \tag{4.4}$$

$$X_d[k] = \sum_{n=0}^{N-1} f_d[n] e^{-j2\pi kn/N} \tag{4.5}$$

where,

N = number of samples

$f_d[n]$ = set of time samples that defines the waveform being transformed

$X_d[k]$ = Fourier coefficients obtained by DFT of $f_d[n]$

The expression (4.5) is called the Discrete Fourier Transform (DFT), and it produces spectral analysis of sampled non-periodic waveforms [158]. Conversely, expression (4.4) does the opposite and is known as the inverse DFT.

Nowadays any commercial signal processing software and most radar systems' hardware incorporate Fourier analysis by means of fast algorithms. These computational efficient algorithms, generally some variation of the Fast Fourier Transforms or FFT, produce the DFT but in much less time than direct application of the summation in the formula. The speed in obtaining results will depend on the algorithm's design, on the employed programming software and on the available hardware [157].

4.3 PREPARING THE DATA FOR FFT ANALYSIS

4.3.1 Sampling rate

One of the key parameters that has to be considered when collecting data is the time interval between points on the recorded signals. This is called the sampling interval $S_f = T_w/N$, where T_w is the time window or range and N the number of samples. It is governed by the *Nyquist Sampling Theorem* which states that "a bandlimited signal can be well represented by its samples without loss of information, provided the sampling rate S_f be at least twice the highest signal frequency" [156]. If this condition is not satisfied, the signal is undersampled and *aliasing* will occur. It will result in a spectral overlap, where components beyond $\frac{1}{2}S_f$ will fold back to frequencies lower than $\frac{1}{2}S_f$, as illustrated in the Figure 4.2.

In practice it is recommended to use at least 3 samples per cycle on the highest frequency component of interest to avoid aliasing [161]. Usually the manufacturers of radar systems provide the users with information regarding the recommended sampling intervals, and/or include "antialiasing filters" in the equipment's design.

During the experiments 1024 samples over a time range of 16 nanoseconds were collected. That is, the sampling frequency was 64 GHz. Using antennas with nominal frequency up to 1 GHz, this rate is well above the minimum required to satisfy the sampling theorem applied to the frequency band of interest.

Once the aliasing problem has been overcome, the choice of the sampling rate will depend more on the kind of information that is required. If the interest is on better definition of the waveforms in the time domain, the option is smaller time intervals (or higher sampling frequency). Conversely, if the aim is better resolution in the frequency domain, the time window has to be increased, since $\Delta f = 1/T_w$.

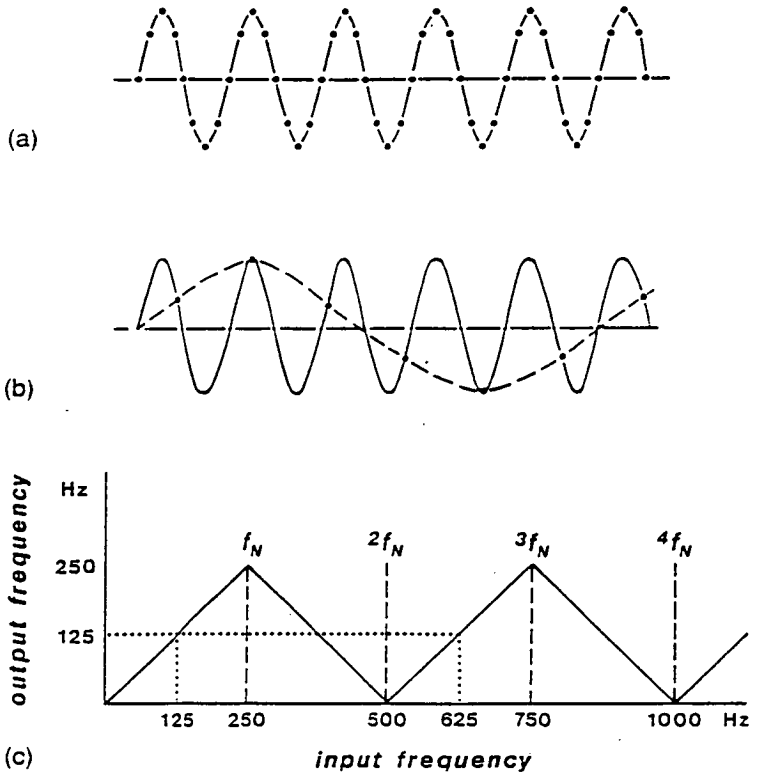

. . . (a) Sine wave frequency less than Nyquist frequency. (b) Sine wave frequency greater than Nyquist frequency showing the fictitious frequency that is generated by aliasing. (c) Relationship between input and output frequencies for a sampling frequency of 500 Hz (Nyquist frequency $f_N = 250$ Hz).

Figure 4.2 The *aliasing* effect, after Kearey [60]

4.3.2 Filtering the data

Although in principle any DSP algorithm may be considered as a "filter", the term is commonly attributed to systems that transmit (or reject) well-defined frequency ranges [157]. Filters can be divided into analog and digital filters, depending on whether they operate on continuous or sampled signals.

In the present research, digital filters are of most interest. They are broadly defined as numerical procedures or algorithms that transform a given signal into a second signal that may produce more desirable properties such as less noise [159]. In

terms of their frequency response, they are required to pass certain bands of frequency and to block the rest. Therefore, they can be designed to reduce unwanted components in a discrete signal. The frequency range is divided into *pass-band* and *stop-band* regions and the particular frequencies that separate them (the band-edge frequencies) are called *cut-off* frequencies [160]. Figure 4.3 depicts these regions for ideal filters.

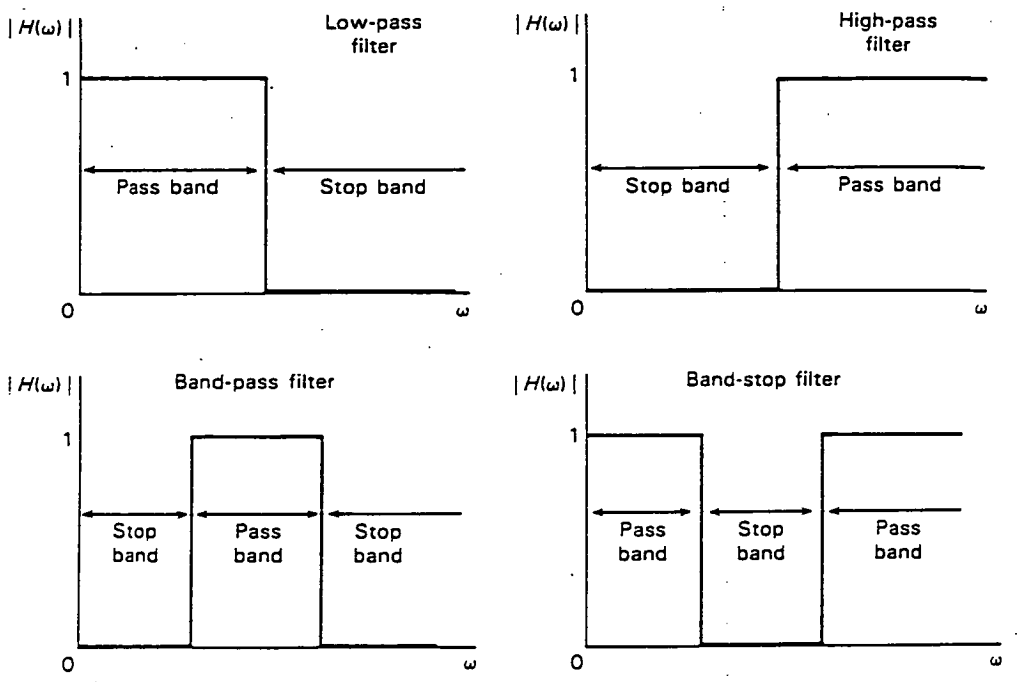

Figure 4.3 Ideal filter characteristics, after Balmer [160]

Regarding the experimental radar data analysis only a high-pass filter is used for spatial filtering and is commonly known as "Background Removal" [162]. It can be made with a simple trace differencing operation, where adjacent traces are subtracted from one another. Its main feature is to suppress slightly varying signals in the data, such as reflections from water tables and "surface reflections", and so to

enhance targets with small spatial dimensions. This was the case for metal bars embedded in concrete. A low-pass filter was used for temporal filtering, to remove high frequency noise normally present on the waveforms along the time axis.

Even though filtering can improve the image of the data, excessive filtering may also deteriorate it by removing frequency components of interest. Since most of the information was expected to be extracted from the spectral analysis, a preliminary filtering exercise was carried out on some experimental data.

Temporal low-pass filter

This filter was applied on all data after recording, using the software provided by the equipment's manufacturer. For the spectral analysis the centre frequency was the main information to be obtained for quantitative evaluation and comparisons. Therefore, the parameters to be set for the filter should not affect the centre frequency in the frequency spectrum.

The Figure 4.4 (a) shows a typical plot in the time domain before and after filtering. Looking at the frequency domain spectrum (b), one may observe that it still contains the whole range of frequencies of the original signal. There is also no apparent shifting of the centre frequency. Only very high frequency components are filtered out, which are not in the bandwidth of interest (> 1.5 GHz).

Spatial high-pass filter (Background Removal)

Background removal was necessary whenever subsurface reflections were obscured by the first signal recorded with radar in the reflection mode, known as "surface reflection" (this subject will be returned to in the chapter 6). Since this is

a) Typical signal in the time domain.

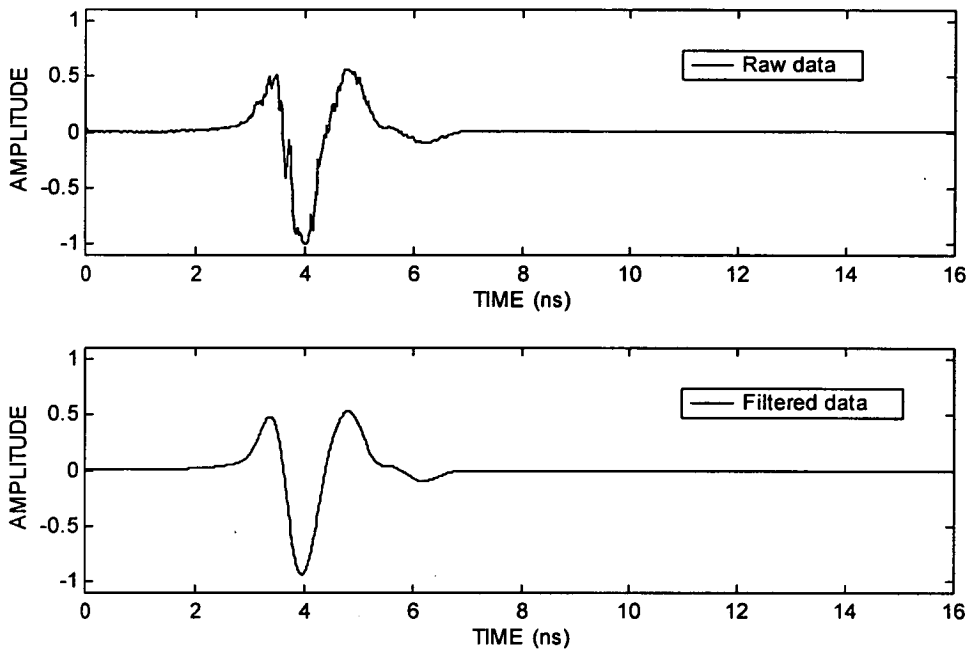

b) Frequency domain spectrum of (a)

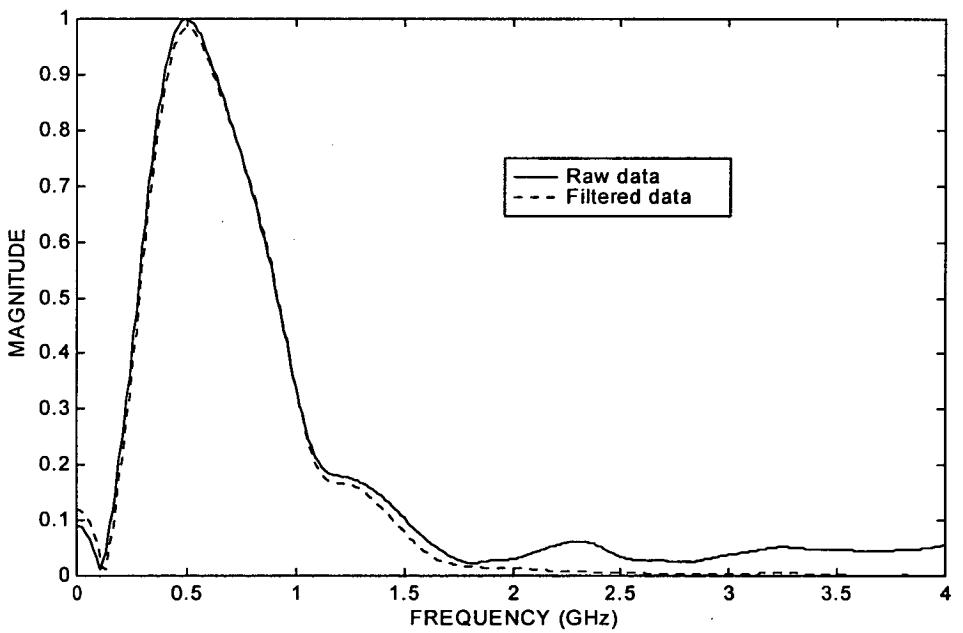

Figure 4.4 Effect of a temporal low-pass filter

normally quite a strong signal, its extraction by filtering can also partially deteriorate reflections scattered from buried targets located close to the surface.

To verify whether a spatial high-pass filter can distort a signal, a single waveform was obtained from a radar scan containing reflections from metal bars embedded in concrete. Figure 4.5 shows a bar reflection, windowed according to section 4.3.3, including the original signal (without the high frequency noise), and after multiple application of the background removal filter.

The resulting frequency spectrum clearly suggests that the frequency range of interest remains essentially unchanged. The centre frequency values are respectively 406, 417 and 427 MHz, with a difference between them of not more than 6%. This difference might be associated with the frequency resolution (see section 4.3.3), and was taken as acceptable. There is a significant reduction in the signal's amplitude, however it was not relevant for the research as the signal attenuation was not within the scope of the investigation.

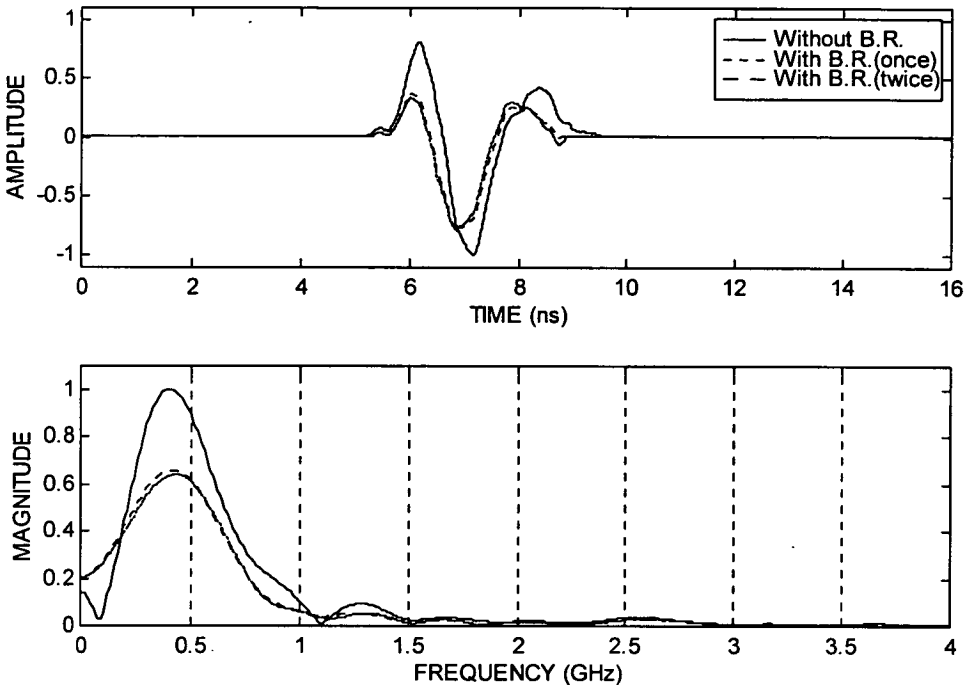

Figure 4.5 Effect of "background removal" (B.R.) on frequency spectrum

4.3.3 Windowing the data

In general terms, windowing means to select specific portions of a signal in the time domain. It can be very helpful when dealing with radar data, where several signal reflections and/or transmissions are normally present. Taking a whole recorded signal, the frequency spectrum may become quite complex, leading to a very difficult interpretation.

Despite the simplicity of the windowing process, the results are not straightforward. Depending on the shape of the window used, problems known as "leakage" may occur. This means that adjacent frequency components with nearly equal magnitude can combine together, making them very difficult to be individually distinguished.

Fortunately, transient waves such as radar pulses do not present the leakage effect, as long as they are totally contained in the window [161]. For the spectral analysis of experimental data only the rectangular window was used.

A typical waveform is depicted in Figure 4.6. It contains the whole recorded signal, as well as the main part of it windowed between 1.3 and 3.7 nanoseconds. This might represent either the reflected wave of main interest or the first arrival if the radar is working in the transmission mode. Thus, any side effects such as secondary reflections and system fluctuations, that can be present before and after the windowed portion, were normally not included. As result, the corresponding frequency spectrum, represented by the dashed line at the bottom of the Figure 4.6, allowed easier interpretation of data and extraction of useful qualitative and quantitative information.

Additional manipulation was carried out in the time domain to improve the resolution in the frequency domain. In most of experimental work, the radar data was recorded with 1024 sample points over a time range of 16 nanoseconds. This gives a sampling rate of 64 points per nanosecond, or a sampling interval of 0.0156 nanoseconds. According to section 4.3.2, the frequency resolution would be

$$\Delta f = \frac{1}{T_w} = \frac{1}{NS_f} = \frac{1}{16} = 0.0625 \text{ GHz} = 62.5 \text{ MHz}$$

To improve the resolution requires one to obtain smaller frequency intervals in the frequency domain. This was possible by artificially increasing the window length, e.g. 16 to 96 nanoseconds, or increasing the number of samples by simply adding zeros after the initial time range. In order to maintain the same definition of the signal in the time domain, the number of samples was increased in the same proportion, resulting in 6144 points.

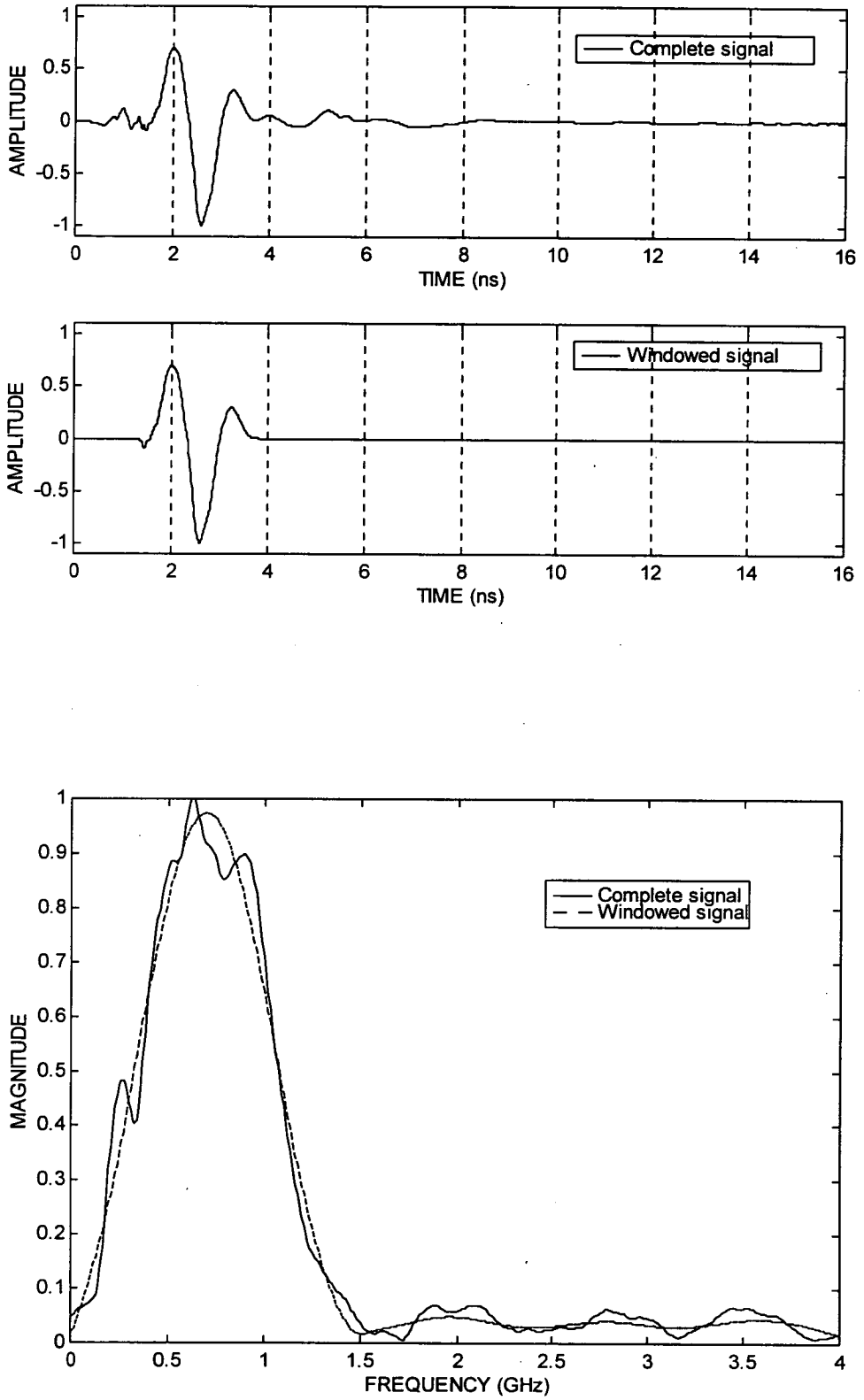

Figure 4.6 The application of a rectangular window on a typical experimental waveform

Consequently the resolution in the frequency domain was improved to

$$\Delta f = \frac{1}{96} = 0.0104 \text{ GHz} = 10.4 \text{ MHz}$$

The resulting frequency interval was considered satisfactory for the research purposes.

4.4 DISCUSSION

The popularity of the spectral analysis and processing of discrete time signals has grown during the past years in areas other than electrical and electronic engineering. Particularly in civil engineering, there is a need, when applying DSP, to understand the potential of techniques such as radar for non-destructive testing of concrete and other building materials.

In this chapter the main aspects regarding signal processing were briefly described, and their use and implications in the experimental data were analysed. Emphasis was given to the frequency domain analysis, signal windowing and signal filtering, as they were the only necessary DSP techniques for the present research purposes.

The DSP techniques can be used to enhance weak signals, to subtract high and low frequency noise, to define targets of interest better and to extract important information for data interpretation. However excessive processing can also degrade data and produce loss of information. Furthermore, one has to identify clearly what sort of information is being looking for, and thus choose the appropriate DSP techniques for each case. Otherwise, incorrect manipulation of data can lead to misleading interpretations. On the other hand, signal processing should not be used deliberately in any practical case. Whenever possible, it should be kept to a

minimum, as it can be very time consuming and represent a high percentage of the final cost of the work.

Filtering was applied only where strictly necessary to produce clean signals in the time domain (temporal low-pass filter) and to enhance shallow targets' reflections obscured by the strong input signal (spatial high-pass filter). It was shown that the filtering process does not produce wave distortion that could significantly affect the frequency spectrum. This aspect was of importance, as the centre frequency was usually the parameter adopted for quantitative evaluation and comparison of results.

4.5 CONCLUSIONS

The main conclusions that can be drawn from this chapter are:

1. Processing techniques, when rationally applied can provide users with very useful qualitative and quantitative information, and make the interpretation of experimental data easier.

2. The use of filters such as temporal low-pass (only for removing high frequency noise), and spatial high-pass (background removal), apparently do not produce significant additional signal distortion. Moreover, the frequency bandwidth of interest still remains in the spectrum.

3. If used excessively, signal processing can be time consuming and may not always produce satisfactory results.

4. To be more effective, processing techniques should be selected only when the user knows what kind of information is being sought. Some skills may be necessary to prepare the data properly in the time domain. This may produce results in the frequency domain which are easier to be interpreted.

CHAPTER 5

NUMERICAL ANALYSIS OF ELECTROMAGNETIC WAVE PROPAGATION THROUGH CONCRETE

CHAPTER 5

5. NUMERICAL ANALYSIS OF ELECTROMAGNETIC WAVE PROPAGATION THROUGH CONCRETE

5.1 INTRODUCTION

When undertaking a radar investigation in civil engineering practice, very little guidance exists on the radar survey design. In general terms "high" centre frequency (900MHz to 1GHz) antennas are used for testing concrete, "medium" centre frequency antennas (100 - 500 MHz) are used for testing masonry and "low" centre frequency (10 - 100 MHz) antennas are used for geophysical testing of soils and rocks.

However very little published data exists to back up the choices made. A limited experimental investigation was undertaken by Bungey *et al.* [101,112] showing the effectiveness of a 1GHz antenna in detecting re-bars in concrete. However this study does not extend to different concrete mixtures or radar antenna. Given that the Bungey *et al.* study was part of a 3-year research project involving an RA, it is clearly impractical to undertake such a study experimentally in the laboratory.

In view of the above, a numerical study was planned and executed to address many of the key issues.

5.2 ELECTROMAGNETIC WAVES - NUMERICAL ANALYSIS FOR RADAR APPLICATIONS ON CONCRETE STRUCTURES

The main objective of the first part of this work was to evaluate numerically the behaviour of electromagnetic waves with changes in the permittivity and conductivity of the material and transmitted centre frequency of the antenna (transducer) into the medium. The idea was to gain a better understanding of how these parameters affect the results when using Ground Penetrating Radar (GPR) on concrete structures.

The range of material properties chosen were typical for concrete, as reported in the literature (section 3.3.5). The frequencies, within the radar range, were chosen on the basis of the antennas commercially available and employed worldwide.

The numerical experiments were carried out on the attenuation and velocity of radar waves as these are the factors that describe the propagation of high frequency radio waves in a medium. These factors depend in turn on the dielectric and conductivity properties of the material [130].

5.2.1 Attenuation

The numerical analysis was carried out using the general equations (3.31) and (3.32) as well as the simplified equation (3.35), which assumes the low loss material condition.

The parameters ε_r and σ were chosen according to values reported in the literature and the frequencies were chosen within the range of commercially available antenna. Higher values for conductivity were examined, although at the moment the reported values were measured at lower frequencies (see section 3.3.6). Therefore,

concrete with lower dielectric constants and higher conductivities have been expected.

It was therefore proposed to simulate a wide range of situations which could be found in concrete structures.

Figures 5.1 and 5.2 show the behaviour of the attenuation as a function of frequency and conductivity for assumed values of the dielectric constant (6 and 12). The frequency independence of the attenuation at lower conductivities and higher dielectric constants can clearly be seen, suggesting the possibility of using the simplified equation. However, the presence of salts in the pore water will increase the conductivity leading to the use of lower frequencies to achieve significant penetration. In this case the values of the attenuation constant given by the simplified equation will be overestimated, and the depth of penetration (or skin depth $= 1/\alpha$) will be underestimated - see section 5.3.5 for further elaboration. The use of three dimensional graphs is very advantageous when more than two variables are involved.

Variations in the signal attenuation through concrete, classified as low loss material ($\tan\delta \ll 1$), based on equation (3.35) are thus independent of frequency (see Figure 5.3). It is important here to point out, for practical applications, what the value of loss tangent should be to classify a material as low loss, since it is usually reported in the literature that a material is assumed to comply with the simplified theory. This subject will be returned to in the next section. In Figures 5.4, 5.5 and 5.6, it can be seen how the loss tangent varies with frequencies of 100, 500 and 1000 MHz respectively, remembering that $\tan\delta = 1$ represents the limit between insulators and conductors.

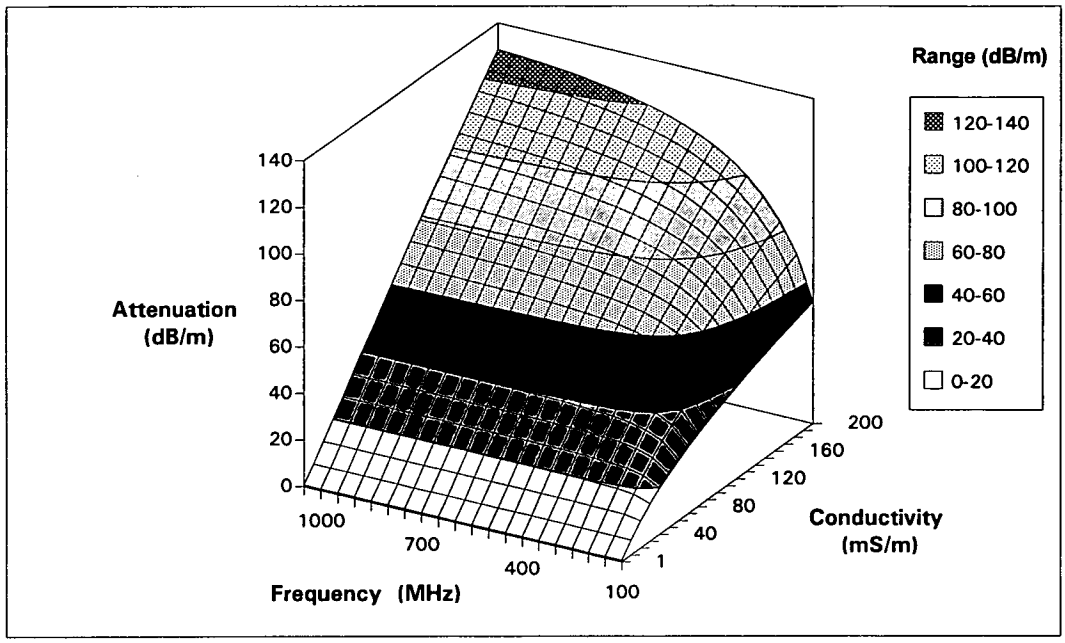

Figure 5.1 Electromagnetic wave attenuation for dielectric constant = 6

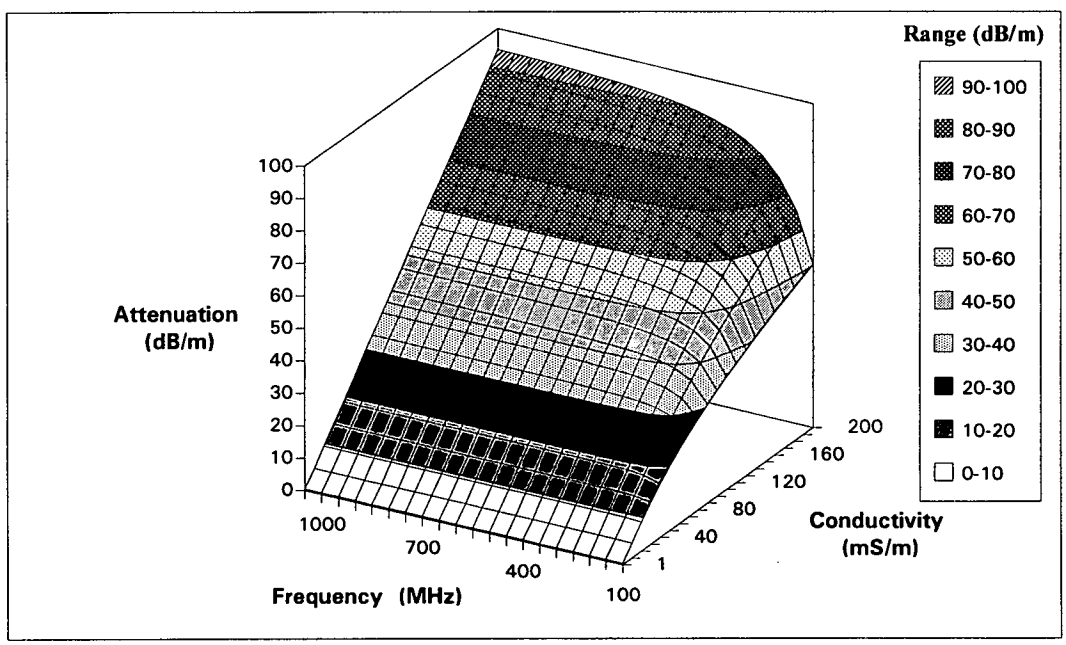

Figure 5.2 Electromagnetic wave attenuation for dielectric constant = 12

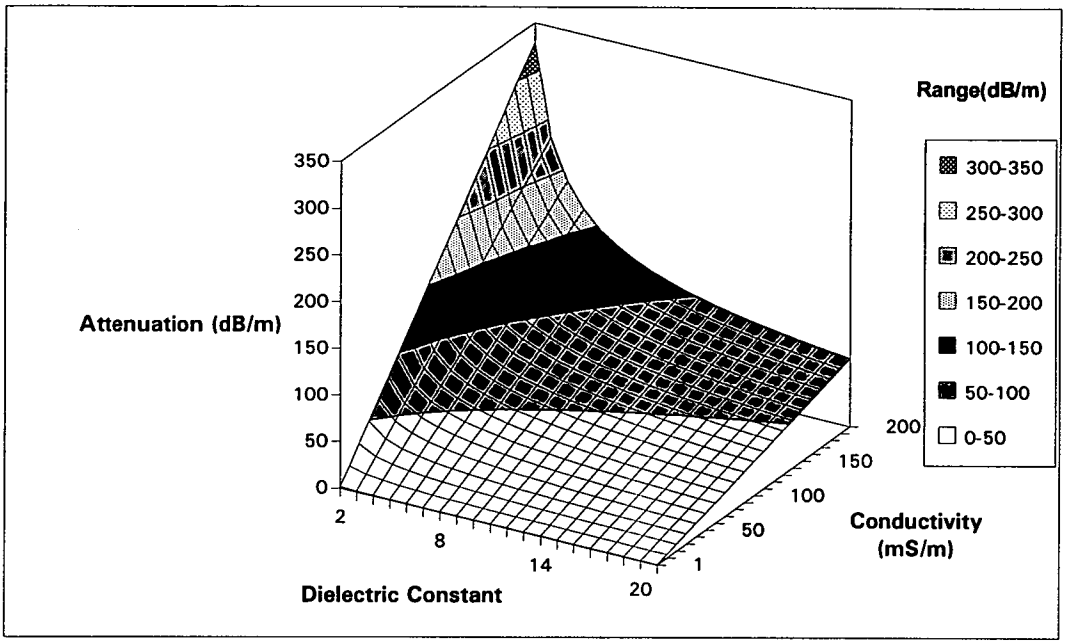

Figure 5.3 Attenuation for lowloss materials

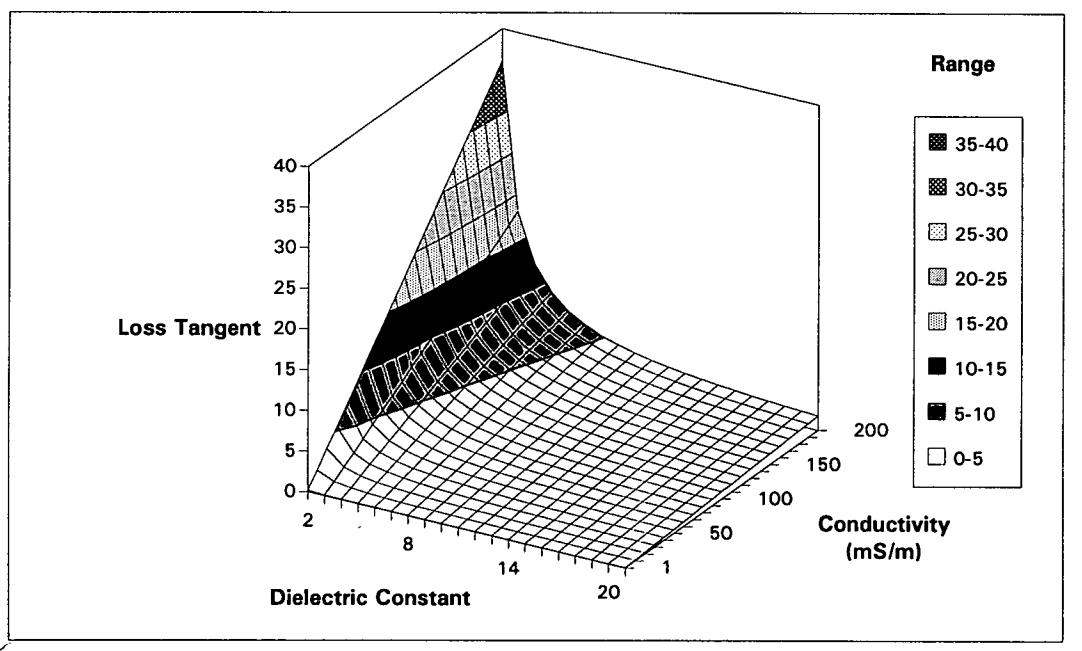

Figure 5.4 Loss tangent for frequency = 100 MHz

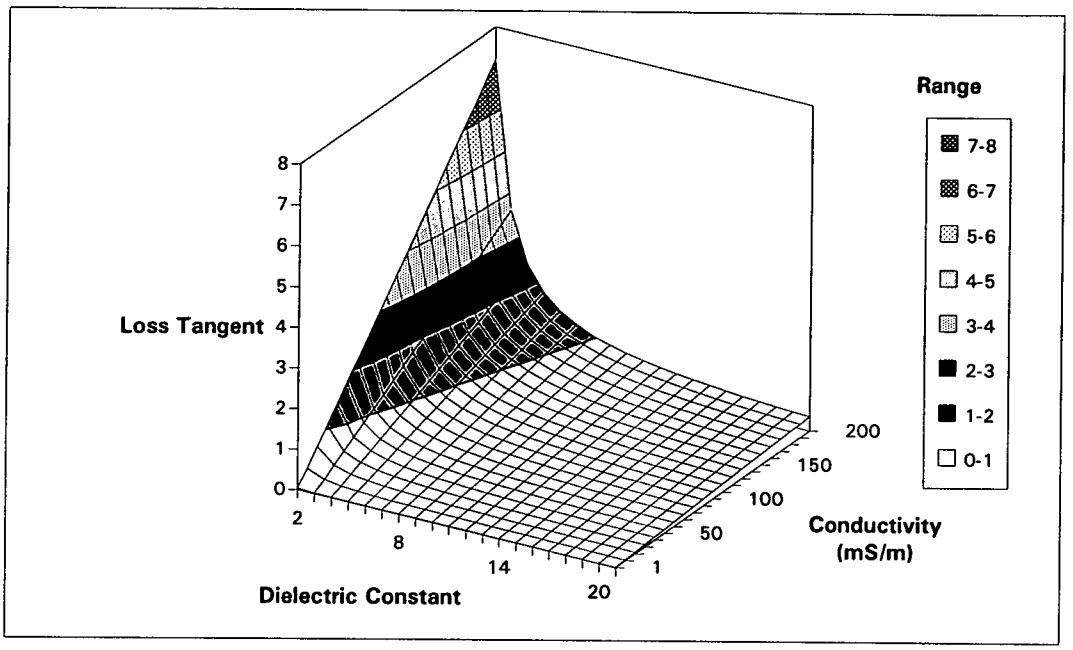

Figure 5.5 Loss tangent for frequency = 500 MHz

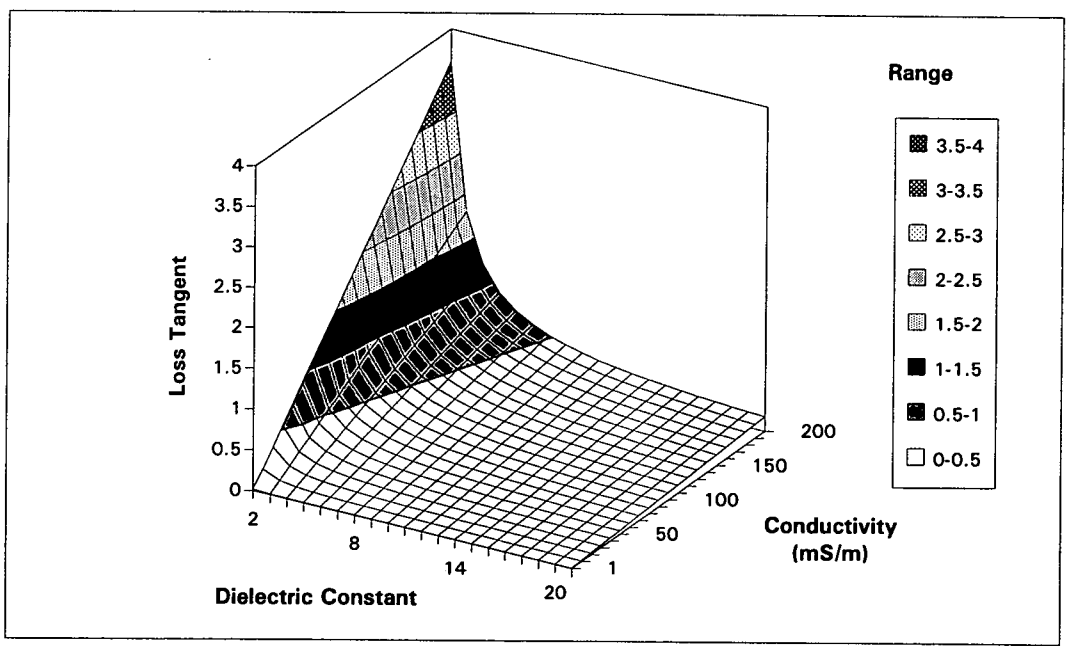

Figure 5.6 Loss tangent for frequency = 1000 MHz

5.2.2 Wave Velocity

Using the equation (3.38) from section 3.3.3, Figures 5.7 and 5.8 were computed and plotted showing 3D graphs of the velocity for dielectric constants 6 and 12 respectively. In these figures the variation of their shape for lower frequencies and higher conductivities can be seen.

The objective here has been to verify the validity of the simplified equation (3.36) when applied to the range of values for concrete as a dielectric material. In order to achieve this, tables were computed to compare the velocity results given by both the theoretical and simplified equations (see Table 5.1 as an example). From these tables the frequency values were chosen which gave the same velocity, assuming that a difference of less than 10% is acceptable. After this, using the equation (3.32), the loss tangent was calculated for each set of ε_r, f and σ values. It was found that the loss tangent essentially resulted about 1, not clearly characterising dielectric materials. The next step was to assume values for $\tan\delta < 0.90$ and to calculate the minimum frequency for each combination of conductivity and dielectric constant to satisfy such a condition. The results are given in Table 5.2, including the respective adjusted commercial antenna centre frequencies, which lead in general to $\tan\delta << 1$, thus validating equation (3.36) for practical applications. The assumption of $\tan\delta < 0.90$ was made because there is no clear idea of what the condition $\tan\delta<<1$ means in practice from a numerical point of view.

It should be remembered that the present work is a numerical study, including probably extreme situations which might not actually be found. It can be concluded, at least for concrete structures, where normally the conductivity expected is less than 100 mS/m, that the simplified equation is quite suitable for estimating velocities in the frequency range normally used (500-1000 MHz).

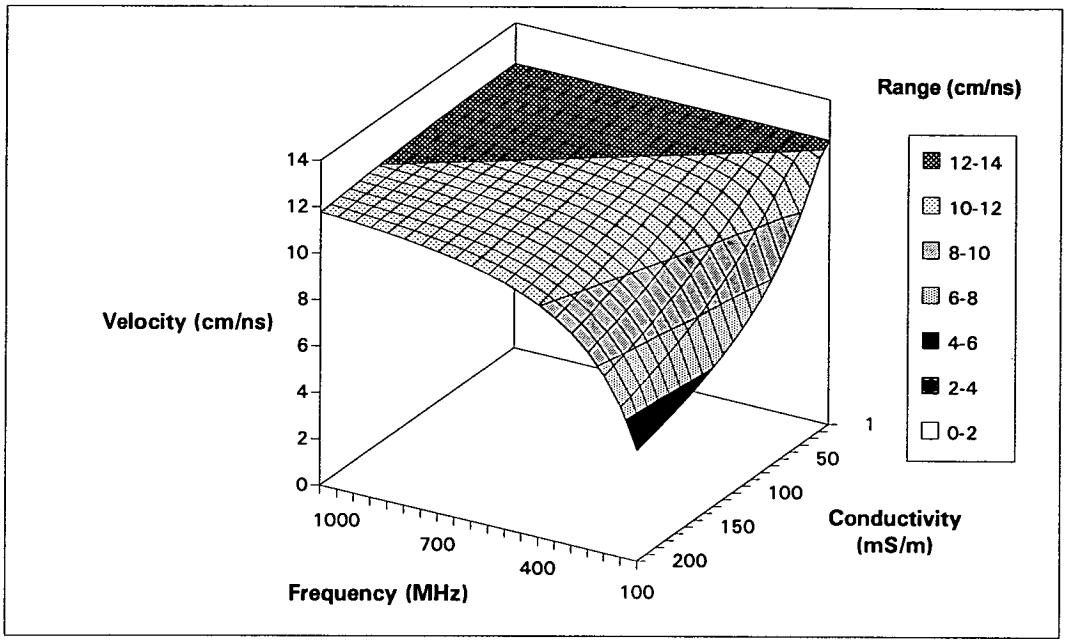

Figure 5.7 Electromagnetic wave velocity for dielectric constant = 6

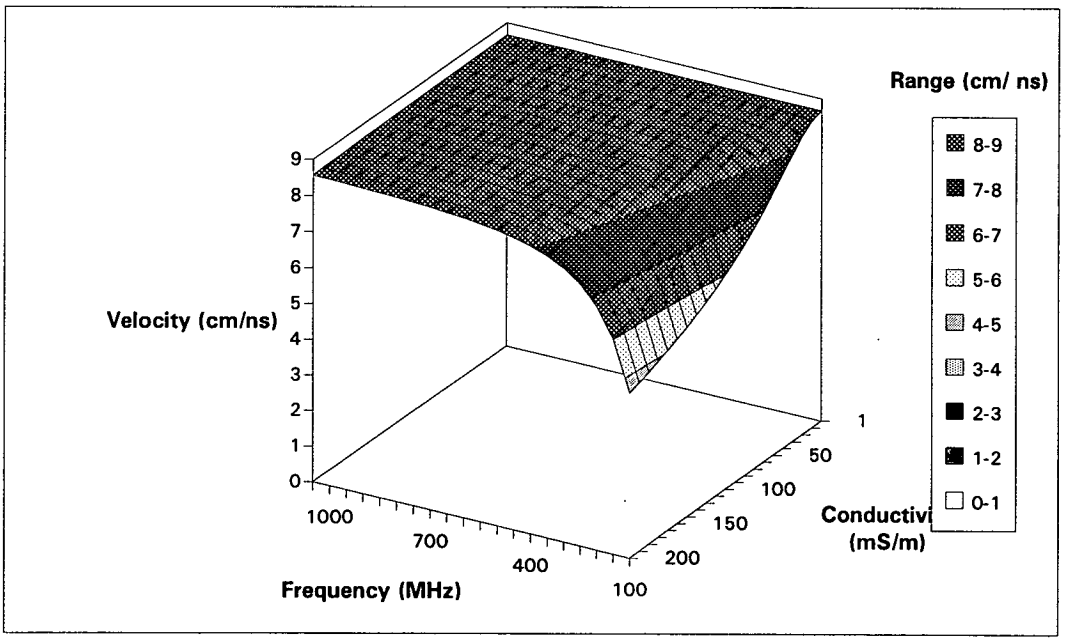

Figure 5.8 Electromagnetic wave velocity for dielectric constant = 12

Table 5.1 Electromagnetic wave velocity (cm/ns)

	Dielectric constant						
f (MHz)	*6*	*7*	*8*	*9*	*10*	*11*	*12*
50	8.49	8.27	8.06	7.86	7.67	7.49	7.32
100	10.35	9.89	9.48	9.10	8.76	8.45	8.16
150	11.15	10.53	10.00	9.53	9.12	8.75	8.42
200	11.55	10.84	10.24	9.72	9.27	8.87	8.52
250	11.77	11.00	10.36	9.81	9.34	8.93	8.57
300	11.90	11.10	10.43	9.87	9.38	8.96	8.59
350	11.99	11.16	10.48	9.90	9.41	8.98	8.61
400	12.04	11.20	10.51	9.92	9.43	9.00	8.62
450	12.09	11.23	10.53	9.94	9.44	9.01	8.63
500	12.11	11.25	10.54	9.95	9.45	9.02	8.64
550	12.14	11.26	10.55	9.96	9.46	9.02	8.64
600	12.15	11.28	10.56	9.97	9.46	9.02	8.64
650	12.17	11.28	10.57	9.97	9.46	9.03	8.65
700	12.18	11.29	10.57	9.97	9.47	9.03	8.65
750	12.19	11.30	10.58	9.98	9.47	9.03	8.65
800	12.19	11.30	10.58	9.98	9.47	9.03	8.65
850	12.20	11.31	10.58	9.98	9.47	9.03	8.65
900	12.21	11.31	10.59	9.98	9.48	9.04	8.65
950	12.21	11.31	10.59	9.99	9.48	9.04	8.65
1000	12.21	11.32	10.59	9.99	9.48	9.04	8.65
Vsimp	12.25	11.34	10.61	10.00	9.49	9.05	8.66

f : transmitted centre frequency

Vsimp : velocity using the simplified formula

Light speed = 30 cm/ns

Conductivity = 50 mS/m

If lower values of frequency to those specified in Table 5.2 were used (or higher conductivities) and thus tan $\delta > 1$ could be achieved, it would be necessary to

consider the material as behaving like a conductor. In this case another simplified equation for calculating velocities should be adopted when tan $\delta >> 1$, where the material behaves as a good conductor [125]:

$$v = \sqrt{\frac{2\omega}{\mu\sigma}} = 10\left(\sqrt{\frac{f}{\sigma}}\right) \quad \text{(cm/ns)} \tag{5.1}$$

where f = centre frequency in MHz

σ = conductivity in mS/m

For example, if $\varepsilon_r = 10$, $\sigma = 100$ mS/m and $f = 100$ MHz the following results will be obtained:

From (3.32): $tan\ \delta = 1.80 > 1$ (conductor)

From (3.38): $v = 7.67$ cm/ns

From (5.1): $v = 10.00$ cm/ns (Difference $\cong 30\%$)

Equations (3.38) and (5.1) will converge to values with differences less than 10% only for $tan\delta > 5$. Using a frequency of 500 MHz, it would imply having $\sigma > 1400$ mS/m (with $\varepsilon_r = 10$), leading to concretes with very high salinity. Therefore, when concrete assumes the characteristics of a conductor, the general equation (3.36) should be more appropriate for calculating wave velocities.

To set up the commercial antenna centre frequencies in Table 5.2 and in all cases afterwards in this chapter, another aspect has been considered. It is known that when an antenna is loaded to a surface, the transmitted signal centre frequency may change - in general to a lower value than the specified by the manufacturer. The latter usually refers to the centre frequency of the transmission in air [154] . It is caused by the loss of some higher frequency components of the frequency spectrum of the signal due to its stronger attenuation with respect to lower frequencies.

Table 5.2 Minimum centre frequency to use the simplified formula for calculating the wave velocity (error < 10% and loss tangent < 0.90)

Material : concrete

	Dielectric constant						
S (mS/m)	*6*	*7*	*8*	*9*	*10*	*11*	*12*
1	3	3	3	2	2	2	2
10	33	29	25	22	20	18	17
20	67	57	50	44	40	36	33
40	133	114	100	89	80	73	67
60	200	171	150	133	120	109	100
80	267	229	200	178	160	145	133
100	333	286	250	222	200	182	167
120	400	343	300	267	240	218	200
140	467	400	350	311	280	255	233
160	533	457	400	356	320	291	267
180	600	514	450	400	360	327	300
200	667	571	500	444	400	364	333

S : conductivity
Frequency in MHz

Using commercial antennas

	Dielectric constant						
S (mS/m)	*6*	*7*	*8*	*9*	*10*	*11*	*12*
1	50	50	50	50	50	50	50
10	50	50	50	50	50	50	50
20	100	80	80	80	80	50	50
40	200	200	200	120	120	100	100
60	300	225	200	200	200	200	200
80	450	300	300	300	225	200	200
100	450	450	300	300	300	300	225
120	500	450	450	450	300	300	300
140	900	500	500	450	450	450	300
160	900	900	500	500	450	450	450
180	900	900	900	500	500	450	450
200	900	900	900	900	500	500	450

To take into account this fact, when choosing the appropriate commercial antenna, the equation below has been adopted which permits an estimate of the centre frequency for mediums with dielectric constant from 1 to 15 [154]:

$$f = \frac{f_0}{\sqrt{\frac{2}{1+\left(\varepsilon_0 / \varepsilon_r\right)}}} \tag{5.2}$$

f = centre frequency of the transmitted signal

f_o = centre frequency of the antenna in air

ε_r = dielectric constant of concrete

ε_o = relative permittivity of air = 1

For the range of dielectric constant 6 to 12, the estimated centre frequency values given by equation (5.2) vary by less than 5 %. Therefore mean values have been assumed according to Table 5.3 below. (Only the most common antenna frequencies are shown).

For greater values of dielectric constant, equation (5.2) gives essentially constant results.

Table 5.3 Transmitted antenna centre frequency in MHz

In air	: 50	100	200	300	500	900	1000
Into concrete	: 38	75	149	224	374	672	747

5.3 GPR SURVEY DESIGN: INFLUENCE OF FREQUENCY

5.3.1 Introduction

In the earlier part of this work it was shown, from a theoretical point of view, what effect of the electrical properties of the material together with the frequency has on electromagnetic wave behaviour. Now the intention is to show how each of these parameters affects a radar survey from a design point of view.

Reflection surveys, such as GPR, are normally designed to provide a specified depth of penetration and a particular degree of resolution of the sub-surface media, in both the vertical and horizontal dimensions [60]. This implies selecting an adequate antenna centre frequency which can offer the best compromise between penetration and resolution. The higher the frequency the better the resolution but the lower the penetration. The opposite will occur for low frequencies.

Selecting the optimal operating frequency for a radar survey is not a simple matter. There are three factors which control the frequency, namely the spatial resolution desired, clutter limitations and depth of penetration [162]. These factors depend essentially on the dielectric constant of the material, but penetration is also strongly dependent on the conductivity.

The following analysis gives some guidance for selecting the antenna centre frequency for a survey design. Annan [162] has considered the factors cited above and has produced a basic reference for the selection of the correct operational frequency of the antenna for geological materials. The results have been worked out by a numerical analysis of the equations proposed, but considering concrete as the main material.

5.3.2 Vertical Resolution (or Depth Resolution)

The vertical resolution is a measure of the ability to recognise individual closely-spaced reflectors, or to distinguish two signals in the time domain. For a reflected pulse represented by a simple wavelet, the maximum resolution possible is between one quarter and one eighth of the dominant wavelength of the pulse [60]. Figure 5.9 shows a seismic model that illustrates the effects of wave interference phenomena on vertical resolution. Even though taken from a seismic example, the basic principles also apply to electromagnetic waves. This is a quite simple model, and in reality it will become more complex if multiple reflections or other interferences are present.

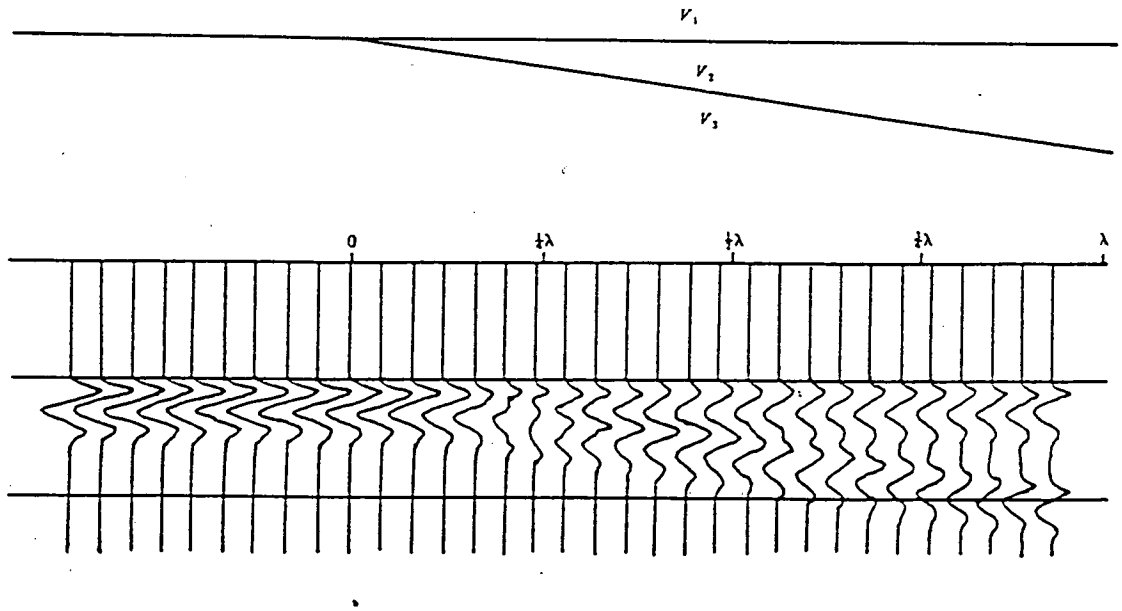

Figure 5.9 Reflection from a wedge showing vertical resolution, after Sheriff [163]

For the present analysis the resolution limit was assumed larger than one quarter, as usually adopted in GPR practical applications (Figure 5.10).

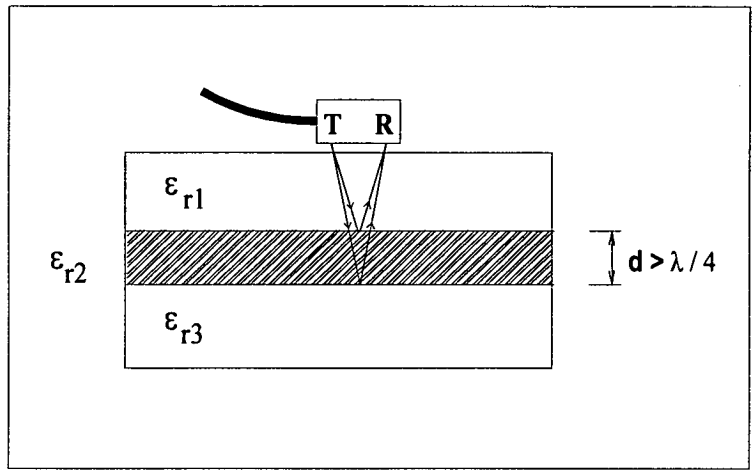

Figure 5.10 Vertical resolution

Acording to section 3.3.4, in a survey design the wavelength can be estimated by equation (3.41) :

$$\lambda = \frac{300}{f\sqrt{\varepsilon_r}}$$

From this equation the following can be derived:

$$f = \frac{300}{\lambda\sqrt{\varepsilon_r}} \tag{5.3}$$

As mentioned before, for vertical resolution $d > \frac{\lambda}{4}$, where "d" is the vertical distance between two reflectors to be resolved. Then from (5.3):

$$f > \frac{75}{d\sqrt{\varepsilon_r}} \tag{5.4}$$

Table 5.4 presents the results which represent the minimum centre frequency recommended for a survey design, when the intention would be adequate vertical resolution. It also presents the adjusted centre frequency values for commercial antenna, based either on Table 5.3 or equation (5.2).

It can be concluded from this study that there is difficulty in resolving reflectors spaced vertically less than 0.05 m apart. When using higher frequency antenna (> 1 GHz) other factors such as "clutter" should be considered, as will be seen in the next section.

It is interesting to note that for higher values of dielectric constants the same resolution can be achieved at lower frequencies, suggesting that the resolution improves at higher water content (the wave velocity is reduced), since there is a signal strong enough to be detected. However, in deciding to use lower frequencies in the presence of higher conductivities, caution should be exercised when using equation (5.3). The general equation for the wave velocity would have to be employed (see section 3.3.3).

Table 5.4 Minimum centre frequency for vertical resolution (MHz)

Material : concrete

	Dielectric constant						
d (m)	*6*	*7*	*8*	*9*	*10*	*11*	*12*
0.05	612	567	530	500	474	452	433
0.10	306	283	265	250	237	226	217
0.20	153	142	133	125	119	113	108
0.30	102	94	88	83	79	75	72
0.40	77	71	66	63	59	57	54
0.50	61	57	53	50	47	45	43
0.60	51	47	44	42	40	38	36
0.70	44	40	38	36	34	32	31
0.80	38	35	33	31	30	28	27
0.90	34	31	29	28	26	25	24
1.00	31	28	27	25	24	23	22

d : vertical distance between two consecutive reflectors.

Using commercial antennas

	Dielectric constant						
d (m)	*6*	*7*	*8*	*9*	*10*	*11*	*12*
0.05	900	900	900	900	900	900	900
0.10	500	450	450	450	300	300	300
0.20	225	200	200	200	200	200	200
0.30	200	120	120	120	120	100	100
0.40	120	100	100	100	80	80	80
0.50	80	80	80	80	80	80	80
0.60	80	80	80	80	80	50	50
0.70	80	50	50	50	50	50	50
0.80	50	50	50	50	50	50	50
0.90	50	50	50	50	50	50	50
1.00	50	50	50	50	50	50	50

5.3.3 Clutter Reduction

Clutter in GPR systems refers to the unwanted radar signals (or scattering losses of electromagnetic energy) returned from material heterogeneity [123,162]. The scattering can be caused by differential packing, porosity and irregular size and shape of grains within the material under investigation, producing reflected energy in random directions. Thus, a target reflection (the wanted signal) may be partially obscured by the scattering or clutter noise.

Scattering may occur when the changes in electrical properties in a material are on the same geometric scale as the size of a wavelength of the signal [164]. In a geological medium the heterogeneity may be represented by voids or stones, and in case of concrete by the larger aggregates (Figure 5.11).

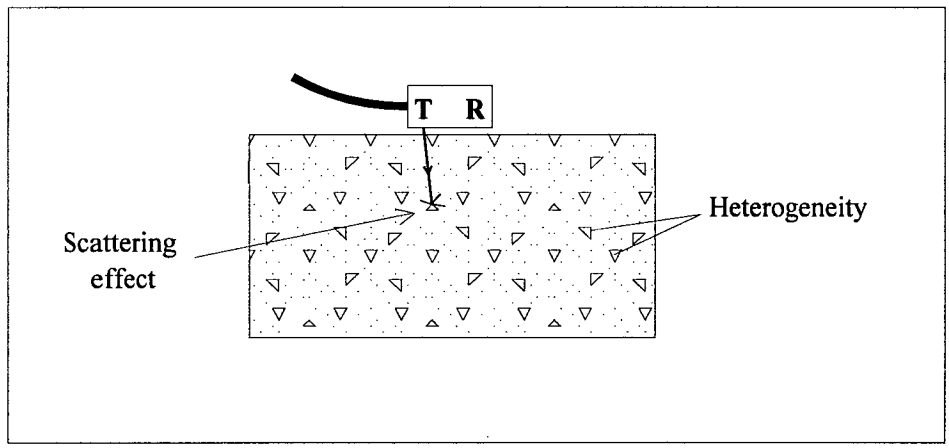

Figure 5.11 Scattering effect due to clutter

To minimise the clutter effect, the dominant signal wavelength (λ) should be much larger than the characteristic dimension of the heterogeneity in the host environment. Annan [162] has suggested λ ten times larger than the characteristic dimension for geological materials. However for concrete, since it is an artificial

material obtained by the mixture of other known materials, there is control over their size. For this reason, this analysis was carried out assuming λ only five times the characteristic dimension of the heterogeneity.

Therefore, from equation (3.41) (section 3.3.3) we obtain:

$$f < \frac{60}{d'\sqrt{\varepsilon_r}} \tag{5.5}$$

d' represents the characteristic dimension of the heterogeneity.

Table 5.5 contains the results as the maximum centre frequency which should be recommended in a survey design on concrete structures for clutter reduction. It also includes the appropriate frequencies when using commercial antenna according to Table 5.3 (or equation 5.2).

As a main conclusion, in building structures where the concrete mixes usually contain aggregates smaller than 50 mm, the use of antennas within the range 500 to 1000 MHz should reduce most of the clutter scattering. For a particular size of aggregates Table 5.5 also indicates that the scattering effect will increase with higher moisture content (or higher values of dielectric constant). In structures where large aggregate would be used, lower frequencies should be selected though the side effect will be less resolution.

Table 5.5 Maximum centre frequency for reducing clutter (MHz)

Material : concrete

	Dielectric constant						
d'(mm)	*6*	*7*	*8*	*9*	*10*	*11*	*12*
10	2449	2268	2121	2000	1897	1809	1732
20	1225	1134	1061	1000	949	905	866
30	816	756	707	667	632	603	577
40	612	567	530	500	474	452	433
50	490	454	424	400	379	362	346
60	408	378	354	333	316	302	289
70	350	324	303	286	271	258	247
80	306	283	265	250	237	226	217
90	272	252	236	222	211	201	192
100	245	227	212	200	190	181	173

d' : characteristic dimension of the heterogeneity

Using commercial antennas

	Dielectric constant						
d'(mm)	*6*	*7*	*8*	*9*	*10*	*11*	*12*
10	>1000	>1000	>1000	>1000	>1000	>1000	>1000
20	1000	1000	1000	1000	1000	1000	1000
30	1000	900	900	500	500	500	500
40	500	500	500	500	500	500	500
50	500	500	500	500	300	300	300
60	500	300	300	300	300	300	300
70	300	300	300	300	300	300	300
80	300	300	300	300	300	200	200
90	300	300	300	200	200	200	200
100	300	300	200	200	200	200	200

5.3.4 Horizontal Resolution (or Plan Resolution)

The horizontal resolution of a subsurface radar system is important where localised targets are being sought and when two of them at the same depth need to be distinguished, otherwise the requirement is for vertical location accuracy [65]. This is the case in the example of concrete structures when the necessity to resolve reinforcing bars may be very important, particularly if the aim is to create conditions to detect features behind them (Figure 5.12).

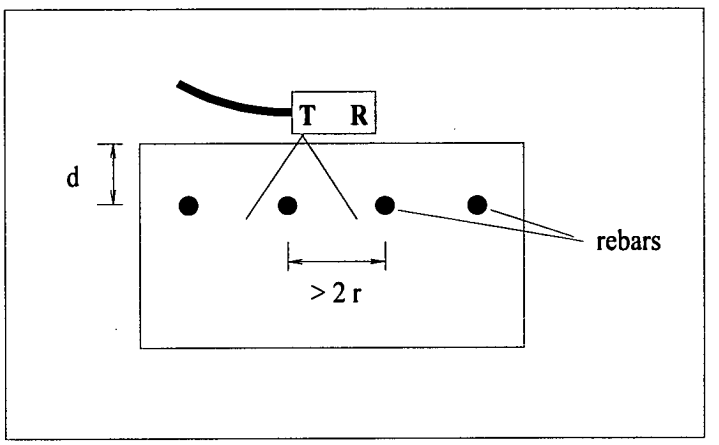

Figure 5.12 Horizonal resolution

There are two main controls on the horizontal resolution of a reflection survey, one being intrinsic to the physical process of reflection and the other being determined by the transducer spacing in the case of bistatic mode operation [60]. Since GPR applied on structures usually involves using transducers which act as transmitter and receiver simultaneously, the bistatic mode was not considered in this study.

In a reflection survey the initial reflected signal will be from the nearest point on the reflector target at depth "d" and will include contributions from all parts of the surrounding circular area that are not distant greater than "$d + \lambda/4$" from the radar

[165]. This is known as the Fresnel zone (Figure 5.13) and its width represents an absolute limit on the horizontal resolution of a reflection survey since reflectors separated by a distance smaller than this cannot be individually distinguished. This has more serious implications when estimating horizontal resolution for shallower targets, as the Fresnel zone describes the near field of an antenna and is dependent on the distance of targets.

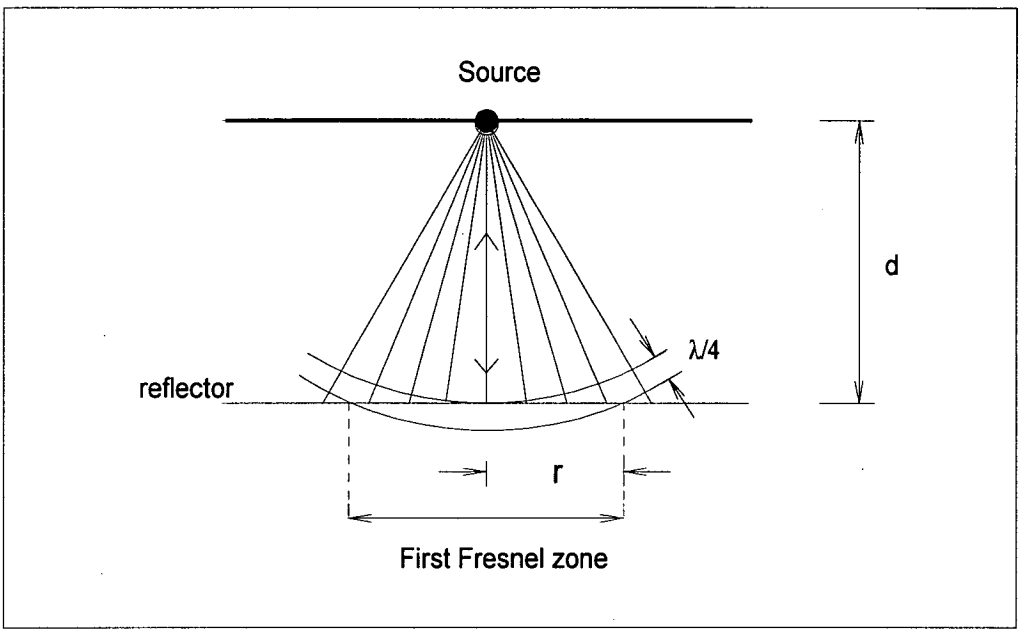

Figure 5.13 First Fresnel zone [60]

Based upon Figure 5.13, the radius (r) of the first Fresnel zone is given by

$$r^2 = \frac{\lambda d}{2} + \frac{\lambda^2}{16} \tag{5.6}$$

Using equation (3.41) and substituting in (5.6) the following equation can be derived

$$r^2 = \frac{150d}{f\sqrt{\varepsilon_r}} + \frac{1}{16}\left[\frac{300}{f\sqrt{\varepsilon_r}}\right]^2 \tag{5.7}$$

d = depth of reflectors.

Thus, two reflectors should be horizontally spaced by more than $2r$ to be distinguishable (Figure 5.12).

Table 5.6 presents the results obtained as a function of the antenna centre frequency and depth of the reflector up to 1.2 m, for concrete with dielectric constant 6 and 12. It can be observed that the resolution improves for higher values of frequency and dielectric constant. Experiments carried out by Bungey [166] have confirmed this.

Regarding the reflectors' horizontal spacing the results also showed coherence with experimental results obtained by Bungey *et al.* [167] using a simulation tank for detecting reinforcing bars with radar. They used a 1 GHz transducer and have concluded that for a cover range of 200-300 mm, bar spacing greater than 200 mm could be resolved, as expected theoretically for either dry or wet concrete (Figure 5.14). However their results do not indicate a clear relationship between horizontal spacing and depth when cover is greater than 200 mm. Their data suggests that they are independent, disagreeing with the theoretical expectation (Figure 5.15).

A possible explanation for this difference is the earlier attenuation with depth of the outer rays of the radiated beam (footprint), as the antenna does not radiate energy with the same intensity at all directions. The footprint will therefore become smaller at greater depths and for materials with higher conductivity, which is equivalent to a relative reduction in the beam width. As result, even though with variable signal intensity, reflectors at different depths could be equally resolved. The assumed model (Eq. 5.7) does not consider this problem. Daniels [65, 129], has proposed an equation based on the distance between the half power points of the spatial response of the scatterer at the plane of the surface as follows,

$$\Delta x = 4d\left(\frac{ln2}{2+\alpha d}\right)^{1/2} \tag{5.8}$$

Δx = horizontal resolution

d = depth of the target

α = attenuation constant

Table 5.6 Minimum space between reflectors for horizontal resolution (in m)

Material : concrete

Dielectric constant = 6

	Centre Frequency (MHz)						
D (m)	*50*	*100*	*200*	*300*	*500*	*900*	*1000*
0.10	1.79	0.98	0.57	0.42	0.30	0.21	0.20
0.20	1.96	1.13	0.69	0.53	0.39	0.28	0.27
0.30	2.12	1.27	0.80	0.63	0.47	0.34	0.32
0.40	2.27	1.39	0.90	0.71	0.53	0.39	0.37
0.50	2.40	1.50	0.98	0.78	0.59	0.43	0.41
0.60	2.53	1.60	1.06	0.84	0.64	0.47	0.45
0.70	2.66	1.70	1.13	0.91	0.69	0.51	0.48
0.80	2.78	1.79	1.20	0.96	0.73	0.54	0.51
0.90	2.89	1.88	1.27	1.02	0.78	0.57	0.54
1.00	3.00	1.96	1.33	1.07	0.82	0.60	0.57
1.10	3.10	2.04	1.39	1.12	0.86	0.63	0.60
1.20	3.20	2.12	1.44	1.16	0.89	0.66	0.63

Dielectric constant = 12

	Centre Frequency (MHz)						
D (m)	*50*	*100*	*200*	*300*	*500*	*900*	*1000*
0.10	1.36	0.76	0.45	0.34	0.25	0.17	0.16
0.20	1.53	0.90	0.57	0.44	0.33	0.24	0.22
0.30	1.67	1.03	0.66	0.52	0.39	0.29	0.27
0.40	1.81	1.13	0.75	0.59	0.45	0.33	0.31
0.50	1.93	1.23	0.82	0.66	0.50	0.37	0.35
0.60	2.05	1.33	0.89	0.71	0.54	0.40	0.38
0.70	2.16	1.41	0.95	0.77	0.59	0.43	0.41
0.80	2.27	1.49	1.01	0.82	0.62	0.46	0.44
0.90	2.37	1.57	1.07	0.86	0.66	0.49	0.46
1.00	2.47	1.64	1.12	0.91	0.70	0.52	0.49
1.10	2.56	1.71	1.18	0.95	0.73	0.54	0.51
1.20	2.65	1.78	1.22	0.99	0.76	0.56	0.53

D : depth of reflectors

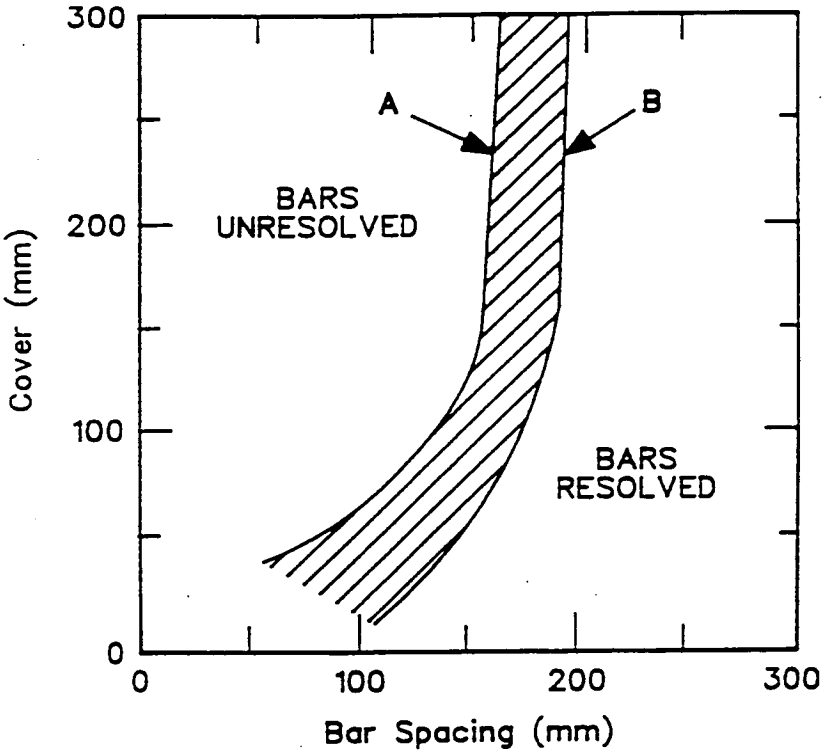

Figure 5.14 Limit of resolution of individual bars, after Bungey *et al.*[167]

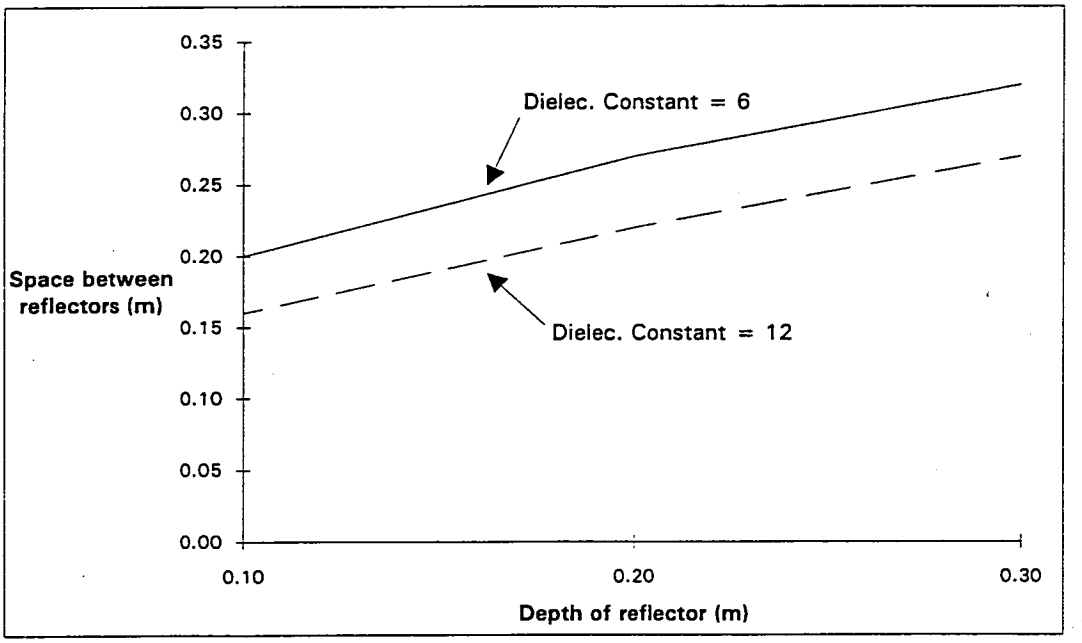

Figure 5.15 Minimum space between reflectors for horizontal resolution

However this equation does not consider the antenna beam pattern, which was approximately taken into account in equation (5.7) as a function of frequency. More experimental data is necessary to see the extension of this effect when using radar on concrete. Some additional dispersion may be attributed to the influence of the bar's diameter. Also targets located at shallower depths can be obscured owing to the initial pulse (a combination of transmission, coupling and surface reflection) which appear on the graphical records. The length of this pulse is usually greater than the nominal value in air.

It is worth mentioning that in the case of metal targets, where total reflection is expected, they might be spaced less than the values given by Table 5.6 and still being distinguishable. However metals give much more intense signal reflections than other building materials due to their very high conductivity. This will cause a strong masking effect with almost total reflection, and as consequence the detection of features located behind the target may be very difficult.

Finally, it is important to stress that values given in Table 5.6 should be considered only as guidance for practical applications, since the Fresnel zone is a concept which is valid for a point source, not taking account of the orientation and size of the antenna. In this case the width of the antenna beam will be usually different at each direction, considering that most commercial antennas are a kind of dipole.

5.3.5 Skin Depth

As seen in section 3.3.2, in a medium which has conductivity the electromagnetic wave is attenuated as it progresses due to losses which occur. If the conductivity is high, the rate of attenuation at radio frequencies is very great and the penetration of the wave may be quite short before being reduced to a small

percentage of its initial strength. Under such circumstances, the "skin depth" is a term that has significance when estimating a useful penetration depth for a sub-surface radar system [141]. However other factors should be taken into account such as the reflector signal strength and clutter. The latter was analysed in section 5.3.3.

At the skin depth the transmitted signal strength will reduce by $1/e$ of its original value [168], and may be determined by equation (5.9) in metres

$$\delta = \frac{1}{\alpha} \tag{5.9}$$

α = Attenuation, in nepers/m, given by (3.30)

For low loss materials, a simplified equation may be obtained from (3.35):

$$\delta = \frac{8.686}{\alpha} = 5.31 \times 10^{-3} \left(\frac{\sqrt{\varepsilon_r}}{\sigma} \right) \tag{5.10}$$

σ: in S/m

For materials classified as good conductors ($tan\delta >> 1$) another simplified equation has to be employed [125] as follows:

$$\delta \cong \frac{16}{\sqrt{f\sigma}} \qquad \text{f: in MHz (Eq. 5.2); } \sigma\text{: in mS/m} \tag{5.11}$$

Using the above equations, Table 5.7 and Figures 5.16 and 5.17 were computed and plotted.

From this table and these graphs the following remarks can be made:

a) Independent of the operational centre frequency, the skin depth varies significantly when the conductivity varies from only 1 to 10 mS/m - with values between 1.3 m and 13.0 m for ε_r = 6; and between 1.8m and 18.0m for ε_r = 12. Conversely it varies less than 1.0 m for conductivities ranging from 20 to 200 mS/m,

Table 5.7 Skin depth (in metres)

Material : concrete
Dielectric constant = *6*

	Centre Frequency (MHz)								
S (mS/m)	*50*	*100*	*200*	*300*	*500*	*900*	*1000*	*SDd*	*SDc*
1	13.00	12.99	12.99	12.99	12.99	12.99	12.99	13.01	1.83
10	1.38	1.32	1.30	1.30	1.30	1.30	1.30	1.30	0.58
20	0.78	0.69	0.66	0.65	0.65	0.65	0.65	0.65	0.41
40	0.48	0.39	0.35	0.33	0.33	0.33	0.33	0.33	0.29
60	0.37	0.29	0.24	0.23	0.22	0.22	0.22	0.22	0.24
80	0.31	0.24	0.19	0.18	0.17	0.16	0.16	0.16	0.20
100	0.27	0.21	0.16	0.15	0.14	0.13	0.13	0.13	0.18
120	0.25	0.18	0.14	0.13	0.12	0.11	0.11	0.11	0.17
140	0.23	0.17	0.13	0.12	0.10	0.10	0.10	0.09	0.15
160	0.21	0.16	0.12	0.10	0.09	0.09	0.08	0.08	0.14
180	0.20	0.15	0.11	0.10	0.08	0.08	0.08	0.07	0.14
200	0.19	0.14	0.10	0.09	0.08	0.07	0.07	0.07	0.13

Dielectric constant = *12*

	Centre Frequency (MHz)								
S (mS/m)	*50*	*100*	*200*	*300*	*500*	*900*	*1000*	*SDd*	*SDc*
1	18.37	18.37	18.36	18.36	18.36	18.36	18.36	18.39	1.87
10	1.87	1.85	1.84	1.84	1.84	1.84	1.84	1.84	0.59
20	0.98	0.94	0.92	0.92	0.92	0.92	0.92	0.92	0.42
40	0.55	0.49	0.47	0.46	0.46	0.46	0.46	0.46	0.29
60	0.41	0.35	0.32	0.31	0.31	0.31	0.31	0.31	0.24
80	0.34	0.28	0.25	0.24	0.23	0.23	0.23	0.23	0.21
100	0.30	0.23	0.20	0.19	0.19	0.18	0.18	0.18	0.19
120	0.26	0.21	0.17	0.16	0.16	0.15	0.15	0.15	0.17
140	0.24	0.19	0.15	0.14	0.14	0.13	0.13	0.13	0.16
160	0.22	0.17	0.14	0.13	0.12	0.12	0.12	0.11	0.15
180	0.21	0.16	0.13	0.12	0.11	0.10	0.10	0.10	0.14
200	0.20	0.15	0.12	0.11	0.10	0.09	0.09	0.09	0.13

S : conductivity
SDd : skin depth using simplified formula for good dielectrics
SDc : skin depth using simplified formula for good conductors and 100 MHz antenna

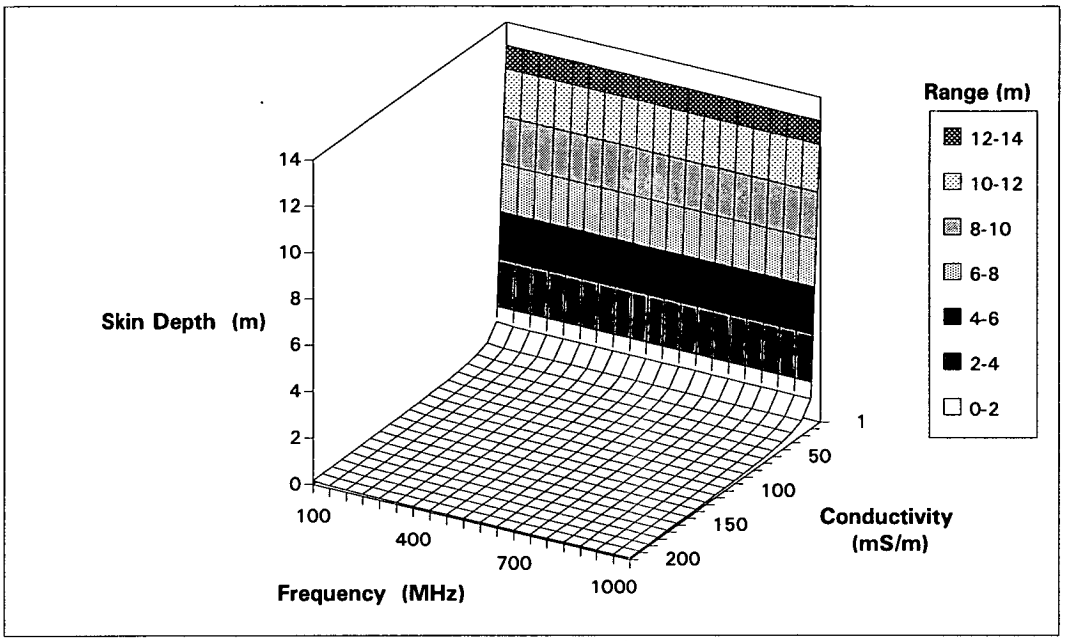

Figure 5.16 Skin depth for dielectric constant = 6

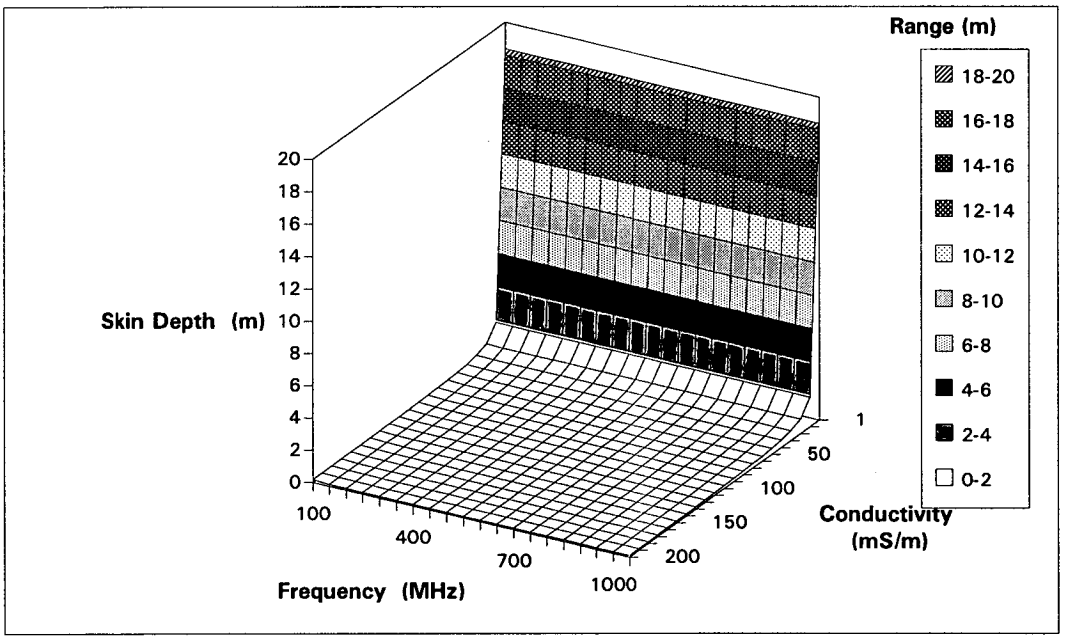

Figure 5.17 Skin depth for dielectric constant = 12

demonstrating that in this case radar will only be useful for shallower probing due to the high attenuation.

b) If the centre frequency of the antenna is between 500 and 1000MHz and the conductivity is less than 120 mS/m, the skin depth may be calculated by the simplified equation (5.10) with an error of less than 10%. It can be also inferred that for conductivities up to 30 mS/m the skin depth is totally independent of frequency.

c) The step line indicated in Table 5.7 represents the interface between insulator and conductive behaviour of concrete for the present study. The values below the line should be compared to values computed by equation (5.11) for each frequency. Therefore, in practice, care has to be taken when employing simplified equations, since their validity depends on the behaviour of the material (insulator or conductor).

d) For the antenna centre frequency range adopted in this work, the shortest nominal wavelength will be between 90 and 120 mm (see Figure 3.2). This means that there will be an operational limit to the use of radar at conductivities higher than 100 mS/m. This is because of the strong signals which theoretically occupy the first 90-120 mm of the vertical records, as can be seen in GPR surveys. In practice these values will be greater because of the coupling effect between transducers and the surface of contact. Thus, objects or interfaces very close to the surface will be obscured. To overcome this problem, some authors [103,131] have suggested interposing another material between the antenna and the surface ($\geq$ 50 mm). This new layer should have approximately the same dielectric constant as the surface material and have good contact to the latter. However, this procedure while theoretically correct has not yet proved to be very successful. More experimental work is required.

Whenever it is possible to post-process data, information from shallower targets might be enhanced using background removal or spatial filtering, as described

in chapter 4. However, this depends on the analyser's skills as data from targets can also be lost.

In practice, depending on the system used, the depth of penetration can be much greater than the skin depth [140]. This is governed by the power of the antenna. In general, for a survey design it is possible to achieve a compromise between frequency, range (ns) and samples per scan. Once the correct antenna centre frequency has been chosen, the number of samples per scan must be defined so that the sampling rate be greater than the Nyquist frequency - at least twice the frequency of the highest frequency present - in order to avoid aliasing of the data (see chapter 4). The range (or time window) may be estimated assuming an average value for the dielectric constant (and so the wave velocity) and the depth of exploration to be recorded.

$$\text{Range (ns)} = \frac{\text{Desired depth of exploration}}{\text{Estimated wave velocity}}$$

This value should be twice in case of using reflection mode.

It is important to point out that estimating a value for the dielectric constant on site may be difficult as it changes with moisture content. Therefore, field trials before commencing survey may be advisable to test the capability of the system to be used.

5.4 CONCLUSIONS

A systematic numerical analysis was undertaken of electromagnetic wave propagation through concrete. In the first part was discussed the behaviour of electromagnetic wave regarding amplitude attenuation and velocity of propagation. In the second part emphasis was given to target resolution (both vertical and horizontal), clutter due to material heterogeneity and depth of penetration. Antennas' centre frequency was proposed as guidance for planning radar surveys.

The most important conclusions drawn from this chapter are summarised below.

1. The commonly held assumption that the simplified expression for wave velocity can be applied to concrete structures may prove erroneous at lower frequencies, especially as the conductivity increases.

2. The suggested centre frequency of the electromagnetic pulse through concrete is expected to be about 75 % of the centre frequency of the antenna as measured in air.

3. Using the concept of Fresnel zone as model for studying horizontal resolution shows a good agreement with experimental results for concrete covers up to 200 mm.

4. On normal structural concrete a 900 MHz antenna may give a cleaner signal than a 1GHz antenna due to the clutter effect. In addition, the larger the dominant particle size in concrete the more energy will be scattered, and therefore the lower the value of the penetration depth at which reflections may be identified.

5. For a particular size of particle, energy scattering in concrete due to clutter will increase with higher moisture content (or higher values of the dielectric constant).

6. For a given frequency the skin depth (a measure of penetration) drops as conductivity increases. If a lower centre frequency is chosen, the simplified equation to work out the attenuation constant may no longer be applicable. It might overestimate the attenuation and therefore underestimate the depth of penetration.

7. The antennas' centre frequency suggested for vertical and horizontal resolution, as well as clutter, should be used as an initial reference only. If a different criteria is assumed, for instance $\lambda/2$ as a maximum resolution, then the centre frequency values have to be adjusted.

CHAPTER 6

EXPERIMENTAL INVESTIGATION OF RADAR PROPAGATION IN CONCRETE

CHAPTER 6

6. EXPERIMENTAL INVESTIGATION OF RADAR PROPAGATION IN CONCRETE

6.1 INTRODUCTION

In most Radar applications, the assumed electrical properties of the materials are usually those obtained from experimental measurements (section 3.3.5). These values are not influenced by operational aspects related to the use of the Radar equipment itself as a non-destructive testing technique.

When employing Radar for measuring dielectric constant values or estimating thicknesses, calculations are based on information recorded in the time domain. This approach requires that the recorded signals are not distorted during their propagation through the medium. Also, in small scale applications such as in non-destructive evaluation, the coupling effect of the antennas may not be ignored.

There are only a few published data concerning the propagation of electromagnetic waves and their consequent distortion. Selmann *et al.* [169] reported the use of 20, 50, 100 and 500 MHz antennas to assess their performance in acquiring information from the bottom and sub-bottom of fresh water river and lakes. The centre frequencies of the actual recorded signals were respectively 23, 40, 83 and 125 MHz. Apart from the first one, the remaining antennas presented lower centre frequency in their received pulse spectra. They also reported the use of the 500 MHz on soil, where the centre frequency fell between 300 and 400 MHz. In a few cases, they even observed recorded signals with higher centre frequencies than the designed values. However these were exceptions, with the majority showing the

tendency of decreased frequencies.

Turner and Siggins [134], recorded data of pulses transmitted by a 120 MHz antenna propagating through granite. They observed that the centre frequency decreased to 79 and 55 MHz, depending on the travelled distance.

Maierhofer *et al.* [108] also reported their preliminary observations of signal attenuation in concrete for 900 MHz antennas. The pulse spectrum in air showed a nominal centre frequency peaking at 1 GHz. They have claimed however that after propagating through concrete apparently frequency components higher than 500 MHz are completely attenuated, causing a shift in the centre frequency down to approximately 500 MHz. In all cases ground coupled antennas were employed.

The important remark that can be made is that none of the researchers has mentioned the interference of the coupling effect in the resulted signals. It is well known that coupling effects exist when using ground coupling antennas or contacting antennas [170]. GPR systems emit pulses with a broad frequency bandwidth. The nominal frequency of antennas specified by the manufacturers and used in the calculations is the centre frequency of the radiated signals. This frequency is measured with the antennas coupled to air. When the antenna is coupled to a medium different from air, the radiation characteristics change with the medium becoming part of the radar system. As result the nominal centre frequency may shift to lower values [171].

Little quantitative information has been published regarding frequency content of recorded signals, especially from concrete structures. It is particularly important in working out either velocities or dielectric constant values, as they are based on time domain data. The simplified equation for velocities (Eq. 3.36) is very sensitive to small variations of time and may easily introduce inaccuracies due to wave shape distortion. The problem will be even more accentuated when working with larger antennas over shorter distances.

To verify the effect of propagation and the coupling effect of electromagnetic waves travelling in concrete at radar frequencies, an experiment was set up and will be described in the following sections.

The experimental data were obtained in the time domain with a GSSI multichannel radar equipment (model SIR 10), and when necessary post-processed using the manufacturer's software. Most analysis was carried out in the frequency domain by applying a Fast Fourier Transform (FFT) to the time domain data.

6.2 DESIGN OF EXPERIMENT

6.2.1 Materials and concrete mix design

The concrete was prepared with ordinary Portland cement to BS12 [172], natural medium sand, coarse aggregate (gravel) and normal supply water. The sand was available at the laboratory and a sieve test was carried out with a dry sample of 1110 grams to verify whether it complied with British Standards (Table 6.1). From this test, according to BS 882 [173], the sand can be classified as grading "M". The percentage of sand passing the 600 μm sieve was also necessary for the mix design. Coarse aggregate was provided by a commercial company. Both cement and coarse aggregate were assumed to fulfil British Standards.

The basic mixture was designed based on a simplified method, proposed in conjunction by the Building Research Establishment, Transport Research Laboratory and the British Cement Association [174]. This design gives a mix proportion of 1 : 1.79 : 3.32 in weight. The surface moisture of aggregates was always determined to correct the water content. See Appendix A for more detail.

Table 6.1 Sieve test results for sand used in concrete (Sample: 1110 g of dry sand)

Sieve	Weight ret. (g)	Total passing (g)	% passing sieve
10 mm	-	1110	100
5 mm	60	1050	95
2.36 mm	215	835	75
1.18 mm	150	685	62
600 μm	122	563	51
300 μm	233	330	30
150 μm	240	90	8
Sieve pan	90		
Total	1110		

As will be described in the following section, a concrete column with variation in concrete porosity was constructed. However, since the concrete strength was not a major concern during the research, standard cubes were moulded only with concrete placed in the first layer, which represents a "sound" concrete. Cubes were crushed at 8, 14, 21, 28 and 60 days and the results are shown in Table 6.2. The specimens were prepared according to BS 1881[175].

The water/cement ratio was maintained constant in all parts of the experimental model, as water has a major influence on dielectric constant values.

Table 6.2 Compressive tests results for concrete

	Compressive strength (N/mm^2)				
	Concrete age (days)				
	8	14	21	28	60
Cube 1	35.9	36.6	42.7	42.3	48.1
Cube 2	32.5	39.4	40.8	46.2	48.0
Average	34.2	38.0	41.8	44.3	48.0

6.2.2 Experimental model

A concrete column was set up for obtaining the experimental data. The column was moulded with five layers of different concrete to simulate the presence of different porosities. Variation in porosity was achieved using a well compacted concrete, concrete without compacting and concrete short of sand. Thus, honeycombing was also expected to influence the radar data.

The choice of a column as the experimental model was advantageous because it could allow collection of data with the antennas either stationary or moving.

No artificial methods were employed to simulate honeycombed concrete. The idea was keep the concrete conditions as close as possible to those which could be found in real structures, despite not giving uniform porous mixtures.

The dimensions of the column were established to be compatible with the size of the antennas. The Figure 6.1 represents a typical layer of concrete.

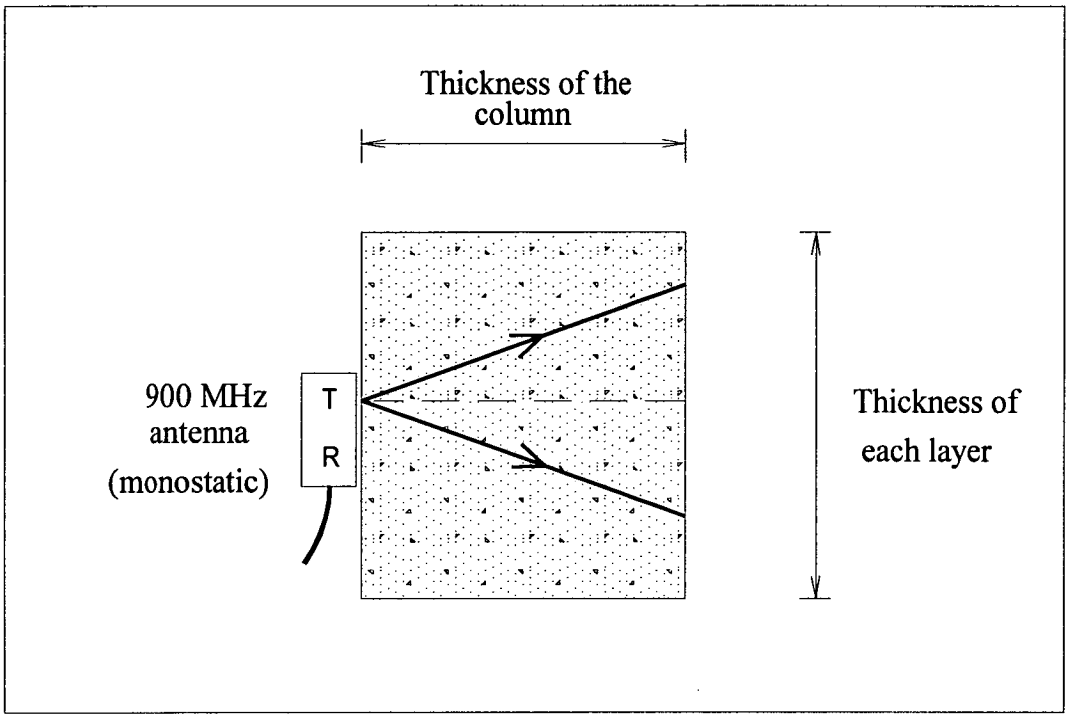

Figure 6.1 Schematic representation of a concrete layer

The thickness of the column was assumed to be at least the signal predominant wavelength in concrete. The wavelength increases with smaller dielectric constant values. Thus, applying equation (3.41) (lowloss materials) for dry concrete (ε_r= 6) and 900 MHz antennas,

$$\lambda = \frac{300}{f\sqrt{\varepsilon_r}} = \frac{300}{900\sqrt{6}} = 0.13 \text{ m}$$

Possible distortion of the waves during propagation can occur which will enlarge the predominant wavelength. Given the presence of the common input signal in the initial part of radar records, a dimension of 0.50 m was adopted.

The thickness of each layer was defined taking as basis Table 5.6 (section 5.3.4). Assuming as maximum depth the column's thickness (0.50 m), ε_r = 6 and 900

MHz antenna, Table 5.6 gives a value 0.43 m. Again a value of 0.50 m was chosen.

The final model resulted in a cross section of 0.50 x 0.50 m and a total height of 2.50 m, as shown in Figure 6.2. The composition of concrete at each layer is described bellow:

- 5th layer (top layer): full mix, well compacted concrete
- 4th layer: 67 % less sand, low compacting
- 3rd layer: 33 % less sand, low compacting
- 2nd layer: full mix, no compacted concrete
- 1st layer (bottom): full mix, well compacted concrete

According to Figure 6.2, two metal bars with diameter 20 mm were embedded at each layer, to produce reflections from variable depths. The dimensions chosen for the model allowed for placing the bars in order to obtain reflections from 100 and 200 mm depths at one side (face D), and 300 and 400 mm depths when readings were taken from the opposite side (face B). Furthermore the bars' vertical spacing was fixed following the suggested values given in Table 5.6 for spatial resolution. This should allow to "see" the deeper bars.

A view of the column after striking the formwork can be seen in Plates 6.1 to 6.3. The variation in the surface texture at each layer is clearly noticeable.

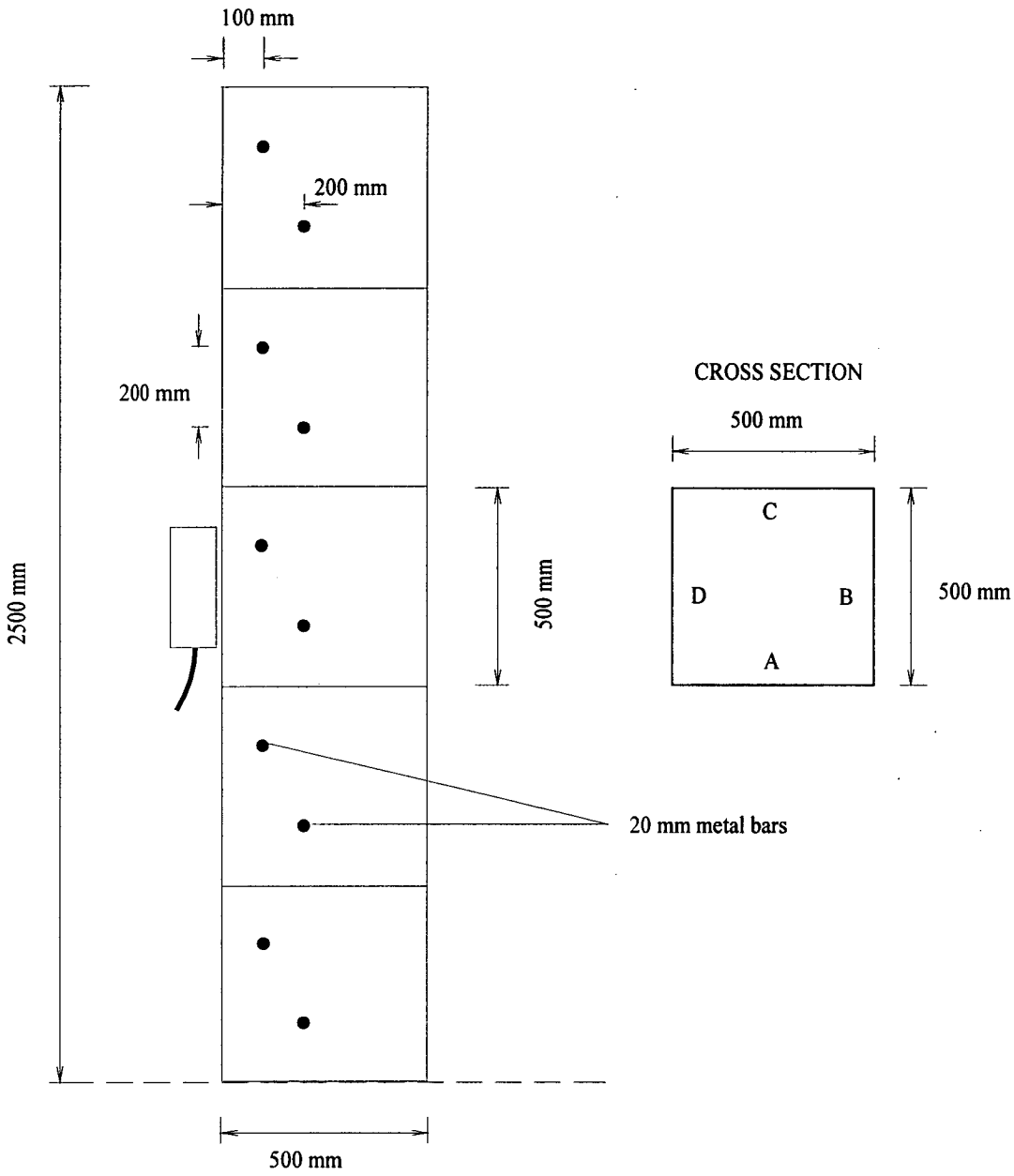

Figure 6.2 Experimental model

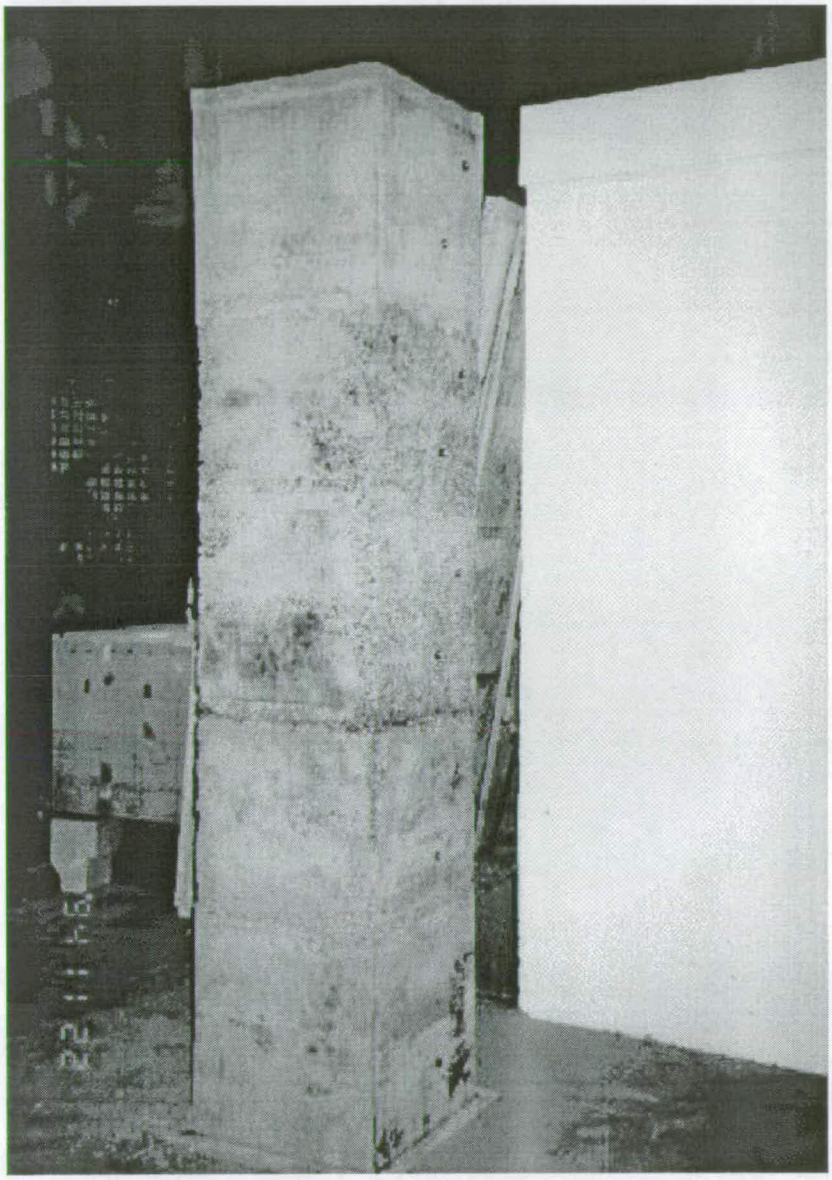

Plate 6.1 General view of concrete column after striking

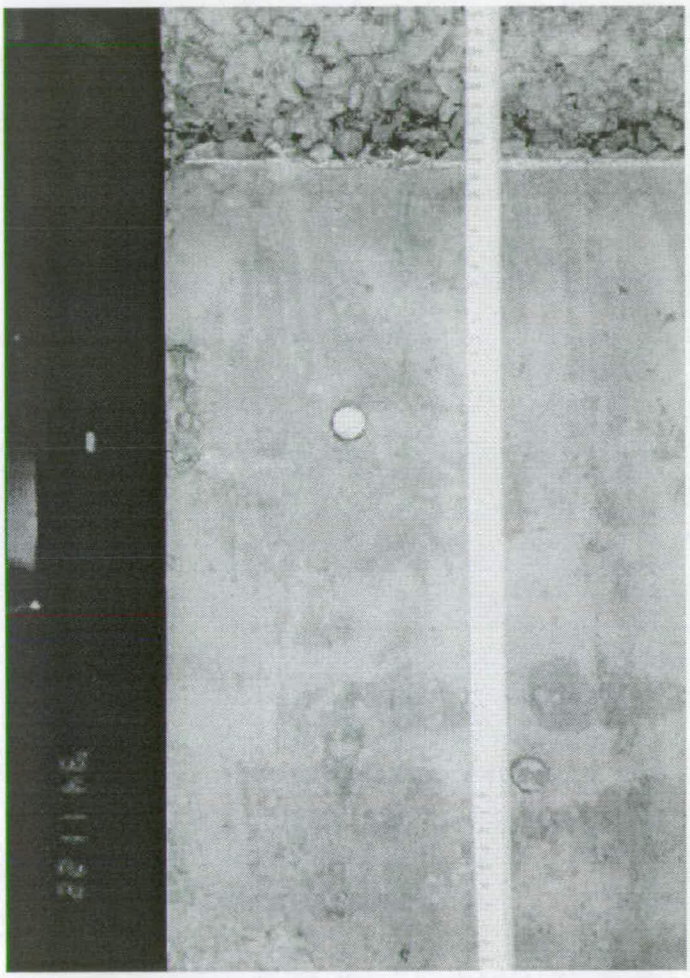

Plate 6.2 Concrete column: transition from 2nd to 3rd layer

Plate 6.3 Concrete column: transition from 4th to 5th layer

6.3 DESCRIPTION OF THE EQUIPMENT

Radar has a quite wide range of potential applications as described in chapter 3. The control unit and monitor are the same no matter the nature of field work: geophysics, engineering, archaeology, etc. Depending on the purpose of the survey the proper antenna has to be chosen, always with the compromise between the depth of exploration and desirable resolution. The latter subjects were numerically analysed in chapter 5.

This section presents a general description of the equipment used during the experimental works. The radar system available was a SIR SYSTEM-10, manufactured by Geophysical Survey Systems, Inc. (GSSI). It is a multichannel system that can automatically display, process and record profiles of subsurface objects or interfaces with up to 4 transducers at same time (See Plate 6.4). Its main features and specifications are listed below [176]:

- Built-in 19 cm EGA monitor for real time and wiggle plot display of the data.
- Data storage unit, which uses 8 mm Exabyte cartridges and has capacity to record and playback up to 2.3 Gbytes of data, either 8 bit or 16 bit.
- Real time digitally controlled gain and functions for high signal to noise data quality.
- Floppy disk drive 3.5", 1.44 Mb.
- Permits post-processing of data either on site or after transferring them to a computer, using a commercial software called RADAN which is provided with the equipment when required.
- Contains a DC and AC plug-in power supply module.
- Transmit pulse repetition rate: 2 to 78 kHz.
- Analogue to digital sampling: 128, 256, 512 or 1024 samples per scan
- RAM memory: 4 Mb (expandable up to 20 Mb);
- Scan rate: 0.2 to 128 scans per second;
- Range: 4 to 10,000 ns;

- Range gain: -26 to 120 dB;
- Filters: vertical (time domain) and horizontal (spatial domain).

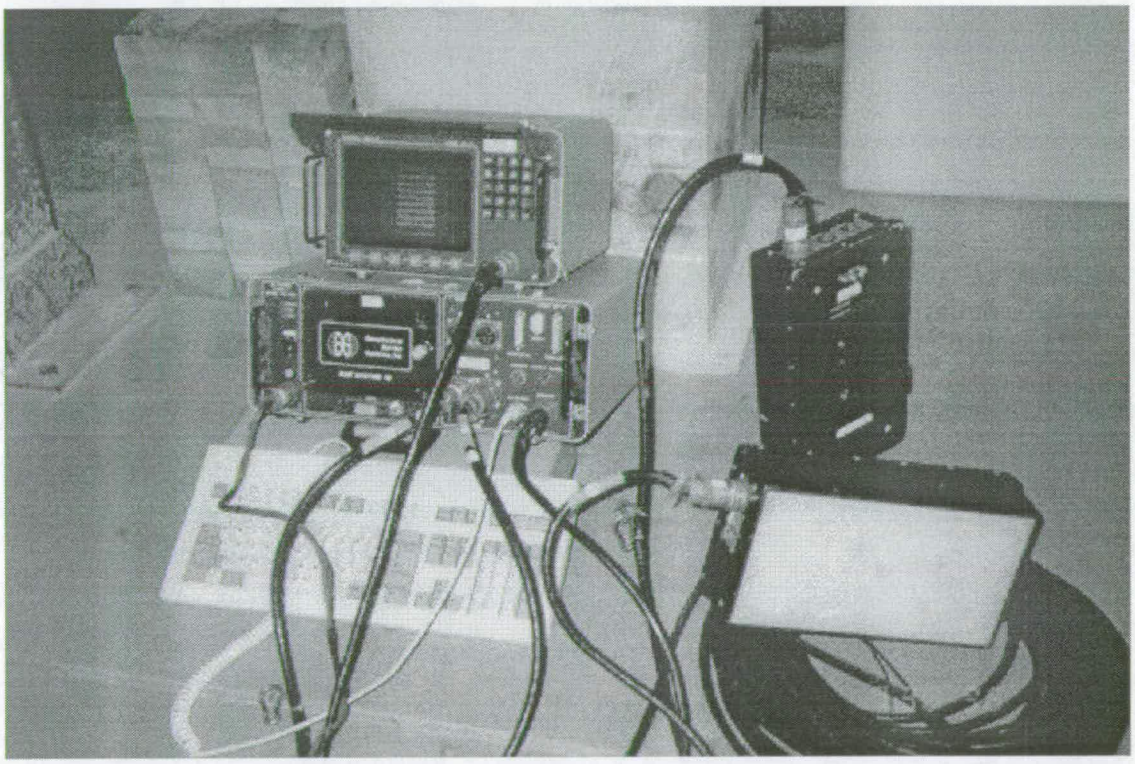

Plate 6.4 SIR-10 GSSI Multichannel Radar System

The connector panel allows one to attach the following facilities:

- Marker, to produce tick marks on the data;
- Survey wheel, for automatic tick marks and horizontal distance scaling;
- Graphic recorder, for real time paper copy output of the data;
- Colour printer;
- Mouse, for use with Radan software and to transfer data to an external computer;
- PC/AT compatible keyboard for editing the data files, for running the Radan software and to modify the menu structures.

This system is compatible with all antennas manufactured by GSSI. Two types of antennas are available, which permit continuous profiling and stationary position data collection.

a) Dipoles or ground-coupled antennas
   - Monostatic: 80, 100, 120, 300, 500, 900, 1000 MHz
   - Bistatic: 15, 20, 30, 40, 80, 120, 300 MHz

b) TEM Horn or air-coupled antennas (non shielded)
   - 1.0 GHz and 2.5 GHz (Bistatic)

These antennas all have a broad bandwidth of frequencies. Most are designed for a ratio" bandwidth/centre frequency" as close as possible to unity. This means that larger values of centre frequency will be associated with the higher range of frequencies, and smaller pulse widths. The significance of this is that signal dispersion and consequently waveform distortion (variation in shape) may be detectable by analysing the frequency spectra.

The bandwidth may be measured in practice as the range of frequencies over which the magnitude exceeds $\sqrt{1/2} \cong 0.71$ times its maximum in the frequency

spectrum[156]. Taking the power spectrum, it would be the range of frequencies that exceeds half the maximum power. The latter is also called the -3 dB bandwidth, if power values are converted to decibels.

For most of the experimental work 900 MHz bowtie monostatic antennas (model 3101) with in-built transmitter and receiver were used. They may be employed either in transmission mode, where one acts effectively as transmitter and the second as receiver, or in reflection mode with only one antenna.

Bowtie antennas are a form of horizontal dipole with a width approximately equal to half a wavelength of the dominant frequency in free space, and are schematically depicted in Figure 6.3. They are designed with an impedance for specific ground conditions. However in practice, due to the variety of materials, the impedance will not match and likely coupling problems will arise with possible changes in the amplitude, shape and phase of the radiated waves.

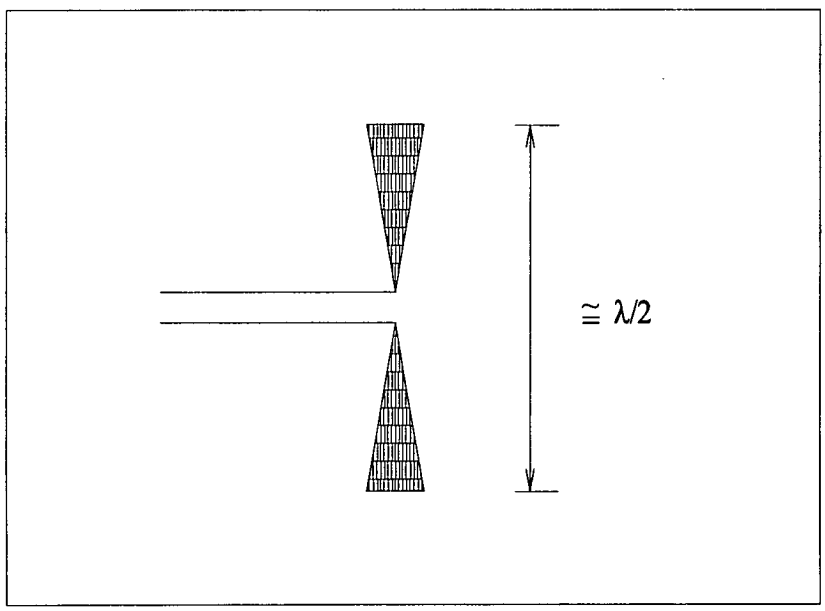

Figure 6.3 Schematic bowtie dipole antenna

A 900 MHz monostatic antenna may then be represented as shown in Figure 6.4.

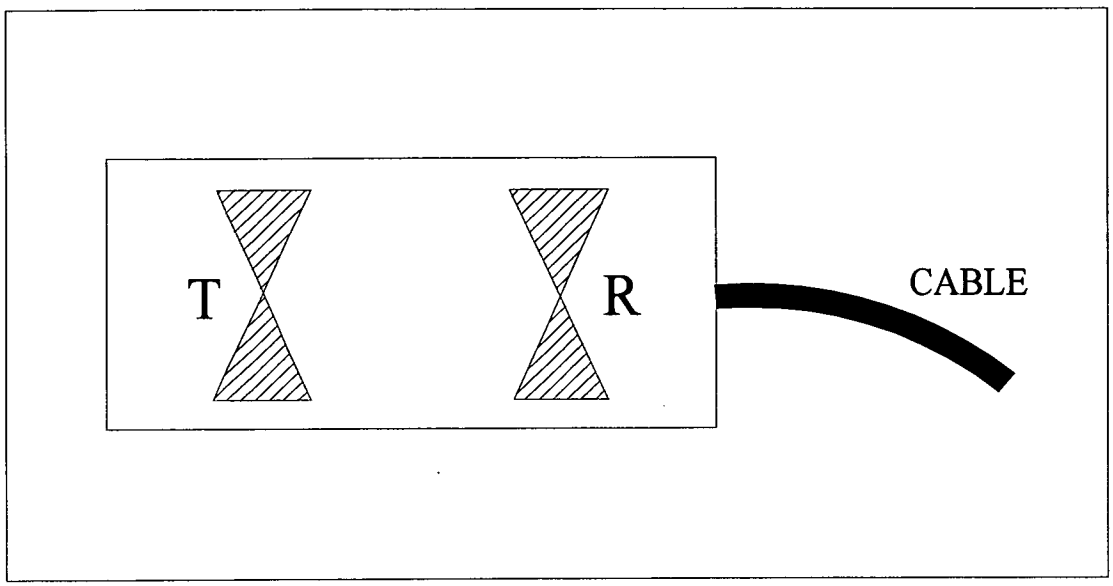

Figure 6.4 900 MHz monostatic antenna - projected view

The basic operative principles of the whole system were already described in section 2.2.4. Radar systems and design of antennas represent a well established and highly specialized field and will not be covered in this work. Further details can be found in Daniels [65], Kraus [62] and Skolnik [177].

6.4 PRELIMINARY TESTING

Before starting to collect radar experimental data from the concrete column, a set of preliminary tests were performed with the antennas to see whether they were working properly. During the whole analysis only the principal part of the recorded signal was considered, as described in chapter 4.

6.4.1 Antennas coupled to air

Manufacturers normally specify the nominal centre frequency with the antennas coupled to air. However, these values may change after using the antennas for long time, due to the electronics decay and/or bad handling. For instance, dropping an antenna may damage the dipoles and thus modify the frequency spectra either of the transmitted or received signals. This problem was once detected when a 1 GHz antenna was tested in air and presented a centre frequency of about 700 MHz rather than the specified one. After carrying out a reciprocity test (described later) it was concluded that the problem was localised at the in-built receiver. Besides, even two new antennas bought at the same time will not necessarily possess an identical frequency range, due to their manual construction.

The two 900 MHz antennas selected for the experiments were then tested in air to check their radiated frequency contents. The results are shown in Figure 6.5, with both antennas giving similar values for the centre frequency (854 MHz and 885 MHz, respectively) and quite close to the specified ones.

6.4.2 Reciprocity test

Here the idea was to evaluate the response of each antenna when working as a receiver to verify the reliability of the recorded signals in the transmission mode. Two 900 MHz antennas were placed 1.00 m apart, one acting as transmitter and the second as receiver, according to Figure 6.6 .

The recorded signals in time domain and respective frequency domain spectrum can be seen in Figure 6.7, which indicates that the antennas were performing coherently.

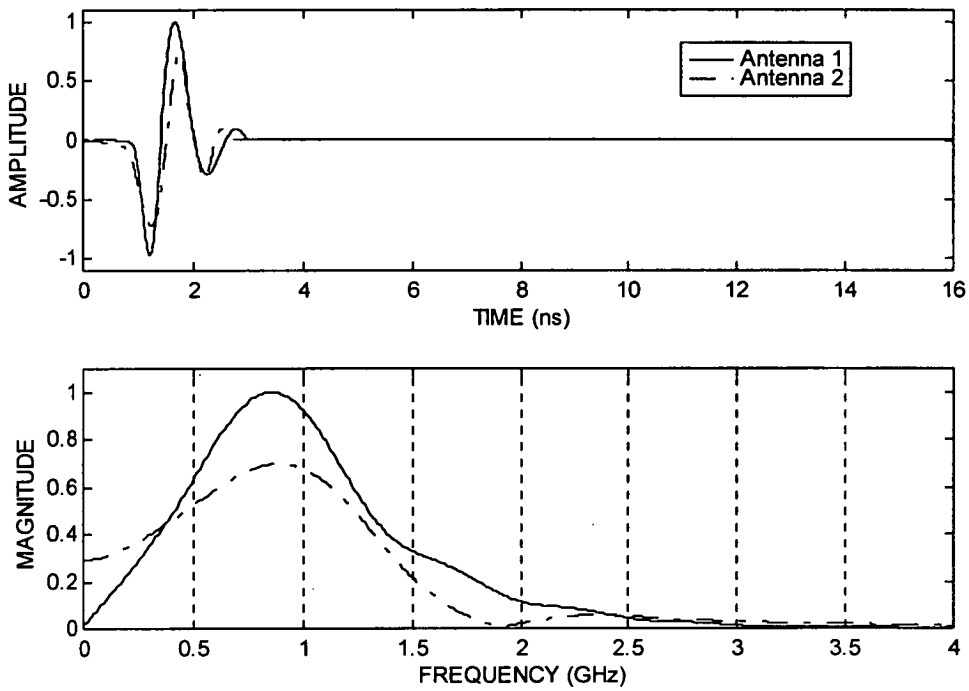

Figure 6.5 900 MHz bowtie monostatic antennas tested in air

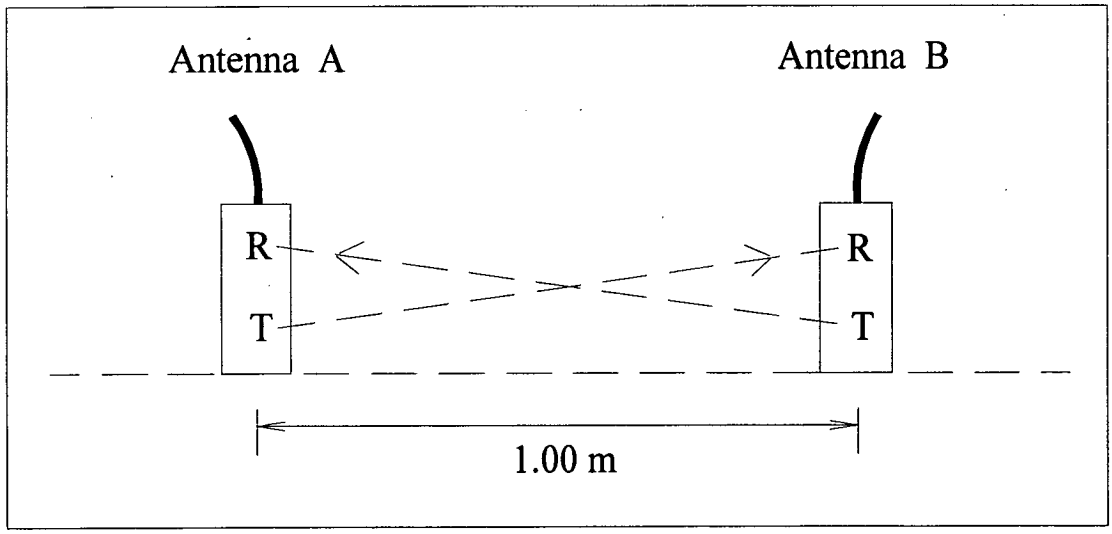

Figure 6.6 Schematic representation for the reciprocity testing

The main quantitative information is listed below.

Transmission from A to B:

Centre frequency= 875 MHz

Peak intensity= 73.8 dB

- 3 dB bandwidth= 609-1140 MHz

Transmission from B to A:

Centre frequency= 885 MHz

Peak intensity= 73.3 dB

- 3 dB bandwidth= 620-1151 MHz

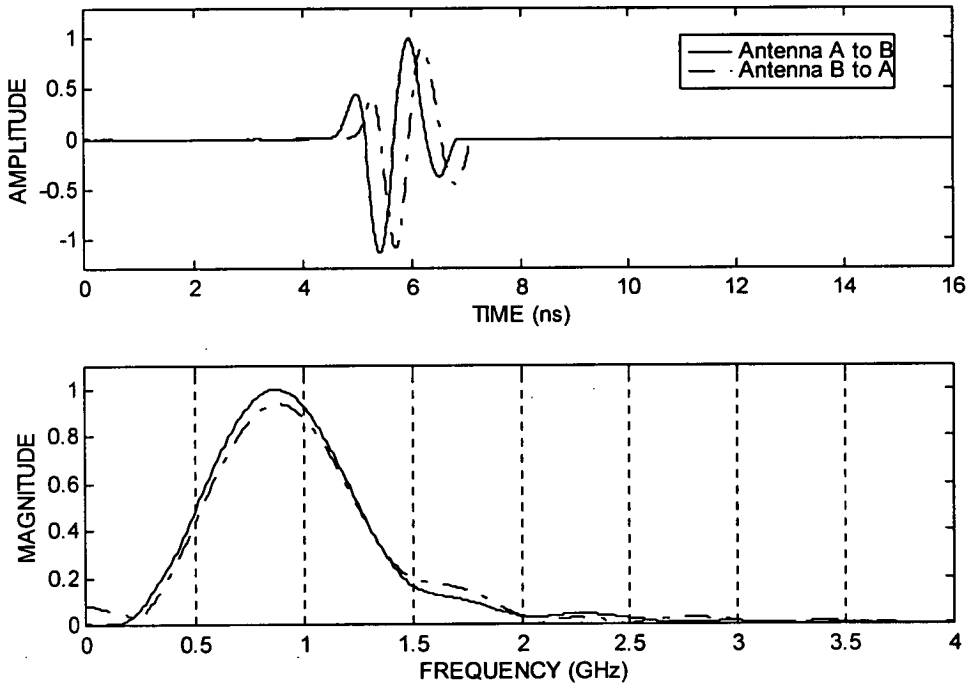

Figure 6.7 Reciprocity testing with 900 MHz bowtie monostatic antennas

6.4.3 Energy spreading

Each antenna radiates the energy following a pattern depending on the field considered: electric or magnetic. Figure 6.8 shows a typical radiation pattern for high frequency antennas. In this experiment the readings in the transmission mode were taken for angles at or close to zero degrees, i.e. the antennas were mostly at opposite

positions. However, due to the spreading effect as the waves propagate, the energy at each particular direction will decrease with distance.

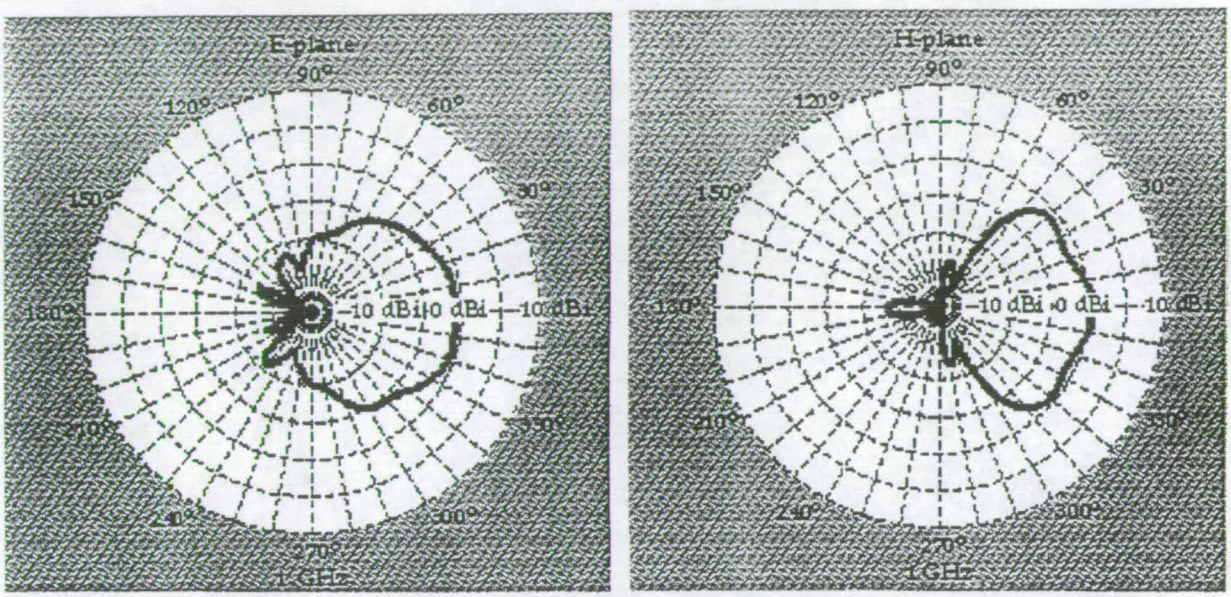

Figure 6.8 Typical radiation pattern for high frequency antennas, after Warhus [178]

In order to see the consequences in terms of frequency spectra, a transmission test was made with two 900 MHz antennas in air (see Fig. 6.9), and also in reflection mode with one antenna directed to a metal plate. The results for the first case can be seen in Figure 6.9, for a distance between antennas 0.50, 1.00 and 1.50 m. Basically the centre frequency remains the same (differences < 10 %), despite showing a decrease in the centre frequency magnitude of nearly 60 % when moving the antennas from a position of 0.50 m to 1.50 m apart.

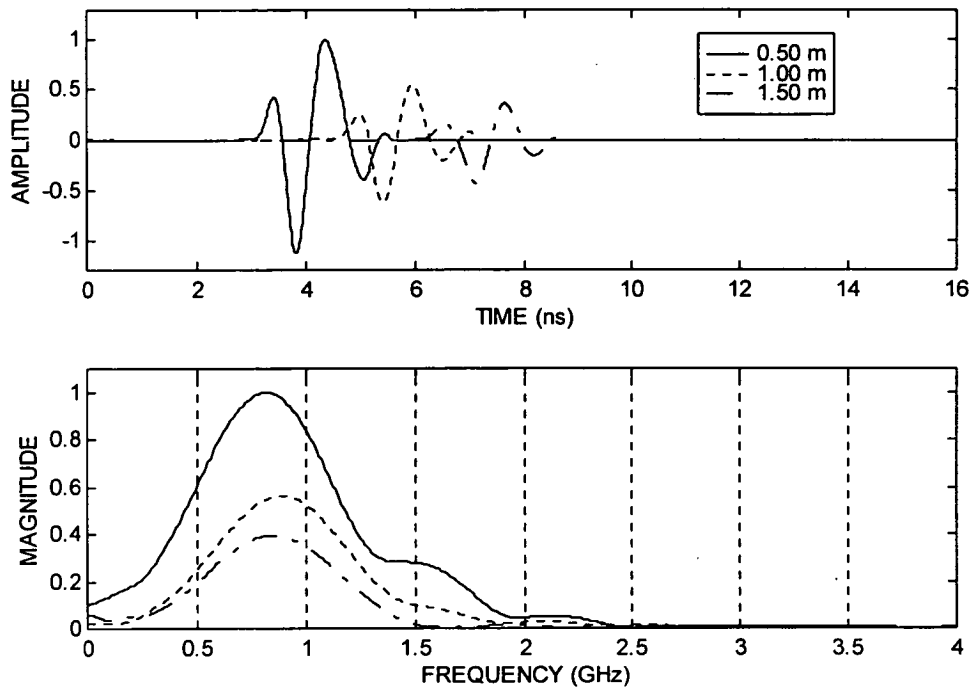

Figure 6.9 Effect of energy geometrical spreading on the main frequency spectra, at distances of 0.50 m, 1.00 m and 1.50 m

Regarding the reflection mode, with one 900 MHz antenna directed against a metal plate (total reflection), the incident waves picked up by the receiver contain practically the same frequency components. As expected, the recorded signals contain much less energy due to the beam spread, as shown in Figure 6.10.

As a main conclusion, no distortion is produced in the waves when propagating in air, for the existing conditions. However different materials representing the media and reflectors may affect the characteristics of the recorded signals. Energy loss will exist and dispersion may occur, mainly owing to absorption and heterogeneity causing scattering.

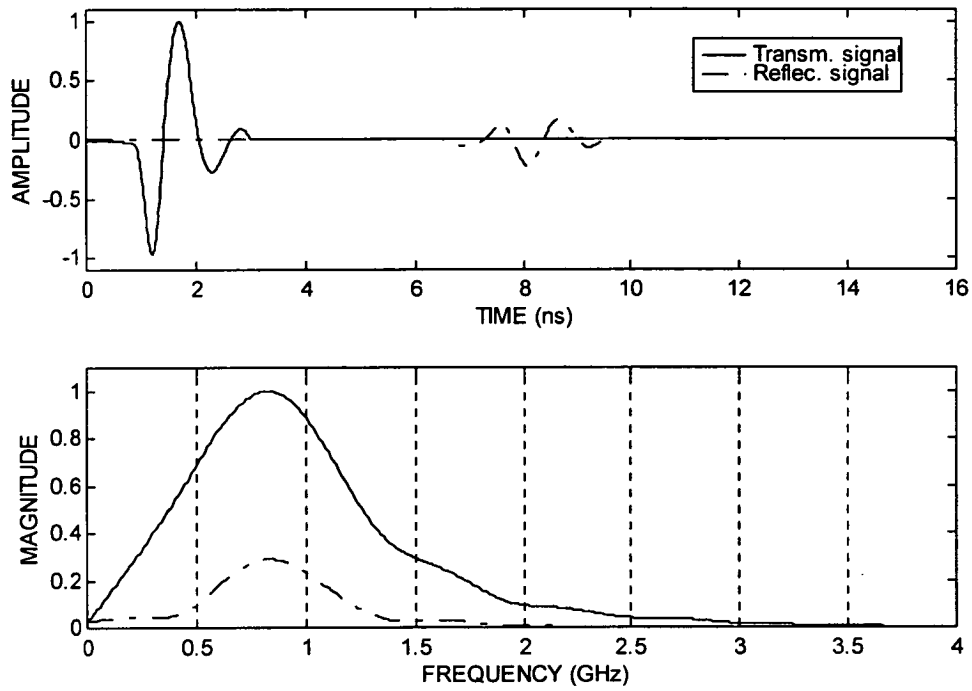

Figure 6.10 Reflected signal from a metal plate (900 MHz antenna, 1.00 m away)

6.4.4 Polarization of antennas

"The polarization of a uniform plane wave refers to the time-varying behaviour of the electric field strength vector at some fixed point in space" [126]. The antennas employed in GPR are normally designed to radiate energy with a predominant orientation of the electric field, classified as linearly polarized antennas. Thus, when using two bowtie antennas the common procedure is to take the readings with the dipoles aligned, thereby achieving the strongest recorded signals.

The polarization of dipole antennas can be verified taking readings firstly with the antennas aligned and after crossing the dipoles. In the present case the 900 MHz antennas were tested and the results are shown in Figure 6.11. The very weak signals recorded for crossed dipoles indicates a good polarization of these antennas.

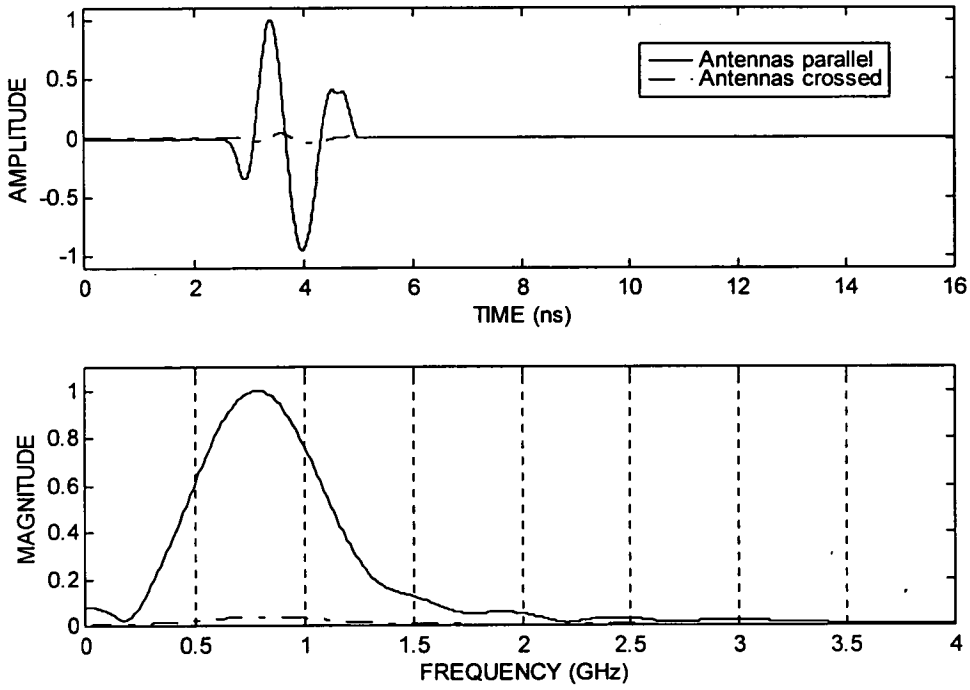

Figure 6.11 Polarization test for a pair of 900 MHz antennas

6.4.5 Influence of the antennas' size and the relative position of the antennas' cables

For transmission mode operation the antennas are normally positioned according to Fig. 6.6, with the cables at the same side. Regarding monostatic antennas, the in-built receiver is located near the cable conector. The distance between transmitter and receiver in a 900 MHz antenna is approximately 16 cm. As a result the travel path length between transmitter and receiver of different antennas will be greater than the horizontal distance between them, as indicated in Figure 6.12 below.

The aim here was to verify the influence of antennas' relative position in the travel time readings. Two 900 MHz antennas were placed 0.50 m apart, initially in air, according to positions "a" and "b" shown in Figure 6.13 as usual in practice.

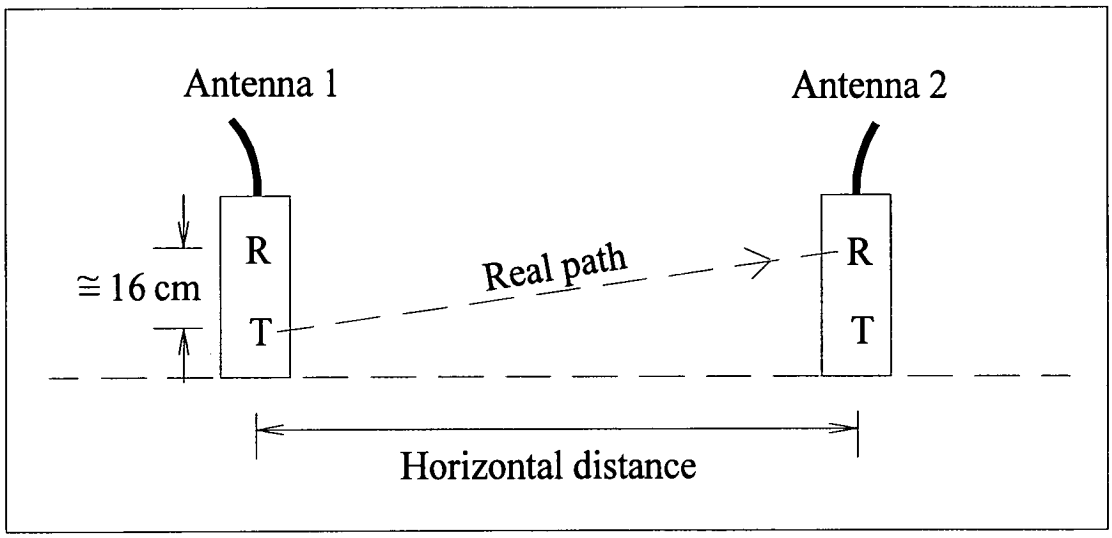

Figure 6.12 Effect of path length using 900 MHz antennas

The signal recorded in time domain and respective frequency spectra are given in Figure 6.14. It is noticeable that there is a small advance in travel time (≅ 0.08 ns) and an increase of nearly 10 % in the magnitude of the centre frequency for the real path (position "b"). For the antennas 1.00 m apart the results are respectively 0.06 ns and 7 %, indicating less influence with increasing distance.

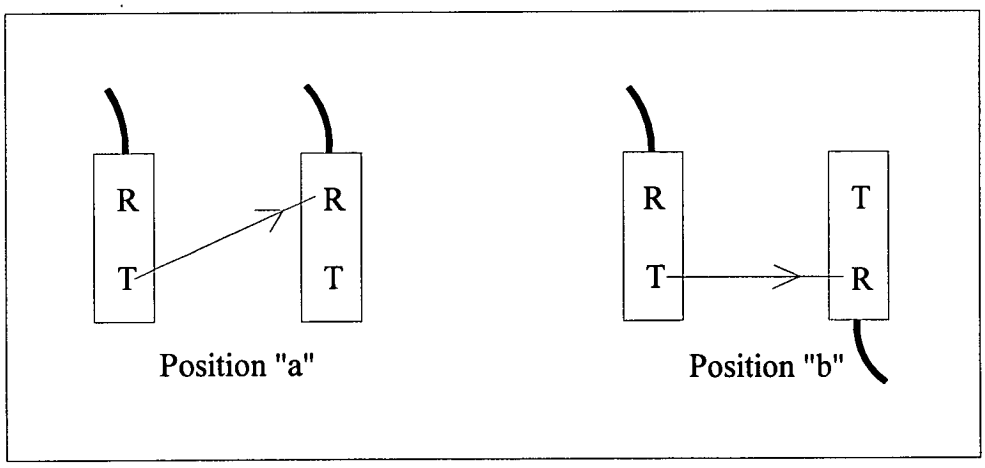

Figure 6.13 Relative positions of antennas for transmission mode

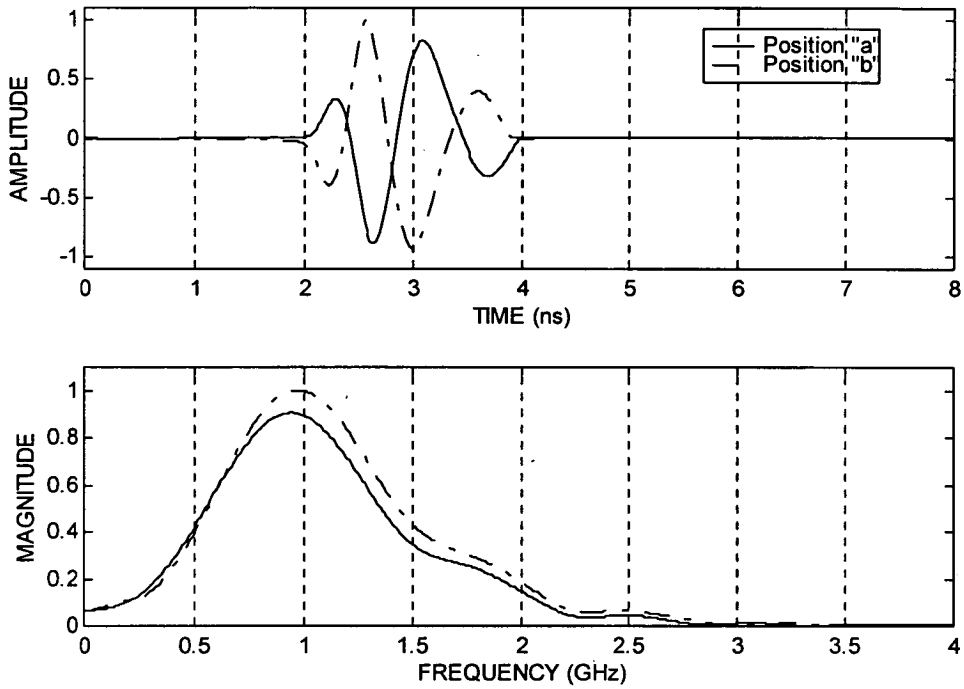

Figure 6.14 Effect of antennas' position in travel time and frequency spectra for transmission mode in air

Another aspect to be observed in Figure 6.14 is the signal phase change according to the position of the receiver. This may confuse the interpretation of the results if the positions of the antennas are used in a random way.

The same test was carried out on the experimental concrete column described in section 6.2.2, for normal laboratory conditions. Typical results can be seen in Figure 6.15, where one can notice a more pronounced variation in travel times. The waves for antennas' position "b" arrived 0.20 to 0.25 ns earlier, and the magnitude of the centre frequency increased 70 to 100 %. The latter may be particularly relevant regarding the level of recorded signals' amplitude for the concrete thickness.

a) Results of 2nd concrete layer

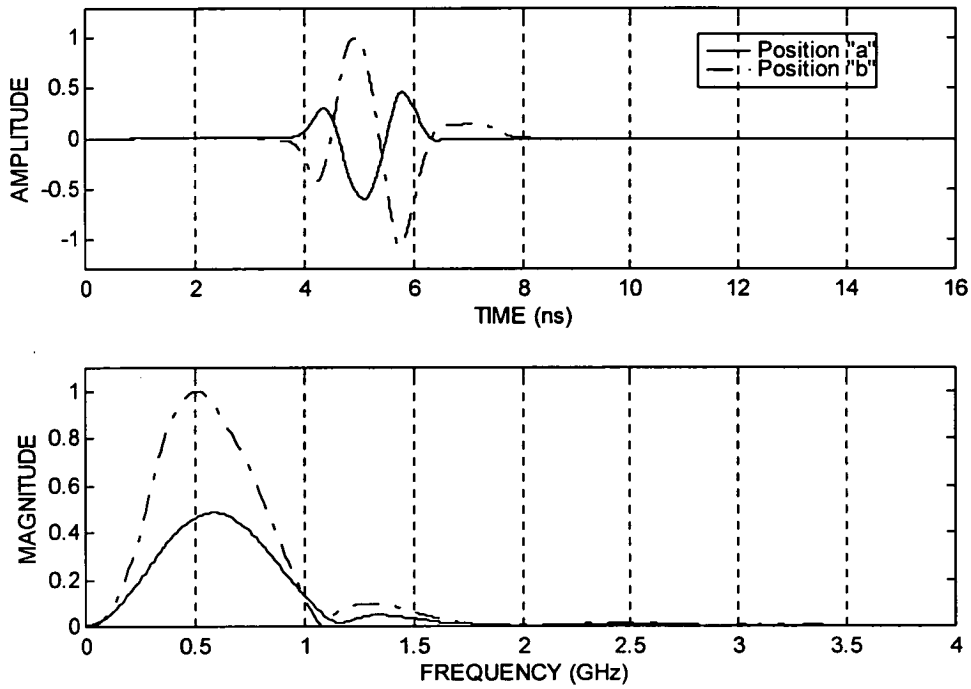

b) Results of 3rd concrete layer

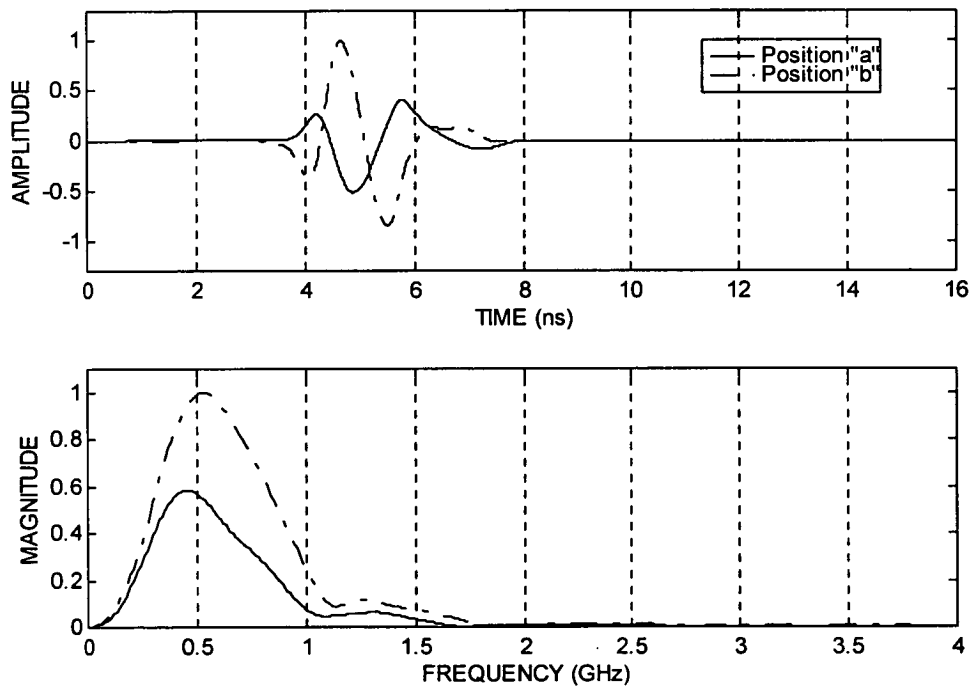

Figure 6.15 Influence of antennas' relative position for waves travelling through concrete at two different layers

A numerical analysis was undertaken in order to see how important the difference in terms of travel time is, for practical purposes, for both transmission and reflection modes. In the first case the following was assumed:

- antennas position "a"
- filling material: concrete with low conductivity
- thickness = 20 cm
- dielectric constant = 6
- real path length (Fig. 6.12) = 25.6 cm (travel time = 2.10 ns)

If the real path is ignored and simply the thickness of concrete is considered for the assumed travel time, the resulting dielectric constant would be 10 (+66 %). For a saturated concrete (ε_r = 12), where an expected travel time is of the order of 3 ns, taking instead the horizontal distance the dielectric constant would compute to be approximately 20.

The implication of this potential anomaly relating to the 900 MHz antenna on the dielectric constant values for other thicknesses can be seen in Figure 6.16. The variation in dielectric constant values will be less than 10 % for thicknesses above 50 cm at any concrete conditions.

In the reflection mode, a monostatic 900 MHz antenna was placed on one side of the column according to Figure 6.17. In this case the size of the antenna (or the physical separation between transmitter and receiver) is the main factor. For the same range of thicknesses assumed in the former case, the results are given in Figure 6.18. Here the variation in ε_r may vary up to 16 %, and will be less than 10 % for thicknesses larger than 25 cm for the same concrete conditions.

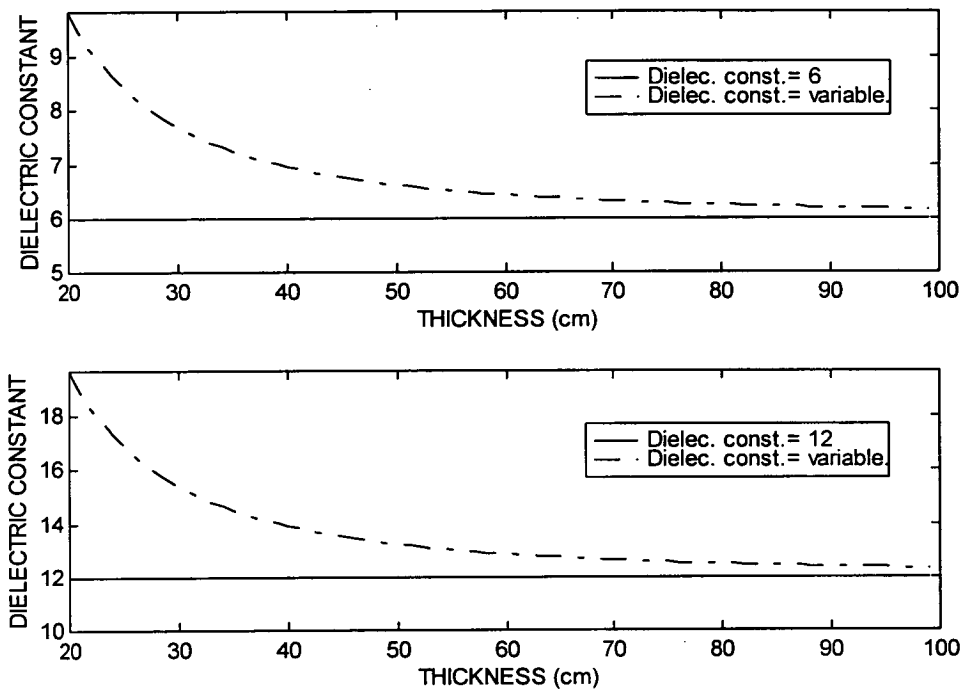

Figure 6.16 Effect of path length on dielectric constant values (transmission mode)

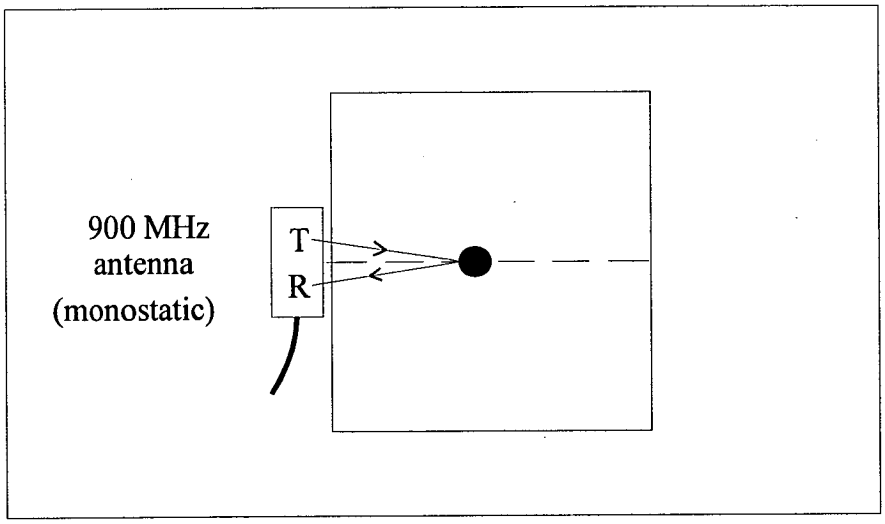

Figure 6.17 Monostatic antenna in reflection mode

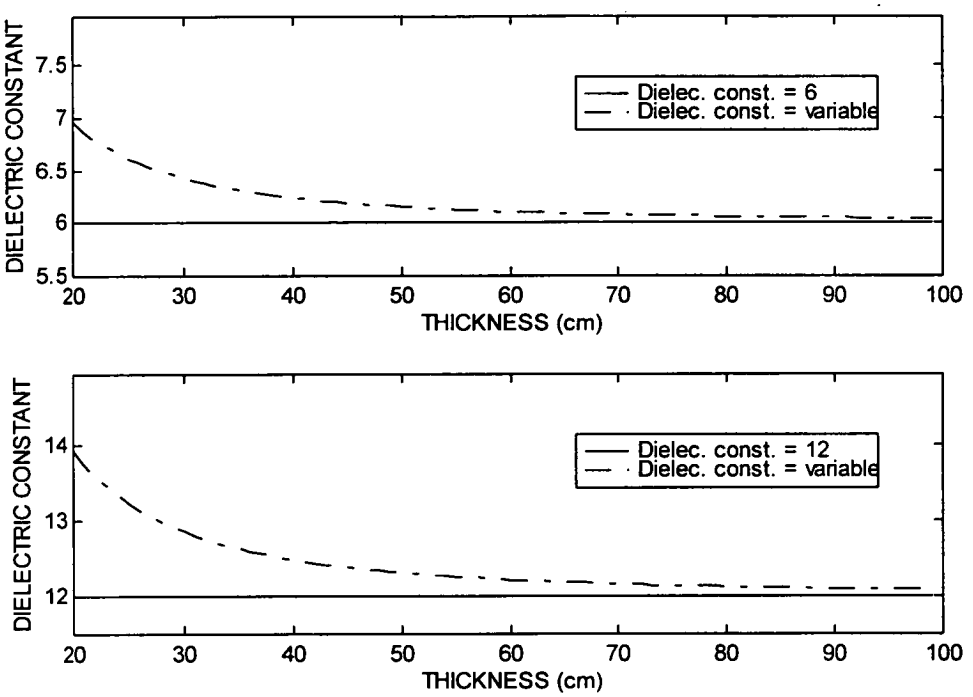

Figure 6.18 Effect of path length on dielectric constant values (reflection mode)

The main conclusion that may be inferred from the present study is that for known travel times the values for dielectric constants may be overestimated by more than 10 % when employing 900 MHz monostatic antennas, depending on the concrete element thickness. This fact should not be ignored in practice when the thickness is less than 25 cm, and the accuracy either in travel time or dielectric constant measurements is a relevant factor.

6.5 EXPERIMENTAL DATA

In the first part of this section the methodology to achieve data from the experimental model will be presented. This will be followed by the data analysis using the principles and assumptions described in chapter 4, as well as discussion and conclusions of the main results.

6.5.1 Set up of the equipment

The technical specifications of the system used were already detailed in section 6.3. The set up parameters were chosen so that the raw data was modified as little as possible. This included:

a) A constant amplitude gain in time domain, when necessary.

b) A fixed time range of 16 ns that always allowed a full display of the reflected or transmitted signals of interest.

c) One or two channels, using the most appropriate one for each mode of operation.

d) An adequate position to obtain a full display of the input antenna signal. This parameter has assumed variable values when the automatic position was set, depending on the antennas, cables and channels chosen. This problem however has no effect during signal post-processing because either advancing and delays in time domain do not change the frequency spectrum contents.

e) No use of special filters to avoid missing data information. After, filtering could be applied whenever convenient.

f) Other parameters:

- Samples per scan = 1024
- Scans per second = 30 - 40
- Transmit pulse rate = 30 - 40 kHz

6.5.2 Data collection

Referring to Figure 6.2, one may observe that data could be collected at the

four sides of the column, with the antennas either steady or in movement. Therefore it was expected to record reflections from the concrete-metal bar interfaces at 90, 190, 290 and 390 mm depth. The main aim was to analyse the coupling effect in the recorded data when the antennas are placed on concrete, as well as, the distortion of the signals as they propagate through concrete. In order to make the analysis clearly, the readings were taken in two stages: reflection from the metal bars employing only one antenna , and transmission with two antennas at opposite sides of the column.

Reflection mode

The antenna was moved with constant speed along the height of the column. They were polarized with the electric field vector parallel to the metal bars to obtain the strongest reflections. Typical Radar linescans are depicted in Figures 6.19 and 6.20. Figure 6.19 shows a scan obtained with the antenna on side D (bar depths of 90 and 190 mm), while Figure 6.20 depicts bar reflections at side B (290 and 390 mm).

The presence of the hyperbolic signatures, characteristic of reflections from circular targets are quite noticeable. Unfortunately reflections from bars at 390 mm were too weak to be detected, and as a consequence only the bar depths of 90, 190 and 290 mm were considered for the next steps of data analysis. It is likely that moisture content of concrete at the time of the testing was the main reason, causing too much attenuation to the waves. It is worthwhile to remember that in the present case the wave path length is in reality about 800 mm.

Transmission mode

Here the readings were taken with two antennas stationary and placed at opposite sides at each layer of the column. The distance between antennas was always 500 mm, and either one or two channels were used. Whenever necessary data were collected in both directions A-C and B-D.

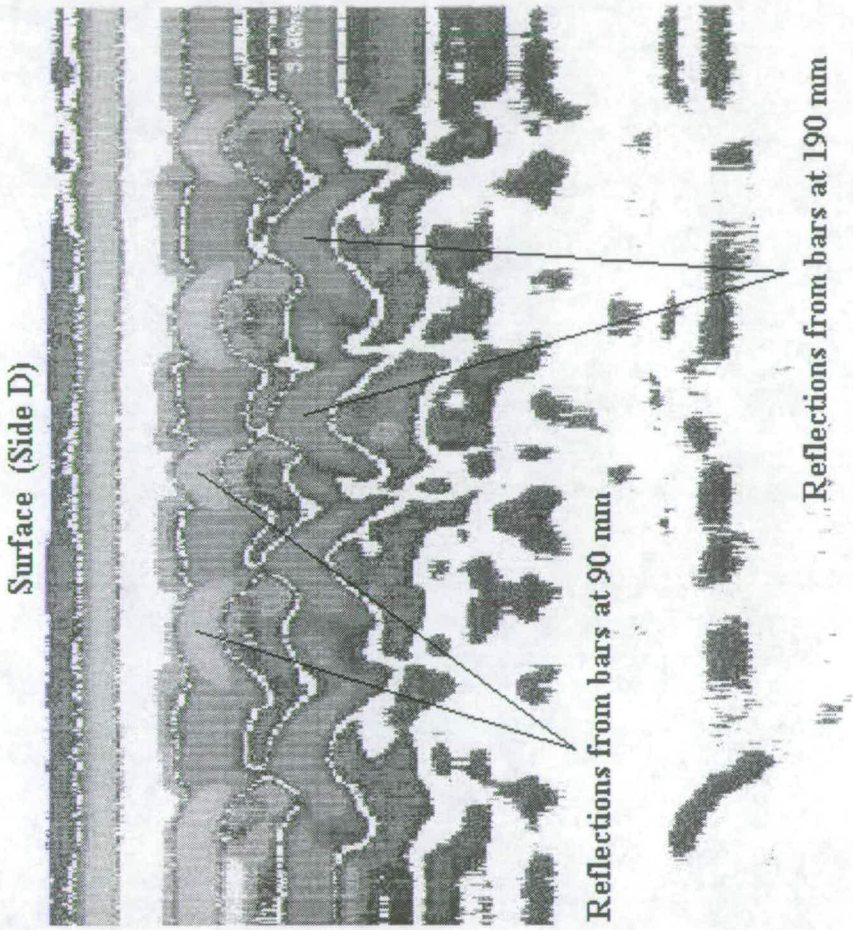

Figure 6.19 Radar scan showing reflections from metal bars at 90 and 190 mm depth (Side D)

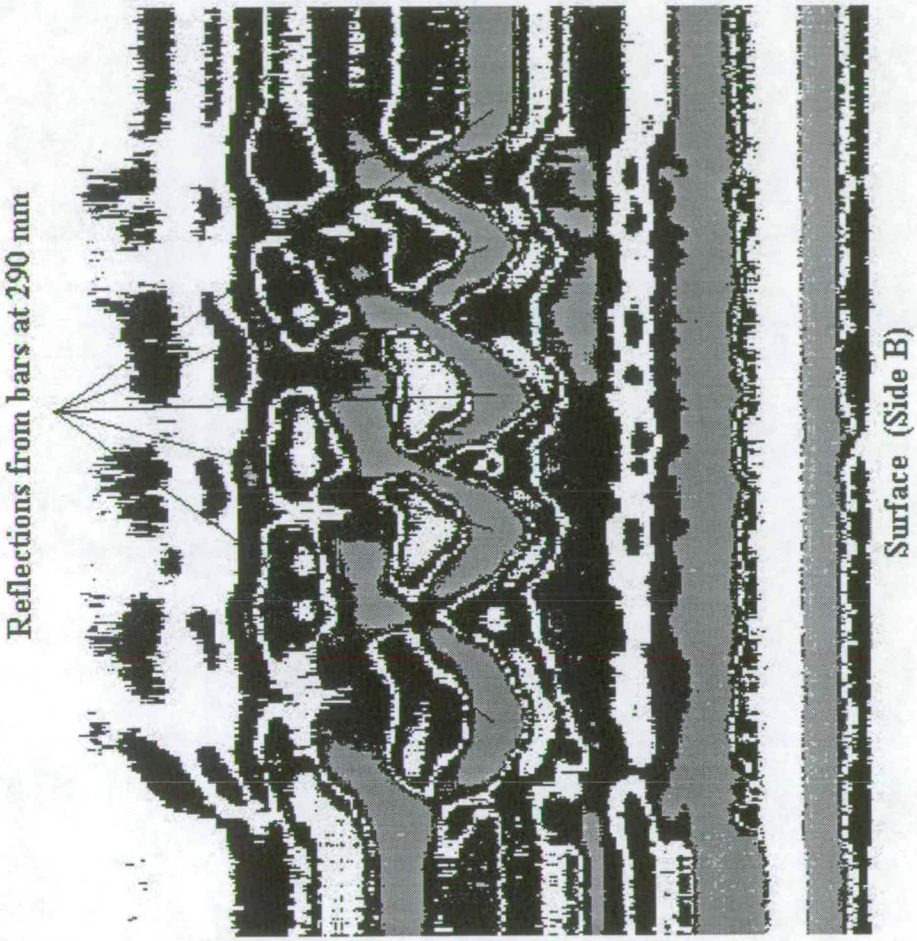

Figure 6.20 Radar scan showing reflections from metal bars at 290 and 390 mm depth (side B), with gain

6.5.3 Signal processing

Files recorded in reflection mode

As mentioned before in section 6.5.1, no special filters were used in the equipment set-up during the data readings. As a consequence, high frequency noise can normally be expected in all data. Given that the use of a temporal low pass filter with a large bandpass does not alter the frequency contents of interest, as verified in chapter 4, all data files were firstly processed in this way. As a result the signals in the time domain come out cleaner.

In fact, the centre frequency of the pulses does not change, which is presently the most important parameter for the interpretation of the results.

Due to the proximity to the surface, primary reflections from bars at 90 and 190 mm have been partially hidden by the strong signal that appears at the beginning of the records. To reveal these reflections a spatial high pass filter (background removal) was applied and the results can be seen in Figure 6.21, derived from the raw data shown in Figure 6.19. The primary reflections are now quite visible and the data still contains the main information for the following signal processing in the frequency domain. This filtering would not be necessary for bars at 300 and 400 mm depth, as their reflections and input signals do not present superposition.

The next step was to obtain single scans corresponding to the antenna when passing over the bars, which represents the strongest reflections and shortest ray path lengths. This was possible using algorithms in the Radan software mentioned in section 6.3, giving as output a single wave plot in the time domain at each vertical bar position. Once having the complete information in the time domain, the data were converted to the frequency domain using the Fast Fourier Transform algorithm (FFT).

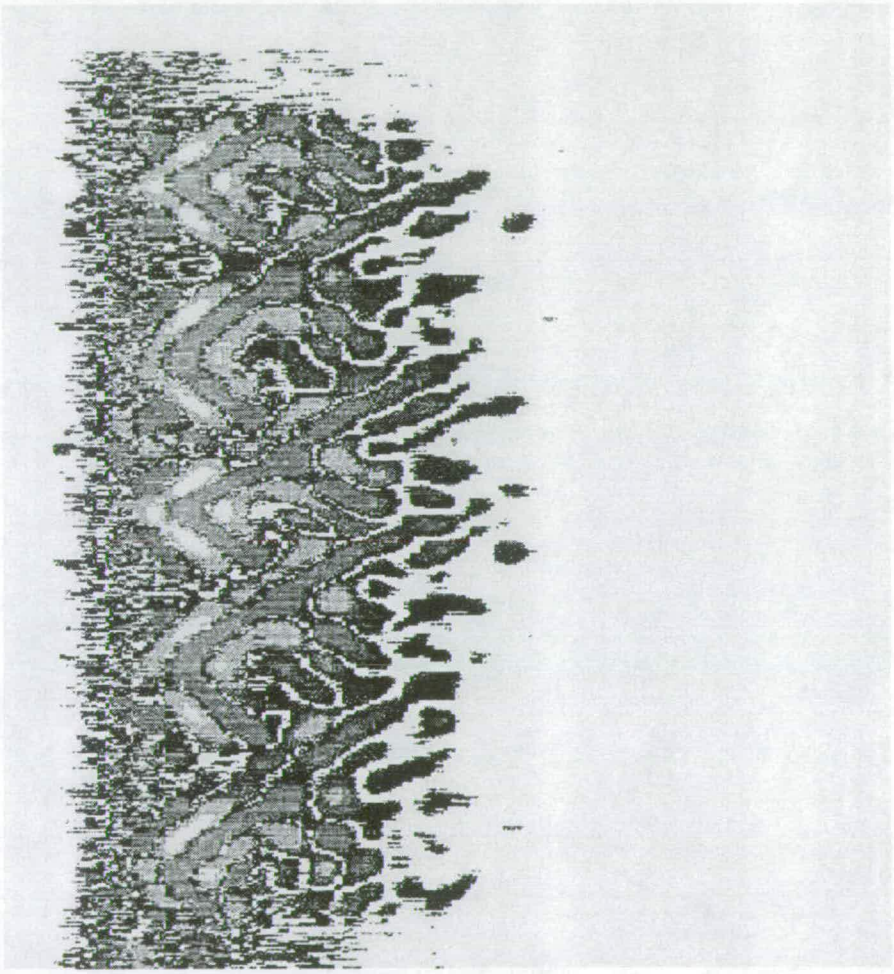

Figure 6.21 Radar data shown in Figure 6.19 after applying horizontal high -pass filter (background removal)

An intermediate step was necessary to convert Radar format data files in common text files, allowing them to be loaded in any commercial graphics software. To do so a small program was written by the technical staff of the Non-Destructive Testing laboratory.

The FFT analysis was carried out using a commercial software called *Matlab* [179], including frequency spectrum, power spectrum and phase spectrum. However due to the aim of the work the results were mostly only presented with the signals in the time domain and their respective frequency spectrum.

Files recorded in transmission mode

In this case all files present constant readings. Therefore background removal is not applicable. Only a temporal low-pass filter was necessary and the single scan files were created by stacking or averaging at least 30 scans of raw data. All the remaining steps were the same as for the reflection mode.

Readings were taken from all five layers, with the objective of verifying, in addition to antenna coupling, the Radar sensitivity to concrete density in terms of travel time, signal distortion and frequency content.

6.5.4 Data analysis

Reflection mode

Individual scans representing reflections from the metal reference bars and corresponding frequency domain spectra are shown in Figures 6.22 to 6.26, for each layer of the concrete column.

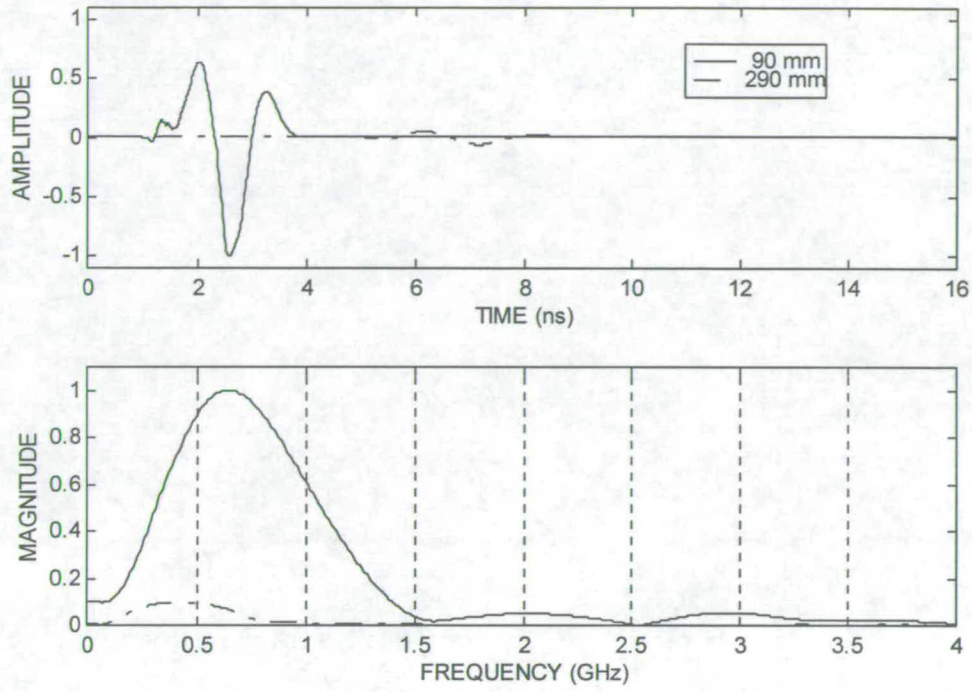

Figure 6.22 Reflections from bars at 1st layer

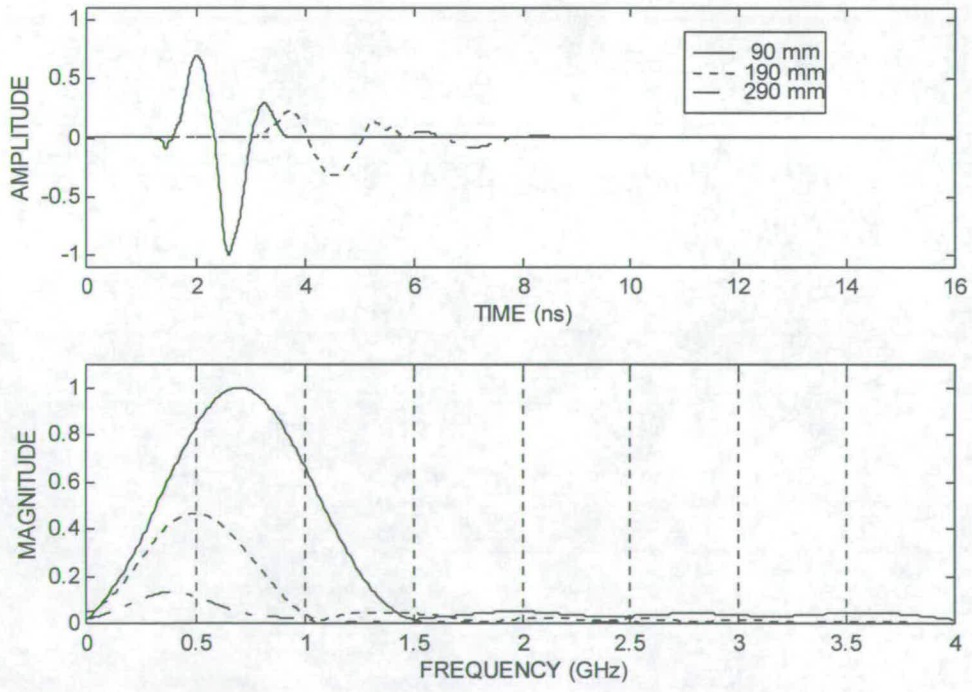

Figure 6.23 Reflections from bars at 2nd layer

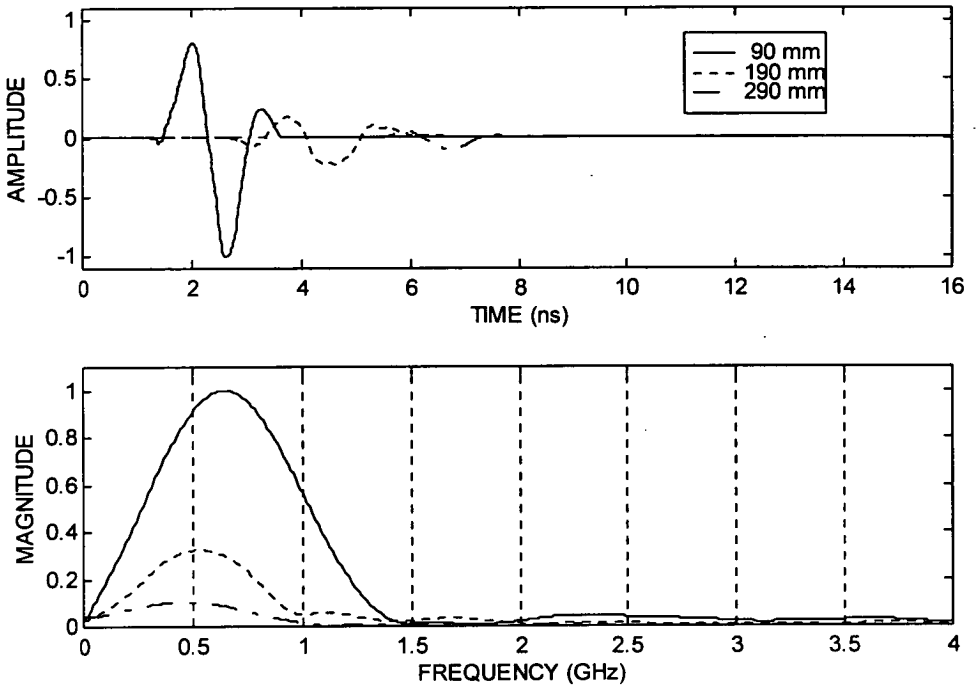

Figure 6.24 Reflections from bars at 3rd layer

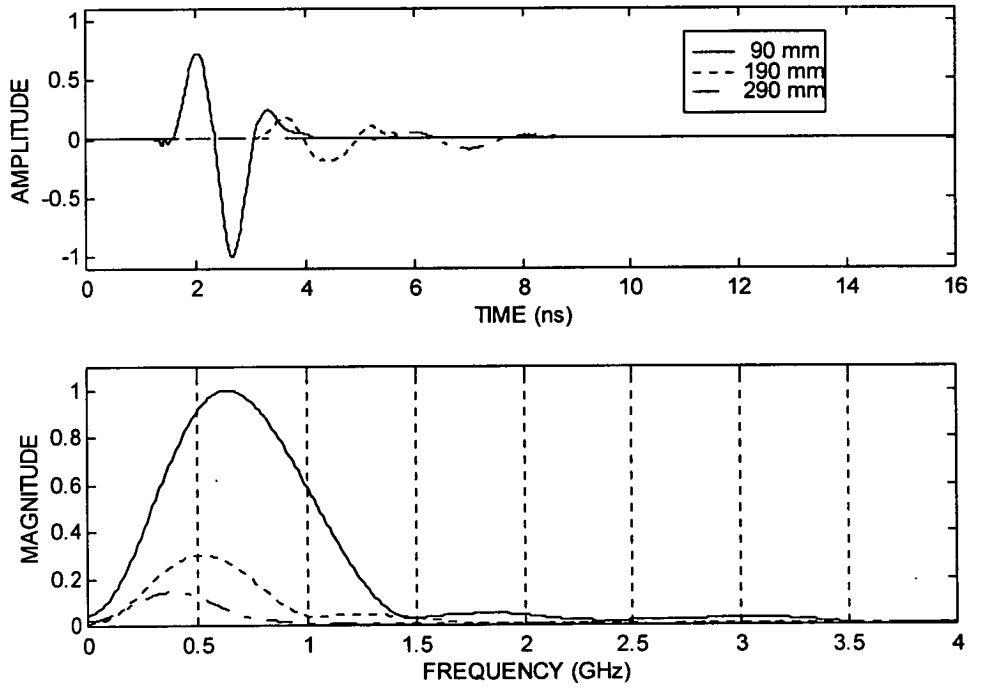

Figure 6.25 Reflections from bars at 4th layer

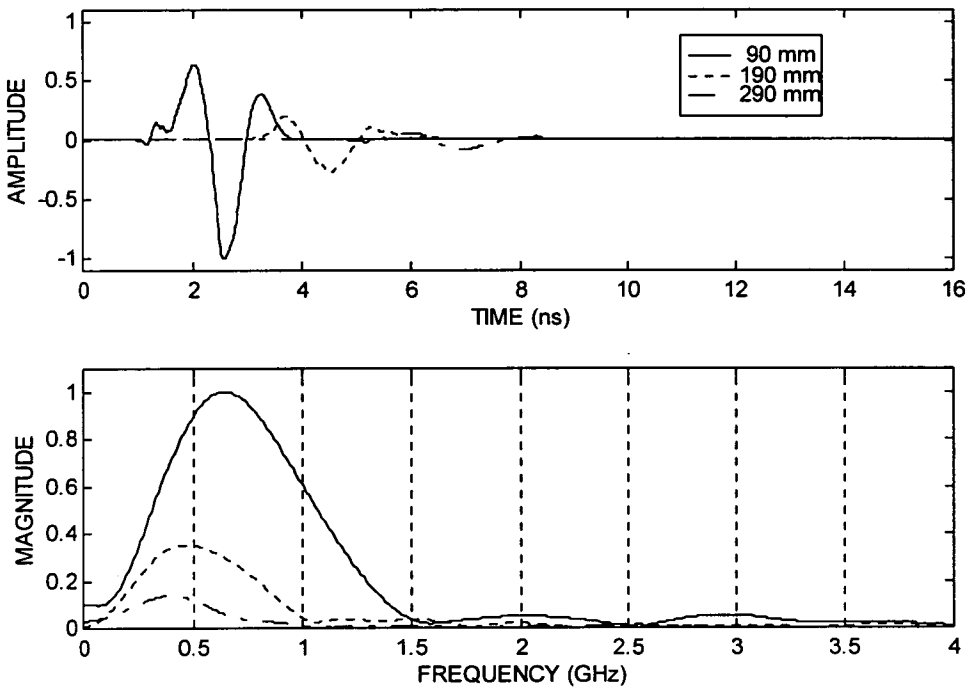

Figure 6.26 Reflections from bars at 5th layer (top)

The spatial high-pass filter does not modify significantly the centre frequency (see chapter 4), and it would not be necessary in all data. However it was applied on all data files for homogeneity purposes, making them comparable. The reflection from the second bar regarding the first layer (Figure 6.22) suffered destructive interference from the floor and was dismissed from the analysis.

The signals in the time domain clearly present severe amplitude attenuation as expected, remembering that the actual path lengths are approximately 240, 412 and 602 mm respectively (influence of the size of the antenna - see section 6.4.5). However the most important feature is shown by the frequency spectra, where the shift in the centre frequency component to lower values for deeper bars is clearly seen. This means that not only energy at higher components is being absorbed, but also distortion of the wave pulses appears to be occurring, with increasing lengths in the recorded signals.

Table 6.3 summarises the values of the centre frequencies for each layer, which are closely related to the pulse lengths involving the two main peaks.

Table 6.3 Centre frequency of bars' reflections

Layer	Bar depth 90 mm	190 mm	290 mm
1	646	-	375
2	698	500	385
3	646	531	469
4	635	521	396
5	646	469	406
Average	654	505	406

Figure 6.27 was plotted taking the average values of Table 6.3 as representative for each bar depth. The dashed line indicates what one might expect of the centre frequency variation by fitting a curve to data at 90, 190 and 290 mm depth.

Also included in Figure 6.27 was a point related to the very first arrived pulse which is a combination of transmit signal, coupling effect and surface reflection (first point of Figure 6.27). It appears as a large band at the top of Figures 6.19 and 6.20 (mistakenly referred only as surface reflection), and a single trace can be seen in Figure 6.28. The latter produces a more severe pulse distortion, that may explain why its centre frequency is smaller than the reflection of the shallower bar. This suggests that the actual pulse sent into concrete is shorter than that seen at the beginning of the records. It means that there is a physical limitation of the in-built receivers of ground coupled antennas, probably due to an impedance mismatch (see section 6.3).

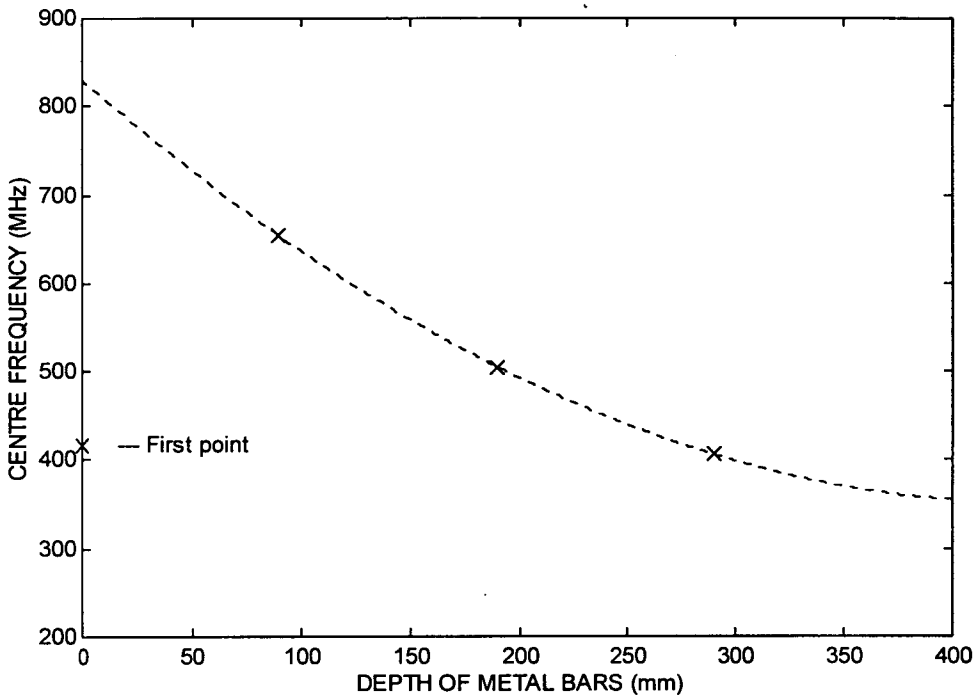

Figure 6.27 Variation of the recorded signal centre frequency with the depth of bars, using a 900 MHz antenna in reflection mode

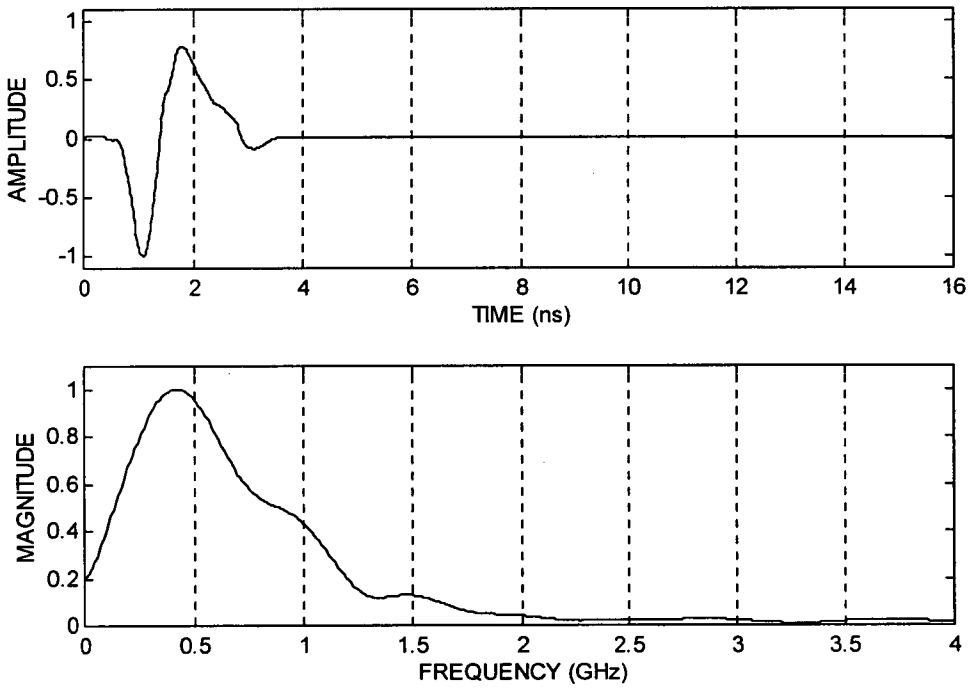

Figure 6.28 Radar "surface reflection" on concrete (900 MHz antenna)

Therefore, even signals coming back from bars at only 90 mm deep with dry concrete cover may experience a recorded centre frequency of nearly 30 % smaller than the specified one. This fact will have direct impact on the actual Radar resolution capabilities, and to some extent ratifies the assumptions made in chapter 5 for the numerical analysis.

As the main conclusion so far, both antenna coupling and energy absorption during propagation should be considered. The difficulty is to distinguish the effect of each factor on the frequency spectra. A first attempt was made by employing the transmission mode, with the second antenna working as receiver placed on the concrete column and far from it. The results are described below.

Regarding the variation of concrete density within the layers, the results at this stage do not suggest any relationship between this parameter and the frequency spectra.

Previous results published by Sellmann *et al.* for radar applied in reflection mode on fresh water lakes and soils [169], and Turner and Siggins using transmission mode through a heavily weathered and fractured granite [134], concluded that the signals will present distortion as they propagate (in both cases a homogeneous medium was assumed). Therefore similar behaviour could be expected in concrete, which is classified as an artificial rock and still normally contains a gradient of moisture (i.e. non-homogeneous). However none of the quoted works mentioned the antenna coupling problem, perhaps because they were working with large depths or thicknesses (of several metres) and thus propagation was the predominant factor. In the present case, where Radar has been regarded as a non-destructive testing technique, the depth range of interest is constrained up to 1.00 m and therefore the coupling effect should not be ignored.

Transmission mode

With a pair of 900 MHz monostatic antennas coupled to concrete the transmission mode was used at all layers and both directions, parallel (A-C) and normal (D-B) to the reference bars. The distance between antennas was always 500 mm. The results for direction D-B are plotted in Figure 6.29 (3rd, 4th and 5th layers only), and direction A-C in Figure 6.30 (all layers).

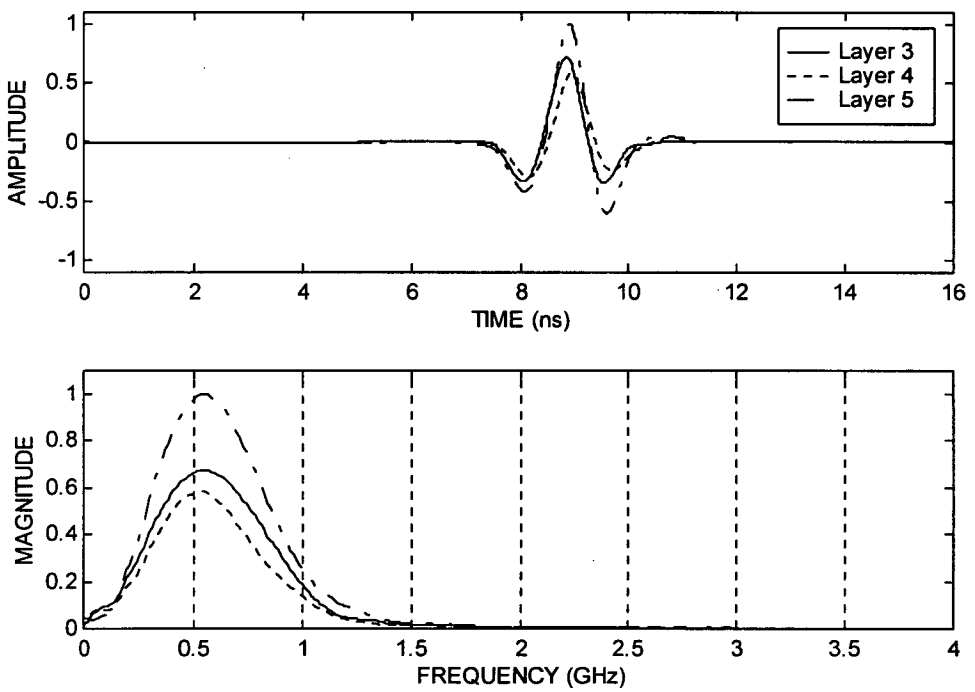

Figure 6.29 Transmission mode - signal at receiver (Direction D-B)

All values of centre frequency are given in Table 6.4 and an overall average is about 528 MHz. The value is within the range of Figure 6.27, being slightly higher than the frequency corresponding to a travel distance of 500 mm, which is equivalent to a bar depth of ~ 237mm. This may be attributed to the different travel path crossing the concrete moisture gradient, to the different mode of propagation (reflection or transmission) and to the different amount of energy that reaches the receiver.

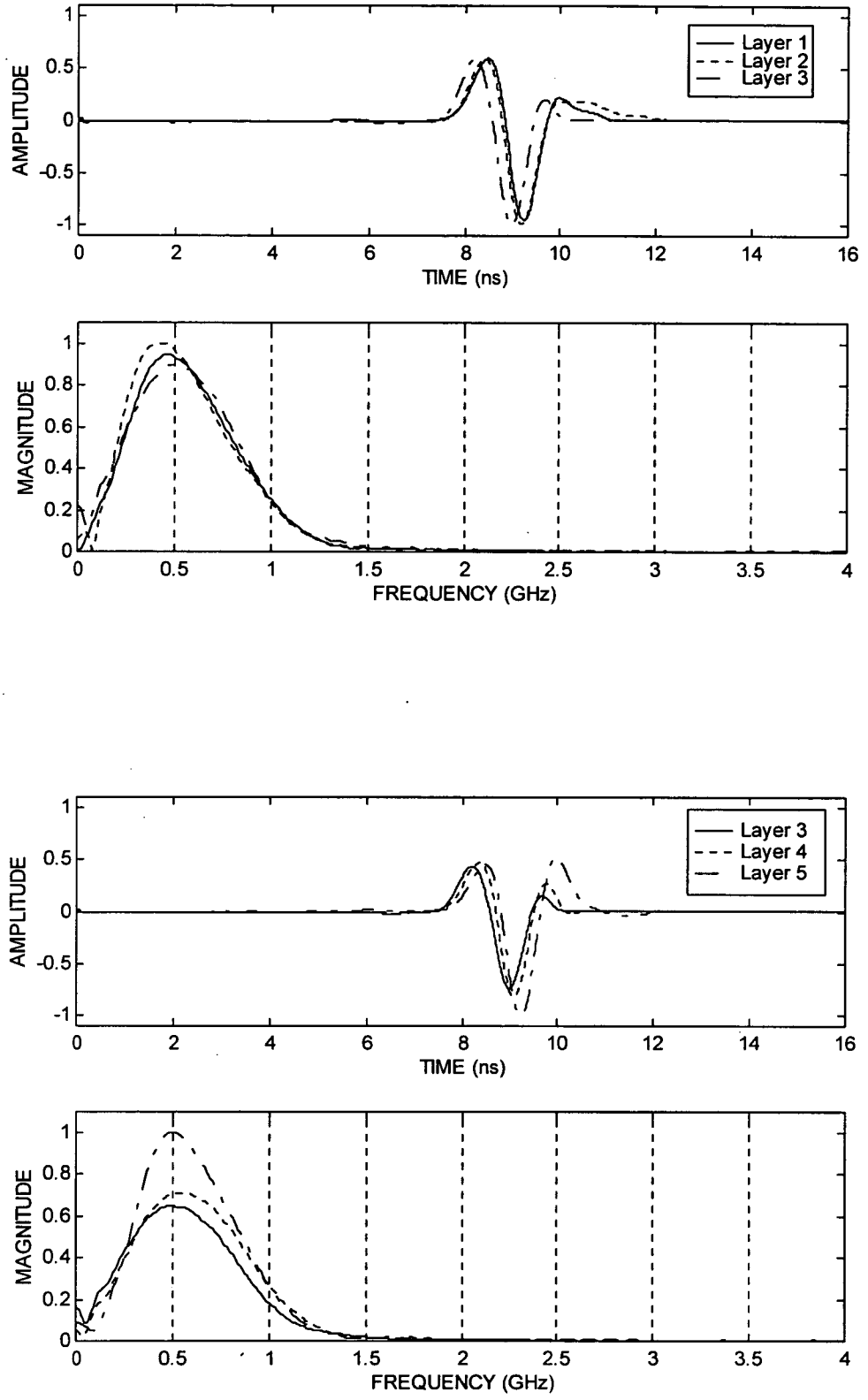

Figure 6.30 Transmission mode - signal at receiver (Direction A-C)

Table 6.4 Centre frequency of recorded signals in transmission mode

Direction	Layer					Average
	1st	2nd	3rd	4th	5th	
A-C	458	448	490	573	500	494
B-D	594	583	552	531	552	562

Here again there is no evidence that the density of concrete might change the frequency spectra. On the other hand, in the time domain Radar proved to be sensitive enough to display a variation in signal arrivals. Denser layers produced bigger delays, and particularly the signal propagating through the 3rd layer in direction A-C travelled faster, suggesting higher concrete porosity. However it does not give any indication about the variation of porosity within the section. This observation matched with a tomographic image obtained from ultrasonic data taken all around the middle section of the same layer (Figure 6.31).

In practice however, it would be very difficult at the moment for Radar to detect concrete porosity due to the presence of heavy reinforcement, or when using the reflection mode, or even due to the cables' position discussed in section 6.4.5. All these factors may affect the recorded data at a same level of the differences detected in the travel times.

The coupling effect is also not clear in the data yet. The next step was to place the receiver away from the column in steps of 50 mm up to 500 mm. Since the concrete density was not shown to influence the frequency spectrum, the test was carried out in only one layer. The recorded waveforms for the receiver coupled and displaced 300 and 500 mm away from the column are depicted in Figure 6.32.

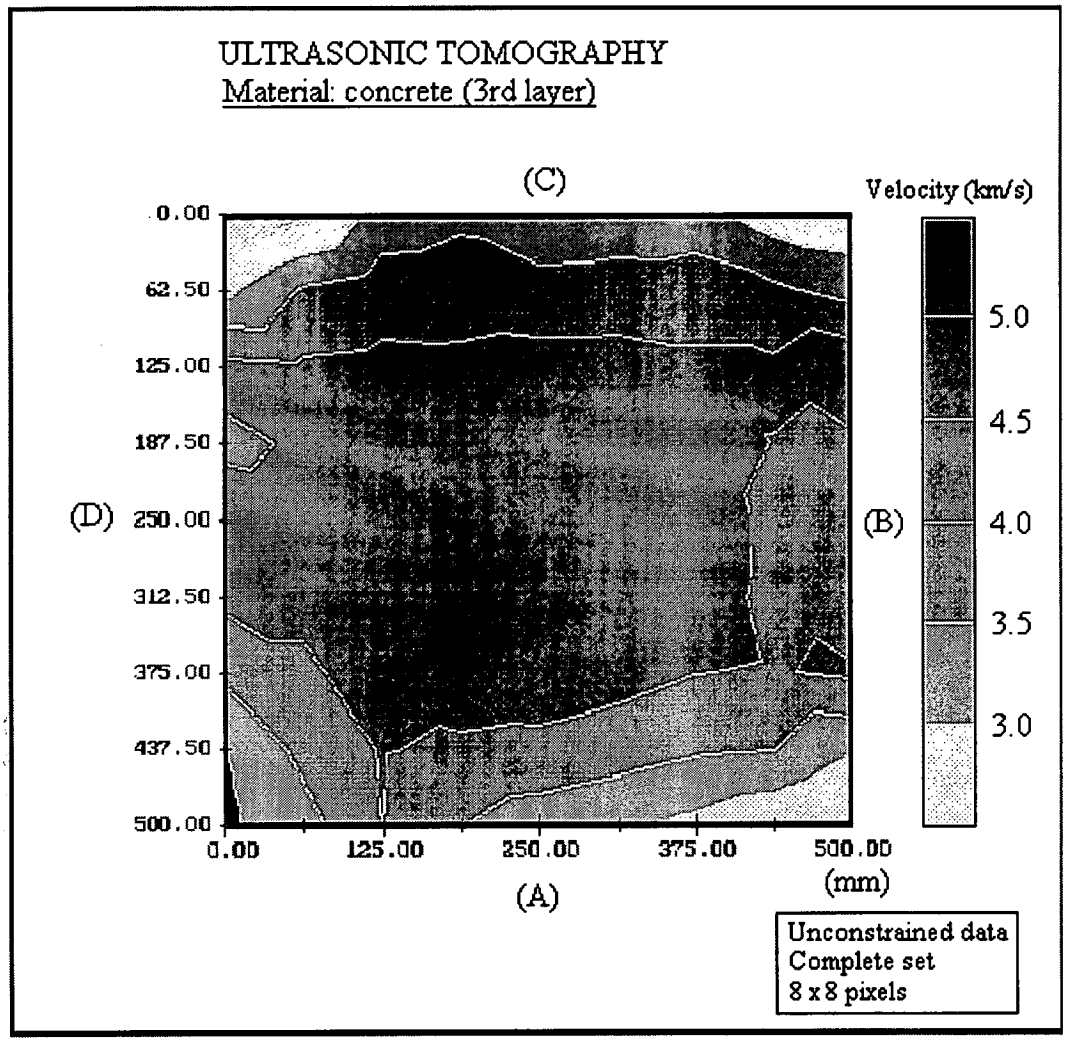

Figure 6.31 Ultrasonic tomographic image of middle section of 3rd layer

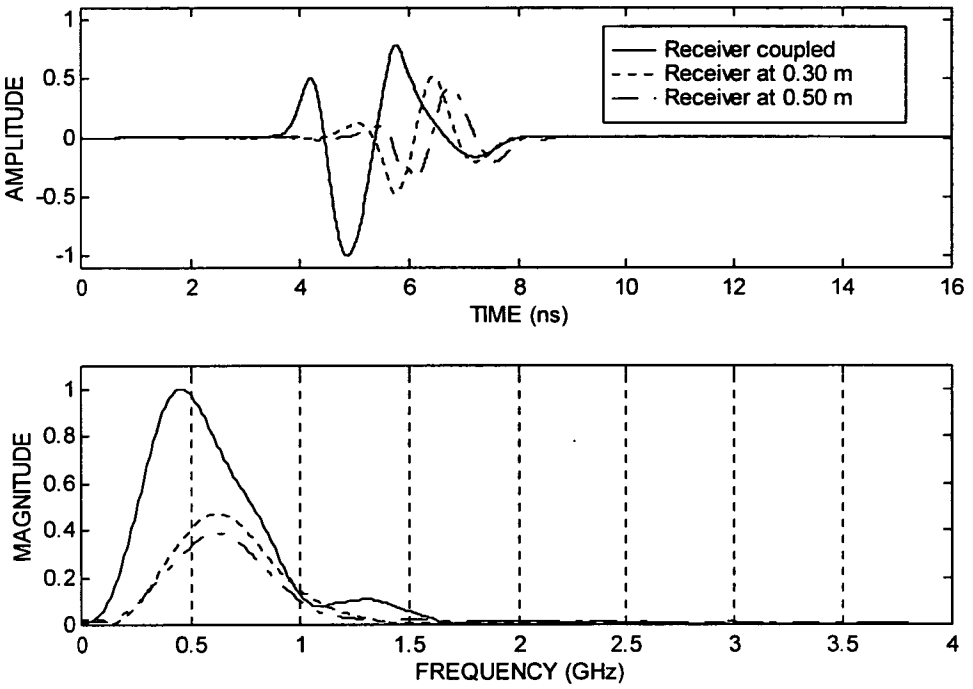

Figure 6.32 900 MHz receiver antenna - coupling effect on concrete

As can be seen in Figure 6.33, the centre frequency for the receiver far from the column resulted in higher values than those for the antenna coupled, even though with smaller amplitudes (due to longer path length and energy spreading in air). The amplitude level is here being represented by the power spectrum intensity of the centre frequency. The main change in the frequency spectra occurs with the receiver positioned within 100 and 150 mm. This indicates that for the experiment conditions coupling exists for the antenna displaced up to 150 mm, which corresponds to approximately one third of the wavelength of the recorded signal (centre frequency $\cong$ 615 MHz). From a first inspection, it suggests that the signals effectively recorded when the antennas are in contact with a medium different from air do not correspond to that actually sent, either in reflection or transmission mode. That is, the antenna coupling may produce greater distortion than wave propagation, depending on the distance travelled.

a) Centre frequency and -3dB bandwidth

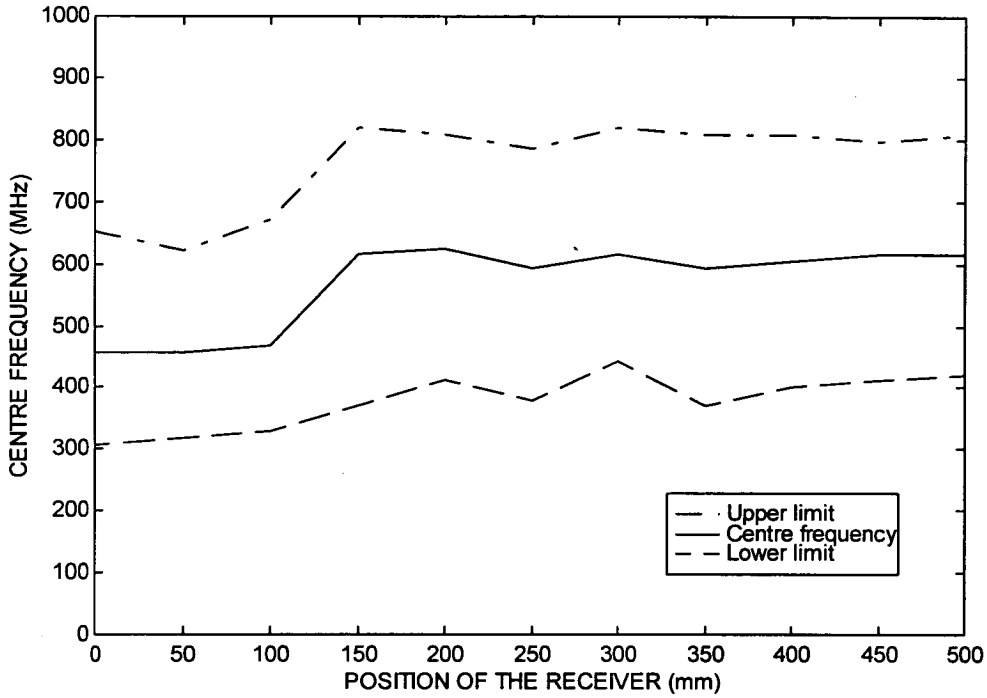

b) Centre frequency and respective power spectrum intensity

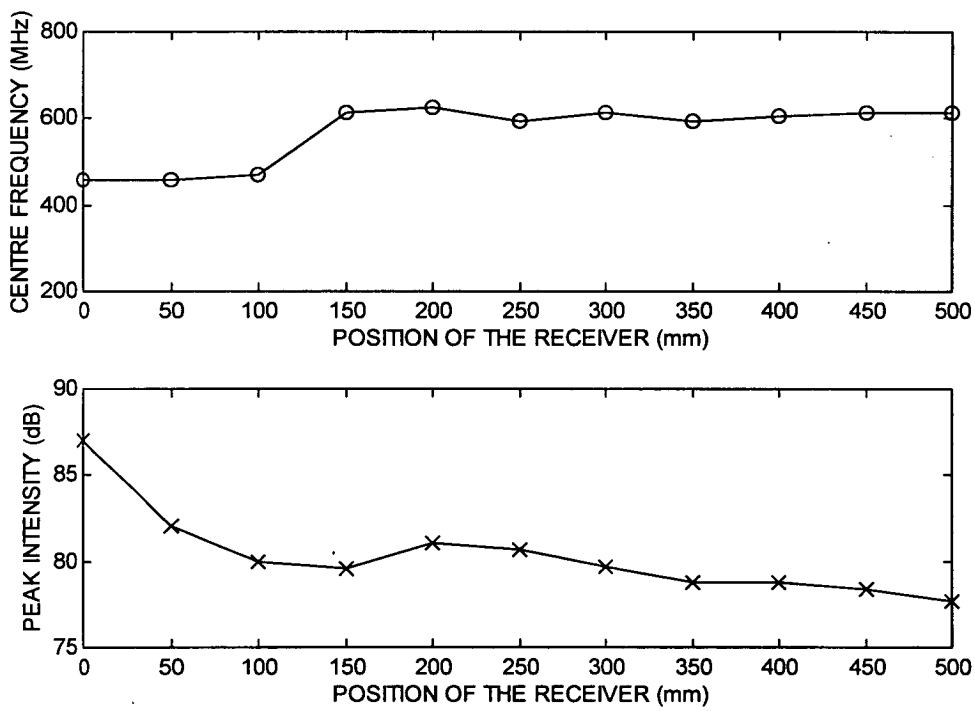

Figure 6.33 Signal behaviour using a pair of 900 MHz antennas

Figure 6.33 may also suggest that using as transmitter a lower frequency antenna, its whole frequency range should then be recorded by a 900 MHz working as a receiver. A test was carried out employing a 500 MHz GSSI antenna (model 3102) as transmitter. The recorded waveform and respective spectra are shown in Figure 6.34, where one can see that the coupling effect is still present. The centre frequency for the receiver coupled and 500 mm far is 396 and 490 MHz respectively. The difference is about 20 %, which is much less than given by the 900 MHz antenna. However the centre frequency for the antenna coupled in both cases are comparable, indicating similar performance. This can also be concluded looking at the bandwidth obtained for the pairs 900/900 MHz and 500/900 MHz: 300-650 (Fig. 6.33a) and 280-505 MHz respectively (not shown).

The signal recorded with the receiver far from the column approximately produces the nominal specified centre frequency of the transmitter coupled to air (490 MHz). This is because the 500 MHz antenna has much more power and thus the signal will penetrate deeper. For this case (concrete thickness of 500 mm), it indicates that the signal keeps its original frequency components.

The main conclusion here is that data can be improved and signals from deeper targets may be recorded when employing pair of antennas with low frequency as transmitter and high as receiver (allo-frequency mode). Similar results were achieved by Mellet [180] using 100, 300 and 500 MHz bi-static antennas, with reciprocal allo-frequency scans recorded along an asphalt driveway.

In order to obtain more detailed information and to reliably conclude about the problems regarding antenna coupling, a new experiment using cement tiles was carried out, which is the subject of the next chapter.

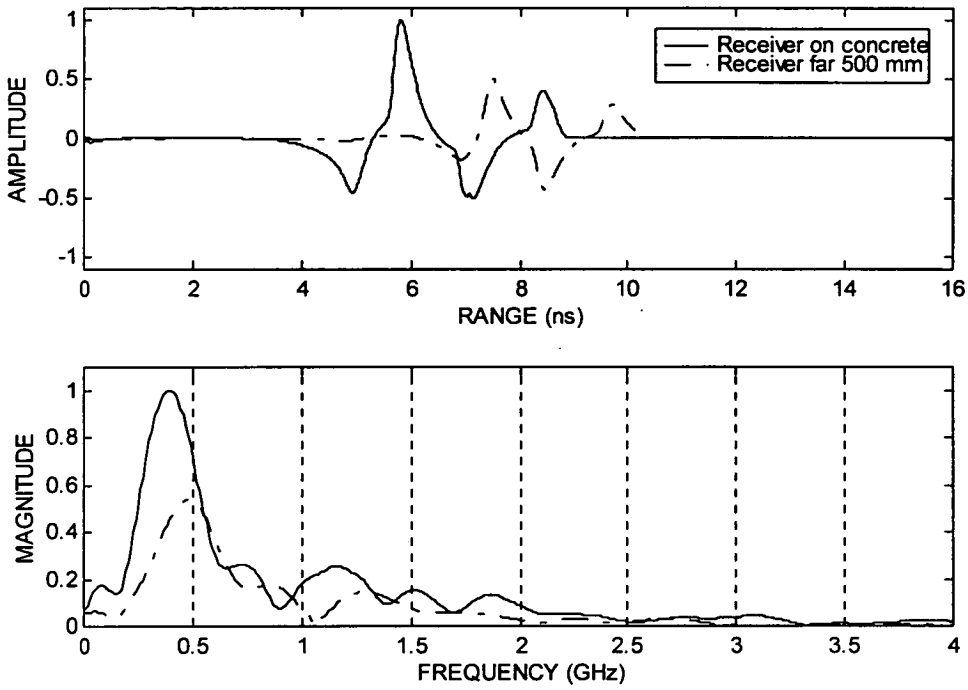

Figure 6.34 Signal performance using 500 MHz as transmitter and 900 MHz as receiver

Finally, it is important to stress that all results of the experiment are valid for the concrete conditions at the time of data readings. As mentioned in section 3.3.3, the dielectric constant of a material is strongly dependent on water content. It is known that concrete normally presents a gradient of moisture, increasing from the surface to the interior, and therefore a variable dielectric constant may be expected. To measure the amount of moisture in existing concrete structures is a very difficult if not impossible task. The same difficulty appeared in the present experiment, and thus it was possible to obtain only an average value of the dielectric constant.

The dielectric constant was estimated employing the transmission mode as shown in Figure 6.35. The position of the antennas were chosen to avoid the influence of their size on the travel time values, as discussed in section 6.4.5. The travel time was taken for each position of the receiver, with an arbitrary origin.

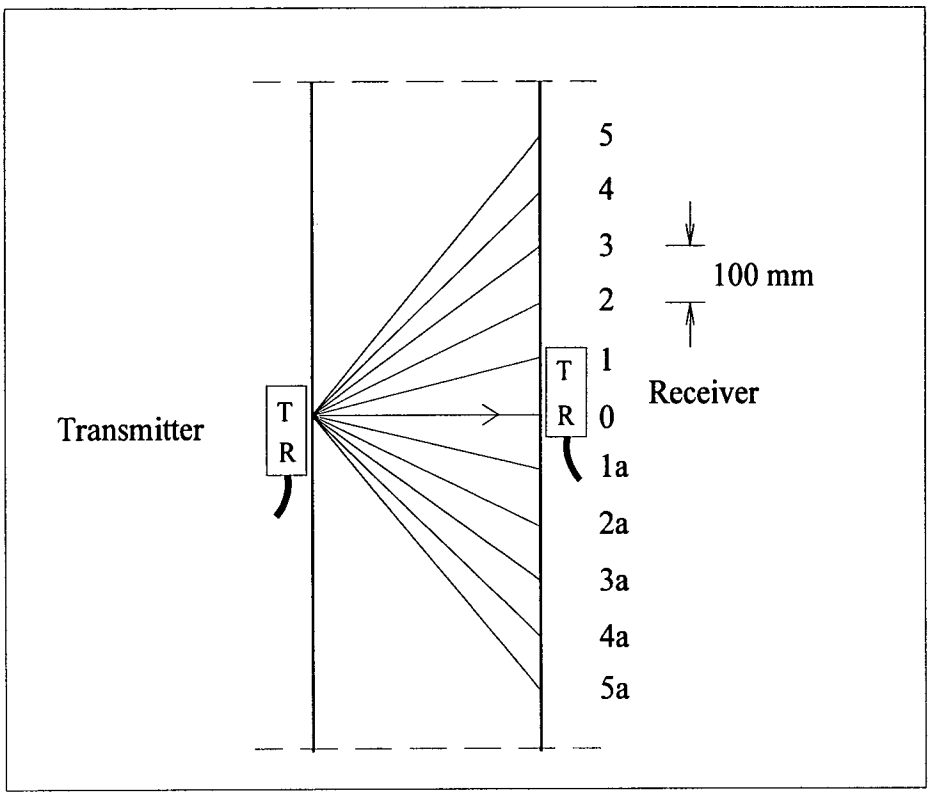

Figure 6.35 Transmission mode for measuring the dielectric constant of concrete

Figure 6.37 contains a plot with the pairs of values distance - time, the latter being the average of points 1-1a, 2-2a, and so on. The reference for time values was the first peak of the recorded signals as indicated in Figure 6.36, which is less affected by the signal distortion. Ideally the correct point should be where the pulse begins. Its accurate determination however has proven to be very difficult in practice due to the presence of signal noise and system fluctuations, being therefore subject to a high level of subjectivity.

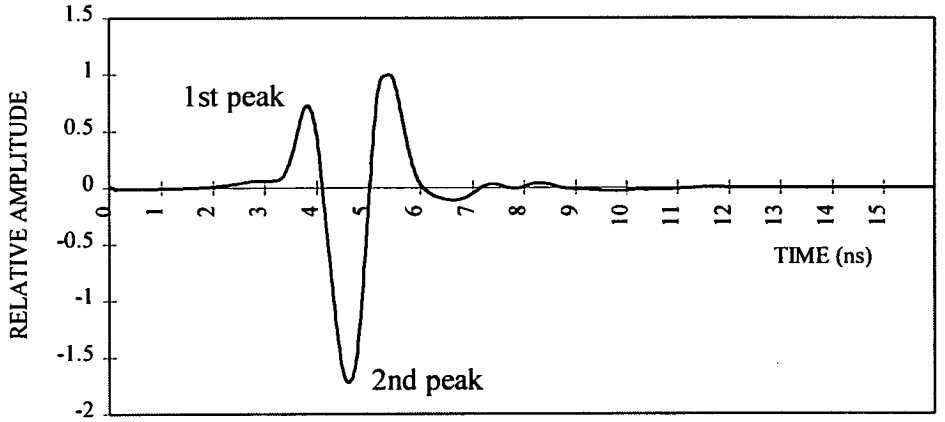

Figure 6.36 Signal peaks used for time measurements

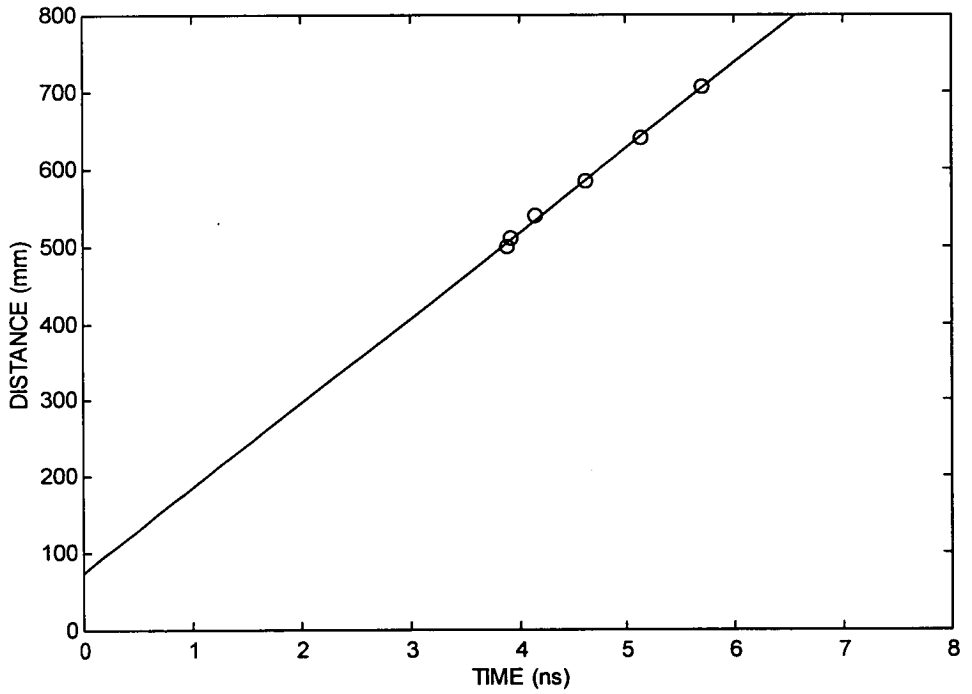

Figure 6.37 Determination of the average wave velocity in concrete

A regression technique was used to fit a straight line as the best curve, the slope of which represents the average wave velocity. In this case a velocity of 11.04 cm/ns was encountered. The corresponding dielectric constant could then be calculated from the simplified equation (3.52),

$$\varepsilon_r = \left(\frac{c}{v}\right)^2 = \left(\frac{30}{11.04}\right)^2 = 7.4$$

This result indicates that the concrete column still contained an amount of moisture above the average of existing air dried structures, for which a value of 6 to 6.5 for the dielectric constant is expected for normal ambient conditions [146].

6.6 SUMMARY OF THE MAIN CONCLUSIONS

1. Radar proved to be sensitive enough to detect variation of concrete density in the time domain for the present material conditions, without however indicating porosity distribution within the concrete.

2. Frequency domain analysis has shown to produce very useful quantitative information regarding signals' distortion. Problems such as the antenna coupling and the change in pulses' shape during propagation can be studied.

3. The actual resolution capability of an antenna may be limited by either a coupling effect or energy dissipation during propagation, or both.

4. Geometrical energy spreading in air does not produce significant signal distortion.

5. Antenna coupling and energy dissipation in lossy media produce changes in Radar pulses, affecting their frequency spectra and shifting the centre frequency normally to a lower value.

6. In this experiment using 900 MHz bow-tie antenna the centre frequency of recorded pulses with the receiver coupled to concrete was limited to about 530 MHz. For the receiver placed up to 500 mm away from the column the same limit resulted about 620 MHz, where the higher frequency components were probably filtered out during propagation. The concrete is acting as a low pass filter.

7. Due to the coupling effect the use of allo-frequency set-up with low frequency antenna as transmitter and high frequency as receiver may produce equivalent performance to a pair of high frequency ones. In addition deeper penetration can be achieved.

8. The actual signal sent into the column should retain most of its original frequency components, but after propagating and recorded they become distorted.

9. The resolution that can be obtained with a coupled antenna should be carefully considered in a survey design, as the centre frequency in air may not be the recommended value in concrete, due to the above aspects.

10. In the case of small thicknesses, the size of monostatic antennas (separation between in-built transmitter and receiver) may affect the measurements of travel times and therefore the determination of dielectric constant values.

11. Further research involving a new experiment was necessary to better identify the effects of the antenna coupling and the wave attenuation during propagation.

CHAPTER 7

EXPERIMENTAL INVESTIGATION OF COUPLING EFFECT OF ANTENNAS

CHAPTER 7

7. EXPERIMENTAL INVESTIGATION OF COUPLING EFFECT OF ANTENNAS

7.1 INTRODUCTION

In chapter 6 several aspects concerning Radar as a non-destructive testing technique on concrete were analysed. One of the main conclusions is that the signals recorded by contact antennas may not correspond to those actually transmitted. Pulse distortion can occur during propagation of the wave due to the attenuation of the high frequency components, as well as due to the antenna coupling. This has a direct implication on travel time measurements for dielectric constant estimation and target resolution.

One of the difficulties encountered during the concrete column experiment was how to control the moisture content. There is a moisture content gradient from the concrete surface, and therefore a varying value for the dielectric constant is expected. However it was only possible to compute an average value that was valid at the time of testing. Also, it was not easy to identify how much coupling and propagation affect the frequency spectra of the recorded pulses.

A new experiment was carried out attempting to overcome the problems mentioned above. A set of commercial cement tiles was used and this is described in more detail in the next section. This experiment permitted simulation of extreme conditions for the moisture content (oven dried and saturated), as well as air dried in the laboratory.

The methodology employed during the tests was basically the same as that applied in the concrete column and their results are compared.

7.2 DESIGN OF EXPERIMENT

7.2.1 Tile material description

In order to obtain results that would be comparable to those of the concrete column experiment, a set of cement tiles with nominal dimensions of 400x400x30 mm was obtained. The average dimensions measured were 397x397x28 mm, and these were used for all calculations.

The apparent density was also obtained for each tile oven dried, in "as-packed" and saturated conditions, by dividing the mass by the respective volume. The results were respectively 2,339, 2,392 and 2,465 kg/m^3, and are typical of a normal structural concrete without reinforcement.

The use of tiles allowed tests to be carried out for different thicknesses and permitted the control of the moisture content for measuring the dielectric constant. Even though each tile could still present a moisture gradient, a reasonably uniform distribution could be assumed in this experiment for the whole set of tiles. The average moisture content of the tiles was determined with respect to oven dry condition using the equation

$$MC = \frac{P_i - P_{od}}{P_{od}} \times 100 \ (\%) \qquad (7.1)$$

where: MC = moisture content percentage

P_i = initial weight

P_{od} = weight after oven dried

The results were 2.3 % for the tiles in normal air and 5.4 % when saturated. The degree of saturation for the air dried condition (in laboratory) was estimated by

equation (7.2), resulting in 41.7 %. For normally exposed mature concrete in site it has been reported a typical value of about 38 % [181], and in the laboratory between 40 and 45 % [146]. Therefore the result found for the tiles is representative.

$$DS = \frac{P_i - P_{od}}{P_{sat} - P_{od}} \times 100 \ (\%) \qquad (7.2)$$

DS = degree of saturation

P_{sat} = saturated weight

7.2.2 Experimental set-up

A set of tiles were placed on a wood table and tested using a pair of 900 MHz monostatic antennas in transmission mode (see Figure 7.1). Views of the actual set-up can be seen in Plates 7.1 and 7.2. When considering the position of the antennas and the distances between them, it was necessary to take into account the effect of their size as discussed in section 6.4.5.

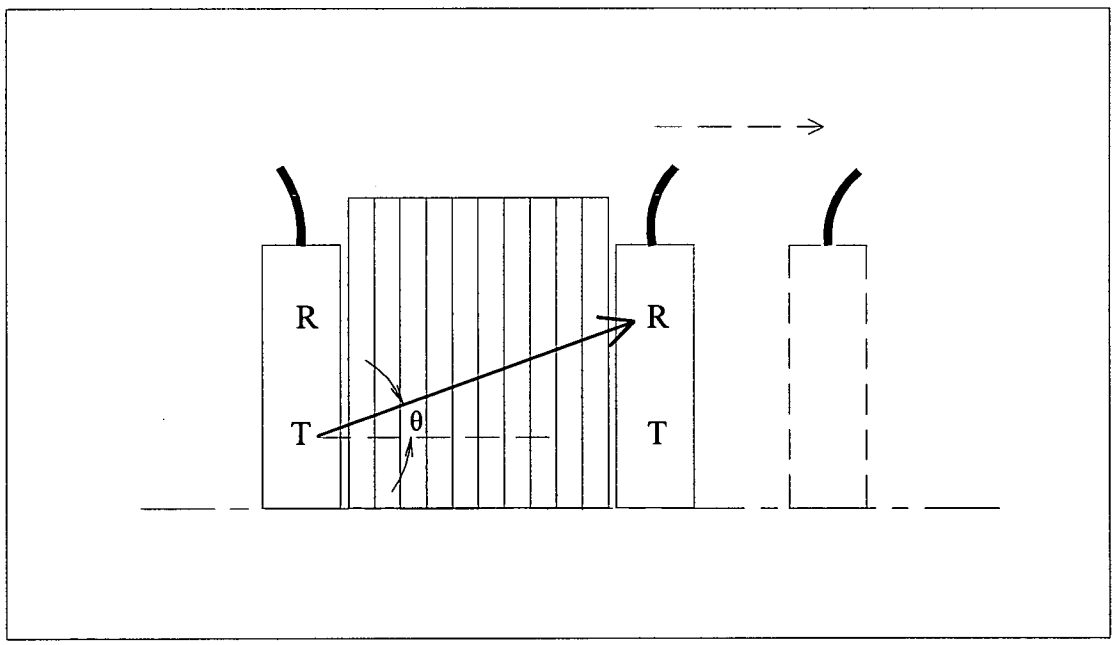

Figure 7.1 Set up for the cement tiles experiment

Precautions were taken to avoid the proximity of objects that could produce unwanted reflections in the recorded data range during the experiment. A wooden table was used to avoid possible interference from the reinforced concrete floor. Even so it was considered that the table itself might produce some secondary reflections, but its presence was considered as a constant factor that would not affect the data analysis. Moreover considering the position of the antennas very little energy from these reflections is expected to reach the receiver.

The tiles came with inevitable geometrical imperfections due to their production process (they are not perfectly plain). As a consequence small air gaps of approximately 1.5 mm between tiles were formed and could affect the results to some extent, mainly when measuring the dielectric constant. This problem was also taken into account during the data analysis and will be highlighted later.

The Radar apparatus and set-up parameters (range, transmit rate, samples/scan, scans/second) used in the concrete column were maintained during the present experiment. Only the gain had to be adjusted to compensate for the high attenuation due to variation in moisture content. When data is compared, it is always corrected for the actual gain.

In order to investigate if the data from this experiment is comparable with those from the concrete column, a preliminary test was carried out. It consisted of using initially 16 tiles ($\cong$ 480 mm) in normal laboratory conditions (air dried). The receiver was displaced from the coupled position by up to 500 mm in regular steps of 50 mm. The results are shown in Figure 7.2 in terms of centre frequency of the recorded signals. It also includes the results obtained for the column, and one can see that both present a similar behaviour. The centre frequency values are not identical due to a different degree of signal distortion associated with materials moisture content. This is confirmed by the dielectric constant measurements, analysed in more detail in the next section.

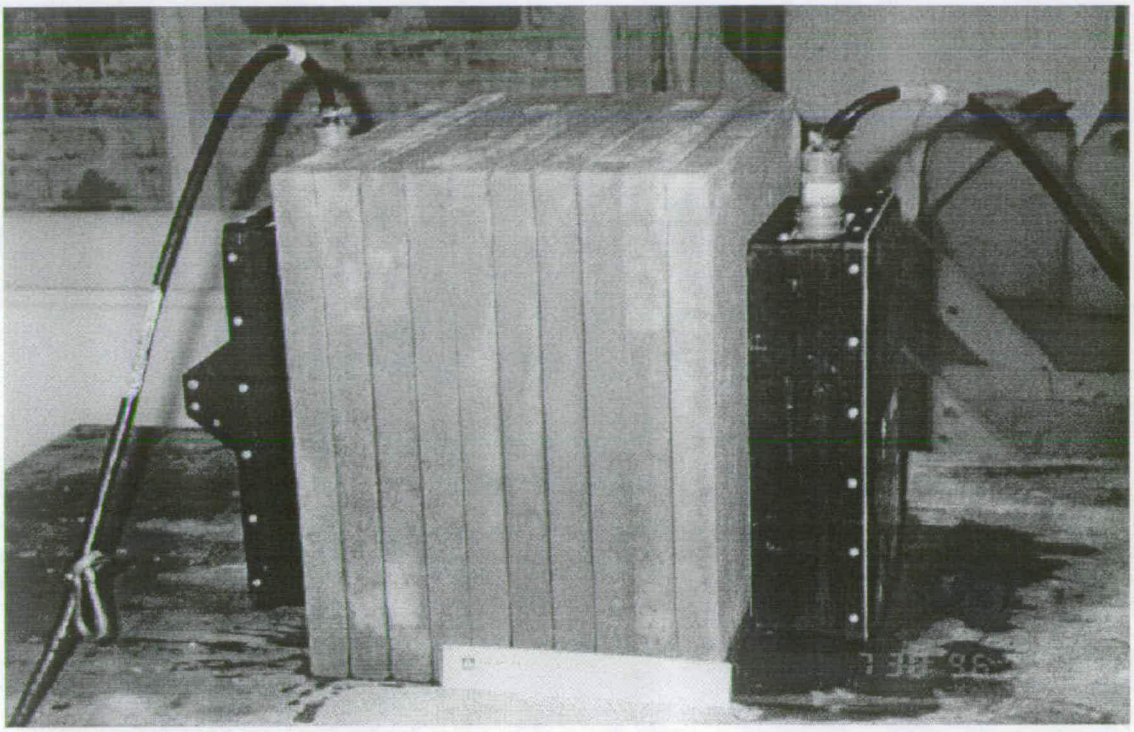

Plate 7.1 Cement tiles experiment (side view)

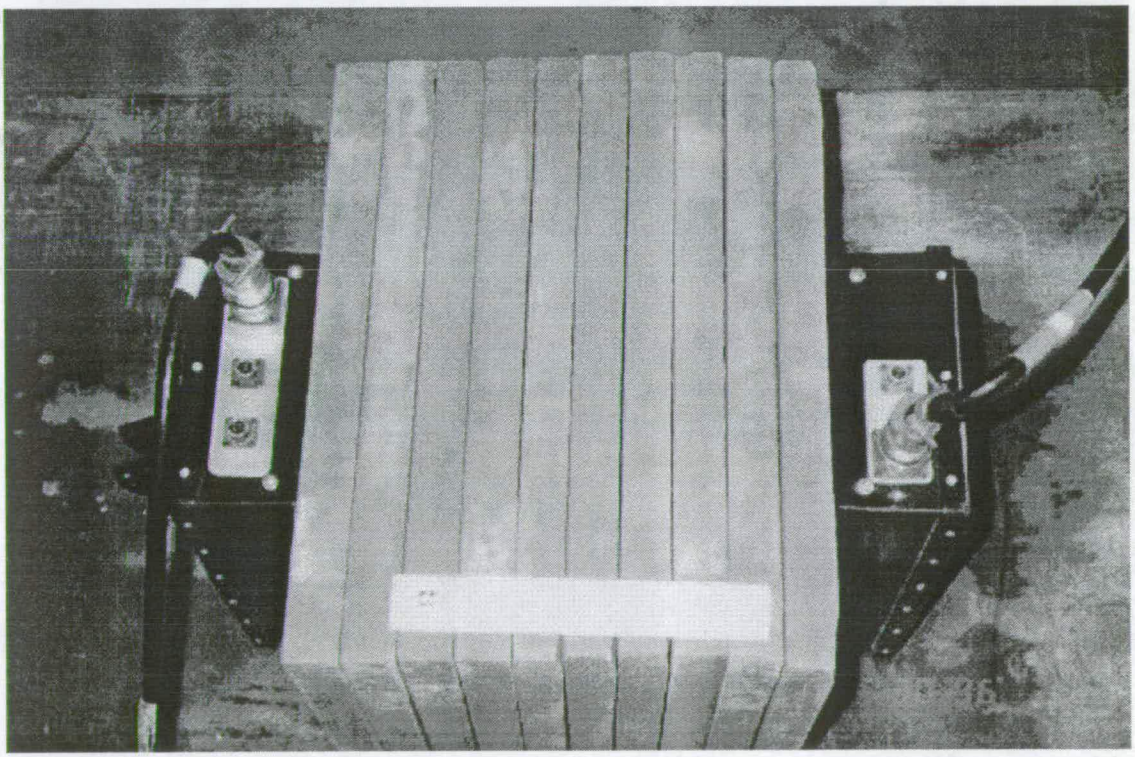

Plate 7.2 Cement tiles experiment (top view)

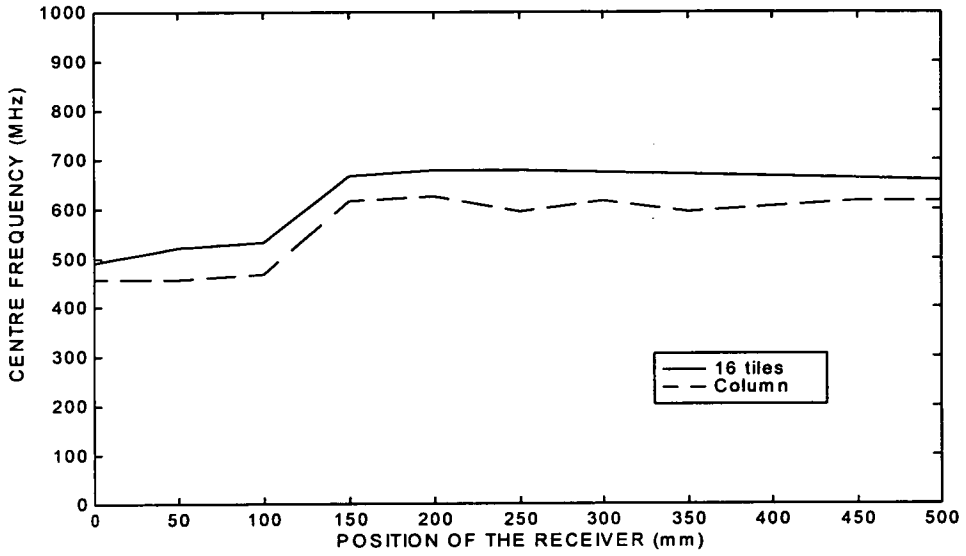

Figure 7.2 Centre frequency for 16 tiles and concrete column

On the other hand the difference was nearly constant throughout the test, leading to the conclusion that the presence of the wooden table is not interfering in the results.

Here again the sudden variation of the centre frequency for the receiver positions within 100 and 150 mm is noticeable. This fact can be seen more clearly in Figure 7.3, which also includes the -3 dB frequency bandwidth. The upper limit increases more rapidly than the lower one, suggesting that higher frequency components are still present when the signals reach the receiver.

A second preliminary test was made using only 10 tiles, and the results compared to the previous one. The main reason for this was to reduce the effect of signal attenuation during propagation and to see whether antenna coupling might be illustrated. Looking at Figure 7.4, one can observe that the frequency variation within 100 and 150 mm is in fact accentuated. Hence, given that the first test confirmed the functionality of the present experimental set-up and because extreme conditions of moisture content would be considered, the following tests were carried out with only 10 tiles (thickness $\cong$ 300 mm).

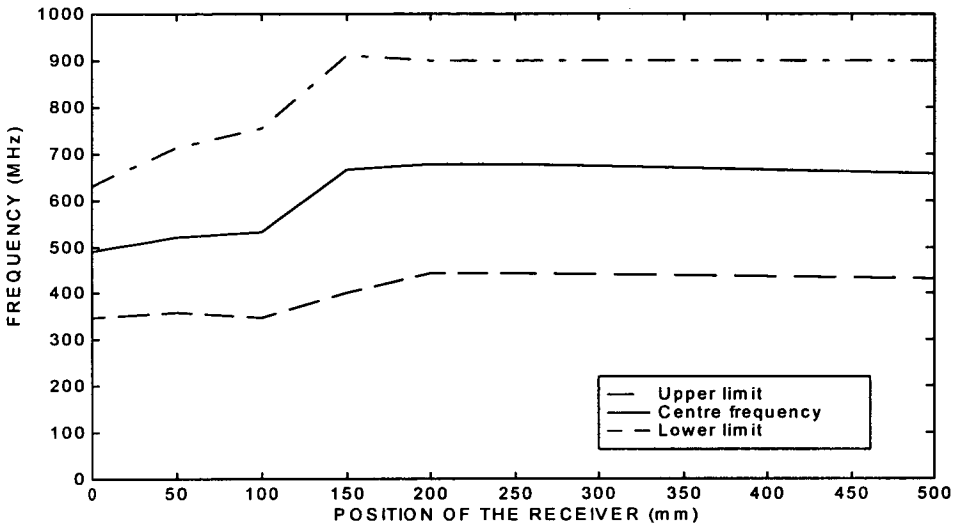

Figure 7.3 Radar results for 16 tiles in normal air dry condition: centre frequency and -3 dB bandwidth

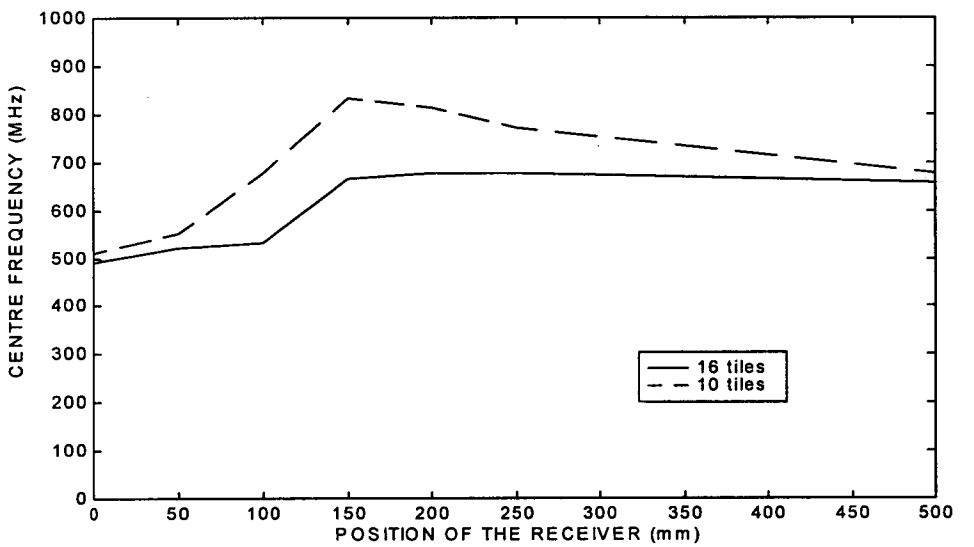

Figure 7.4 Centre frequency for 16 tiles and 10 tiles

7.3 EXPERIMENTAL RESULTS

7.3.1 Dielectric constant

As mentioned in the previous section, this experiment was designed to investigate concrete with moisture contents in extreme conditions as well as for the normal laboratory environment: oven dried, saturated in water and air dried. Therefore the tiles will present a range of electrical properties, particularly the dielectric constant. Since mains water supply was used and no chemical reactions were involved, the conductivity should remain low in all cases. Thus, the condition of low loss material could be assumed and the simplified equation for calculating the velocity applied (Eq. 3.36).

The methodology to obtain the travel times had to be changed. In the concrete column they were measured by moving the receiver by regular distances (see Figure 6.35) relative to a centre position. In these tests, the transmitter and receiver were placed according to Figure 7.1 on sets of different numbers of tiles (10, 12, 14 and 16). Travel times are proportional to distance, and therefore the velocity of propagation is constant. The dielectric constant can then be calculated by equation (3.54) reproduced below,

$$\varepsilon_r = \left(\frac{ct}{d}\right)^2$$

It is important to stress again that due to the size of the antennas the distance "d" is the real path length, which is not simply the thickness of the tiles (see section 6.4.5).

As mentioned earlier, the tiles were not geometrically perfect, and when assembled small air gaps between them existed (≅1.5 mm). This fact was taken into account in the calculation by subtracting the corresponding time propagation in air from the times measured in the experiment. As the direct wave paths between

transmitter and receiver were always in the diagonal direction (which increases the distances), an air gap of 1.5/cosθ mm was assumed. The estimated real path length was then determined with the average thickness of the tiles (≅ 28 mm). All this information is summarised in Table 7.1 below.

Table 7.1 Correction of waves path length

No. of tiles	No. of air gaps	Thickness of tiles (mm)	Air gaps Diagonal path (mm)	Time in air (ns)	Tiles Diagonal path (mm)*
10	9	280	15	0.05	322
12	11	336	18	0.06	372
14	13	392	21	0.07	423
16	15	448	24	0.08	476

* The distance between the in-built transmitter and receiver is 160 mm.

The corrected time readings are shown in Table 7.2. This table contains two columns for each tile condition, corresponding to the first and second peaks of the signals in the time domain, according to Figure 6.36 (see chapter 6). It also contains the resulting values for the wave velocity and the dielectric constant.

As can be seen, the difference in the dielectric constant values between the peaks is not constant. For oven dry condition this difference is about 8 %, but when saturated it becomes over 30 %. The second peaks also always give higher dielectric constants. From this analysis one may infer that signal distortion during wave propagation exists, and affects the travel time measurements. For this reason, results given by the first peaks were finally adopted.

Table 7.2 Waves' relative travel times

No. of tiles	Oven dried		Air dried		Saturated	
	1st peak	2nd peak	1st peak	2nd peak	1st peak	2nd peak
10	1.39	1.95	1.68	2.28	2.20	2.83
12	1.82	2.35	2.14	2.79	2.74	3.41
14	2.23	2.84	2.62	3.27	3.29	4.23
16	2.64	3.22	3.04	3.82	3.94	4.76
Velocity (cm/ns)	12.3	11.9	11.2	10.1	8.9	7.7
ε_r	5.9	6.4	7.1	8.9	11.4	15.2

Simply taking the tiles' thickness as the path length, the dielectric constant would compute as 5, 6 and 9.6 respectively for oven dry, air dry and saturated. It represents an average reduction of about 19 %, which is quite significant. When compared to the example studied in section 6.4.5 (effect of antennas' size), can be observed that the opposite occurred. There a fixed travel time was assumed and simply the material thickness compared to the real path length between the antennas. In the present case times are fixed relative to an unknown origin and the path length does not increase in the same proportion as the tiles' thickness in a same interval of time. The latter is explained in Figure 7.5.

The lines indicated by "D" (path length) and "d" (tiles' thickness) do not have the same slope. As a result, for a same interval of time (t_2 - t_1) Figure 7.5 shows that $y_1 > y_2$, and therefore different values for the dielectric constant are computed. The correct path length is "D", and it is given by $D = \sqrt{d^2 + s^2}$.

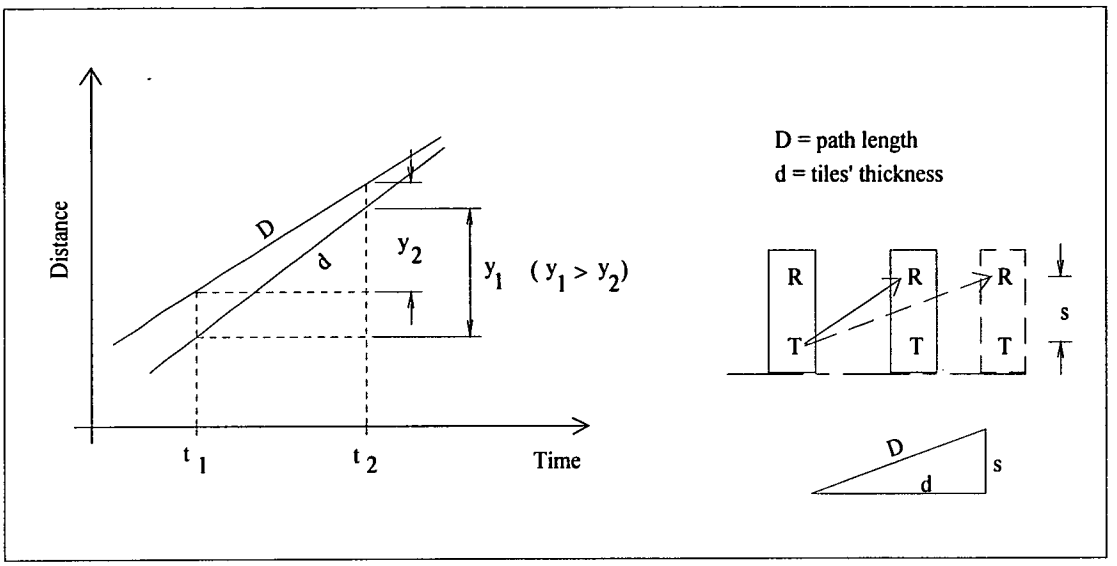

Figure 7.5 Influence of path length on dielectric constant

Figure 7.6 shows a plot of distance versus time for all tiles conditions. The variation of the lines' slope can clearly be seen, confirming the influence of moisture on wave velocity.

The dielectric constant estimated for the column's concrete is higher than for the air dried tiles. It suggests that the concrete in the column contains more moisture and therefore more signal distortion is expected. This is consistent with the difference in centre frequencies shown in Figure 7.2.

7.3.2 Signal distortion due to antenna coupling

To obtain data about the effect of the antenna coupling with the surface, a set of 10 tiles to distort the transmitted pulse was placed according to Figure 7.1, and the Radar used in transmission mode. The receiver was moved away from the tiles in steps of 50 mm up to 500 mm. First the readings were taken with the tiles in normal

laboratory air conditions. Next they were put in an oven to dry out at 100 °C for a period of one week, and the whole process was repeated. Finally the tiles were immersed in water for one week to saturate them.

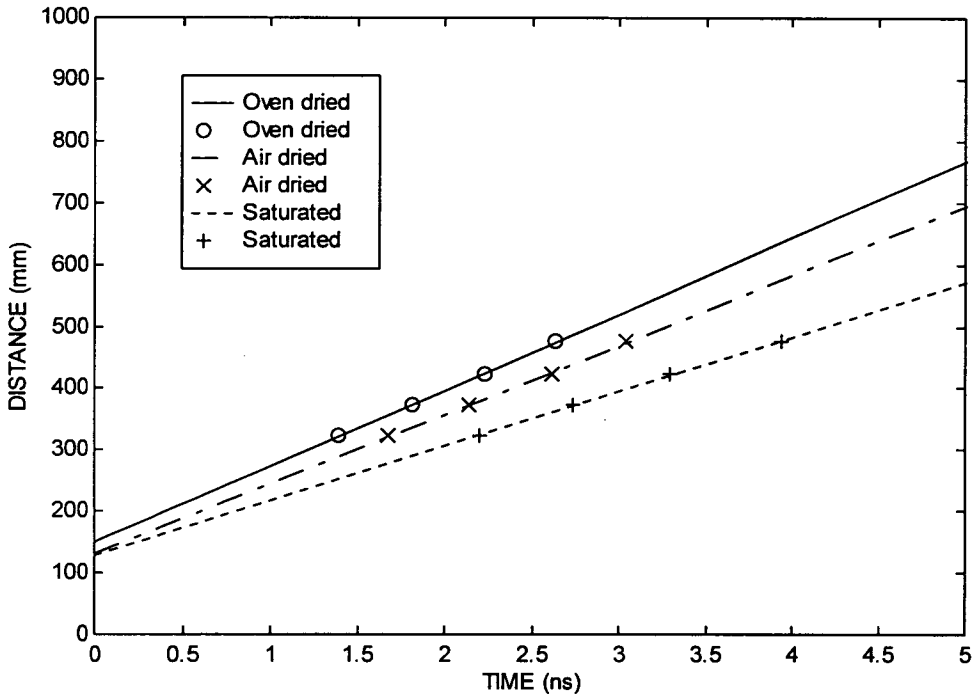

Figure 7.6 Travel path length V. Time (1st peak values)

The Figure 7.7 contains the signals in the time domain and corresponding frequency domain spectra, with the receiver in contact with the tiles. Figure 7.8 contains the same information for the receiver positioned 250 mm from tiles. In both situations the influence of moisture content on signal distortion, time delay and amplitude attenuation is quite visible.

Figures 7.9, 7.10 and 7.11 show plots for the centre frequency and -3 dB bandwidth limits respectively for each moisture condition and all receiver positions.

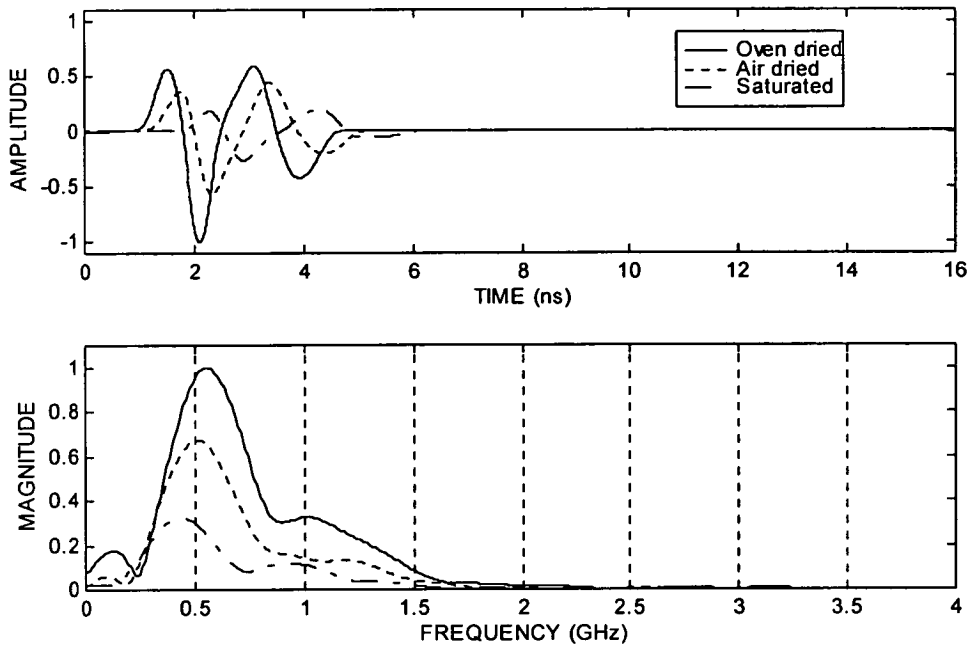

Figure 7.7 Recorded signals with the receiver in contact with the tiles (trans. mode)

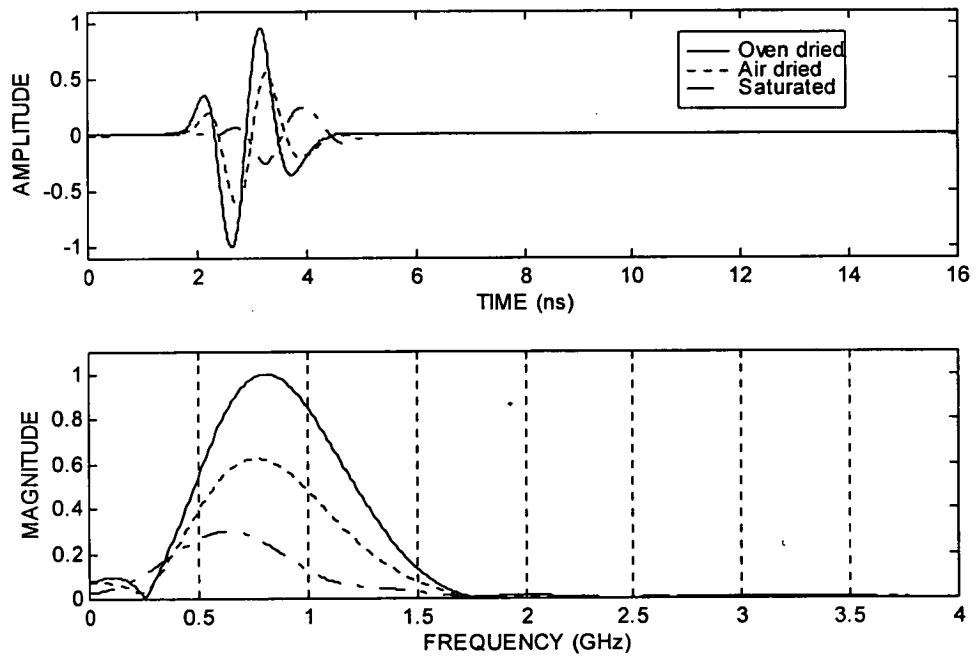

Figure 7.8 Recorded signals with the receiver 250 mm far from tiles (trans. mode)

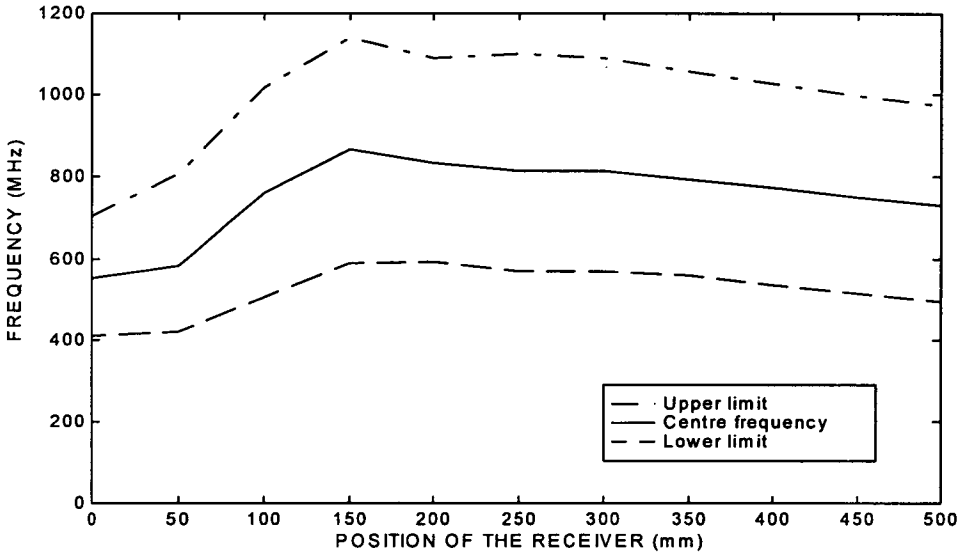

Figure 7.9 Frequency domain results for the oven dried tiles

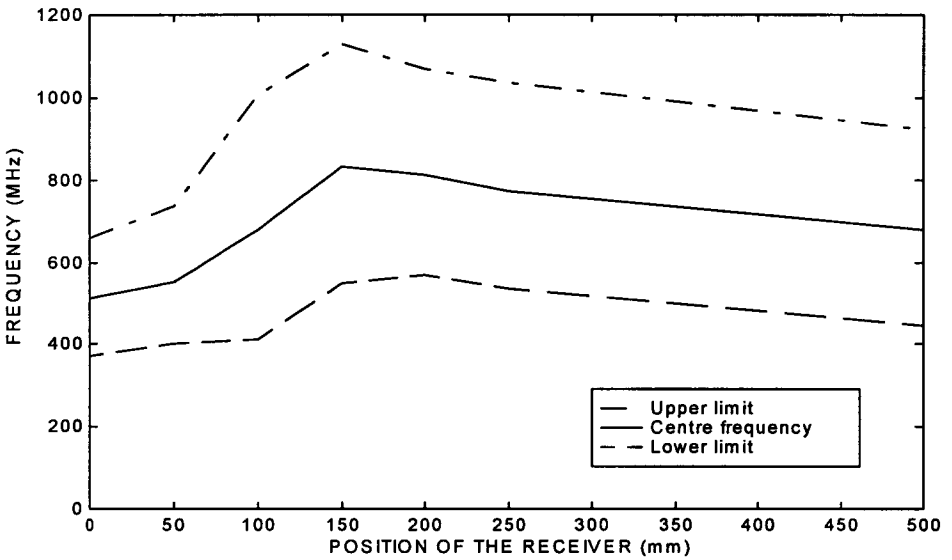

Figure 7.10 Frequency domain results for the air dried tiles

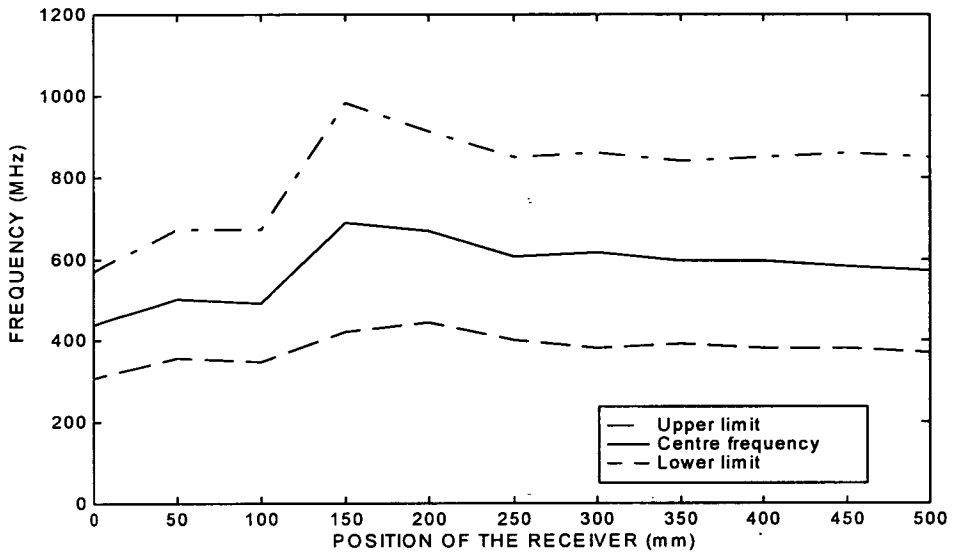

Figure 7.11 Frequency domain results for the saturated tiles

Figure 7.12 allows one to compare their centre frequencies and respective energy decay, the latter represented by the corresponding value of the intensity in the power spectrum. Analysing these plots, the characteristic behaviour they have in common is the increasing centre frequency for the receiver positions up to 150 mm, and then slightly reducing afterwards. It is essentially associated with the appearance of the high frequency components as indicated by the upper limit of the -3 dB bandwidth. This confirms the conclusion arrived in the column experiment, that the antenna coupling occurs for the receiver up to about 150 mm.

In order to explain what is causing the coupling effect, Figures 7.13, 7.14 and 7.15, for three positions of the receiver within 100 and 160 mm, were plotted. They contain the signals in the time domain and respective frequency spectra. All of them show two characteristic peaks in the frequency domain.

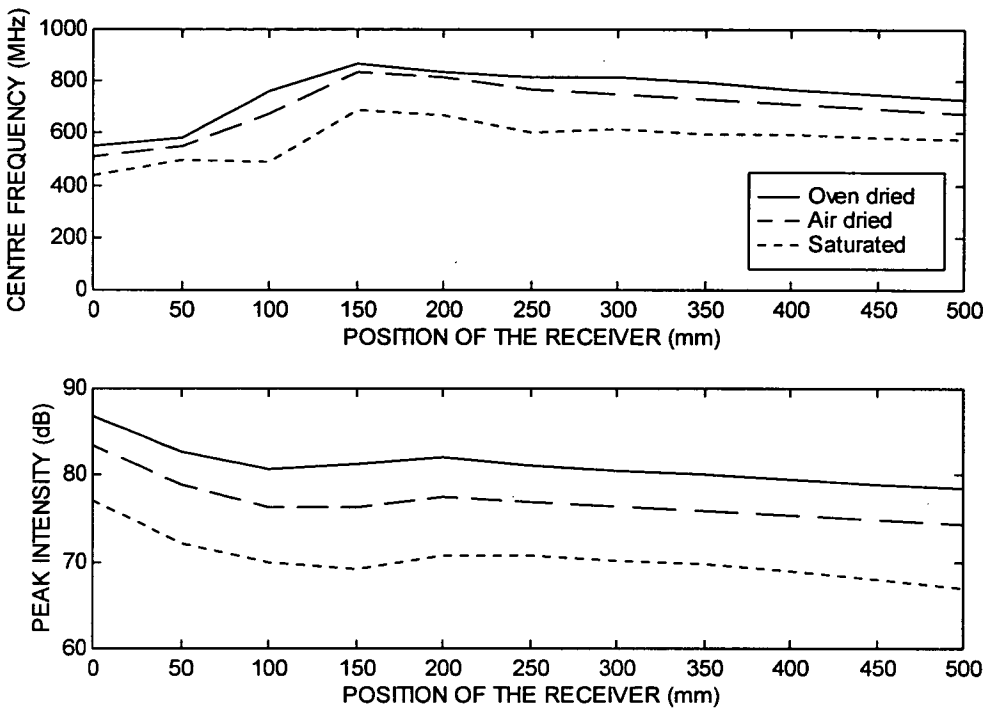

Figure 7.12 Variation of centre frequency and corresponding power spectrum intensity for all tiles' conditions

Analysing the signals more closely in the time domain, their second positive peak changes significantly in amplitude and width despite the small antenna displacement. Furthermore, for the antenna in the farthest position a complete wave can be seen after the main pulse. When the antenna is coupled, these waves superpose and as consequence a destructive interference occurs in this case. Depending on the position of the receiver, the first or the second peak in the frequency domain will dominate the results. However, when the receiver is coupled only one main peak will be visible at lower frequencies (see Figure 7.7). This suggests that the actual targets' reflections may be distorted to some extent and lower frequencies or larger pulse lengths will predominate in their recorded data. The practical implication will be a reduced capability of Radar to resolve subsurface targets. These figures also illustrate the temporary increase in the amplitude for the receiver positioned within the specified distance range, already shown in Figure 7.12.

a) Time domain

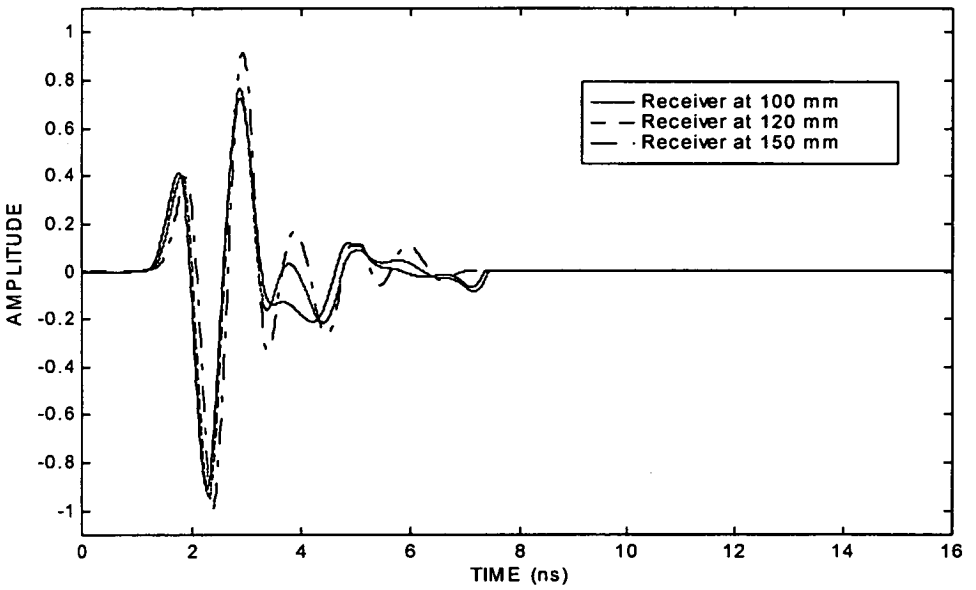

b) Frequency domain

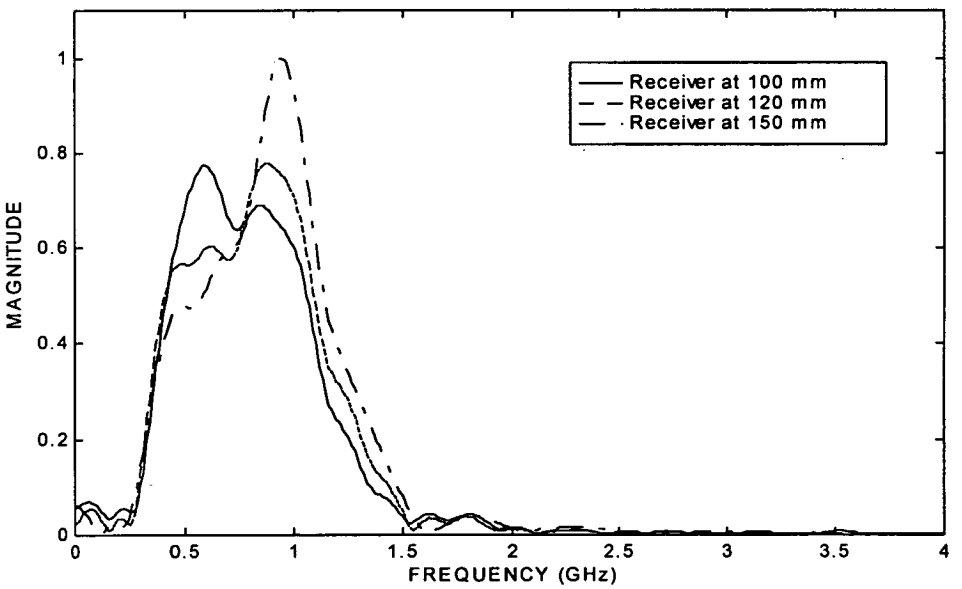

Figure 7.13 Coupling effect for tiles oven dried

a) Time domain

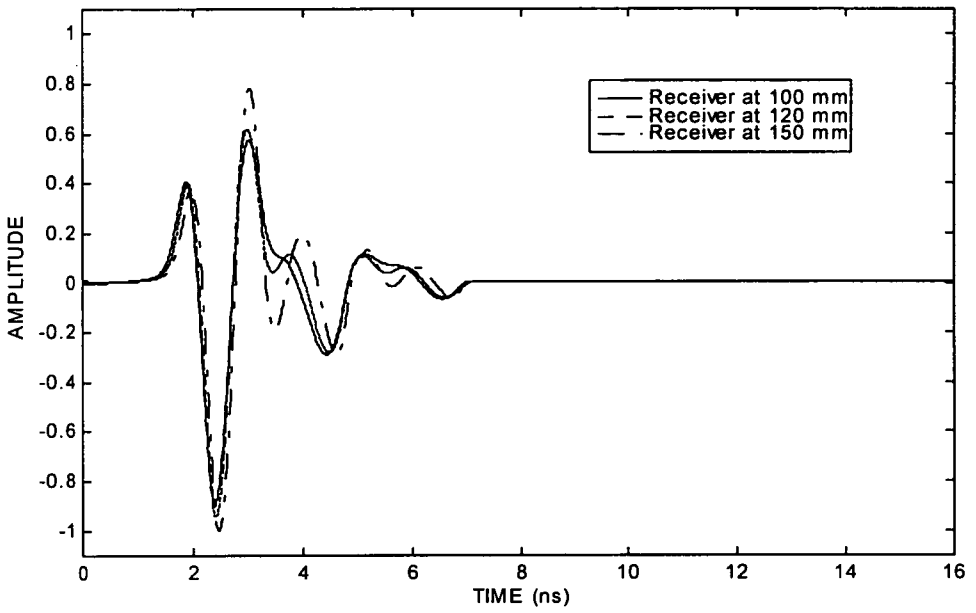

b) Frequency domain

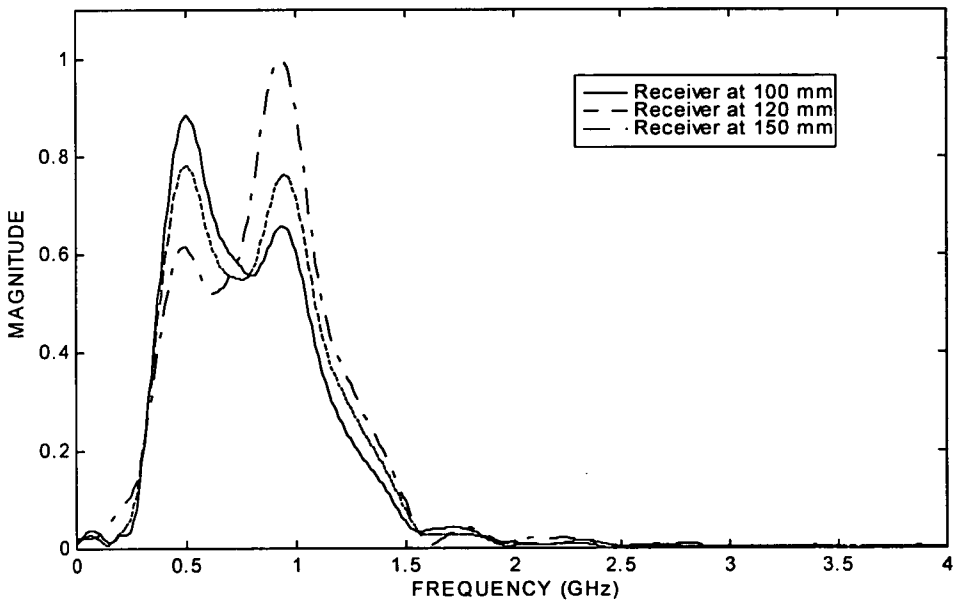

Figure 7.14 Coupling effect in air dried tiles

a) Time domain

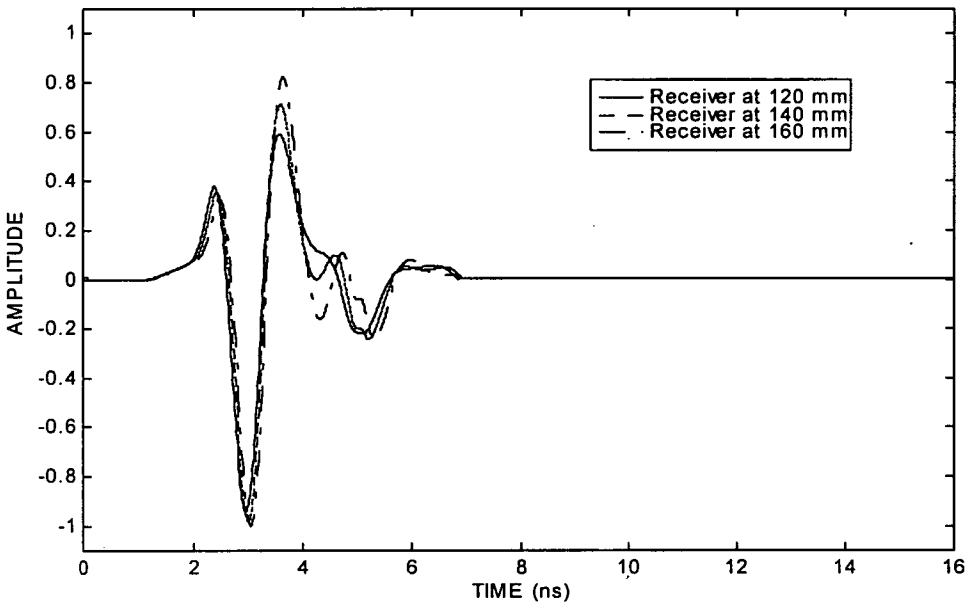

b) Frequency domain

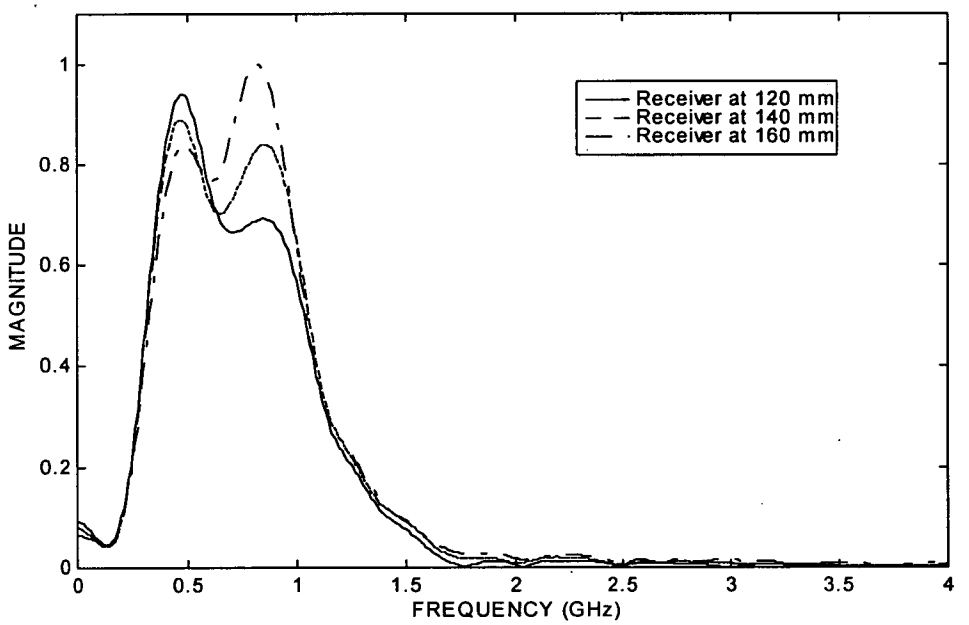

Figure 7.15 Coupling effect in saturated tiles

The second apparent wave mentioned before, may be attributed to multiple reflections between the receiver and the surface (ringing). This is a Radar operational problem that will always occur in practice when using contact antennas, either in transmission or reflection mode.

In the reflection mode, the first recorded signals will be a combination of the direct transmit pulse and the surface reflection. In practice however the combined pulse is often referred to as the " surface reflection" and always appears as a large band at the beginning of radar data. It appears that the ringing between the antenna and the interface air/material is present in all recorded data afterwards. The ringing intensity might be associated with the angle of incidence and refraction of the reflected rays (from the subsurface) at that interface. According to the Snell's law of refraction (equation 3.48), when the rays pass from a medium with dielectric constant ε_{r1} to another medium with dielectric constant ε_{r2}, and $\varepsilon_{r1} > \varepsilon_{r2}$, total refraction or large angles can occur for the transmitted rays. For low loss materials equation (3.48) can be rewritten as follows

$$\theta_t = sin^{-1}\left(sin\theta_i \frac{\sqrt{\varepsilon_{r1}}}{\sqrt{\varepsilon_{r2}}} \right) \qquad (7.3)$$

or,

$$\theta_i = sin^{-1}\left(sin\theta_t \frac{\sqrt{\varepsilon_{r2}}}{\sqrt{\varepsilon_{r1}}} \right) \qquad (7.4)$$

Thus, for a material with $\varepsilon_{r1} = 7$, total refraction ($\theta_t = 90°$) happens for incident angles $\theta_I \geq 22°$. It also suggests that the ringing effect will be reduced for greater angles of incidence (the refracted rays propagate along the interface air/material).

To complete the experiment, the signals were recorded with the antenna set in the reflection mode. The results are shown in Figure 7.16, which suggests that larger "surface reflections" will appear as the moisture content increases. The first 2.5 to 3

ns of the Radar data will be occupied by the large input signal. The practical consequence is that targets close to the surface will be obscured in the recorded data. In the concrete column experiment (chapter 6) this corresponded to depths up to 200 mm.

The distortion of the recorded pulses and the influence of the moisture content are again visible. Transmission mode was preferred during the experiments because it had the advantage of permitting the identification of the actual transmitted signal into the medium and its attenuation.

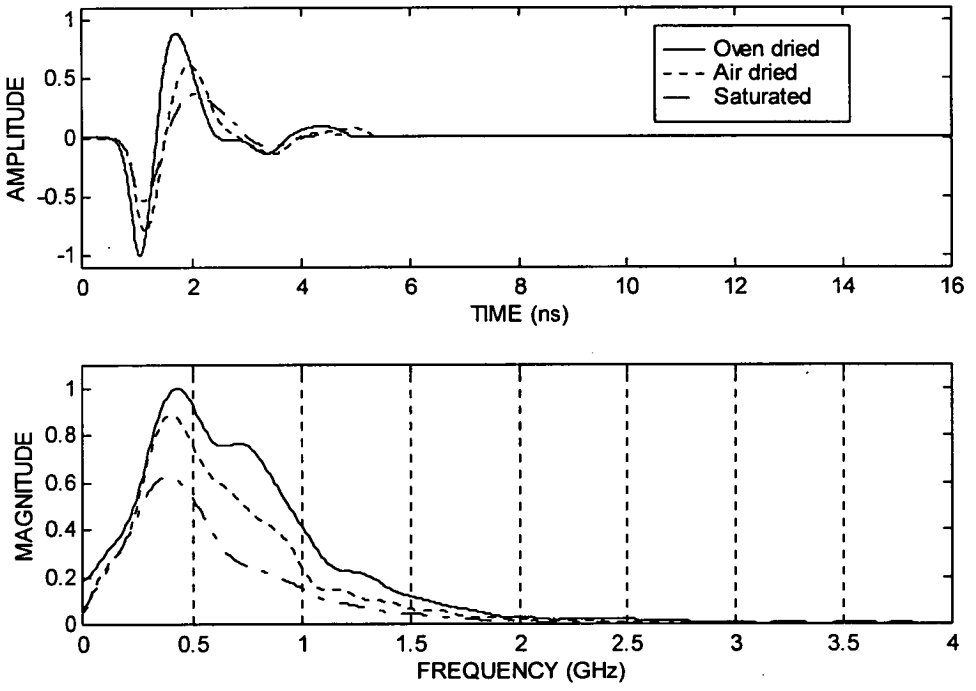

Figure 7.16 "Surface reflection" of a 900 MHz monostatic antenna on tiles

7.4 CONCLUSIONS

This chapter describes and contains the results of an experiment employing Radar on a set of commercial cement tiles.

The use of tiles permitted the simulation of extreme conditions for the moisture content. The values estimated for the dielectric constant ranged from 5.8 to 11.3, and therefore were comparable to those usually reported in the literature for concrete. The conclusions of this experiment can therefore be extended to common structural concrete.

The main aim of the experiment was to see the effect of the antenna coupling on the recorded data, and to check the preliminary results given by the concrete column.

The transmission mode was mostly used because it allowed isolation of the receiver. Data could then be collected with the receiver in contact with the tiles and away from them. The main advantage of this approach was that coupling and the transmitted signal could be clearly identified in the data. Also, it allowed the presence of moisture to be taken into account, when investigating the signal propagation through the tiles.

The specific conclusions that can be inferred from this chapter are:

1. The influence of the size of the antennas was investigated in relation to the estimation of the dielectric constant values of the tiles in terms of path length of the pulse. If the thickness of the tiles was considered, rather than the actual diagonal path length, then the values would be underestimated by 19 %.

2. Signal distortion affects travel time measurements, thus different references on a wave in the time domain (signal peaks) can produce variable results for the wave's

velocity. Equation (3.54) is very sensitive to small variations of time, and therefore dielectric constant values may change significantly. For example, taking the travel times given by the first two peaks, the difference was over 30 % for the saturated tiles.

3. This experiment confirms that a coupling effect between an antenna and concrete surface will happen for any moisture conditions: oven dried, air dried or saturated.

4. When using a 900 MHz monostatic antenna as transmitter, the first recorded signal (or "surface reflection") may occupy up to 3 ns of the Radar data.

5. Recorded signals may always contain some distortion due to coupling. The degree of distortion may be associated with the waves' refraction in the interface solid (or liquid) medium/air. However more research is necessary to confirm this conclusion.

6. The signals retain most of their original frequency components when transmitted into a medium different from air. It was more evident for the dry tiles, where the centre frequency of the recorded signals reached values over 850 MHz. This value is equivalent to the nominal centre frequency for the 900 MHz antennas in air.

7. When the materials contain moisture, amplitude attenuation and shape distortion will occur. High conductivity will increase these problems further.

8. When using contact antennas in the reflection mode, it is not easy to separately identify the distortion produced in the recorded signals by coupling or attenuation during propagation. They will always appear as a combined effect.

9. Further research is necessary to verify how much antenna coupling, moisture, salinity, particle size and travel distance may individually contribute to the wave's distortion.

CHAPTER 8

GENERAL DISCUSSION OF FINDINGS

CHAPTER 8

8. GENERAL DISCUSSION OF FINDINGS

8.1 INTRODUCTION

The work reported throughout this thesis has focused mainly on using Radar as a non-destructive testing technique on concrete. It started with a numerical analysis of electromagnetic wave propagation through concrete as described in chapter 5. The next step was to develop an experimental programme using concrete to obtain information about antenna coupling and signal distortion during propagation. An experimental concrete column was constructed with material variations. Lack of vibration and different mix proportions were used to produce variation in concrete porosity, and to observe their influence on signal behaviour in both the time and frequency domain. The results obtained were valid for a particular moisture content and its distribution within the concrete. This led to a second experimental programme in the laboratory, employing commercial cement tiles.

The use of cement tiles allowed the simulation of extreme conditions of the moisture content: oven dry and saturated. The limit values obtained for the dielectric constant were 5.9 and 11.4 respectively, clearly indicating that the corresponding radar results could be extended to normal structural concrete. In addition, a uniform distribution of moisture could be approximated for the whole model.

The results from the experiments have led to a better understanding of the problems associated with an antenna coupled to concrete and the subsequent wave propagation. Their influence on the frequency spectra and time measurements were

analysed and the relating implications were highlighted. The main aspects of the findings are discussed in the following sections.

8.2 RESOLUTION

A systematic numerical analysis was undertaken of electromagnetic wave propagation through concrete. This covered signal attenuation and velocity as well as aspects that can give support for more effectively designing a radar survey, such as vertical and horizontal resolution, clutter and depth of penetration.

The electrical properties were chosen according to the figures reported in the literature for concrete. The antennas' centre frequency used were those specified by the manufacturer for the antennas coupled to air. During the analysis these were adjusted to take into account possible changes when the antennas are coupled to a medium different from air, based upon the reference [154]. All the results obtained, despite not yet fully confirmed experimentally, are mainly addressed to potential radar users that are not familiar with the relevant theory. From this numerical experiment, field applications may then be better planned and more successful results can be expected.

Since it was a numerical study, initial assumptions were made, particularly for the maximum resolution and for the pulse's centre frequency. The resolution was assumed to be larger than $\lambda/4$ and therefore minimum or maximum limits for the frequency were obtained for each case. When suggesting the corresponding commercial antenna's centre frequency in air, possible signal distortion was considered. These assumptions were based on previous geological applications, and further refinement can be made for other materials such as concrete. For instance, the maximum resolution might turn out to be $\lambda/2$. While numerically it is an easy task to be performed, only practice or experimental research will confirm whether the quoted parameters are suitable.

All the assumptions mentioned above may however become invalid if the signal's frequency components are not well known. The experiments have confirmed that the nominal frequency in air cannot be used as reference for calculating resolution capabilities of radar. This was taken into account in the numerical study, but based on an empirical formula and considering only variation in the dielectric constant. The possible change in wave shape, with the pulse length becoming larger during their propagation, is normally ignored or unknown in the civil engineering field. The latter has not been given yet due attention by researches regarding building materials. This is quite evident by the small number of publications in the literature. Papers regarding civil engineering applications have only mentioned the problem without quantifying it.

An experimental programme was then carried out to obtain some additional systematic results. First, a column was designed containing layers of concrete with different sand contents and placed with and without vibration. Special attention was given to the frequency spectra of the reflected signals coming from metal bars located at various depths. The results were expected to give a realistic basis for the assumptions made in the numerical study.

Nine hundred MHz antennas were used during the tests, and the results for the signal centre frequency are summarised in Table 8.1. The average dielectric constant was 7.4, and due to the moisture gradient, real values may be expected between 6 (surface zones) and 10 (internal zones), depending on the ambient conditions.

The equation (5.2) (chapter 5) suggests an average centre frequency of 672 MHz for 900 MHz antennas transmitting pulses into concrete. This value matches quite well for bar depths up to 90 mm (or travel distance $\cong$ 210 mm). For deeper bars the centre frequency becomes lower and therefore the pulses become larger.

What one has to bear in mind is that equation (5.2) gives the expected centre frequency for a transmitted signal and the values shown in Table 8.1 are the centre frequencies of recorded signals. Referring to the conclusions reached in the experiment described in chapter 7, the signals transmitted by the antennas into a medium different from air still contain most of their original frequency components. During the propagation the waves become more distorted and the centre frequency shifts to a lower value. As a result, one may infer that targets at certain depths might be resolved when the signals reach them, but may not be distinguishable in the recorded data. It is important to stress, that the influence of the antenna coupling is already included in Table 8.1, as coupling and propagation appear as a combined effect.

Table 8.1 Variation of centre frequency with depth (900 MHz antennas in reflection mode)

Depth of bars	Shortest path length (Approx. values)	Centre frequency of recorded signals
90 mm	~ 240 mm	~ 650 MHz
190 mm	~ 410 mm	~ 500 MHz
290 mm	~ 600 mm	~ 400 MHz

The resulting centre frequencies might be considered for estimating the capabilty of radar resolution when working with 900 MHz antennas.

Additional experimental work will be necessary to obtain more quantitative information for calibrating the results given by the numerical analysis. It should include different antennas, larger aggregate size, different mix proportions and salinity. Small variations in porosity, such as in the present case, do not seem to influence the frequency response of the recorded data.

8.3 TIME DOMAIN MEASUREMENTS

Travel time readings

Travel time readings are mainly used to work out the depth of targets when the dielectric properties of the materials are known (or the velocity of wave propagation is known). Conversely, if the distances are known the dielectric constant can be estimated.

The most accurate results will be obtained if the start point or sample of the transmitted or received pulse can be identified in the data records. In practice this is very difficult due to the presence of noise, system fluctuations and secondary reflections. The latter is more evident in the received signals. This is why the peaks of waveforms are usually chosen as reference points to calculate the travel times.

According to the experiments, it could clearly be shown that the signal peaks can easily introduce inaccuracies in the travel time readings. It is caused by the change in the pulse shapes, which become larger as they propagate through a medium different from air, as discussed before. Differences in the dielectric constant values have reached up to 33 % when the material was saturated. Higher conductivity may worsen the problem even more.

The shape distortion affects all points in a waveform, increasing toward its tail. Therefore, accuracy will be improved if points located at the beginning can be identified. During the research reported in this thesis, the point corresponding to the first small positive peak was chosen whenever possible (see Figure 6.36).

Size of the antennas

Another possible source of error can be associated with the size of the antennas. Its influence can be noticed for instance, when using 900 MHz monostatic antennas in the transmission mode and dealing with material thicknesses up to 500 mm (or up to 250 mm in the reflection mode). The real path length is dependent on the separation of the in-built transmitter and receiver. This aspect is quite often omitted in practice by Radar users, especially those not well familiar with the technique. This may be related to the fact that in most cases only qualitative aspects are involved in the surveys. Moreover, the equipment specification given by the manufacturer normally does not provide users with all the necessary information regarding the antenna internal geometry.

Concrete porosity

One of the potential applications of Radar is to detect the variation of concrete porosity, as mentioned in chapter 3. This would allow one to find the regions of poor concrete, commonly associated with poor compaction, material segregation and mix proportion. Until now however, Radar has not seen to be able to detect such problems in practice. A few cases of success have been reported, but only when the problem was localised (equivalent to an air void) and could be visualised in the recorded data.

In the concrete column experiment described in chapter 6, it was actually possible to detect poorer concrete, not as a different pattern on the displayed data, but as small time advances when compared to sound concrete (see Figure 6.30). The problem was mainly localised near to the surface area as shown by a ultrasonic tomographic image (Figure 6.31). However it was not possible to extract this information from the single time domain traces.

In practice, the presence of heavy reinforcement and uneven surfaces may completely mask the ability of Radar to detect variations in material porosity. Nevertheless, the small time delays caused by poorer compaction may represent an additional source of errors in time measurements. This can affect the estimation of thicknesses and dielectric constant values with Radar either in transmission or reflection mode.

CHAPTER 9

OVERALL CONCLUSIONS AND RECOMMENDATIONS

CHAPTER 9

9. OVERALL CONCLUSIONS AND RECOMMENDATIONS

This chapter aims to present an overview of the main conclusions reached during the research. In order to give continuity to the work reported in this thesis, a set of recommendations for future research is presented.

9.1 OVERALL CONCLUSIONS

a) Radar has been confirmed as a powerful tool as a non-destructive testing technique, as long as one is aware of its limitations and how to improve its capabilities. It is fast in data acquisition and permits the collection of large amounts of data that can be easily transferred to a computer for post-processing. Despite needing skilled people for data analysis and interpretation, the equipment itself can be easily operated with little training.

b) A radar field survey when carefully designed can increase the chances of success. Case histories may play an important role in this, especially the unsuccessful ones. However, there is still a lack of technical specifications that might serve as guidance for radar users who do not want (or cannot) spend time to handle the background theory. The standardisation of radar as a well-established non-destructive testing technique is still in its early stages. Meanwhile, the results given in chapter 5 and conclusions reached in the experimental work can be extremely helpful.

c) Special laboratory setups with sophisticated antennas have been used to study radar on concrete. Also new systems with very high frequency antennas are being proposed mainly for bridge deck inspections (depth < 300 mm). Most of these systems employ air coupled antennas, which do not present coupling problems. However for structures or buildings in general, the commercial systems available to potential users are still limited to the kind used during the experiments reported in this thesis. Usually contact antennas are employed to achieve more penetration and thus coupling will always be present. The limitations of this equipment are still not completely known.

d) The nominal centre frequency of transmitted pulses in air specified by the manufacturer cannot be adopted to define whether sub-surface targets can be resolved. Antenna coupling and signal shape changes during propagation may drastically limit the maximum resolution.

e) The centre frequency of pulses transmitted into concrete by a 900 MHz antenna given by the empirical equation (5.2) (adopted for the numerical study) is 672 MHz, about 75 % of the value measured in air. However experimental data indicates that the actual centre frequency can fall below 400 MHz, depending on the material's moisture content and signal path length. Therefore the tables presented in chapter 5 for resolution and clutter may have to be adjusted.

f) In the time domain Radar may detect concrete with variable porosity. This potential application of radar may be useful for quality control of concrete. However the degree of sensitivity has to be better studied as the movement of the antenna on uneven surfaces and the presence of heavy reinforcement may lead to erroneous interpretation of the data.

g) The frequency spectrum of the transmitted pulses into concrete is affected by the antenna coupling depending on the dielectric properties of the material near the

surface. If the surface is dry the pulse's spectrum initially retains most of the original frequency components, changing afterwards due to distortion during propagation.

h) When dealing with shallow targets, the size of the monostatic antennas (or the separation between in-built transmitter and receiver) cannot be ignored. It may significantly affect calculated wave velocities.

i) The wave velocity may be frequency dependent at lower frequencies, mainly at higher conductivities. Therefore when concrete assumes characteristics of a conductor the simplified equation for calculating wave velocities will overestimate the results.

j) For the range of commercial contact antennas at present available, the vertical resolution (or depth resolution) will in practice be greater than 0.05 m.

k) At short range times applications of radar, clutter may be a significant problem. For smaller depths higher frequency antennas are used. Therefore energy scattering in concrete will be increased, and may affect the quality of the recorded data.

l) The horizontal resolution can be estimated for target depths up to 200 mm using the concept of Fresnel zone. For deeper targets, the model has to be improved to take into account the possible reduction of the width of the radar beam with depth due to signal attenuation.

9.2 RECOMMENDATIONS FOR FUTURE RESEARCH

a) To study signal amplitude, attenuation, and shape distortion due to clutter, involving concrete with larger sizes of aggregates.

b) With more contrasting models, to verify the influence of material porosity on signal distortion.

c) To obtain equations that might estimate the wave's attenuation and shape distortion, which could be used for forward modelling. Computer simulation may then preview the radar response in specific applications.

d) To improve the model adopted in the numerical analysis for horizontal resolution, taken into account the attenuation of the outer rays of the radar beam.

e) To study the wave attenuation in building materials as a function of moisture content. This would allow better quantification of the useful depth of penetration. If one is using models like that used in the experiment described in chapter 7, one may have good control of the amount of moisture and could easily set up different thicknesses. Salinity could also be incorporated by adding salt to the water when saturating the material.

f) Concrete is a pre-prepared material that can, after hardening, present variable properties, depending on the mix proportions, particle size, degree of vibration, etc. All these factors may affect the electrical properties of the concrete. Very little published experimental data is available. Therefore more research is necessary to verify their influence on the electromagnetic behaviour of concrete.

g) Experimental work is required to obtain more quantitative information regarding target detection in concrete, to calibrate the numerical results proposed in chapter 5. In addition, it would allow more realistic criteria for the maximum resolution to be established.

h) To improve the empirical equation adopted in chapter 5 for estimating the centre frequency of transmitted pulses, taking into account its variation during propagation.

i) To test other antennas that may be employed on concrete, and to verify their performance concerning the aspects covered in the present thesis, such as the influence of antennas' size and signal distortion.

CHAPTER 10

REFERENCES

CHAPTER 10

10. REFERENCES

1. Bungey, J. H. and Millard, S. G. (1996). *Testing of concrete in structures.* Blackie Academic & Professional, 3rd ed., 286 pp.

2. Rigden, S. R., Burley, E., Poole, A. and Christer, A. (1989). "Inspection practices for concrete structures in the UK." *The life of structures*, G. S. T. Armer ed., Butterworths, pp. 137-144.

3. Uomoto, T. and Misra, S. (1993)."Non-destructive evaluation of RC structures - recent developments in Japan." *Proc. Int. Conf. on Non-Destructive Testing in Civil Engineering*, Liverpool, The Brit. Instn. of NDT, Vol. I, pp. 65-77.

4. Weil, G. (1995)."Non-destructive testing of bridge, highway and airport pavements." *Proc. Int. Symp. on Non-Destructive Testing in Civil Engineering (NDT-CE)*, Berlin, DGZfP, Vol. 1, pp. 467-474.

5. Halder, A. and Zhao, Z. (1996)."Fatigue reliability evaluation, updating and maintenance of steel bridges using NDI." *Proc. NSF Workshop on Structural Reliability in Bridge Engineering*, University of Colorado, Boulder, McGraw-Hill Inc, pp. 179-184.

6. Perenchio, W. F. (1989). "The condition survey." *Concrete International*, **11**(1), pp. 59-62.

7. Tomsett, H. N. (1987)."Non destructive testing of concrete." *Proc. 4th European Confer.*, London, The Br. Instn. of NDT, Vol. 1, pp. 289-301.

8. Filipczynski, L., Pawloswki, Z. and Wehr, J. (1966). *Ultrasonic methods of testing materials*. Butterworths, (Translation), London, 280 pp.

9. Hull, B. and John, J. (1988). *Non-destructive testing*. Mc Millan Education Ltd., London, 144 pp.

10. Tomsett, H. N. (1980). "The practical use of ultrasonic pulse velocity measurements in the assessment of concrete quality." *Magazine of Concrete Research*, **32**(110), pp. 7-16.

11. Sansalone, M. and Carino, N. J. (1991). "Stress wave propagation methods." *Handbook on non-destructive testing of concrete*, M. V. Malhotra and N. J. Carino, Eds., CRC Press, Boston, Chap. 12, pp. 275-304.

12. Jones, R. (1962). *Non-destructive testing of concrete.* Cambridge University Press, Cambridge, 101 pp.

13. James Electronics Inc. *"Instruction manual for model C-4899, V-Meter."* Chicago, Illinois, USA.

14. CNS Electronics Ltd. *"PUNDIT- Manual of instructions and operation."* 61-63 Holmes Rd, London.

15. Naik, T. R. and Malhotra, V. M. (1991). "The ultrasonic pulse velocity method." *Handbook on non-destructive testing of concrete*, V. M. Malhotra and N. J. Carino, Eds., CRC Press, Boston, Chap. 7, pp. 169-188.

16. Dixon, S., Edwards, C. and Palmer, S. B. (1995). "Experiment to monitor adhesive cure using electromagnetic acoustic transducers." *Insight*, **37**(12), pp. 969-973.

17. Atkinson, R. H. and Schuller, M. P. (1994). "Characterization of concrete condition using acoustic tomographic imaging." *Rep. Phase I SBIR*, Boulder, Colorado, U.S. Nuclear Regulatory Commission.

18. Colla, C., Forde, M. C., McCann, D. M. and Das, P. C. (1995)."Investigation of masonry arch bridges using non-contacting NDT." *Proc. 6th Int. Conf. on Structural Faults and Repair*, London, Engineering Technics Press, Vol. 1, pp. 235-239.

19. Jalinoos, F., Olson, L. D. and Sack, D. A. (1995)."Use of combined acoustic impact echo and crossmedium tomography methods for defect characterization in concrete civil structures." *Proc. 6th Int. Conf. on Structural Faults and Repair*, London, Engineering Technics Press, Vol. 2, pp. 43-49.

20. Atkinson, R. H., Schuller, M. P. and Frank, D. A. (1995)."Acoustic tomography studies of reinforced concrete." *Proc. 6th Int. Conf. on Structural Faults and Repair*, London, Engineering Technics Press, Vol. 2, pp. 39-42.

21. Olson Engineering Inc. *"Condition assessment of buildings and bridges."* Golden, CO, Publicity material.

22. Popovics, S., Komlos, K. and Popovics, J. (1995)."Comparison of DIN/ISO 8047 (Entwurf) to several standards on determination of ultrasonic pulse velocity in concrete." *Proc. Int. Symp. on Non-Destructive Testing in Civil Engineering (NDT-CE)*, Berlin, DGZfP, Vol. 1, pp. 521-528.

23. BS 1881: Part 203. *"Recommendations for measurement of velocity of ultrasonic pulses in concrete."* British Standards Institution, London.

24. Schuller, M. P. and Woodham, D. B. (1996)."Evaluating structural damage and deterioration using tomographic velocity reconstructions." *Proc. NSF Workshop on Structural Reliability in Bridge Engineering*, University of Colorado, Boulder, McGraw-Hill Inc, pp. 334-337.

25. ACI Committee 364 (1993). "Guide for evaluation of concrete structures prior to rehabilitation." *ACI Materials J.*, **90**(5), Committee Report ACI 364.1R, pp. 479-498.

26. Hillger, W. (1993)."Imaging of defects in concrete by ultrasonic pulse-echo technique." *Proc. 5th Int. Conf. on Structural Faults and Repair*, Edinburgh, Engineering Technics Press, Vol. 3, pp. 59-65.

27. Krause, M. *et al.* (1995)."Comparison of pulse-echo methods for testing concrete." *Proc. Int. Symp. on Non-Destructive Testing in Civil Engineering (NDT-CE)*, Berlin, DGZfP, Vol. 1, pp. 281-295.

28. Tasker, C. G., Milne, J. M. and Smith, R. L. (1990). "Recent work at the National NDT Centre on concrete inspection." *The British J. of Non-Destructive Testing*, **32**(7), pp. 355-359.

29. Scruby, C. B., Dewhurst, R. J., Hutchins, D. A. and Palmer, S. B. (1982). *"Research techniques in NDT."* Academic Press, British Standards Institution BS:1881 (1986) Part 203., pp. 281-327.

30. Bushell, A. C., Edwards, C. and Palmer, S. B. (1991). "Laser-generated surface waves on plates of varying thickness." *The British J. of Non-Destructive Testing*, **33**(4), pp. 177-182.

31. Jansohn, R., Kroggel, O. and Ratmann, M. (1995)."Detection of thickness, voids, honeycombs and tendons utilising ultrasonic impulse-echo technique." *Proc. Int. Symp. on Non-Destructive Testing in Civil Engineering (NDT-CE)*, Berlin, DGZfP, Vol. 1, pp. 419-427.

32. Sansalone, M. and Carino, N. J. (1988). "Impact-echo method: detecting honeycombing, the depth of surface-opening cracks, and ungrouted ducts." *Concrete International*, **10**(4), pp. 38-46.

33. Carino, N. J. and Sansalone, M. (1992). "Detection of voids in grouted ducts using the impact-echo method." *ACI Materials Journal*, **89**(3), pp. 296-303.

34. Carino, N. J., Sansalone, M. and Hsu, N. N. (1986). "Flaw detection in concrete by frequency spectrum analysis of impact-echo waveforms." *International advances in nondestructive testing*, Gordon and Breach Sciences Publishers S.A.(UK), pp. 117-146.

35. Chan, H. F. C., Heywood, C. and Forde, M. C. (1987)."Developments in transiet shock pile testing." *Proc. Int. Conf. Foundations & Tunnels-87*, Eng. Technics Press, Edinburgh, Vol. 1, pp. 245-261.

36. Fegen, I., Forde, M. C. and Whittington, H. W. (1979)."The detection of voids in concrete piles using sonic methods." *Proc. 4ème Colloque International sur les Méthodes de Contrôle Non Destructif*, Grenoble, pp. 40-46.

37. Sansalone, M. and Carino, N. J. (1989). "Detecting delaminations in concrete slabs with and without overlays using the impact-echo method." *ACI Materials J.*, **86**(2), pp. 175-184.

38. Davis, A. G. and Dunn, C. S. (1974). "From theory to field experience with the non-destructive vibration testing of piles." *Proc. Instn. Civ. Engrs.*, **57**(Dec.), Part 2, pp. 571-593.

39. Forde, M. C. (1996)."Invited special paper: Reliability of NDE in bridge assessment." *Proc. NSF Workshop on Structural Reliability in Bridge Engineering*, University of Colorado at Boulder, McGraw-Hill Inc, pp. 162-171.

40. Carino, N. J. and Sansalone, M. (1990). "Flaw detection in concrete using the impact-echo method." *Bridge evaluation, repair and rehabilitation*, A. S. Nowak, ed., Kluwer Academic Publishers, pp. 101-118.

41. Sansalone, M. and Streett, W. (1995)."Use of the impact-echo method and field instrument for non-destructive testing of concrete strucutures." *Proc. Int. Symp. on Non-Destructive Testing in Civil Engineering (NDT-CE)*, Berlin, DGZfP, Vol. 1, pp. 495-502.

42. Martin, J. and Forde, M. C. (1995). "Influence of concrete properties on impulse hammer spectrum and compression wave velocity." *Construction and Building Materials*, **9**(4), pp. 245-255.

43. Olson, L. D., Sack, D. A. and Phelps, G. C. (1992)."Sonic NDE of bridges and other concrete structures." *Proc. Nondestructive Evaluation of Civil Structures and Materials*, Boulder, Colorado, pp. 279-295.

44. Robert, A., Baillon, L. and Huet, C. (1995)."Improving the interpretation of infrared and ground penetrating radar used for non-destructive testing of civil engineering structures." *Proc. Int. Symp. on Non-Destructive Testing in Civil Engineering*, Berlin, Vol. 1, pp. 375-382.

45. Weil, G. J. (1991). "Infrared thermographic techniques." *Handbook on non-destructive testing of concrete*, M. V. Malhotra and N. J. Carino, Eds., CRC Press, Boston, Chap. 13, pp. 305-316.

46. Kern, D. Q. (1984). *Process heat transfer*. Mc Graw-Hill, 22 ed, 871 pp.

47. Manning, D. G. and Masliwec, T. (1990)."Operational experience using radar and thermography for bridge deck condition survey." *Proc. Conf. on Nondestructive Evaluation of Civil Structures and Materials*, Boulder, Colorado, pp. 233-244.

48. Kaasinen, H. (1993). "Assessing the quality of the waterproofing of bridges using thermography." *The British J. of Non-Destructive Testing*, **35**(6), pp. 301-304.

49. de Bosset, C. and Robert, A. (1995)."Non-destructive testing methods applied to bridge decks in order to localize the defects associated with the waterproof membrane." *Proc. Int. Symp. on Non-Destructive Testing in Civil Engineering (NDT-CE)*, Berlin, DGZfP, Vol. 1, pp. 713-720.

50. Weil, G. J. (1993)."Non-destructive testing of bridge, highway and airport pavements." *Proc. 5th Int. Conf. on Structural Faults and Repair*, Edinburgh, Engineering Technics Press, Vol. 2, pp. 71-80.

51. Weil, G. J. (1989)."Nondestructive remote sensing of subsurface utility distribution pipe problems using infrared thermography." *Proc. 2nd Int. Conf. on Pipeline Constr. Cong.*, Centrum Hamburg.

52. Ward, I. C. (1994). "The use of a thermal imaging system in building and air-conditioning applications." *Insight*, **36**(7), pp. 511-513.

53. Titman, D. J. (1993)."Advances in the use of thermal imaging techniques in civil engineering." *Proc. Int. Conf. on Non-Destructive Testing in Civil Engineering*, Liverpool, The Brit. Instn. of NDT, Vol. II, pp. 845-855.

54. ASTM D 4788 *"Test method for detecting delaminations in bridge decks using infrared thermography."*

55. Weil, G. J. (1992)."Non-destructive testing of bridge, highway and airport pavements." *Proc. Nondestructive Evaluation of Civil Structures and Materials*, Boulder, Colorado, pp. 385-394.

56. Malhotra, V. M. (1984). "In situ/nondestructive testing of concrete - a global review." American Concrete Institute, SP 82-1, pp. 1-16.

57. Mitchell, T. W. (1991). "Radioactive/nuclear methods." *Handbook on non-destructive testing of concrete*, M. V. Malhotra and N. J. Carino, Eds., CRC Press, Boston, Chap. 10, pp. 227-252.

58. Hönig, A. (1993)."Radiation - one of the NDT methods in civil engineering." *Proc. Int. Conf. on Non-Destructive Testing in Civil Engineering*, Liverpool, The Brit. Instn. of NDT, Vol. I, pp. 25-44.

59. BS 1881: Part 205. *"Recommendations for radiography of concrete."* British Standards Institution, London.

60. Kearey, P. and Brooks, M. (1991). *An introduction to geophysical exploration.* Blackwell Scientific Publications, Oxford, 2nd ed, 254 pp.

61. Clemena, G. G. (1991). "Short-pulse radar methods." *Handbook on non-destructive testing of concrete*, CRC Press, Boston, Chap. 11, pp. 252-274.

62. Kraus, J. D. (1988). *Antennas*. McGraw-Hill Book Company, New York, 892 pp.

63. Walter, C. H. (1965). *Traveling wave antennas*. McGraw-Hill, New York, 429 pp.

64. Chung, T., Carter, C. R., Masliwec, T. and Manning, D. G. (1992). "Impulse radar evaluation of asphalt-covered bridge decks." *IEEE Trans. on Aerospace and Electronic Systems*, **28**(1), pp. 125-137.

65. Daniels, D. J., Gunton, D. J. and Scott, H. F. (1988). "Introduction to sub-surface radar." *Proc. Inst. Elect. Engrs.*, **135-F**(4), pp. 278-320.

66. Scullion, T. and Saarenketo, T. (1995)."Ground penetrating radar technique in monitoring defects in roads and highways." *Proc. Symp. on the Application of Geophysics to Engineering and Environmental Problems - SAGEEP' 95*, Orlando-Florida, pp. 63-72.

67. Bertram, C. L., Campbell, K. J. and Sandler, S. S. (1972)."Locating large masses of ground ice with an impulse radar system." *Proc. 8th Int. Symp. on Remote Sensing*, Willow Run Laboratory, University of Michigan.

68. Morey, R. M. and Harrington Jr, W. S. (1972). "Feasibility of electromagnetic subsurface profiling." *Rep. EPA-R2-72-082,* U.S. Environmental Protection Agency, Washington D.C.

69. Campbell, K. J. and Orange, A. S. (1974). *"A continuous profile of sea ice and freshwater ice thickness by impulse radar."* Polar Rec., 17.31.

70. Morey, R. M. (1974)."Application of downward looking impulse radar." *Proc. 13th Annu. Canadian Hydrographic Conf.*, Canada Centre for Inland Waters, Burlington, Ontario, Canada.

71. Brown, W. E. (1971)."Lunar subsurface exploration with coherent radar." *Proc. Conf. Lunar Geophys.*, Lunar Science Inst., Houston, pp. 113-127.

72. Porcello, L. J. *et al.* (1974). "The Apollo lunar sounder radar system." *Proc. IEEE*, **62**, pp. 769-783.

73. Alongi, A. V. (1973)."A short-pulse high-resolution radar for cadaver detection." *Proc. 1st Int. Electronic Crime Countermeasures Conf.*, pp. 79-87.

74. Bowders, J. J. and Koerner, R. M. (1982). "Buried container detection using ground-probing radar." *J. Hazard. Mater.*, **7**, pp. 1-17.

75. Lord, A. E. and Koerner, R. M. (1987). "Nondestructive testing techniques to detect contained subsurface hazardous." *Rep. EPA/600/2-87/078,* Drexel University, Philadelphia.

76. Haeni, F. P. and Trent, R. E. (1988)."Measuring scour with ground-penetrating radar, sonar, and seismic geographical methods." *Proc. 67th Annu. Meet. of the Transportation Research Board,* Washington D.C.

77. Davidson, N., Padaratz, I. and Forde, M. C. (1995)."Quantification of bridge scour using impulse radar." *Proc. Int. Symp. on Non-Destructive Testing in Civil Engineering (NDT-CE)*, Berlin, DGZfP, Vol. 1, pp. 61-68.

78. Millard, S. G. and Thomas, C. (1995). "Assessment of bridge pier scour using impulse radar." *Proc. Instn. Civ. Engrs. Structs. & Bldgs.*, **110**(May), pp. 216-227.

79. Davidson, N. C., Hardy, M. S. A., Broughton, K. J., Forde, M. C. and Das, P. C. (1996)."Investigation of bridge scour using digital impulse radar." *Proc. 3rd Conf. on Nondestructive Evaluation of Civil Structures and Materials*, Boulder, Colorado, pp. 69-79.

80. Caldecott, R., Terzuoli, A. J. and Hall, J. P. (1979)."Underground transmission 1- An underground mapping system using impulse radar." *Proc. 7th IEEE/PES Transmission and Distribution Conf. and Expos.*, pp. 99-107.

81. Olver, A. D., Cuthbert, L. G., Nicolaides, M. and Carr, A. G. (1982)."Portable FMCW radar for locating buried pipes." *Proc. Radar 82 Conf.*, London, IEE Conf. Publication 216, pp. 413-418.

82. Botros, A. Z., Olver, A. D., Cuthbert, L. G. and Farmer, G. (1984). "Microwave detection of hidden objects in walls." *Electron. Lett.*, **20**, pp. 379-380.

83. Fenning, P. J. and Brown, A. J. (1995)."Ground probing radar investigation within pipes and tunnels." *Proc. 6th Int. Conf. on Structural Faults and Repair*, London, Engineering Technics Press, Vol. 3, pp. 101-105.

84. Bertram, C. L., Morey, R. M. and Sandler, S. S. (1974). "Feasibility study for rapid evaluation of airfield pavements." *Rep. AFWL-TR-71-178,* U.S. Air Force Weapons Laboratory.

85. Clemena, G. G. and McGhee, K. H. (1980). *"Applicability of radar subsurface profiling in estimating sidewalk undermining."* Transport. Res. Rec., 752, pp. 21-28.

86. Kovacs, A. and Morey, R. M. (1980). "Detection of cavities under concrete pavement." *Rep. 83-18,* U.S. Cold Region Research and Engineering Laboratory (CRREL), pp. 41.

87. Clemena, G. G., Sprinkle, M. M. and Long Jr., R. R. (1987). "Use of ground penetrating radar for detecting voids under concrete pavement." *Rep. No. 1109,* Transportation Research Board.

88. Holt, F. B. and Eales, J. W. (1987). "Non-destructive evaluation of pavements." *Concrete International,* **9**(6), pp. 41-45.

89. Manning, D. and F., H. (1983). "Detecting deterioration in asphalt-covered bridge decks." Transp. Res. Rec. No. 899, pp. 10.

90. Clemena, G. G. (1983). "Non-destructive inspection of overlaid bridge decks with ground-penetrating radar." *Rep. No. 899,* Transp. Res. Board, pp. 21-32.

91. Cantor, T. (1984). "Review of penetrating radar as applied to nondestructive evaluation of concrete." In-Situ/Non-Destructive Testing of Concrete Institute, Detroit, pp. 581-601.

92. Maser, K. R. (1993)."Highway speed radar for pavement and bridge deck evaluation." *Proc. Int. Conf. on Non-Destructive Testing in Civil Engineering,* Liverpool, The Brit. Instn. of NDT, Vol. I, pp. 187-209.

93. Saarenketo, T. and Soderqvist, M. K. (1993)."GPR applications for bridge deck evaluations in Finland." *Proc. Int. Conf. on Non-Destructive Testing in Civil Engineering,* Liverpool, The Brit. Instn. of NDT, Vol. I, pp. 211-226.

94. Chung, T., Carter, C. R., Masliwec, T. and Manning, D. G. (1994). "Impulse radar evaluation of concrete, asphalt and waterproofing membrane." *IEEE Trans. on Aerospace and Electronic Systems,* **30**(2), pp. 404-415.

95. Maijala, P., Saarenketo, T. and Valtanen, P. (1994)."Correlation of some parameters in GPR measurement data with quality properties of pavements and concrete bridge decks." *Proc. 5th Int. Conf. on Ground Penetrating Radar,* Kitchener, Ontario, Canada, Vol. 1, pp. 393-406.

96. Fenning, P. J., Jack, A. G. and Veness, J. K. (1993)."Ground probing radar applications in site investigation." *Proc. Int. Conf. on Non-Destructive Testing in Civil Engineering,* Liverpool, The Brit. Instn. of NDT, Vol. I, pp. 113-140.

97. Roddis, W. M. K., Maser, K. R. and Gisi, A. J. (1992). *"Radar pavement thickness evaluations for varying base conditions."* Transp. Res. Board, Washington D.C., Transp. Res. Rec. No. 1355.

98. Maser, K., Kristiansen, J., Schellenberger, W. and Fippinger, F. (1995)."Evaluation of pavement thickness using ground penetrating radar." *Proc. Int.. Symp. on Non-Destructive Testing in Civil Engineering (NDT-CE)*, Berlin, DGZfP, Vol. 1, pp. 655-662.

99. Vaughan, C. J. (1986). "Ground-penetrating radar surveys used in archaeological investigations." *Geophysics*, **51**(3), pp. 595-604.

100. Imai, T., Sakayama, T. and Kanemori, T. (1987). "Use of ground-probing radar and resistivity surveys for archaeological investigations." *Geophysics*, **52**, pp. 137-150.

101. Bungey, J. H., Millard, S. G. and Shaw, M. R. (1991)."Use of sub-surface radar for structural assessment of in-situ concrete." *Proc. ACI International Conference*, Hong Kong, ACI, pp. 128-31.

102. Fenning, P. J., Matthews, S. L. and Veness, K. J. (1989)."Radar inspection of concrete structures." *Proc. Int. Conf. on Structural Faults and Repair*, London, Engineering Technics Press, Vol. 2, pp. 219-229.

103. Bailey, M. (1989)."The use of ground penetrating impulse radar in the investigation of structural faults." *Proc. 4th Int. Conf. on Structural Faults and Repairs-89*, London, Engineering Technics Press, Vol. 1, pp. 11-18.

104. de Vekey, R. C., Ballard, G. and Adderson, B. W. (1989)."The effectiveness of radar for the investigation of complex LPS joints." *Proc. Int. Seminar of the Life of Structures - Physical Testing*, Cambridge, University Press-UK, pp. 116-126.

105. Cooke, R. S., Ashhurst, D. M., McCavitt, N. and Forde, M. C. (1993)."Digital radar assessment of Besses O'TH' Barn post-tensioned precast concrete segmental rail bridge." *Proc. 5th Int. Conf. on Structural Faults and Repair*, Edinburgh, Engineering Technics Press, Vol. 1, pp. 305-313.

106. Flohrer, C. and Bernhardt, B. (1993)."Detection of prestressed steel tendons behind reinforcement bars, detection of voids in concrete structures - a suitable application for radar systems." *Proc. Int. Conf. on Non-Destructive Testing in Civil Engineering*, Liverpool, The Brit. Instn. of NDT, Vol. II, pp. 227-234.

107. Jack, A. G. (1993)."Surface penetrating radar for inspecting bridge superstructures and postensioning cable ducts." *Proc. 5th Int. Conf. on Structural Faults and Repair*, Edinburgh, Engineering Technics Press, Vol. 1, pp. 293-296.

108. Maierhofer, C., Borchardt, K. and Henschen, J. (1995)."Application and optimization of impulse-radar for non-destructive testing in civil engineering." *Proc. Int.. Symp. on Non-Destructive Testing in Civil Engineering (NDT-CE)*, Berlin, DGZfP, Vol. 1, pp. 663-672.

109. Chidiac, J., Rainer, J., Davis, L. and Johnson, B. (1995)."Use of impulse radar for investigating the integrity of stone-masonry walls." *Proc. Int. Symp. on Non-Destructive Testing in Civil Engineering (NDT-CE)*, Berlin, DGZfP, Vol. 1, pp. 487-494.

110. Forde, M. C., McCavitt, N. and Binda, L. (1993)."Identification of moisture cappilarity in masonry using digital impulse radar." *Proc. 5th Int. Conf. on Structural Faults and Repair*, Edinburgh, Engineering Technics Press, Vol. 2, pp. 397-403.

111. Colla, C., Das, P., McCann, D. and Forde, M. C. (1995)."Investigation of stone masonry bridges using sonics, electromagnetics and impulse radar." *Proc. Int. Symp. on Non-Destructive Testing in Civil Engineering*, Berlin, Vol. 1, pp. 629-636.

112. Bungey, J. H., Millard, S. G. and Shaw, M. R. (1993). "A simulation tank to aid interpretation of radar results on concrete." *Magazine of Concrete Research*, **45**(164), pp. 187-195.

113. Büyüköztürk, O. and Rhim, H. C. (1995)."Radar using imaging of concrete specimens for non-destructive testing." *Proc. 6th Int. Conf. on Structural Faults and Repair*, London, Engineering Technics Press, Vol. 2, pp. 307-310.

114. Coffey, J. M. (1987)."Mathematical modelling of NDT techniques." *Proc. 4th European Conference*, London, The British Inst. of Non-Destructive Testing, Vol. 1, pp. 79-93.

115. Goodman, D. and Nishimura, Y. (1992)."2-D synthetic radargrams for archaeological investigation." *Proc. 4th Int. Conf. on Ground Penetrating Radar*, Finland Geol. Sur., pp. 339-343.

116. Goodman, D. (1994). "Ground penetrating radar simulation in engineering and archaeology." *Geophysics*, **59**(2), pp. 224-232.

117. McCavitt, N. and Forde, M. C. (1991). "The application of the method of convolution to the simulation of the response of masonry arch bridges to ground probing radar." *J. of Non-Destructive Testing & Evaluation*, **6**(3), pp. 179-194.

118. Park, S., Uomoto, T. and Yoshizawa, M. (1995)."Analysis of radar response on subsurface objects in concrete by simulation techniques." *Proc. Int. Symp. on Non-Destructive Testing in Civil Engineering (NDT-CE)*, Berlin, DGZfP, Vol. 1, pp. 673-680.

119. Giannopoulos, A., Tealby, J. M. and Tsokas, G. N. (1994)."Numerical modelling of ground penetrating radar." *Proc. 56th Meeting of the European Association of Exploration Geophysicists (Extended abstracts)*, Vienna, Austria, p. P127.

120. Chen, H. L. R., Halabe, U. B., Sam, Z. and Bhandarkar, V. (1994). "Impulse radar reflection waveforms of simulated reinforced concrete bridge decks." *Materials Evaluation*, **52**(12), pp. 1382-1388.

121. Pichot, C. and Trouillet, P. (1990)."Diagnosis of reinforced structures: an active microwave imaging system." *Proc. NATO Advanced Research Workshop on Bridge Evaluation*, Kluwer Academic Publishers, pp. 201-215.

122. Mast, J. E. and Johansson, E. M. (1994)."Three-dimensional ground penetrating radar imaging using multi-frequency diffraction tomography." *Proc. SPIE-The International Society for Optical Engineering, Advanced Microwave and Millimeter-Wave Detectors*, Vol. 2275, pp. 196-204.

123. Olver, A. D. and Cuthbert, L. G. (1988). "FMCW radar for hidden object detection." *Proc. Instn. Electr. Engrs.*, **135-F**(4), pp. 354-361.

124. Paul, C. R. and Nasar, S. (1987). *Introduction to electromagnetic fields*. McGraw-Hill, 2nd ed.

125. Cheng, D. K. (1989). *Field and wave electromagnetics*. Addison-Wesley Publishing Company, USA, 703 pp.

126. Jordan, E. C. and Balmain, K. G. (1968). *Electromagnetic waves and radiating systems*. Prentice Hall, New Jersey, 753 pp.

127. Von Hippel, A. R. (1954). *Dielectric materials and applications*. Chapman and Hall Ltd., London, 438 pp.

128. Hoekstra, P. and Delaney, A. (1974). "Dielectric properties of soils at UHF and microwaves frequencies." *J. Geophys. Res.*, **79**, pp. 1699-1708.

129. Daniels, D.J. (1996). "Surface-penetrating radar". *Electronics & Communication Engineering Journal,* (August), pp. 165-182.

130. Davis, J. L. and Annan, A. P. (1989). "Ground-penetrating radar for high-resolution mapping of soil and rock stratigraphy." *Geophysical Prospecting*, **37**(5), pp. 531-551.

131. Bungey, J. H. and Millard, S. G. (1993). "Radar inspection of structures." *Proc. Instn Civ. Engrs Structs & Bldgs*, **99**(May), pp. 173-186.

132. Annan, A. P. and Davies, J. L. (1977). *"Radar range analysis for geological materials."* Report of Activities, Geological Survey of Canada, Paper 77-1B, pp. 117-124.

133. Corson, D. and Lorrain, P. (1962). *Introduction to electromagnetic fields and waves*. W.H. Freeman and Company, London.

134. Turner, G. and Siggins, A. F. (1994). "Constant Q attenuation of subsurface radar pulses." *Geophysics*, **59**(8), pp. 1192-1200.

135. Hasted, J. B. (1973). *Aqueous dielectrics*. Chapman and Hall, London, 302 pp.

136. Sen, P. N., Scala, C. and Cohen, M. H. (1981). "A self-similar model for sedimentary rocks with application to the dielectric constant of fused glass beds." *Geophysics*, **46**, pp. 781-795.

137. Millard, S. G., Bungey, J. H. and Shaw, M. R. (1993)."The assessment of concrete quality using pulsed radar reflection and transmission techniques." *Proc. Int. Conf. on Non-Destructive Testing in Civil Engineering*, Liverpool, The Brit. Instn. of NDT, Vol. I, pp. 161-185.

138. Ulriksen, P. (1982). "Application of impulse radar to Civil Engineering." Doctoral Thesis, Department of Engineering Geology, Lund University of Technology, Lund, 175 pp.

139. Krause, M., Maierhofer, C. and Wiggenhauser, H. (1995)."Thickness measurement of concrete elements using radar and ultrasonic." *Proc. 6th Int. Conf. on Structural Faults and Repair*, London, Engineering Technics Press, Vol. 2, pp. 17-24.

140. McCann, D., Jackson, P. D. and Fenning, P. J. (1988). "Comparison of the seismic and ground probing radar methods in geological surveying." *Proc. Inst. Elect. Engrs.*, **135-F**, pp. 380-390.

141. Reynolds, J. M. and Taylor, D. I. (1992)."The use of sub-surface imaging techniques in the investigation of contaminated sites." *Proc. Polluted and Marginal Land-92*, London, Engineering Technics Press, pp. 121-131.

142. Millard, S. G. and Gowers, K. R. (1992). "Resistivity assessment of in-situ concrete: the influence of conductive and resistive surface layers." *Proc. Instn. Civ. Engrs.*, **94**(Nov.), pp. 389-396.

143. Castle, G. S. P. and Roberts, J. (1974). "A microwave instrument for the continuous monitoring of the water content of crude oil." *Proc. IEEE*, **62**(1), pp. 103-108.

144. Al-Qadi, I. L. (1994)."Variation of the dielectric properties of Portland cement concrete during curing time over low RF frequencies." *Proc. 73rd Annual Meeting*, Transportation Research Board, Paper No. 940480.

145. Wilson, J. G. and Whittington, H. W. (1990). "Variations in the electrical properties of concrete with change in frequency." *Proc. Instn. Elect. Engrs.*, **137-Part A**(5), pp. 246-254.

146. Shaw, M. R., Millard, S. G., Houlden, M. A., Austin, B. A. and Bungey, J. H. (1993). "A large diameter transmission line for the measurement of the relative permittivity of construction materials." *British Journal of NDT*, **35**(12), pp. 696-704.

147. Baillon, L., Robert, A. and Huet, C. (1995)."Design and calibration of a dielectric measurement cell for concrete with large grain heterogeneities." *Proc. Int. Symp. on Non-Destructive Testing in Civil Engineering*, Berlin, Vol. 2, (Poster), pp. 1053-1062.

148. Feng, S. and Sen, P. N. (1985). "Geometrical model of conductive and dielectric properties of partially saturated rocks." *J. Appl. Phys.*, **58**(8), pp. 3236-3243.

149. Halabe, U. B., Sotoodehnia, A., Maser, K.R. and Kausel, E.A. (1993). "Modeling the electromagnetic properties of concrete." *ACI Materials Journal*, **90**(6), pp. 552-563.

150. Endres, A. L. and Knight, R. (1992). "A theoretical treatment of the effects of microscopic fluid distribution on the dielectric properties of partially saturated rocks." *Geophysical Prospecting*, **40**, pp. 307-324.

151. Tsui, F. and Mathews, S. L. (1995)."Analytical modelling of the dielectric properties of concrete for sub-surface radar applications." *Proc. 6th Int. Conf. on Structural Faults and Repair*, London, Engineering Technics Press, Vol. 2, pp. 25-31.

152. Stogryn, A. (1971). "Equations for calculating the dielectric constant of saline water." *IEEE Trans. on Microwave Theory and Techniques*, **MTT-19**(Aug.), pp. 733-736.

153. Klein, L. A. and Swift, C. T. (1976). "An improved model for the dielectric constant of sea water at microwave frequencies." *IEEE Trans. on Antennas and Propagation*, **AP-25**(1), pp. 104-111.

154. Petroy, D. E. (1994)."Assessment of ground penetrating radar-applicability to specific site investigations: simple methods for pre-survey estimation of likely dielectric constants, target resolution and reflection strengths." *Proc. SAGEEP-94*, Massachusetts, 21p.

155. Darracot, B. W. and Lake, M. I. (1981). "An appraisal of ground probing radar for the site investigation in Britain." *Ground Engineering*, **14**(April), pp. 14-18.

156. Ambardar, A. (1995). *Analog and digital signal processing*. PWS Publishing Company, Boston, 700 pp.

157. Lynn, P. A. and Fuerst, W. (1989). *Introductory digital signal processing with computer applications*. John Willey & Sons.

158. Kraniauskas, P. (1992). *Transforms in signals and systems*. Addison-Wesley Publishers, 558 pp.

159. Kuc, R. (1982). *Introduction to digital processing*. McGraw-Hill International Editions.

160. Balmer, L. (1991). *Signals and systems - an introduction*. Prentice Hall International, 466 pp.

161. Ramirez, R. W. (1985). *The FFT - Fundamentals and Concepts*. Prentice-Hall Inc., New Jersey, 178 pp.

162. Annan, A. P. (1992). *"Ground penetrating radar - workshop notes."* Sensor and Software Inc., Canada, 128p.

163. Sheriff, R. E. and Geldart, L. P. (1982). *Exploration seismology: history, theory and acquisition*. Cambridge University Press, Vol. 1.

164. Olhoeft, G. R. (1986)."Electrical properties from 10^{-3} to 10^{9} Hz - physics and chemistry." *Proc. 2nd Int. Symp. on the Physics and Chemistry of Porous Media*, Schlumberger-Doll ,Ridgefield, CT, Am. Inst. Phys, pp. 281-298.

165. Cook, J. C. (1975). "Radar transparencies of mine and tunnel rocks." *Geophysics*, **40**(5), pp. 865-885.

166. Bungey, J. H. (1992)."Principles of sub-surface radar surveying." *Proc. Conf. on Polluted and Marginal Land-92*, London, Engineering Technics Press, pp. 115-120.

167. Bungey, J. H., Shaw, M. R. and Millard, S. G. (1993)."The influence of reinforcing steel on radar surveys of concrete structures." *Proc. 5th Int. Conf. on Structural Faults and Repairs-93*, Edinburgh, Engineering Technics Press, Vol. 3, pp. 43-50.

168. Forde, M. C. and McCavitt, N. (1993). "Impulse radar testing of structures." *Proc. Instn. Civ. Engrs. Structs. and Bldgs.*, **99**(Feb), pp. 96-99.

169. Sellmann, P. V., Delaney, A. J. and Arcone, S. A. (1993)."Observations of radar performance for bottom and sub-bottom information in fresh water." *Proc. Second Government Workshop on GPR - Advanced Groun Penetrating Radar : Technologies and Applications*, Ohio, pp. 59-70.

170. Smith, G. S. (1984). "Directive properties of antennas into a material half-space." *IEEE Trans. Antennas*, **AP-32**, pp. 232-247.

171. Daniels, J. J. (1989)."Ground penetrating radar." *Proc. Symp. on the Application of Geophysics to Engineering and Environmental Problems - SAGEEP'89*, pp. 62-142.

172. BS12. *"Specification for ordinary and rapid-hardening Portland cement."* British Standards Institution, London.

173. BS882. *"Specification for aggregates from natural sources for concrete."* British Standards Institution, London.

174. Murdock, L. J., Brook, K. M. and Dewar, J. D. (1991). *Concrete-materials & Practice*. Edward Arnold, London, 6th ed, 470 pp.

175. BS1881. *"Testing concrete."* British Standards Institution, London.

176. GSSI (1991). "Sir10 Manual."

177. Skolnik, M. I. (1970). *Radar handbook*. McGraw-Hill, New York.

178. Warhus, J. P., Scott, D. N., Jeffrey, E. M. and Johansson, E. M. (1993). *"Advanced ground-penetrating, imaging radar for bridge inspection."* Engineering Research, Development and Technology, Lawrence Livermore National Laboratory, Livermore, California.

179. Anon (1995). *Matlab reference guide*. The MathWorks Inc.

180. Mellett, J. S. (1995)."Use of bistatic allo-frequency antennas in ground-penetrating radar (GPR) investigations." *Proc. SAGEEP 95, Symposium on the Application of Geophysics to Engineering and Environmental Problems*, Orlando-Florida, pp. 405-411.

181. Levitt, M. (1988). *Magazine of Concrete Research*, **40**(145), pp. 238-239.

APPENDICES

A. CONCRETE MIX DESIGN

B. PUBLISHED PAPERS

APPENDIX A

CONCRETE MIX DESIGN

This appendix presents the concrete mix design regarding the construction of the concrete column referred to in chapter 6. It was designed based on a simplified method, proposed in conjunction by the Building Research Establishment, Transport Research Laboratory and the British Cement Association [173].

For the mix design the following assumptions were made:

- Average strength at 28 days $\geq 30+10 = 40$ N/mm^2
- Concrete slump = 50 mm
- Maximum aggregate size = 20 mm
- Percentage of sand passing 600 μm = 50 % (Table 6.1 - See section 6.2.1)

Next are presented the steps of the mix design:

a) Free water/cement ratio = 0.52 (Figure A1, for uncrushed aggregates)

b) Free water content = 180 kg/m^3 (Table A1)

c) Cement content= 180 / 0.50 = 360 kg/m^3 (Assuming w/c= 0.50, $f_{c\,28} > 40$ N/mm^2)

d) Plastic density = 2380 kg/m^3 (Figure A2)

e) Aggregate content = 3280-360-180 = 1840 kg/m^3

f) Proportion of fine aggregate = 35 % (Figure A3)

g) Sand content = 0.35 x 1840 = 644 kg/m^3

h) Gravel content = 1840 - 644 = 1196 kg/m^3

The resultant mix proportion was 1 : 1.79 : 3.32 by weight. The main tables and figures considered for the design are reproduced below.

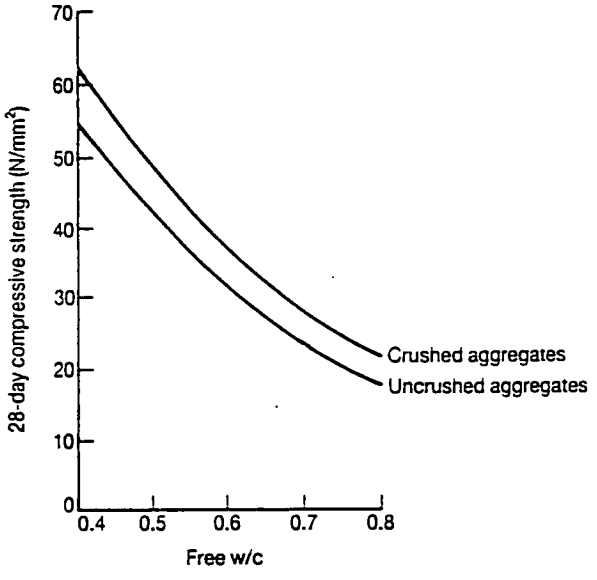

Figure A1 Assumed relationships between strength at 28 days and free w/c for concrete made with OPC to BS12, after Murdock [173]

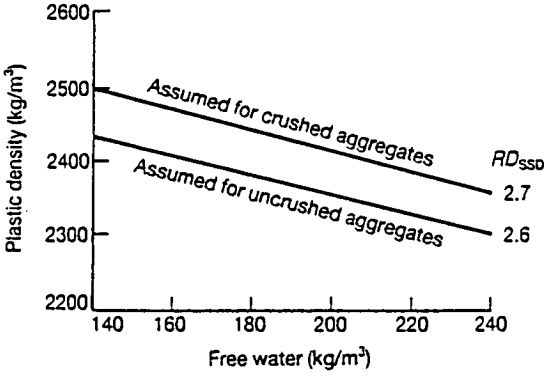

Figure A2 Assumed relationships between plastic density and free water content, after Murdock [173]

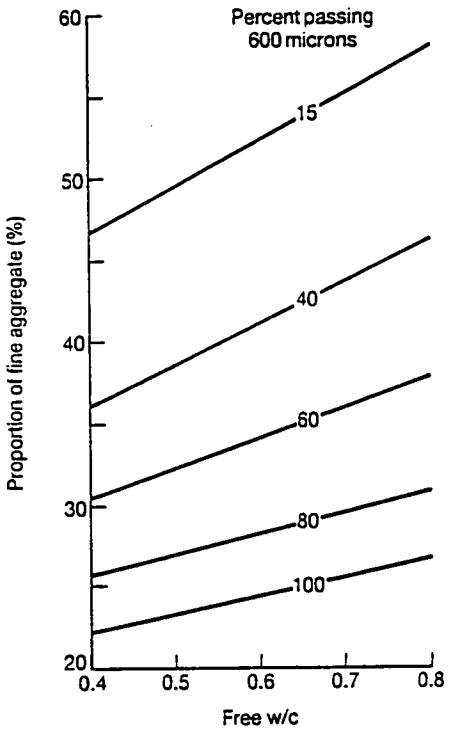

Figure A3 Example of relationship between percentage fine aggregate and free w/c for concrete of 50 mm slump made with 20 mm aggregate, after Murdock [173]

Table A1 Assumed free water contents of concrete made with uncrushed aggregates [173]

Maximum aggregate size	Free water (kg/m^3)			
	Slump			
	25	50	75	100
10	185	205	215	220
20	165	180	190	195
40	145	160	170	175

APPENDIX B

PUBLISHED PAPERS FROM THIS THESIS

1. Padaratz, I.J. and Forde, M.C. (1994). "Limits of effectiveness of digital impulse radar in contaminated land site investigation." *Proc. 3rd Int. Conf. Polluted and Marginal Land - 94*, Brunel Univ., June 1994, Engineering Technics Press, pp. 397-402.

2. Padaratz, I.J. and Forde, M.C. (1995). "A theoretical evaluation of impulse radar wave propagation through concrete." *J. Non-destructive Testing and Evaluation*, **12**, pp. 9-32.

3. Padaratz, I.J. and Forde, M.C. (1995). "Influence of antenna frequency on impulse radar surveys of concrete structures." *Proc. 6th Int. Conf. on Structural Faults and Repair*, London, July 1995, Vol. 2, Engineering Technics Press, pp. 331-336.

4. Davidson, N.C., Padaratz, I.J. and Forde, M.C. (1995). "Quantification of bridge scour using impulse radar ." *Proc. Int. Symp. on Non-Destructive Testing in Civil Engineering (NDT-CE)*, BAM, Berlin, Germany, September 1995, Vol. 1, pp. 61-68.